New coupled Thermo-Hydro-Mechanical-Chemical formulations with consideration of swelling and dissolution

Yue MA

Submitted in accordance with the requirements for the degree of

Doctor of Philosophy

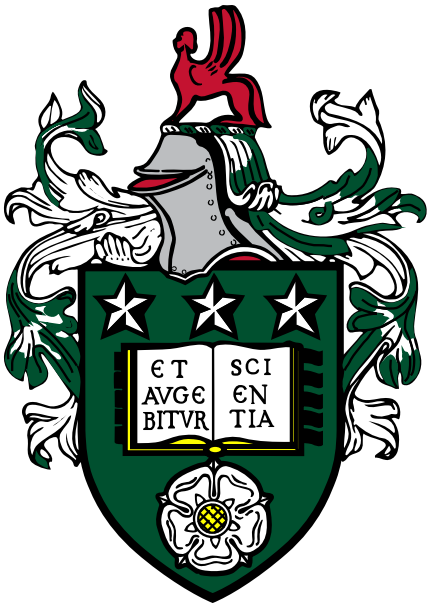

The University of Leeds

School of Civil Engineering

April 2022

DECLARATION

The candidate confirms that the work submitted is his own, except where work which has formed part of jointly authored publications has been included. The contribution of the candidate and the other authors to this work has been explicitly indicated below. The candidate confirms that appropriate credit has been given within the thesis where reference has been made to the work of others.

Publication 1 has been reproduced in some aspects of chapters 3 and 4; Publication 2 has been reproduced in some aspects of chapters 5; Publication 3 has been reproduced in some aspects of chapters 2 and 6.

1. **Ma, Y**., Chen, X.H., Yu, H.S., 2020. An extension of Biot's theory with molecular influence based on Mixture-Coupling Theory: Mathematical model. International Journal of Solids and Structures, 2020, 191, pp.76-86.
2. **Ma, Y**., Chen, X.H., Hosking, L.J., Yu, H.S., Thomas, H.R., Norris, S., 2021. The influence of coupled physical swelling and chemical reactions on deformable geomaterials. International Journal for Numerical and Analytical Methods in Geomechanics, 2021, 45(1), pp.64-82.
3. **Ma, Y**., Ge, S., Yang, H., Chen, X.H. Coupled Thermo-Hydro-Mechanical-Chemical processes with reactive dissolution by non-equilibrium thermodynamics. Submitted to Journal of the Mechanics and Physics of Solids (Under Review)

In the first and the second publications, the candidate carried out the mathematical derivation, numerical simulation, original draft writing, and response to review comments. Dr Xiaohui Chen provided guidance on theory derivation and draft writing. Other co-authors reviewed and provided comments on the manuscripts. In the third paper, the candidate carried out the mathematical derivation, numerical simulation, and original draft writing. Mr Shangqi Ge and Mr He Yang contributed to the draft writing,

reviewed the manuscript, and provided comments. Dr Xiaohui Chen provided guidance on theory derivation.

ACKNOWLEDGEMENT

I would gratefully acknowledge the final support of the Civil Engineering Research Excellence Award provided by the School of Civil Engineering at the University of Leeds.

I would like to give my utmost gratitude to my supervisor Dr Xiaohui Chen for providing guidance, feedback, and support throughout my PhD period. His knowledge, experience and encouragement are essential for this project. He also provides the teaching assistant position for me to gain teaching experience. I would also like to thank my co-supervisors Prof Hai-Sui Yu and Prof Doug Stewart for their strong support and helpful suggestions.

I would like to thank Dr Amirul Khan, he has kindly shared his opinions and comments on my research.

I would like to thank the members of the Geomodelling and AI group, including Mr Yousef Baqer, Dr Cuicui Liu, Mr Sulaiman Abdullah, Mr Jiangwei Zhang, Dr Liyang Xu, Mr Kai Wang, Mr He Yang, Mr Shangqi Ge, et.al. They have given valuable suggestions and comments on my research work.

I have spent a very happy time in the School of Civil Engineering, I would like to thank Mr Siyuan Lin, Mr Jihua Zhai, Mrs Meng Li, Mrs Yuyan Huang, Mr Licong Cao, Mr Kongming Yan, Mr Hao Li, Mr Xiaohong Zhu, Ms Haoyue Qiao. Sorry for those left out but they have my gratitude.

Finally, I would like to thank my family for their continuous support.

ABSTRACT

This thesis fundamentally extends the new theory, Mixture-Coupling Theory (MCT), to develop a new Thermo-Hydro-Mechanical-Chemical model by including swelling (e.g., hydration) and dissolution in soils/rocks, with the engineering application focusing on nuclear waste disposal.

The Mixture-Coupling Theory is based on non-equilibrium thermodynamics and continuum mechanics. This thesis firstly builds an advanced Hydro-Mechanical (HM) coupled model by incorporating the swelling and dissolution influence. The model is then extended to unsaturated conditions. Afterwards, the unsaturated Hydro-Mechanical-Chemical (HMC) model is developed, and finally, a new coupled Thermo-Hydro-Mechanical-Chemical (THMC) formulation with consideration of swelling and dissolution is derived. All the numerical simulations in this thesis are for demonstration purpose with application in the field of nuclear waste disposal.

Deep geological disposal is a major approach to treat high-level nuclear waste, in which the nuclear waste is isolated in the deep geological rock formation at a depth of hundreds of meters or several kilometres below the surface. The waste is kept away from the biosphere by a multi-barrier system consisting of artificial barriers (bentonite, concrete, et al.) and the natural surrounding rock. The swelling of backfill bentonite and clay-rich rock, and the chemically induced reaction (e.g., dissolution) have a significant influence on the integrity and stability of the engineered barriers and significantly affect the THMC process.

The new coupled Thermo-Hydro-Mechanical-Chemical (THMC) model with consideration of swelling and dissolution achieves a deeper understanding of the rock/clay behaviour of the multi-barrier system and provides a more realistic prediction for nuclear waste disposal safety assessment.

LIST OF ABBREVIATIONS

HM	Hydro-Mechanical
HMC	Hydro-Mechanical-Chemical
MCT	Mixture-Coupling Theory
THM	Thermo-Hydro-Mechanical
THMC	Thermo-Hydro-Mechanical-Chemical

CONTENT

LIST OF FIGURES

LIST OF TABLES

LIST OF SYMBOLS

English symbols:

A	Affinity
A_s	Solid affinity
A_{sf}	Surface area
c^{β}	Concentration of chemical β
C^f	Specific heat capacities of the fluid
C^s	Specific heat capacities of the solid
C_s	Specific moisture content
C_s^p	Defined as $C_s^p = \phi \partial S^f / \partial p^f$
$\mathbf{d}$	Displacement tensor
D_{diff}	Diffusion Coefficient
$\mathbf{E}$	Green strain
$\mathbf{F}$	Solid deformation gradient
G	Shear modulus
h^w	Enthalpy of water
h^f	Enthalpy of fluid
h^c	Enthalpy of chemical
h^{β}	Enthalpy of fluid component β
$\mathbf{I}$	Unit tensor
$\mathbf{I}^c$	Flux of chemical c
$\mathbf{I}^d$	Flux of dissolved solid/chemical
$\mathbf{I}^f$	Flux of pore fluid
$\mathbf{I}^w$	Flux of water
J	Determinant of $\mathbf{F}$
$\mathbf{J}^c$	Chemical flux
$\mathbf{J}^{\beta}$	Chemical flux of fluid component β
$\mathbf{I}_{\eta}$	Entropy flow exchange with the surroundings
k	Absolute permeability

K	Bulk modulus
K_{eq}	Equilibrium constant
k_{rate}	Rate constant
k_{rf}	Relative permeability
K_f	Bulk modulus of fluid
K_s	Bulk modulus of the solid grain
K_w	Bulk modulus of water
M	Biot's modulus
m^c	Mass density of chemical c in the reference configuration
m^w	Mass density of water in the reference configuration
m_{bound}	Bounded water mass density in the reference configuration
$m_{dissolve}$	Dissolved mass density in the reference configuration
m_r^β	Source term, representing mass of β due to chemical reaction
m_r	Source term for chemical c
M_b	Molar mass of mineral B
M_c	Molar mass of chemical C
$\mathbf{n}$	Outward unit normal vector
p_{atm}	Atmospheric pressure
p^f	Porefluid pressure
p^{pore}	Pore pressure
Q	Void compressibility
q	Void coefficient
R	Gas constant
$\mathbf{q}$	Total heat flux
$\mathbf{q}^f$	Heat flow carried by fluid
$\mathbf{q}'$	Heat flux by convection (Reduced heat flow)
q^f	Heat density of pore fluid, relative to the mixture volume
q^s	Heat density of solid, relative to the mixture volume
q^f_{bound}	Heat density of the bounded fluid

q_s^s	Thermo density of solid, relative to the solid volume
R	Source term
r^β	Dissolution/precipitation rate of chemical β
S^f	Saturation of pore fluid
T	Temperature
$\mathbf{T}$	Second Piola-Kirchhoff stress
$\mathbf{u}$	Darcy velocity
$\mathbf{v}^f$	Velocity of fluid
$\mathbf{v}^d$	Velocity of dissolved solid/chemical
$\mathbf{v}^s$	Velocity of the solid
$\mathbf{v}^w$	Velocity of water
w^c	Mass fraction of chemical c
x^β	Mole fraction of β
V	Volume of the mixture
V_{fluid}	Volume of pore fluid
V_s	Volume of the solid part

Greek Symbols:

α_f	Thermal expansion coefficient of fluid
α_s	Thermal expansion coefficient of solid
α_μ^c	Temperature coefficient of chemical potential of fluid component C
γ	Entropy produced per unit volume
δ_{ij}	Kronecker delta
ε	Internal energy
ε_d	Strain resulting from dissolution
ε_{kk}	Strain tensor
ζ	Biot coefficient
η^d	Entropy induced by dissolution
η	Entropy density

η^f	Entropy density of fluid
η^s	Entropy density of solid
η^{mix}	Entropy density of the mixture
η^{wet}	Entropy density of the wetted matrix
η^f_{bound}	Entropy density of the bounded fluid
H^{wet}	Entropy density of the wetted matrix in the reference configuration
θ	Poisson's ration
λ	Thermal conductivity
μ^c	Chemical potential of pore fluid component C
μ^d	Chemical potential of dissolved solid/chemical
μ^w	Chemical potential of pore water
μ^β	Chemical potential of pore fluid component β
μ^c_{bound}	Chemical potential of bounded chemical C
μ^w_{bound}	Chemical potential of bounded water
μ^β_{bound}	Chemical potential of bounded fluid component β
μ^β_t	True chemical potential of β
ν	Dynamic viscosity
ν_c	Stoichiometric coefficient for chemical c
ξ	Reaction extent
ρ^c	Mixture density of chemical
ρ^d	Mixture density of dissolved solid/chemical
ρ^f	Mixture density of fluid
ρ^w	Mixture density of water
ρ^β	Mixture density of fluid component β
ρ^c_f	Phase density of chemical
ρ^d_f	Phase density of dissolved solid/chemical
ρ^f_f	Phase density of fluid
ρ^w_f	Phase density of water

ρ_f^β	Phase density of the fluid component β
ρ_s^s	Phase density of solid
ρ_t^b	True mass density of mineral B
ρ_{ex}^β	Mixture density of fluid component β that entered into interlayer space
ρ_{bound}^β	Mixture density of bounded fluid component β
ρ_{pore}^β	Mixture density of pore fluid component β
$\boldsymbol{\sigma}$	Stress tensor
σ_{ij}	Stress tensor
$\boldsymbol{\sigma}'$	Effective stress tensor
ϕ	Porosity
ϕ^f	Volume fraction of pore fluid
ψ	Helmholtz free energy density in the current configuration
ψ_{pore}	Helmholtz free energy density of the pore space
Ψ	Helmholtz free energy density in the reference configuration
ω_p	Precipitation coefficient
ω_d	Dissolution coefficient
ω_r	Reaction coefficient
ω_R	Stress change coefficient due to dissolution/precipitation
ω_s	Swelling coefficient
ω_s^c	Swelling coefficient for chemical C
ω_s^w	Swelling coefficient for water
ω_s^β	Swelling coefficient for fluid component β
ς	increment of water content

LIST OF PUBLICATIONS

1. Publication list (Papers directly contributing to the thesis): The first paper contributes to the major part of chapter 4 and chapter 3; the second paper contributes to the majority of chapter 5; the third paper contributes to chapter 6.

(1) Ma, Y., Chen, X.H., Yu, H.S., 2020. An extension of Biot's theory with molecular influence based on Mixture-Coupling Theory: Mathematical model. International Journal of Solids and Structures, 2020, 191, pp.76-86. **(IF: 3.9, Top 1% in Applied Mathematics)**

(2) Ma, Y., Chen, X.H., Hosking, L.J., Yu, H.S., Thomas, H.R., Norris, S., 2021. The influence of coupled physical swelling and chemical reactions on deformable geomaterials. International Journal for Numerical and Analytical Methods in Geomechanics, 2021, 45(1), pp.64-82. (**IF: 4.26, Q1, Top 3% Journal in Computational Mechanics**)

(3) Yue MA, Shangqi GE, He Yang, Xiaohui Chen. Coupled Thermo-Hydro-Mechanical-Chemical processes with reactive dissolution by non-equilibrium thermodynamics. Journal of the Mechanics and Physics of Solids (Under Review)

2. Other papers indirect contributing to the knowledge of the thesis

(1) Ma, Y., Chen, X.H, Hosking L.J., Yu, H.S. Thomas HR., 2022. THMC constitutive model for membrane geomaterials based on Mixture-Coupling Theory. International Journal of Engineering Science, 2022, 171: 103605. (**IF: 8.843. Q1, Top 1% Journal in Engineering (miscellaneous)**)

(2) Abdullah, S., Ma, Y., Chen, X.H, Khan, A., 2022. A Fully Coupled Hydro-Mechanical-Gas Model Based on Mixture-Coupling Theory. Transport in porous media. (Accepted)

(3) Liu, C., Ma, Y., Banwart, S. A., Chen, X.H, Du, W., Yin, Y., Guo, H., 2022. Kinetic Modeling for a Novel Permeable Reactive Biobarrier for In Situ Remediation

of PAH-Contaminated Groundwater. Journal of Geotechnical and Geoenvironmental Engineering, 148(5), 04022024.

(4) Feng, J., Ma, Y., Liu, Z., 2021. A Study on the Creep Characteristics of Airport Viscous Subsoil Based on Unsaturated Stress Level. Geofluids, 2021.

(5) Chen, J., Chen, X.H, Wang, M., Thornton, S., Wang, Y., Ma, Y., 2019. The couplings of rock/carbonate groundwater/cement leachate. Environmental Geotechnics, 7(7), pp.467-477.

Chapter 1 Introduction

1.1 Nuclear waste disposal and the importance of THMC model

Since the first commercial nuclear power station started operation in the 1950s, there have been about 440 power reactors now (WNA, 2022). Nuclear energy has become the world's second-largest source of low-carbon power and provides 11% of the world's electricity (WNA, 2022). However, the spent nuclear fuel after usage is still radioactive and harmful, which must be managed carefully.

Due to the long half-life of some radioactive elements, such as uranium, the radiation of the spent fuel will remain harmful for a long time. Hence, it is crucial to isolate these wastes from human beings and the environment for many thousands of years (NEA, 2013). Various isolation options have been put forwarded and discussed, such as geological disposal, disposal in outer space, rock melting, disposal at subduction zones, sea disposal, sub-seabed disposal, and disposal in ice sheets (NDA, 2015). Nevertheless, most of them are discarded because of political or safety reasons (NEA, 2008). The only well-accepted disposal approach is deep geological disposal, which has been discussed, studied, and even constructed.

The concept of deep geological disposal is: Disposal holes or tunnels are constructed in a site in the natural rock formation to be the residence of nuclear waste. The site is hundreds of meters or several kilometres below the surface and the host rock works as a natural barrier for protecting the waste. The nuclear waste is packed with metal containers and placed inside the disposal holes, and the empty room between the container and the hole wall is backfilled with bentonite. The container, bentonite and concrete are referred to as the engineered multi-barrier and the host rock is the natural barrier (Ericsson, 1999, Freiesleben, 2013). Figure 1.1 and Figure 1.2 show the Swiss

concept of nuclear waste repository and the concept of the multi-barrier system, respectively.

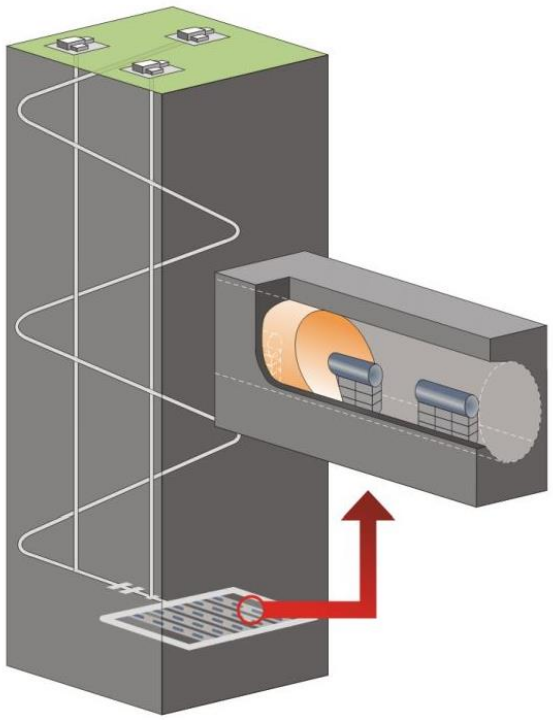

Figure 1. 1 Swiss concept of deep geological repository (NDA, 2010a)

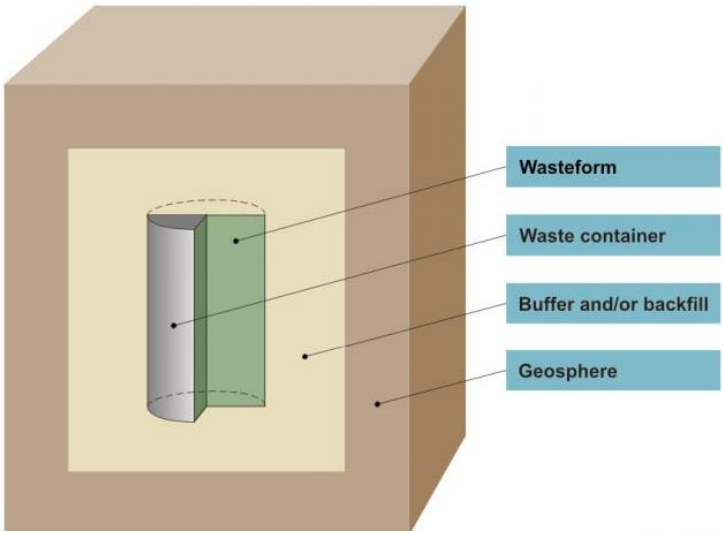

Figure 1. 2 Multi-barrier system – illustration of key components (NDA, 2010b)

According to the radiation level, nuclear waste can be classified as (BEIS, 2018, NDA, 2019): 1. High-level waste (HLW). The temperature may significantly rise due to

radioactivity; 2. Intermediate-level waste (ILW), which exceeds the upper boundaries of Low-level waste, but does not undergo significant temperature raise; 3. Low-level waste (LLW), of which the alpha activity is no more than 4 Giga becquerels per ton or the beta/gamma activity no more than 12 Giga becquerels per ton; 4. Very low-level waste (VLLW), can be disposed as common industrial waste. In UK, LLW and VLLW make up over 95% of the total volume of nuclear waste, but HLW and ILW contribute to over 99.9% of total radioactivity (BEIS, 2018). It is suggested that all HLW, most ILW and a small fraction of LLW should be stored and disposed by the deep geological facility (Alexander and McKinley, 2011, BEIS, 2018, NDA, 2019).

From the above classification, high temperature is the main feature of HLW. For HLW, the temperature influence must be considered during waste storage and disposal, while for the rest, the temperature is not required to be taken into consideration (BEIS, 2018, NDA, 2019). The engineered and natural barriers of deep geological facility such as the clay barrier and host rock, once prepared and placed, will be progressively affected by a series of geological processes, which could mainly be described as thermal (T), hydro (H), mechanical (M) and chemical (C) processes. These processes do not affect the geoengineering infrastructure individually but synchronously, more than that, there is an interaction between them, which means some properties and parameters in one process may be affected by the others (Sijing and Enzhi, 2004), ‘Mutual feedbacks of the influences then lead to a combined process of development, the so-called coupled processes’ (Sijing and Enzhi, 2004), the term coupled process can also be described as: one process affects the initiation and progress of the others and in turn, it’s also affected by the other process. Therefore, the behaviour of rock/soil cannot be predicted with confidence by considering each process independently (Chan et al., 1996, Jing and Feng, 2003, Sun, 2005, Tsang et al., 2009). The coupled modelling of thermal (T), hydraulic (H), mechanical (M), and chemical (M) process is very important for the analysis, estimation and prediction of the stability and safety of geoengineering infrastructure.

1.2 THMC model in other application fields

The initial purpose for developing THMC coupling is the demand for safety analysis of nuclear waste disposal in the last 1980s (Jing and Feng, 2003). Now, the coupled THMC modelling has been applied in some other fields including mining engineering, ground pollution and chemical engineering, geothermal engineering, structural engineering and mining engineering (Peter, 2011). Some other THMC coupling application areas are presented here.

1.2.1 Carbon capture and storage

In recent years, a lot of unusual climate change, e.g. rising sea level, melting of snow, ice and permafrost in permanently frozen, resulting from enhancement of greenhouse gas by the increasing concentration and carbon dioxide (CO_2) and other gases, have been reported (Gluyas and Mathias, 2013).

A series of approaches are required to solve the climate change problem, including improving energy efficiency and using alternative energy sources (Wielopolski, 2011, Bandyopadhyay, 2014) or reducing greenhouse gas (especially CO_2). 'Predictions of the increased use of energy globally during this century and continued reliance on fossil fuels point to a further rise in greenhouse gas emissions' (Wielopolski, 2011), and now, reducing greenhouse is the major research topic. The concentration of CO_2 increased from 270 ppm before the industrial revolution (Gluyas and Mathias, 2013) to 320 ppm in 1965 (Keeling et al., 1976) and then to 368 ppm in 2000 (ESRL, 2017) and then to 401 ppm in 2016 (ESRL, 2017). There is a pressing need to reduce the concentration of CO_2.

The method, carbon capture and storage, also called carbon sequestration, has been recognized as a cost-effective way to reduce carbon dioxide by global development

organizations, environmental regulatory groups and industrial coalitions (Al-Fattah et al., 2011).

After the CO_2 was injected into the aquifer, CO_2 would be held in porous formation by a combination of trapping mechanisms (Figure 1.3), categorized as 1): Structural trapping: confinement CO_2 phase with low permeability caprocks; 2): Residual trapping: trapping by capillary force and remaining disconnected blots of CO_2 phase; 3): Mineral trapping: conversion to mineral precipitation by interaction with water and rock; 4): Solubility trapping: dissolution into underground water (Han et al., 2010, Saadatpoor et al., 2010, Zhang et al., 2015, Zhang et al., 2016b).

Injection of massive CO_2 will induce strong coupled thermo-hydro-mechanical-chemical processes (Yin et al., 2011). The high pressure CO_2 will change the stress field and the transport of CO_2 flux may react with the host formation, meanwhile, the temperature, either from the injected CO_2 flux or from the natural source, will influence the stress, transport or reactive processes.

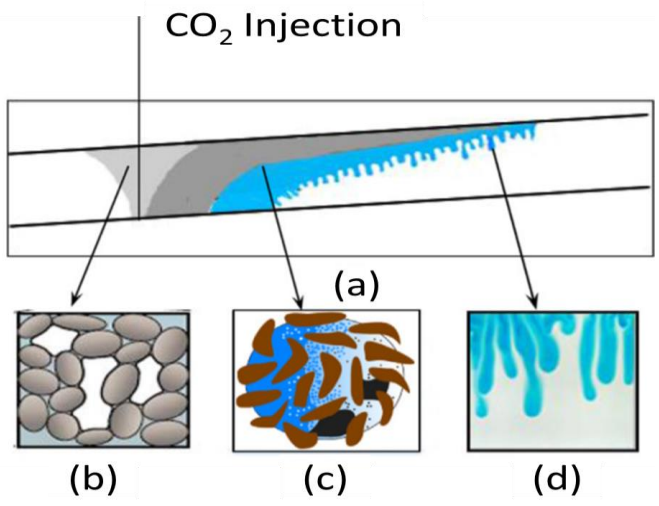

Figure 1. 3 Trapping mechanism of CO2 sequestration: (a) Structural Trapping; (b) Residual Trapping; (c) Mineral Trapping; (d) Solubility Trapping (Zhang et al., 2016b)

1.2.2 Wellbore stability

Access boreholes are required in many engineering applications, including the development of oil, gas, and geothermal energy, deep geological storage of nuclear waste and disposal of liquid and slurried solid wastes (Yin et al., 2010). Although a lot of new technologies have been used, borehole instability remains one of the most challenging issues in terms of the cost to drill and complete a well (Mohammed, 2017).

It is estimated that the substantial economic losses of about US$ 8 billion per year worldwide are caused by wellbore instability (Peng and Zhang, 2007), and over 40% of all drilling-related nonproductive time is wasted (Yan et al., 2013).

The main factors associated with wellbore instability during drilling operation are mechanical behaviour, pore water evolution, heat flux, chemical transport and reaction (Yin et al., 2010). As there are interactions between pore water, temperature, stress and geochemistry, it becomes a coupled THMC problem.

1.2.3 More application areas

Apart from these application areas, there are more research fields for THMC modelling, such as landfill (Kowalsky et al., 2014), tunnelling in the cold region (Lai et al., 1999), geothermal system (Xiong et al., 2013, Nandanwar and Anderson, 2014), cemented tailings backfill (Ghirian and Fall, 2013, Ghirian, 2016, Lu et al., 2017), sedimentary rocks to past glaciations (Nasir et al., 2013).

1.3 The key novel mechanisms focused in this study for THMC model

1.3.1 Swelling of clay/clay-rich rock

In nuclear waste disposal, compacted bentonite is used as the backfill material due to its low permeability and good compatibility with the leachate contaminants. However,

the swelling phenomenon of bentonite requires careful consideration to address its impact on the Thermo, Hydro, Mechanical and Chemical processes and the overall behaviour of the engineering barrier.

The swelling mechanism is a combination of physical-chemical reactions involving water and stress relief (ISRM., 1989), it can be categorized into three kinds: mechanical swelling, hydration swelling and osmotic swelling (Einstein, 1996). Mechanical swelling is caused by the dissipation of negative excess pore pressure, it can be viewed as an inverse process of consolidation. Osmotic swelling results from the large difference between the ion concentration close to the clay surfaces and the ions in the pore water. Dissolved minerals release a large amount of positive charges, e.g. Na+, K+, into clay layers and these positive charges will attract water molecules into the layers, resulting in the widening of the space.

Hydration swelling is the result of exchangeable cations. In dry montmorillonite, the clay layers lie very close to each other and the distance between the two layers is about 10 $\mathring{A}$ (Viani et al., 1983, Quirk and Marcelja, 1997). The exchangeable cations are absorbed on the layer surfaces (Viani et al., 1983). When in contact with water, the cations will hydrate and order themselves on a plane halfway between the clay layers. The hydration results in the widening between the two layers, and the distance increase to 12.5, 15.5, 19 and 22.5 corresponding to 1, 2, 3 and 4 $\mathring{A}$ layers of water molecules absorbed into the layers (Quirk and Marcelja, 1997). Figure 1.4 briefly illustrates hydration swelling and osmotic swelling.

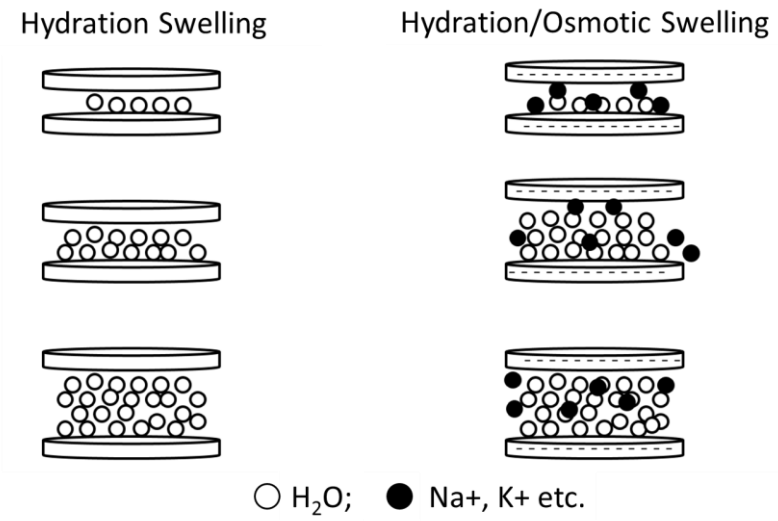

Figure 1. 4 Hydration swelling and osmotic swelling (Ma et al., 2020)

1.3.2 Dissolution of minerals

Dissolution is another common phenomenon in rock/clay. It happens when fluid flows in porous media such as rocks in numerous geological and industrial settings like carbon capture and storage, enhanced oil recovery, pollution transport, nuclear waste disposal, etc. When in contact with water, the water-rock reaction starts and moves forward toward equilibrium until equilibrium by dissolving or leaching rock-forming minerals into the solution (Yadav and Chakrapani, 2006). If the solution is diluted by newly entered fluid, more minerals will be dissolved to maintain the equilibrium (Zhao, 2014). Limited minerals can be dissolved by the reaction of primary minerals with pure water, while most minerals are dissolved by acids provided by plant activity and bacterial metabolism (Bricker, 1988) as well as CO2 dissolved in water. As the minerals are dissolved by fluid, the pore space growths and channel size evolutes significantly (Fredd and Fogler, 1998, Ciantia et al., 2015), leading to change in porosity and permeability and other physical, mechanical characteristic of the porous media (Emmanuel and Berkowitz, 2007). And, in turn, changes in porosity and permeability will have a feedback effect on fluid flow (Zhao, 2014). A scanning electron microscope

(SEM) image (Ciantia et al., 2015) (Figure 1.5) shows a clear reduction of bond and particle size of calcarenites after 6 hours of chemical dissolution.

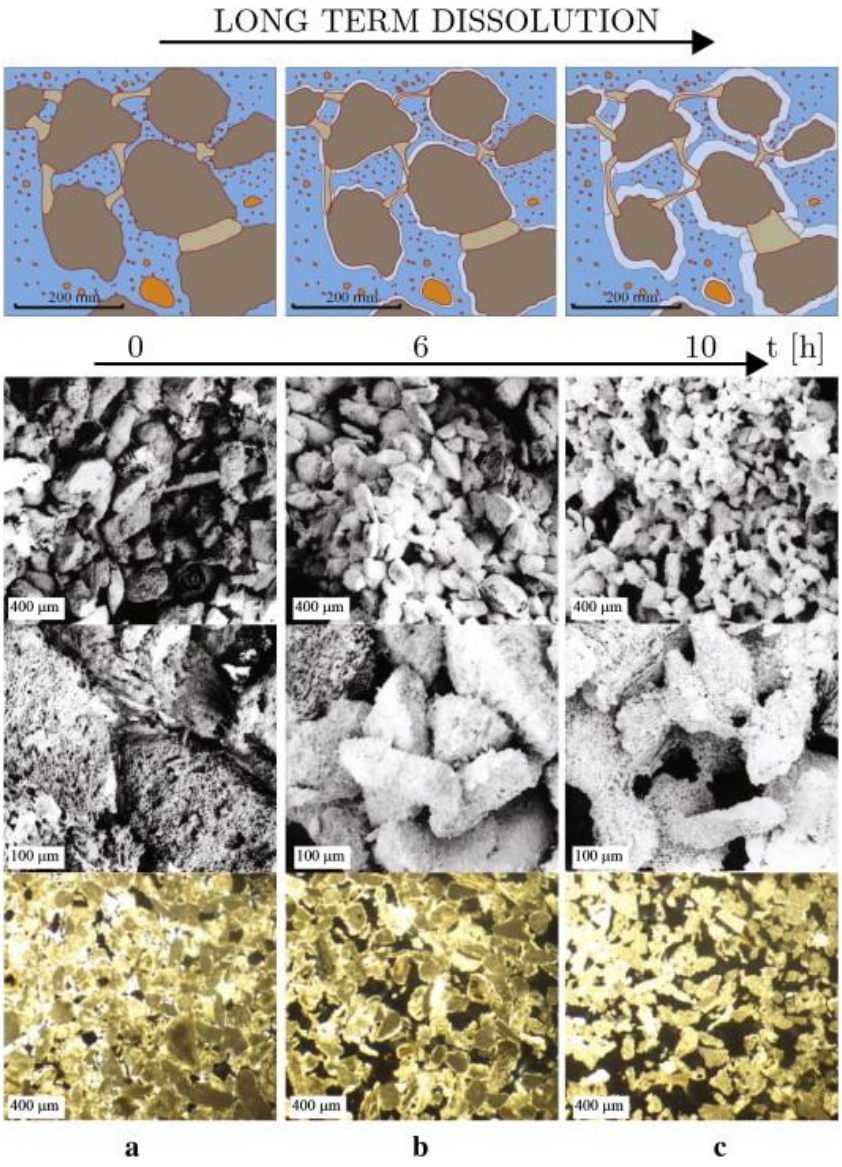

Figure 1. 5 Pore size change due to dissolution in Calcarenites (Ciantia et al., 2015)

1.4 Layout of the thesis

The thesis aims to develop new THMC theoretical and numerical models, with consideration of swelling and dissolution, to study the complex couplings between the geochemical, hydrogeological, thermal, and mechanical processes in the subsurface system. The overall aim is achieved through several objectives, including 1: Building a basic coupled hydro-Mechanical (HM) formulation for the saturated condition and

extending it to unsaturated condition; 2. Taking the chemical modulus to form a reactive-diffusion-advection HMC model; 3. Incorporates the thermal process into the developed HMC model to build a THMC model.

All the objectives are fulfilled, and the aim is achieved, and the layout of the thesis is arranged as:

Chapter 1 introduces the engineering background of this research, including nuclear waste disposal, carbon capture and storage, wellbore stability, etc. The key novel mechanism, namely, swelling and dissolution, are introduced to build the foundation for further research work.

Chapter 2 provides a literature review on the research of multiphysics coupling in porous media. It firstly introduces the concept of porous media and the basic laws to govern the mechanical, hydro, chemical and thermal behaviour. Different couplings between these processes are summarized later, followed by a review of the mathematical descriptions of these couplings. Next, the research on the swelling and dissolution in the THMC framework is reviewed, since these researches are based on different approaches, an introduction and a review on the mechanics approach, the mixture theory and the Mixture-Coupling Theory are provided.

Chapter 3 presents the mathematical derivation of the coupled saturated HM coupling model with consideration of swelling and dissolution based on the Mixture-Coupling Theory. Two parameters, the swelling parameter and dissolution parameter, are introduced into the classic Biot's poroelasticity. A numerical simulation is presented to show the role of swelling and dissolution.

Chapter 4 extends the derivation in chapter 3 to the unsaturated case by considering the

saturation of pore fluid but neglecting the gas phase. Saturation terms are incorporated into the Biot type equation. The model developed in chapter 3 and chapter 4 build the influence of swelling and dissolution in a commonly known framework, making them friendly to engineers.

Chapter 5 gives the coupled HMC model with swelling and dissolution. The swelling influence is linked to the fluid pressure, and the dissolution influence is represented by an independent term. The numerical simulations show that the swelling influence stopped in a limited time scale, while the dissolution influence shows its effect in a long time scale.

Chapter 6 presents the most rigorous derivation of swelling and dissolution in the THMC framework by the Mixture-Coupling Theory. It considers the entropy production due to pore mass becoming bounded mass, as well as the entropy production caused by mineral dissolution. Different from pre chapters and existing research, the transport law for hydraulic, chemical and thermal processes all contain a term that represents the influence of bounded mass.

Chapter 7 gives the conclusion of the thesis and recommendations for future work. This thesis has built a complete framework for swelling and dissolution in THMC coupling research. Throughout the derivations, some assumptions and simplifications are adopted to simplify the discussion, which also opens the door for further research to make different assumptions or explore more complicated cases.

Chapter 2 Literature review

2.1 Porous media

Porous media is a material formed by a solid skeleton with voids or pores which allow fluid to pass through. A typical example of natural porous media is the soil or rock which covers the earth's surface or forms the earth's crust. When the pore space is fully filled with liquid (e.g., water, oil), the media is saturated; when partially filled with liquid and partially filled with gas, it is unsaturated.

In geotechnical engineering, the research on porous media mainly focuses on deformation and mas/energy transport, which have been extensively explored by many researchers for over 100 years. The basic laws describing the deformation and mass/energy transport phenomenon are the Terzaghi effective stress principle, Darcy's Law, Fick's law, and Fourier's Law, as shown in equations (2.1) to (2.4).

1. Terzaghi effective stress principle

$$\boldsymbol{\sigma}' = \boldsymbol{\sigma} - p^w \mathbf{I} \tag{2.1}$$

2. Darcy's Law

$$\mathbf{u} = -\frac{\mathrm{k}}{v}\nabla p \tag{2.2}$$

3. Fick's law

$$\mathbf{J}^c = -D_{diff}\nabla c^c \tag{2.3}$$

4. Fourier's law

$$\mathbf{q}' = -\lambda \nabla T \tag{2.4}$$

where $\boldsymbol{\sigma}$ is the total stress tensor, $\boldsymbol{\sigma}'$ is the effective stress tensor, p^w is the water pressure, $\mathbf{I}$ is the unit tensor, $\mathbf{u}$, $\mathbf{J}^c$, $\mathbf{q}'$ are the water flux, chemical flux and heat flux (flux by conduction) respectively; c^c and T are chemical concentration and

temperature; k is permeability, v is viscosity, λ is thermal conductivity, D_{diff} is the chemical diffusion coefficient.

The four equations describe the stress (mechanical), fluid transport (hydro), chemical diffusion (chemical) and heat conduction (thermal) in porous media, which are the very basic processes considered in multi-physics coupling research. The effective principle is a very simple coupling in a way that the mechanical process is coupled with the hydraulic process through water pressure. Most of the existing THMC coupling equations for porous media can be viewed as a further extension, modification, integration or combination of these four equations. A good understanding of the basic four equations will be helpful to understand the complex coupled equations.

2.2 Interaction between thermal, hydro, mechanical and chemical processes

In the last section and chapter 1, processes affecting geo-engineering are classified into T, H, M and C. Each process has its source and may influence the other processes or be influenced by the other processes. For example, in nuclear waste disposal, the heat may be generated by the radiation of high-level waste, and the high temperature could affect the stress distribution and accelerate the chemical reaction, also, the temperature may be reduced by heat convection through groundwater transport. It is important to identify the detailed factors in each process so that one can evaluate their influence on soil or rock mass and how they affect other processes.

However, due to the extremely complex environment, researchers prefer to primarily focus on some main processes and factors, and some less important ones would be ignored. Some of the major factors in each process and their interactions are shown in Table 2.1

Table 2. 1 THMC factors and interaction (Tsang, 1991, Jing and Feng, 2003, Chen and Brouwers, 2010, Ghirian, 2016, Thomas et al., 2002)

	Mechanical (M)	**Hydraulic (H)**	**Thermal (T)**	**Chemical (C)**
M	Stress, deformation, damage, strength and failure in matrix; initiation, growth, displacement of fractures. Source: in-site stress, gravity, excavation, etc.	Stress-deformation-damage effects on matrix porosity and permeability, and fracture transmissivity and network connectivity (well-defined coupling)	Mechanical work conservation into heat increment. (coupling effect not well defined and usually negligible)	Mechanical alteration to transport path and flow properties by deformation, damage and fracturing.
H	Effective stress of matrix; aperture-pressure-stiffness function of fractures; capillary and swelling pressures-relative saturation. (well-defined coupling models)	Darcian or non-Darcian fluid flow in matrix and fractures. Source: surface water infiltration, groundwater, oil/gas flow in energy reservoirs, hot/cool injection in geothermal energy fields.	Heat convection by fluid velocity field (well-defined coupling models)	Effects on pressure, velocity, saturation and dehydration/rehydration cycles on solid/gas solution, precipitation and solute retardation. (well-defined coupling models in geochemistry, less understood in rock mechanics)
T	Thermal stress and expansion of matrix; closure, opening, damage and/or irreversible deformation of fractures. (well-defined coupling models)	Fluid buoyancy and viscosity change; fluid phase change (evaporation and condensation); thermal diffusion of moisture flow. (well-defined coupling models)	Heat conduction, convection & radiation Sources: radioactive waste decay, geothermal gradient, hot/cool water injection and pumping, cooling by natural gas storage	Temperature effect on reaction rate and chemical stability of minerals, elements (well-defined coupling models in geochemistry, less understood in rock mechanics)
C	Strength and deformability alteration and damage of rock/ soils due to chemical reaction. (coupling mechanism not well understood)	Flow property changes of matrix and fractures due to chemical reaction (by gas solution and exsolution, solid dissolution and precipitation)	Heat release or consumption due to chemical reaction. (well defined coupling models in chemistry, less understood in rock mechanics)	Inter-species reaction, precipitation/dissolution, complexation, advection, dispersion, mineral alteration, diffusion, sorption and decay

2.3 Development of THMC model

The complexity of multiphase fluid and heat flow, geomechanics, geochemical reactions, and the strong non-linearities in the mass and energy conservation equations make it a challenging issue to model the THMC processes within a coupled procedure mathematically (Zhang et al., 2012, Zhang et al., 2016a). Because of the complexity of the interaction between T, H, M, C processes, the development of THMC coupling theories has gone through a long way.

Considering different possibilities of interaction between the four processes, the number of couplings is 11, i.e., TH, TM, TC, HM, HC, MC, THM, THC, HMC, TMC, THMC. To date, all of them have been researched to varying degrees. Looking back at the development history, the research starts from two ways coupling and then extended to three ways coupling and then four ways coupling. This thesis will follow the path of HM, HMC and THMC, thus, the literature review will also focus on HM, HMC and THMC coupling with the same layout.

2.3.1 HM model

The earliest Hydro-Mechanical coupling research is the Terzaghi effective stress principle (von Terzaghi, 1923, Terzaghi, 1943), which describes the influence of water pressure on stress behaviour. It is a simple one-way coupling as no stress influence on the fluid transport is considered, but it is one of the most important theories in soil/rock mechanics. The initial effective stress principle is proposed for one-dimension saturated porous media, it assumes the soil to be homogenous and isotropic, and the solid and fluid to be incompressible. Biot extended Terzaghi's one-dimension theory to a more general three-dimension in which the compressibility of solid and fluid are considered (Biot, 1941). Moreover, the water amount change due to stress response is considered, making it a fully coupled Hydro-Mechanical framework. The model was further

extended to the general anisotropic elastic case (Biot, 1955) and nonlinear elastic case (Biot, 1973).

The general Biot consolidation theory for isotropic linear elastic porous media can be written as a mixed stiffness form (Detournay and Cheng, 1993, Rutqvist and Stephansson, 2003, Merxhani, 2016)

$$\begin{aligned} \sigma_{ij} &= (K - \frac{2G}{3})\varepsilon_{kk}\delta_{ij} + 2G\varepsilon_{ij} - \zeta p^w \delta_{ij} \\ \varsigma &= -\zeta\varepsilon_{ii} + \frac{1}{M} p^w \end{aligned} \tag{2.5}$$

where K is the bulk modulus, G is the shear modulus, ε_{ij} is the strain tensor, ζ is the Biot's coefficient, ς is the increment of water content, M is the Biot's modulus, δ_{ij} is the Kronecker delta. M can be linked to the bulk modulus of the solid grain K_s and the bulk modulus of water K_w; ζ can be linked to the bulk modulus of the solid grain K_s and the bulk modulus of the solid matrix K (Cosenza et al., 2002). These two modulus can be obtained through pressure-volume relationship in compression tests.

$$\frac{1}{M} = \frac{\zeta - \phi}{K_s} + \frac{\phi}{K_w},\ \zeta = 1 - \frac{K}{K_s} \tag{2.6}$$

Equation (2.5) deals with the elastic response and pore fluid in porous media, it has been called the Biot poroelasticity, theory of poroelasticity, or Biot theory.

From equation (2.5), the effective stress now becomes:

$$\sigma'_{ij} = \sigma_{ij} - \zeta p^w \delta_{ij} \tag{2.7}$$

which differs from the Terzaghi effective stress (2.1) in the coefficient ζ. ζ is a coefficient that ranges from 1 to 0, therefore, Terzaghi effective stress is a specific case with ζ being 1.

Then, based on the pioneering work of Terzaghi and Biot, more research work is

furtherly carried out. Verruijt (1969) applied Biot theory to predict aquifer behaviour; Rice and Cleary (1976) redefined the material constant and adopted more familiar parameters from soil and rock mechanics. Some researchers (Morland, 1972, Atkin and Craine, 1976, Bowen, 1980, Bowen, 1982, Katsube and Carroll, 1987, Rajagopal and Tao, 2005) re-examined Biot's theory within the context of mixture theory. Coussy (Coussy, 1995, Coussy, 2004) derived the Biot theory through a thermodynamics approach.

The original Biot theory is for the saturated condition, and the Hydro-Mechanical coupling equations are later developed for more complicated cases to consider the multiphase phase flow. Vaunat et al. (2000) described the retention curve in an encompassing way, covering all the possible soil states in the void ratio-water ratio-suction space. Then they developed an elastoplastic HM model with considering the hysteresis of water storage mechanism and its dependence on the void ratio (Vaunat et al., 2000). Based on the sub-loading plasticity for unsaturated soil and the stress-saturation approach, an advanced H-M model for unsaturated soil with different initial densities is presented (Zhou and Sheng, 2015). Sun and Sun (2012) developed an elastoplastic constitutive model for HM coupling with the degree of saturation and void ratio taken into account. Among them, remarkable work was the constitutive model proposed by Lewis (Lewis and Schrefler, 1998), which is a fully coupled Hydro-mechanical-Gas model and the relevant numerical solution.

The Hydro-Mechanical coupling research is not only for porous media but can be also applied to fractured porous media (Berryman and Wang, 1995, Callari and Federico, 2000, Berryman, 2002, Khalili, 2003, Borja and Koliji, 2009, Boutin and Royer, 2015, Choo et al., 2016, Song et al., 2019). Since this thesis focuses on traditional porous media, no further attention will be paid to these areas.

2.3.2 HMC model

The chemical process is very common in porous media. The major chemical process includes diffusion, dissolution, precipitation, transport, complexation, etc. If dissolution takes place, minerals in the solid particle will be dissolved, resulting in the increment of pore size and further growth of permeability. Precipitation may clog up the fluid path. Other processes all have different influences on the porous media. Because the chemical process is so complicated, research on chemical process coupling still requires much further depth.

The above-mentioned chemical processes may induce significant influence on mechanical process or hydraulic process and in turn, be influenced. The widest noticed interactions between chemical and hydraulic processes are the advection and osmosis phenomenon. The former is the chemical transport with the hydraulic flow and the latter is the fluid flow change due to chemicals.

In porous media, the transport of chemical species is not only controlled by the concentration gradient but also controlled by the fluid flow, therefore the migration of chemical species in porous media is usually described by the Advection-Diffusion-Reaction Equation, which describes the coupling of chemical migration with the hydraulic flow.

$$\frac{\partial c^c}{\partial t} = -\mathbf{v}^w \cdot \nabla c^c + \nabla \cdot (D_{diff} \nabla c^c) + R \tag{2.8}$$

in which R is the source term, representing the change of concentration due to chemical reaction or other source terms.

On the other hand, the presence of chemical species in fluid flow may induce the osmosis phenomenon, which is a result of concentration difference and has been explored by some researchers (Ghassemi and Diek, 2003, Ghassemi et al., 2009, Zheng

et al., 2011, Chen and Hicks, 2013, Chen et al., 2016, Chen et al., 2018, Ma et al., 2022).

Unlike the well-defined interaction between hydraulic and chemical processes, the interaction between mechanical and chemical processes is still at an early age. The mechanical influence on the chemical process is normally considered to be weak. Although the pressure solution, which is the mineral dissolution at stressed contact (Yasuhara et al., 2016), has received some attention (Taron and Elsworth, 2010, Yasuhara et al., 2016, Ogata et al., 2019), very limited research has been conducted to explore the mechanical influence on the chemical process. On the other hand, the chemical influence on the mechanical process is very strong and therefore received wide attention. The presence of chemical species may affect the mechanical behaviour both physically (e.g. swelling, adsorption) and chemically (e.g. dissolution, precipitation). However, the mechanism and results are so complicated that no well-accepted mathematical models have been developed yet. Although the chemical influence is well recognized, the HMC coupling research is not the mainstream. This is because most multiphysics coupling research adopts the mechanics approach (see section 2.5.1), which lacks the ability to build the coupling between mechanical process and chemical process due to the natural gap between geomechanics and geochemistry. This thesis tries to address the swelling and dissolution influence on mechanical behaviour, and a review of current research on swelling and dissolution in the THMC framework can be found in section 2.4.

2.3.3 THMC model

The early THMC coupled model was presented by incorporating chemical reactions into an existing THM model (Thomas et al., 2001, Gens et al., 2002, Thomas et al., 2002). In the presence of temperature, the stress and mass content in equation (2.5) turns into (Ghassemi et al., 2009, Gao et al., 2021)

$$\begin{aligned}\sigma_{ij} &= (K-\frac{2G}{3})\varepsilon_{kk}\delta_{ij}+2G\varepsilon_{ij}-\zeta p^{w}\delta_{ij}-K\alpha_{s}T \\ \varsigma &= -\zeta\varepsilon_{ii}+\frac{1}{M}p^{w}-\left((\zeta-\phi)\alpha_{s}+\phi\alpha_{f}\right)T\end{aligned} \tag{2.9}$$

where α_s is the thermal expansion coefficient of the solid, K is the bulk modulus.

Such a relationship describes the temperature influence on the mechanical and hydraulic field. Moreover, the hydraulic field can be affected by temperature indirectly through the fluid viscosity ν (Zheng et al., 2011)

$$\nu(T) = 0.661(T-229)^{-1.562} \tag{2.10}$$

For the chemical process, the most well-known temperature influence is that the chemical reaction can be accelerated under high temperature, such an interaction is normally presented in the reaction rate, e.g. the source term in equation (2.8). Another interaction is the diffusion coefficient as an equation of temperature, written as (Zheng and Samper, 2008)

$$D_{diff}(T) = D_{diff}(T_0)\frac{T}{T_0}\frac{\nu(T_0)}{\nu(T)} \tag{2.11}$$

However, when it comes to the temperature being affected, things are much simpler. The heat induced by mechanical deformation and chemical reaction is normally ignored. Some researchers adopt the deformation-induced heat as an equation of bulk modulus and thermal expansion coefficient (Tong et al., 2010, Fan et al., 2019). However, for the mechanical stress considered in THMC research, either elastic, plastic or creep, the rate of deformation is slow, and the scale is small, therefore the heat generated is negligible. Although sometimes massive geological movement may release a great amount of heat, THMC applications are normally settled in stable rock formations to avoid being subjected to such mass movement. Like mechanical deformation, the chemical reaction in porous media could generate a very limited amount of heat, which is usually neglected.

The most often considered coupling in the thermal process is the heat advection due to fluid flow. The fluid transport can carry heat to raise or decrease the temperature, therefore, the heat transport in porous media can be described by the heat conduction and advection equation as

$$\frac{\partial}{\partial t}\left\{\left[(1-\phi)\rho_s^s C^s + \phi\rho_f^f C^f\right]T\right\} - \nabla^T \lambda \nabla T + \nabla \cdot C^f T \rho_f^f \mathbf{u} = 0 \qquad (2.12)$$

where ρ_s^s and ρ_f^f are the phase density of solid and fluid, which are the mass of solid (fluid) against the volume of solid (fluid); C^s and C^f are the specific heat capacity of the solid and fluid, ϕ is the porosity.

2.4 Swelling and dissolution in THMC framework

2.4.1 Swelling in THMC framework

The swelling phenomenon in clay or clay-rich rock has attracted the attention of researchers for many years. Lots of experimental works have been done to explore the mechanism or the impact of swelling. These works are normally conducted at the microscale to reveal the swelling mechanism by technology such as X-ray diffraction (Mooney et al., 1952, Norrish, 1954, Brown, 1982, Viani et al., 1983, Fukushima et al., 1988, Zhou, 1995, Drits et al., 1997, Amorim et al., 2007, Chavali et al., 2017), thermo-gravimetric analysis (Shanmugharaj et al., 2006, Diaz-Perez et al., 2007, Zhang et al., 2019), or at the macroscale to explore the impact of swelling, such as swelling pressure (Cuisinier and Masrouri, 2004, Cuisinier and Masrouri, 2005, Zhang et al., 2007, Castellanos et al., 2008, Nowamooz et al., 2009, Weimin et al., 2014, Chen et al., 2017).

The experimental findings greatly contribute to the theoretical and numerical modelling work. Modelling research on swelling is also conducted at the microscale and macroscale. Microscale modelling usually adopts the classical statistical mechanics based on Monte Carlo and the Molecular Dynamics method (Skipper et al., 1995, Karaborni et al., 1996, Shroll and Smith, 1999, Tambach et al., 2004, Anderson et al.,

2010), these modellings show the molecular arrangement during swelling in molecular scale, hence are not practical for engineering applications. Macroscale modellings build the equation with macroscale properties, such as pressure, strain, temperature, and volume fraction, therefore, there are practical for engineering.

Macroscale modelling is generally achieved through micromechanics viewpoint and macromechanics viewpoint (Lewis and Schrefler, 1987). The micromechanics viewpoint, such as the hybrid mixture theory (Murad et al., 1995, Moyne and Murad, 2002, Gray and Miller, 2014) and the double structure theory (Gens and Alonso, 1992, Guimarães et al., 2014), starts at the microscale and arrives at the macroscale formulations, and the macromechanics viewpoint, such as the mixture theory and the Mixture-Coupling Theory, however, directly work on the macroscale and forms the constitutive relations without consideration the scale or effects on the microstructure. Different swelling models within the THMC framework have been developed by these approaches or theories, such as the ones by mixture theory (Loret et al., 2002, Kleinfelter et al., 2007, Chen et al., 2016), the ones by hybrid mixture theory (Bennethum and Cushman, 1996, Murad and Cushman, 2000), or the one by double structure theory (Sánchez et al., 2005). Among them, a noticeable one is the model proposed by Loret (Loret et al., 2002) using mixture theory, which has received wide attention and has been extended to different levels (Lei et al., 2014, Lei et al., 2016).

In terms of the swelling model developed by Mixture-Coupling Theory, Heidug and Wong (1996) firstly developed the saturated HMC model to account for the swelling influence, in which a swelling parameter is introduced to represent the swelling influence on mechanical behaviour. This model has became the foundation of some further research. In Heidug's model, the chemical potential of solute is linked to the solute mass fraction through a logarithmic function, resulting in the difficulty in developing analytical solutions for the stress-strain response (Ghassemi and Diek,

2003). To solve this issue, Ghassemi and Diek (2003) used a linear relationship for chemical potential and mass fraction, which made the constitutive relationship more friendly and received wide acceptance (Roshan and Rahman, 2011, Roshan and Aghighi, 2012, Kivi et al., 2015, Ma et al., 2018, Gao et al., 2021). Ghassemi and co-workers further extended their model to involve thermo process (Ghassemi et al., 2009, Zhou and Ghassemi, 2009), however, they failed to consider the temperature influence on chemical potential, which was later refined by adopting a linear relationship to describe the chemical potential dependency on temperature (Roshan and Oeser, 2012, Gao et al., 2021). While the above researches are for saturated conditions, Chen and co-workers managed to cover the unsaturated case (Chen, 2013, Chen et al., 2016).

All the aforementioned research contributed greatly to the modelling of swelling within the THMC framework, however, they all ignored one point. From the swelling mechanics, some amount of water is bounded in the clay platelet, unlike the free pore fluid, this part of water does not flow. Since it was formerly part of the pore fluid, it must play a role of 'sink term' in the conservation equation of pore fluid. Although the aforementioned research derived the mass density of bounded mass, none of them derived it as the 'sink source' in the fluid transport equation, this is primarily because in the original Heidug's research, the mass density of pore fluid and bounded fluid is not distinguished and the entropy production due to free fluid becoming bounded fluid is not considered.

2.4.2 Dissolution in THMC framework

Dissolution, as an independent process, has been explored extensively for a long time. However, very limited research has been done for dissolution in the THMC framework. Most existing THMC frameworks, when referring to 'reactive', only consider the chemical transport being influenced by mineral dissolution or porosity/permeability alteration but failed to directly link the mechanical-chemical process, like the ones

(Guimaraes et al., 2006, Zheng et al., 2010, Yin et al., 2011, Xiong et al., 2013, Nasir et al., 2014, Bea et al., 2016). The strong influence of chemical dissolution on stress-strain response has been observed in laboratory experiments (Amanullah et al., 1994, Qi et al., 2009, Ciantia et al., 2015, Momeni et al., 2017, Chen et al., 2020, Lin et al., 2020). The stress-strain curve of a dissolved rock sample in an unconfined compression test is much lower compared to the one of an intact sample and the mechanical properties, e.g., Young's modulus significantly decreased.

The mathematical modelling of the Mechanical-Chemical coupling has been explored widely by the mechanics approach. Some research tried to reduce the mechanical properties, e.g. bulk modulus and shear modulus, to represent the chemical dissolution influence (Zhang et al., 2016b), yet how the mechanical properties reduce is not discussed. Based on the principle of damage mechanics, Sun et al. (2020) and Fan et al. (2019) introduced the damage variable to reduce the mechanical properties. Similar research adopting damage mechanics also can be found in Chen et al. (2007), Lyu et al. (2018), Gerard et al. (1998). Unlike the above research, based on experimental results, Hu et al. (2012) and Jia et al. (2017) not only set the mechanical properties, e.g. bulk modulus and shear modulus, as a function of the introduced 'chemical damage variable', but also embedded this variable into the stress-strain relationship. Tao et al. (2019) introduced a strain caused by the dissolution/precipitation from the solid matrix and defined the strain as the percentage of dissolved mineral volume against the total mineral volume. This method is more friendly and applicable in THMC research as the dissolved mineral volume can be estimated through geochemical kinetic modelling. However, he failed to explore deeper on this strain as it was only presented in the porosity change model.

The above works are based on the mechanics approach (see section 2.5.1). As for research by mixture theory or other modifications of mixture theory, Kuhl et al. (2004)

introduced a chemical internal variable to relate chemical reaction and mechanical damage. Gawin (Gawin et al., 2003, Gawin et al., 2008) developed a coupled HMC model to model the calcium leaching in cementitious material, in which the strength properties of chemically degraded material during the reactive transport process are proposed. Coussy (2004) and other researchers (Haxaire and Djeran-Maigre, 2009, Zhang and Zhong, 2017b, Zhang and Zhong, 2018) adopted the thermodynamics consistency way to model the chemical dissolution, in which the thermodynamics variable, reaction extent, was introduced into the stress-strain relationship to describe the strain resulting from chemical dissolution. The variable, reaction extent, is a very important concept in geochemistry and can be easily estimated by geochemical kinetic modelling, making it a good choice for the chemical-mechanical modelling.

2.5 Mechanics approach, mixture theory, Mixture-Coupling Theory

This section introduces the approaches for modelling the multiphysics coupling in porous media. Generally speaking, there are two approaches, the mechanics approach and the mixture theory approach. These two approaches have been adopted by many researchers and generated great outcomings; meanwhile, they are modified or refined to derive new branches or theories, including the Mixture-Coupling Theory adopted in this thesis. Other approaches may exist, but they are either not widely accepted or do not have a significant academic impact, consequently, they are not mentioned here.

2.5.1 Mechanics approach

The mechanics approach is based on the classic consolidation theory of Terzaghi (Terzaghi, 1943) and Biot (Biot, 1962, Biot and Temple, 1972). This approach focuses on the macroscopic process of THMC (e.g., pressure, displacement, concentration, temperature) and directly analyses the stress-strain relationship by continuum mechanics or soil/rock mechanics. This makes it very practical since the equations may be specially developed for the intended specific application, especially when dealing

with physical-physical coupling such as solid-fluid coupling. A lot of research has been done by using this approach including those for saturated HM coupling (Meroi et al., 1995), multiphase flow coupling (Lewis and Schrefler, 1987, Xikui and Zienkiewicz, 1992, Lewis and Schrefler, 1998, Schrefler and Scotta, 2001), THM or THMC coupling (Thomas, 1985, Thomas, 1988, Thomas et al., 1998, Gens et al., 2004, Gens et al., 2005, Seetharam et al., 2007, Zheng and Samper, 2008, Gens et al., 2010, Zheng et al., 2010)

However, such an approach is not based on a systematic theory, therefore, it lacks the self-development capacity to incorporate more processes, such as chemical process or biological process (Laloui et al., 2003). This approach focuses on the macroscopic process of THMC, using macroscopic variables, i.e., pressure/ displacement/temperature/concentration, to build the constitutive relationships without understanding of the microscopic mechanism, making it difficult to couple the chemical process. Therefore, when trying to incorporate chemical processes, it has to borrow equations from geochemistry to form the constitutive relations due to the gap between geochemistry and geomechanics. The resulting constitutive relations are highly semi-empirical and could not explain the inherent coupling mechanism and rely heavily on experiments. The results are often questioned on their accuracy since they are not obtained through rigorous mathematical derivation, and they must be validated and verified against experimental observations.

2.5.2 Mixture theory

Mixture theory is firstly developed by Truesdell (Truesdell, 1957) and extended by Bowen (Bowen, 1976, Bowen, 1980, Bowen, 1982, Bowen, 1984) and further modified by Humphrey and Rajagopal (Humphrey and Rajagopal, 2002, Humphrey and Rajagopal, 2003, Rajagopal, 2007). This approach ‘provides a means for studying the motions of bodies made up of several constituents by generalizing the equations and principles of the mechanics of a single continuum’ (Massoudi, 2003).

The basic assumption in mixture theory is: each point in the domain is regarded to be occupied by the particle belonging to each of the constituents of the mixture in a homogenized sense, and each constituent of the mixture is regarded as a single continuum (Rajagopal, 2007, Siddique et al., 2017). Each constituent of the mixture obeys the balance law of mass, momentum and energy. Moreover, the mixture, as a whole, satisfies the entropy inequality in addition to the balance laws (Miao et al., 1999). Moreover, 'the Mixture theory provides a systematic framework to treat the thermomechanics of interacting continua even when there is interconversion taking place between the constituents' (Rajagopal and Tao, 2005). In this case, the balance law of mass, momentum and energy of one constituent will take into account the contribution of those from other constituents (Rajagopal and Tao, 1995).

Mixture theory has been adopted by many researchers to explore different couplings in porous media. Some researchers re-examined or extended the Biot theory by using the mixture theory, their research shows that the classic Biot theory is a specific case of the equations derived from the Mixture theory (Morland, 1972, Atkin and Craine, 1976, Bowen, 1980, Prévost, 1980, Bowen, 1982, Prevost, 1982, Katsube and Carroll, 1987). The transport laws, e.g. Fick's law, Darcy's law, are also rederived by Mixture theory (Atkin and Craine, 1976, Rajagopal and Tao, 1995). Grasley and Rajagopal (2012) revisited the notion of suction and derived new expressions for total, matric and osmotic suction for unsaturated geomaterials. The new expressions explained the behaviour that is incorrectly explained by the traditional theory (Grasley and Rajagopal, 2012). Some more complicated models considering different coupling were also developed (Hueckel, 1992, Karalis, 1992, Huyghe and Janssen, 1999, Massoudi and Antaki, 2008, Massoudi, 2010, Cui and Fall, 2015, Lu et al., 2017, Akaki and Kimoto, 2020).

'Mixture theory maintains the individuality of the solid and fluid phase and forms the

constitutive equations for each phase separately' (Heidug and Wong, 1996), this makes it very powerful in modelling the coupling between different phases. However, the challenge is that the 'interaction information between the phases is very difficult to obtain, and this lack of information must very often be filled by physical intuition and ad hoc assumptions' (Heidug and Wong, 1996).

2.5.3 Mixture-Coupling Theory

To overcome the challenge in mixture theory, Heidug and Wong (1996) modified mixture theory by adopting Biot's poroelasticity viewing a fluid-infiltrated rock/soil as a single continuum instead of explicitly discriminating between the solid and fluid phase. Such a view enables researchers to 'employ the thermodynamic force-flux couplings, rather than introducing body forces between the constituents in the constituent equilibrium equations (or constituent equations of motion in the general case) as in classic mixture theory' (Ma et al., 2022).

The new theory was called 'modified mixture theory' before and was renamed as 'Mixture-Coupling Theory' by Chen et al. (2016) to address the core of the theory and to distinguish it from other modifications or branches of mixture theory (Chen et al., 2018). 'This approach combines Biot's theory and non-equilibrium thermodynamics. It simplifies the variables of interactions between solids particles which are normally difficult to obtain in geomaterials and enables incorporating the well-developed continuum mechanics for solids deformation' (Ma et al., 2022). As Mixture-Coupling Theory adopts the fundamental principles of non-equilibrium thermodynamics (e.g. entropy), it could build a smooth link between geomechanics and geochemistry (Ma et al., 2020).

Mixture-Coupling Theory was first developed to model the swelling phenomenon in saturated porous media (Heidug and Wong, 1996), and was then refined by Ghassemi

and co-workers (Ghassemi and Diek, 2003, Ghassemi et al., 2009) in terms of the swelling part. The theory was later extended to model the unsaturated porous media (Chen and Hicks, 2011, Chen, 2013). Further on, the thermal and chemical osmosis phenomenon were taken into account (Chen and Hicks, 2013, Chen et al., 2013, Chen et al., 2018). The derivation of the thermal process in some of the above citations is not so rigorous or complete, for example, in Ghassemi et al. (2009), the thermal transport equation only considered the heat conduction, but ignored the heat advection part; in Chen et al. (2013), the free energy balance equation failed to consider the temperature variation. The most rigorous and complete derivation of the thermal process so far is presented by Ma et al. (2022). Apart from porous media, Mixture-Coupling Theory is also applied to dual continuum media (Aghighi et al., 2021)

2.6 Summary

This chapter presents a general introduction to the relevant literature. It first introduces the concept of porous media and the basic processes (mechanical, hydro, chemical and thermal), as well as the basic equations of these processes. These concepts build the foundation of the following coupling research. Later, the couplings between these processes are reviewed including the hydro-mechanical (HM) model, hydro-mechanical-chemical (HMC) model, and thermo-hydro-mechanical-chemical (THMC) model. The basic concepts and governing equations for these couplings are introduced, and the research progress is reviewed, giving the basic framework of the following chapters. As the swelling and dissolution influence is the key research point, the current research progress of swelling and dissolution in the THMC framework is thoroughly reviewed, which shows the drawbacks in current research and proves the need to conduct this thesis. Finally, the approaches used to develop the coupled equations are introduced and compared, demonstrating the advantages of the approach adopted in this thesis.

Chapter 3 Saturated coupled Hydraulic-Mechanical constitutive model with swelling and dissolution

Many contemporary geotechnical engineering applications create a Chemical Disturbed Zone, where chemical reactions occurring at the molecular scale strongly change the engineering properties of rocks/soils (NNL, 2016). Applications include carbon capture and storage, shale gas extraction, acid mine drainage, nuclear waste disposal, hyper alkaline industrial wastes (e.g. steel slags and “red muds” from aluminium extraction), and accidental chemical spills (Moyce et al., 2014, Chen et al., 2015).

Minerals in rocks/soils may dissolve into groundwater until they reach thermodynamic equilibrium (Yadav and Chakrapani, 2006). Most minerals react slowly in groundwater, however, when the pore fluid is replaced by reactive solutions or the life cycle of the engineering application is long enough (e.g. 100 years for nuclear waste disposal), the chemical processes will result in significant changes to the physical properties of the ground (e.g. the porosity, permeability, and strength) (Fredd and Fogler, 1998, Emmanuel and Berkowitz, 2007, Zhao, 2014).

The swelling of rocks/soils is another engineering problem caused by molecular influence. Typically, two major mechanisms of swelling are observed in the clay platelets within a soil/rock, i.e. hydration swelling and osmotic swelling (Chen, 2013). Hydration swelling is the result of exchangeable cations of the dry clay. One to four water layers can be added between clay platelets due to cations hydrate, resulting in the space expansion between clay layers. Osmotic swelling results from the large difference of the ion concentration close to the clay surfaces or in the pore water.

In this chapter, a novel mathematical formulation of the hydro-mechanical coupled

model based on Mixture-Coupling Theory is obtained, and the strong couplings between mineral dissolution and swelling are included. Helmholtz free energy is used to give the relationship between these couplings. The fully coupled formulations, which include dissolving and swelling, are obtained. Finally, the finite element method is used to solve the governing equations for demonstration purpose. The results show that both swelling and dissolving have a significant influence on the stress and strain change of the porous media rock.

The developed model in this chapter is a further extension and modification of the classic Biot's theory to involve swelling and dissolution influence. The saturated HM model developed in this chapter leads to the development of the unsaturated HM model in the next chapter and builds the foundation for the following chapters, including the HMC model in chapter 5 and the THMC model in chapter 6.

3.1 Balance equations and dissipative process

A domain V, which is big enough to include solid and fluid, has been selected within the soil/rock, with the assumption that S is its boundary attached to the solid phase, allowing only movement of fluid across.

3.1.1 Balance equation

(1) Helmholtz free energy change should account for the deformation energy, transport energy and entropy production (Haase, 1990). The balance equation for the saturated condition can be derived as (Chen and Hicks, 2009, Chen, 2013):

$$\frac{D}{Dt}\int_V \psi dV = \int_S \boldsymbol{\sigma}\mathbf{n}\cdot\mathbf{v}^s dS - \int_S \mu^w \mathbf{I}^w \cdot \mathbf{n} dS - \int_S \mu^d \mathbf{I}^d \cdot \mathbf{n} dS - T\int_V \gamma dV \qquad (3.1)$$

in which $\mathbf{I}^w$ and $\mathbf{I}^d$ are the mass flux of water and dissolved chemicals, which can be defined as

$$\mathbf{I}^w = \rho^w\left(\mathbf{v}^w - \mathbf{v}^s\right) \text{ and } \mathbf{I}^d = \rho^d\left(\mathbf{v}^d - \mathbf{v}^s\right) \qquad (3.2)$$

where ρ^w, ρ^d are the mass density of water and dissolved chemical, which are defined relative to the volume of the mixture; $\mathbf{v}^w$, $\mathbf{v}^d$, $\mathbf{v}^s$ are the velocity of water, dissolved chemical and the solid matrix.

Other notations include: ψ is Helmholtz free energy density, $\boldsymbol{\sigma}$ is the Cauchy stress tensor, μ^w is the chemical potential of water, μ^d is the chemical potential of dissolved chemicals, T is temperature, γ is the entropy produced per unit volume.

Let ∂_t be the time derivative and ∇ be the gradient, the material time derivative is

$$\frac{D}{Dt} = \partial_t + \mathbf{v}^s \cdot \nabla \tag{3.3}$$

The derivative version of the balance equation (3.1) for the Helmholtz free energy is expressed as

$$\dot{\psi} + \psi \nabla \cdot \mathbf{v}^s - \nabla \cdot \left(\boldsymbol{\sigma} \mathbf{v}^s\right) + \nabla \cdot \left(\mu^w \mathbf{I}^w\right) + \nabla \cdot \left(\mu^d \mathbf{I}^d\right) = -T\gamma \le 0 \tag{3.4}$$

(2) Balance equation for water mass is

$$\frac{D}{Dt}\left(\int_V \rho^w dV\right) = -\int_S \mathbf{I}^w \cdot \mathbf{n} dS \tag{3.5}$$

The derivative version is

$$\dot{\rho}^w + \rho^w \nabla \cdot \mathbf{v}^s + \nabla \cdot \mathbf{I}^w = 0 \tag{3.6}$$

ρ^w is related to the phase density ρ_f^w through

$$\rho^w = \phi \rho_f^w \tag{3.7}$$

In this thesis, three kinds of densities (mass/heat/entropy density) for the solid-fluid mixture are defined: mixture density, phase density and true density. Let β represent any component (water or chemical species) in the pore fluid, then, the definition of these densities are

1. Mixture density: The mass is relative to the solid-fluid mixture volume.

$$\rho^{\beta} = \frac{Mass\ of\ \ pore\ \ fluid\ component\ \beta}{Volume\ of\ \ the\ mixture} \tag{3.8}$$

2. Phase density: The mass is relative to the solid/fluid volume. It is denoted with the abbreviation of the phase name with 's' for solid phase, and 'f ' for fluid phase. For example, ρ_f^{β} is the phase density of pore fluid component β, which equals the mass of pore fluid component divided by pore fluid volume:

$$\rho_f^{\beta} = \frac{Mass\ of\ \ pore\ \ fluid\ component\ \beta}{Volume\ of\ \ the\ \ pore\ \ fluid} \tag{3.9}$$

3. True density: The mass is relative to the volume of each component. It is denoted with the abbreviation of 't'. When there is only water but no chemical in the pore fluid, the phase density of water becomes the same as the 'true density' or 'intrinsic density'.

The mixture density and true density are widely used in literature, but the phase density is not. The definition of the mixture density is for the cases that a fluid with multi-components or a solid with multi-minerals (not considered in this thesis). The definition of the three densities is not only for mass but also for energy, heat or entropy.

3.1.2 Dissipative progress and saturated Darcy's law

The dissipation mechanism considered is the pore fluid passing through the solid matrix, the corresponding entropy production can be obtained through non-equilibrium thermodynamics (Katchalsky and Curran, 1965)

$$0 \le T\gamma = -\mathbf{I}^{w} \cdot \nabla\mu^{w} - \mathbf{I}^{d} \cdot \nabla\mu^{d} \tag{3.10}$$

If neglect the transport of dissolved chemical/solid, equation (3.10) can be simplified as

$$0 \le T\gamma = -\mathbf{I}^{w} \cdot \nabla\mu^{w} \tag{3.11}$$

The Darcy's Law can be obtained by using the Phenomenological Equation (Chen, 2013)

$$\mathbf{u} = -\frac{\mathrm{k}}{\nu}\nabla p^f \tag{3.12}$$

where $\mathbf{u}$ is the Darcy velocity, k is the permeability, ν is the viscosity of the pore fluid, and p^f is the pore fluid pressure. Note here: The chemical influence on fluid transport (e.g., osmosis) is not considered here to simplify the discussion.

3.2 State equations for swelling and dissolution

There are two types of water in a swelling/dissolving rock; 1) water in the pores which can be described using non-equilibrium thermodynamics, and 2) water in the clay platelets which has a strong feel of intermolecular and surface forces and thermodynamics is not applied (Israelachvili, 1991); The solids can be classed as two types; 1) the solid structure which follows the continuum thermodynamics (mechanics) and 2) the dissolving chemicals follows the intermolecular and surface forces. The dissolving chemicals do not contribute to the strength of the rock and surrounding the wetting place of the pores (Figure 3.1).

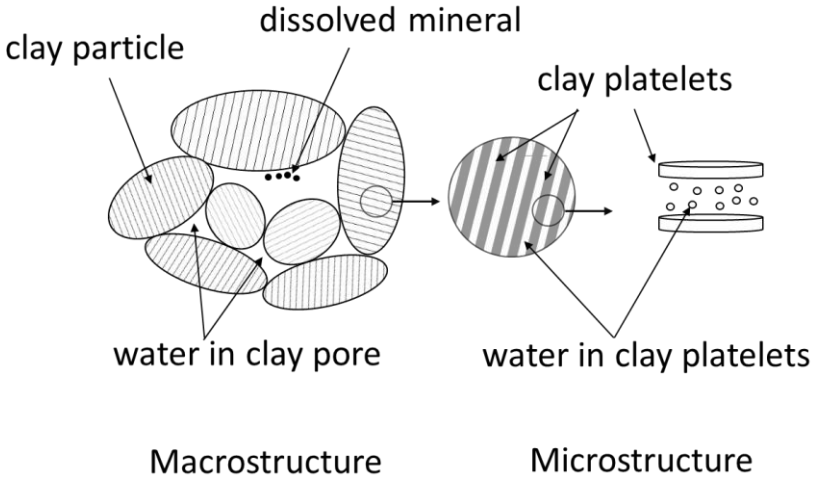

Figure 3. 1 Water types and solid types

3.2.1 Helmholtz free energy of pore space

Take the pore space as the research object, then, based on classical thermodynamics,

the free energy density of pore space can be written as

$$\psi_{pore} = -p^f + \rho_f^w \mu^w + \rho_f^d \mu^d \tag{3.13}$$

where p^f is the pore fluid pressure, ρ_f^w, ρ_f^d are the phase density of pore water and dissolved chemicals.

From equation (3.13), it leads to

$$\dot{\psi}_{pore} = -\dot{p}^f + \dot{\rho}_f^w \mu^w + \rho_f^w \dot{\mu}^w + \dot{\rho}_f^d \mu^d + \rho_f^d \dot{\mu}^d \tag{3.14}$$

According to the Gibbs-Duhem equation in constant temperature, there is

$$\dot{p}^f = \rho_f^w \dot{\mu}^w + \rho_f^d \dot{\mu}^d \tag{3.15}$$

With equation (3.14) and (3.15), there is

$$\dot{\psi}_{pore} = \dot{\rho}_f^w \mu^w + \dot{\rho}_f^d \mu^d \tag{3.16}$$

3.2.2 Basic equation for deformation

It is assumed that the rock maintains mechanical equilibrium so that $\nabla \cdot \boldsymbol{\sigma} = \mathbf{0}$. With the entropy production (3.10), balance equation (3.4) and ignoring the transport flux $\mathbf{I}^d$, the equation for ψ is

$$\dot{\psi} + \psi \nabla \cdot \mathbf{v}^s - \left(\boldsymbol{\sigma} : \nabla \mathbf{v}^s \right) + \mu^w \nabla \cdot \mathbf{I}^w = 0 \tag{3.17}$$

Remark: In the derivation of equation (3.17), the flux $\mathbf{I}^d$ is ignored, which is based on the assumption that the dissolved chemicals do not flow out through the boundary. Equation (3.17) describes the free energy change of the system, including the mechanical energy and the mass energy. Since the dissolved chemicals remain in the system, equation (3.17) contains the water flux $\mathbf{I}^w$ only but excludes dissolved chemical flux $\mathbf{I}^d$. If assuming that the dissolved chemicals could flow out through the boundary, equation (3.17) would include the dissolved chemical flux $\mathbf{I}^d$, as

$$\dot{\psi} + \psi \nabla \cdot \mathbf{v}^s - \left(\boldsymbol{\sigma} : \nabla \mathbf{v}^s \right) + \mu^w \nabla \cdot \mathbf{I}^w + \mu^d \nabla \cdot \mathbf{I}^d = 0 \tag{3.18}$$

Equations (3.17) and (3.18) are the free energy change of the mixture system under different assumptions (dissolved chemicals transport or not transport), using either of them, the final constitutive equation of mechanical behaviour will be the same. This is because the mechanical behaviour depends only on the occurrence of solid mineral dissolution instead of the transport of dissolved species.

To measure the rock's deformation state, classic continuum mechanics has been considered here. First, an arbitrary reference configuration $\mathbf{X}$ is selected, then at the time t the position is $\mathbf{x}$. The expression of Green strain $\mathbf{E}$, the deformation gradient $\mathbf{F}$,

$$\mathbf{F} = \frac{\partial \mathbf{x}}{\partial \mathbf{X}}(\mathbf{X}, t),\ \mathbf{E} = \frac{1}{2}\left(\mathbf{F}^{\mathrm{T}}\mathbf{F} - \mathbf{I}\right), \tag{3.19}$$

The relationship between second Piola-Kirchhoff stress $\mathbf{T}$ and Cauchy stress $\boldsymbol{\sigma}$ is

$$\mathbf{T} = J\mathbf{F}^{-1}\boldsymbol{\sigma}\mathbf{F}^{-T}$$

where J (the Jacobian of $\mathbf{F}$) is

$$J = \frac{dV}{dV_0},\ \dot{J} = Jdiv\nu_s \tag{3.20}$$

From the partial masses equation (3.6) and equation (3.17), the free energy equation (3.17) can be converted to the free energy in the reference configuration as

$$\dot{\Psi} = tr\left(\mathbf{T}\dot{\mathbf{E}}\right) + \mu^w \dot{m}^w \tag{3.21}$$

$$\Psi = J\psi,\ m^w = J\rho^w \tag{3.22}$$

where Ψ is the Helmholtz free energy in the reference configuration, m^w is water mass density in the reference configuration.

3.2.3 Free energy density of the wetted mineral matrix

Because the free energy of the mineral matrix includes the fluid 'bound' between the clay platelets, the free energy can be obtained by subtracting the contribution of the pore fluid $J\phi\psi_{pore}$ from the total free energy of the solid/ fluid system Ψ. The free energy density of the wetted mineral matrix is

$$\left(\Psi - J\phi\psi_{pore}\right)^{\cdot} = tr\left(\mathbf{T}\dot{\mathbf{E}}\right) + \mu^w \dot{m}^w_{bound} + p^f \dot{\upsilon} - \mu^d \dot{m}_{dissolve} \tag{3.23}$$

in which $\upsilon = J\phi$ is denoted as pore volume per unit referential volume. $m^w_{bound} = J\rho^w - J\phi\rho^w_f$ is the mass density of bounded water at the reference configuration, $m_{dissolve}$ is the mass density of dissolved minerals in the reference configuration.

For the reason of convenience, the dual potential can be expressed as

$$W = \left(\Psi - J\phi\psi_{pore}\right) - p^f \upsilon - \mu^w m^w_{bound} + \mu^d m_{dissolve} \tag{3.24}$$

where W can be regarded as a function of $\mathbf{E}$, p^f, μ^w, μ^d, so the expression of $\mathbf{T}$, υ, m^w_{bound}, $m_{dissolve}$ can be given. Equation (3.24) implies the time derivative of $W\left(\mathbf{E}, p^f, \mu^w, \mu^d\right)$ satisfies the relation

$$\dot{W}\left(\mathbf{E}, p^f, \mu^w, \mu^d\right) = tr\left(\mathbf{T}\dot{\mathbf{E}}\right) - \dot{p}^f \upsilon - \dot{\mu}^w m^w_{bound} + \dot{\mu}^d m_{dissolve} \tag{3.25}$$

There must be

$$T_{ij} = \left(\frac{\partial W}{\partial E_{ij}}\right)_{p^f, \mu^w, \mu^d}, \ \upsilon = -\left(\frac{\partial W}{\partial p^f}\right)_{E_{ij}, \mu^w, \mu^d},$$

$$m^w_{bound} = -\left(\frac{\partial W}{\partial \mu^w}\right)_{E_{ij}, p^f, \mu^d}, \ m^d_{dissolve} = -\left(\frac{\partial W}{\partial \mu^d}\right)_{E_{ij}, p^f, \mu^w} \tag{3.26}$$

From equation (3.25), there is

$$\dot{W}(\mathbf{E}, p^f, \mu^w, \mu^d) = \left(\frac{\partial W}{\partial E_{ij}}\right)_{p^f, \mu^w, \mu^d} \dot{E}_{ij} + \left(\frac{\partial W}{\partial p^f}\right)_{E_{ij}, \mu^w, \mu^d} \dot{p}^f + \left(\frac{\partial W}{\partial \mu^w}\right)_{E_{ij}, p^f, \mu^d} \dot{\mu}^w + \left(\frac{\partial W}{\partial \mu^d}\right)_{E_{ij}, p^f, \mu^w} \dot{\mu}^d \tag{3.27}$$

If equation (3.27) is differentiated with respect to time, the fundamental constitutive equations for the evolution of stress, pore volume fraction, the mass densities in the bound water, and the mass density of dissolved chemicals can be obtained.

$$\dot{T}_{ij} = L_{ijkl}\dot{E}_{kl} - M_{ij}\dot{p}^f + S_{ij}\dot{\mu}^w - H_{ij}\dot{\mu}^d \tag{3.28}$$

$$\dot{\upsilon} = M_{ij}\dot{E}_{ij} + Q\dot{p}^{f} + B\dot{\mu}^{w} + B^{d}\dot{\mu}^{d} \tag{3.29}$$

$$\dot{m}^{w}_{bound} = -S_{ij}\dot{E}_{ij} + B\dot{p}^{f} + Z\dot{\mu}^{w} + X\dot{\mu}^{d} \tag{3.30}$$

$$\dot{m}_{dissolve} = H_{ij}\dot{E}_{ij} - B^{d}\dot{p}^{f} - X\dot{\mu}^{w} + Y\dot{\mu}^{d} \tag{3.31}$$

where the parameters L_{ijkl}, M_{ij}, S_{ij}, H_{ij}, B, X, Y, Z, B^{d} are as following group equations

$$\begin{aligned}
L_{ijkl} &= \left(\frac{\partial T_{ij}}{\partial E_{kl}}\right)_{p^{f},\mu^{w},\mu^{d}} = \left(\frac{\partial T_{kl}}{\partial E_{ij}}\right)_{p^{f},\mu^{w},\mu^{d}} \\
M_{ij} &= -\left(\frac{\partial T_{ij}}{\partial p^{f}}\right)_{E_{ij},\mu^{w},\mu^{d}} = \left(\frac{\partial \upsilon}{\partial E_{ij}}\right)_{p^{f},\mu^{w},\mu^{d}} \\
S_{ij} &= \left(\frac{\partial T_{ij}}{\partial \mu^{w}}\right)_{E_{ij},p^{f},\mu^{d}} = -\left(\frac{\partial m_{bound}}{\partial E_{ij}}\right)_{p^{f},\mu^{w},\mu^{d}} \\
H_{ij} &= \left(\frac{\partial T_{ij}}{\partial \mu^{d}}\right)_{E_{ij},p^{f},\mu^{w}} = \left(\frac{\partial m_{dissolve}}{\partial E_{ij}}\right)_{p^{f},\mu^{w},\mu^{d}} \\
Z &= \left(\frac{\partial m_{bound}}{\partial \mu^{w}}\right)_{E_{ij},p^{f},\mu^{d}} \\
B &= \left(\frac{\partial \upsilon}{\partial \mu^{w}}\right)_{E_{ij},p^{f},\mu^{d}} = \left(\frac{\partial m_{bound}}{\partial p^{f}}\right)_{E_{ij},\mu^{w},\mu^{d}} \\
Q &= \left(\frac{\partial \upsilon}{\partial p^{f}}\right)_{E_{ij},\mu^{w},\mu^{d}} \\
Y &= \left(\frac{\partial m_{dissolve}}{\partial \mu^{d}}\right)_{E_{ij},p^{f},\mu^{w}} \\
X &= \left(\frac{\partial m_{bound}}{\partial \mu^{d}}\right)_{E_{ij},p^{f},\mu^{w}} = -\left(\frac{\partial m_{dissolve}}{\partial \mu^{w}}\right)_{E_{ij},p^{f},\mu^{d}} \\
B^{d} &= -\left(\frac{\partial m_{dissolve}}{\partial p^{f}}\right)_{E_{ij},\mu^{w},\mu^{d}} = \left(\frac{\partial m_{bound}}{\partial \mu^{d}}\right)_{E_{ij},p^{f},\mu^{w}}
\end{aligned} \tag{3.32}$$

3.3 Coupled Hydro-Mechanical constitutive equations

3.3.1 Mechanical behaviour

Equations (3.28)-(3.31) give the general coupled equations for mechanical behaviour, water pressure, and chemical potential including non-linear, large deformation, and anisotropic conditions.

As the attention of this thesis is focused on the coupled dissolution and swelling influence, therefore, a few assumptions are made to simplify the discussion.

i) Small strain condition, which leads to the replacement of Green Strain tensor E_{ij} by strain tensor ε_{ij}, and Piola-Kirchhoff stress T_{ij} by Cauchy stress σ_{ij}.

ii) The parameters L_{ijkl}, M_{ij}, S_{ij}, Z, B, Q are material-dependent constants and the material is isotropic, therefore, the tensors M_{ij}, S_{ij} are diagonal and can be written in the below forms:

$$M_{ij} = \zeta\delta_{ij},\ S_{ij} = \omega_s\delta_{ij},\ H_{ij} = \omega_d\delta_{ij} \tag{3.33}$$

iii) The deformation is limited in the elastic region, then the stiffness can be written as a fourth-order isotropic tensor

$$L_{ijkl} = G\left(\delta_{ik}\delta_{jl} + \delta_{il}\delta_{jk}\right) + \left(K - \frac{2G}{3}\right)\delta_{ij}\delta_{kl} \tag{3.34}$$

Here G denotes the rock's shear modulus and K denotes the bulk modulus.

From the above assumptions and simplifications, the governing stress equation (3.28) can be simplified to

$$\dot{\sigma}_{ij} = \left(K - \frac{2G}{3}\right)\dot{\varepsilon}_{kk}\delta_{ij} + 2G\dot{\varepsilon}_{ij} - \zeta\, p^f\delta_{ij} + \omega_s\dot{\mu}^w\delta_{ij} + \omega_d\dot{\mu}^d\delta_{ij} \tag{3.35}$$

where the quantity ζ is related to the bulk modulus K and K_s in a manner from poroelasticity through the equation $\zeta = 1 - \left(K / K_s\right)$, K_s is the bulk modulus of the

solid grains.

By introducing equation (3.15), and assuming that the linear relationship $\dot{\mu}^d = x\dot{\mu}^w$ (note here, this relationship can be further modified), then the stress equation (3.35) can be rewritten as

$$\dot{\sigma}_{ij} = \left(K - \frac{2G}{3} \right) \dot{\varepsilon}_{kk} \delta_{ij} + 2G\dot{\varepsilon}_{ij} - \left(\zeta - \frac{\omega_s}{\rho_f^w + x\rho_f^d} + \frac{x\omega_d}{\rho_f^w + x\rho_f^d} \right) \dot{p}^f \delta_{ij} \qquad (3.36)$$

By assuming mechanical equilibrium condition $\partial\sigma_{ij} / \partial x_j = 0$, and using displacement variables $d_i \left(i = 1,2,3 \right)$ through $\varepsilon_{ij} = \frac{1}{2}\left(d_{i,j} + d_{j,i} \right)$, it leads to

$$G\nabla^2 \mathbf{d} + \left(\frac{G}{1-2\theta} \right) \nabla(\nabla \cdot \mathbf{d}) - \left(\zeta - \frac{\omega_s}{\rho_f^w + x\rho_f^d} + \frac{x\omega_d}{\rho_f^w + x\rho_f^d} \right) \dot{p}^f = 0 \qquad (3.37)$$

where $\mathbf{d}$ is the displacement tensor, θ is Pison's ratio.

Equation (3.37) presents a formula including both the swelling and dissolution influence on the mechanical behaviour.

3.3.2 Fluid-phase

From the fluid partial mass equation (3.6), fluid density relationship (3.7) and Euler identity (3.20), if neglecting the swelling/dissolution influence on pore fluid mass, the conservation equation of pore fluid can be written as

$$\left(\upsilon \rho_f^f \right)^{\cdot} + \nabla \cdot \left(\rho_f^f \mathbf{u} \right) = 0 \qquad (3.38)$$

Expanding the first term in equation (3.38) leads to

$$\dot{\upsilon}\rho_f^f + \upsilon\dot{\rho}_f^f + \nabla \cdot \left(\rho_f^f \mathbf{u} \right) = 0 \qquad (3.39)$$

in which the fluid density change can be written as

$$\dot{\rho}_f^f = \frac{\partial \rho_f^f}{\partial t} = \frac{\partial \rho_f^f}{\partial p^f} \frac{\partial p^f}{\partial t} = \rho_f^f \frac{1}{K_f} \frac{\partial p^f}{\partial t} \qquad (3.40)$$

where $K_f = \rho_f^f \dfrac{\partial p^f}{\partial \rho_f^f}$ is the bulk modulus of the pore fluid.

From the assumptions and simplifications in section 3.3.1, the porosity change equation (3.29) becomes

$$\dot{\upsilon} = \zeta \dot{\varepsilon}_{ii} + Q\dot{p}^f + B\dot{\mu}^w + B^d \dot{\mu}^d \tag{3.41}$$

If neglecting the dissolution influence, with the Gibbs-Duhem equation, the porosity change equation (3.41) can be written as

$$\dot{\upsilon} = \zeta \dot{\varepsilon}_{ii} + \left(Q + \frac{B}{\rho_f^f} \right) \dot{p}^f \tag{3.42}$$

where the coefficients Q and B are

$$Q = \left(1/K_s\right)\left(\zeta - \phi\right) \tag{3.43}$$

$$B = \left(1/K\right)\left(\zeta - 1\right)\omega_s \tag{3.44}$$

Invoking equation (3.42) and (3.40) into (3.39), it leads to

$$\rho_f^f \zeta \dot{\varepsilon}_{ii} + \rho_f^f \left[\left(Q + \frac{B}{\rho_f^f} \right) + \frac{\upsilon}{K_f} \right] \dot{p}^f + \nabla \cdot \left(\rho_f^f \mathbf{u} \right) = 0 \tag{3.45}$$

Neglecting the space variation of fluid density, e.g. $\nabla \rho_f^f = 0$, and with the Darcy velocity (3.12), the final hydraulic equation can be obtained as

$$\zeta \nabla \cdot \dot{\mathbf{d}} + \left[\left(Q + \frac{B}{\rho_f^f} \right) + \frac{\upsilon}{K_f} \right] \dot{p}^f - \frac{k}{\nu} \nabla^2 p^f = 0 \tag{3.46}$$

3.3.3 Equation Validation

The basic Biot consolidation theory has been well-accepted by researchers and engineers. However, the complexity of the swelling and dissolution process, especially when the two processes occur simultaneously, has retarded the experimental work. The lack of experimental data makes it difficult to validate the presented model by experiments.

The coupled equations (3.37) and (3.46) can be validated by comparing with the equations developed by Lewis and Schrefler (1987) through using the mechanics approach. Equation (3.37) and equation (3.46) can be viewed as a further extension of the equations in Lewis and Schrefler (1987) by incorporating the coupled swelling and dissolution term $\frac{\omega_s}{\rho_f^w + x\rho_f^d} + \frac{x\omega_d}{\rho_f^w + x\rho_f^d}$ into the mechanical equation and the $\frac{B}{\rho_f^f}$ term into the hydraulic equation. The classic Biot consideration theory can be viewed as a specific or simplified case of the developed model.

3.4 Numerical simulation

In this section, a simple one-dimension numerical modelling is presented to show the influence of swelling and dissolution in the Bio type equation. The governing equations (3.37) and (3.46) with primary variable $\mathbf{d}$, p^f are implemented by the classic finite element method proposed by Lewis and Schrefler (1987) through using the software COMSOL Multiphysics (Version 5.4). The basic Solid Mechanics and Darcy's Law modulus in COMSOL are used and are extended to incorporate the swelling coefficient and the dissolution coefficient, as well as the coupling of pressure and strain.

3.4.1 conceptual model

3.4.1.1Model geometry and boundary condition

The geometry of the numerical model is presented in Figure 3.2. A one-dimensional rectangle with 0.15m width and 0.3m height is selected to represent a host rock around the nuclear waste disposal. The left boundary A is fixed while the right boundary B is free, and both of them are permeable, allowing fluid to pass through. The upper and lower boundary are on rollers and impermeable. Under the above boundary conditions, the domain could only allow changes in the horizontal direction, therefore, one

observation line (the dotted line in Fig 3.2) lying in the central of the domain is selected to track the change along the horizontal direction.

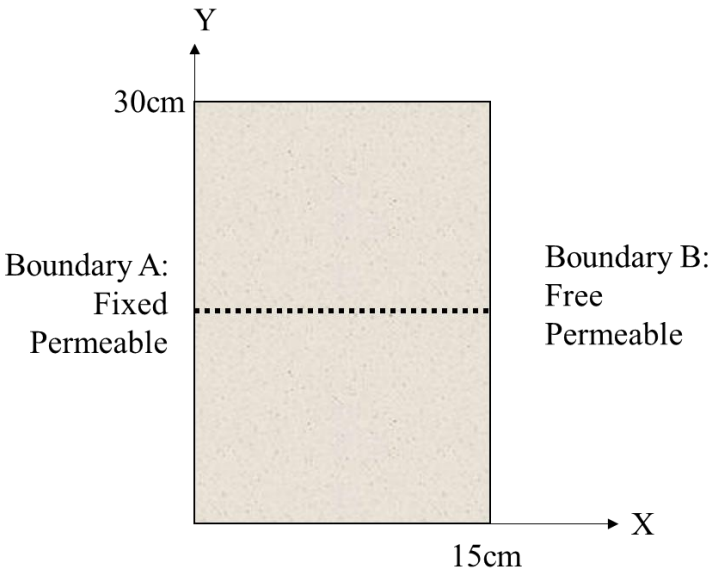

Figure 3.2 Numerical modelling geometry and boundary condition

The sample is assumed to be in mechanical equilibrium and the initial effective stress is zero. The domain initially contains fluid at a pressure of 20MPa and maintains this value at the right boundary. At the beginning, the pressure at the left boundary drops to 4MPa to simulate external disturbance. In such as condition, the fluid will flow from the right toward the left due to the pressure gradient. As the press loses, loading will be beard by the solid matrix, hence, deformation and effective stress/strain generate.

3.4.1.2 Parameters

In the mechanical equation (3.37), the dissolution term can be complex expressions. To simplify the discussion and show the influence of swelling and dissolution, it is assumed that $\mathrm{dv} = \dfrac{x\omega_d}{\rho_f^w + x\rho_f^d} = 0.05$ and $\mathrm{sw} = \dfrac{\omega_s}{\rho_f^w + x\rho_f^d} = 0.2$. The coefficient $\left(Q + \dfrac{B}{\rho_f^f}\right) + \dfrac{\upsilon}{K_f}$ in association with the fluid pressure in equation (3.46) is regarded to

be one term and named as void coefficient $q = \left(Q + \frac{B}{\rho_f^f} \right) + \frac{\upsilon}{K_f}$

Other parameters adopted in the numerical simulation are listed in table 3.1. The material considered is the Tournemire argillite, which contains clay minerals. It is regarded to be traditional porous media without considering the fracture. The mechanical properties, i.e., Young's modulus and Poisson's ratio, as well as the hydraulic permeability are collected from the Tournemire argillite experiments (Rejeb and Cabrera, 2004); the Biot's coefficient is collected from the numerical modelling case for Tournemire argillite (Maßmann et al., 2006); the void coefficient is assumed.

Table 3. 1 Material parameters (Rejeb and Cabrera, 2004, Maßmann et al., 2006)

Parameters	Physical meaning	Values and units
ρ_f^f	Density of water	1000kg/m^3
k / ν	absolute permeability/dynamic viscosity	10^{-19}m/s
E	Young's modulus	9270MPa
θ	Poisson's ratio	0.2
ζ	Biot's coefficient	1
q	Void coefficient	0.0005MPa^{-1}
sw	Swelling parameter	0.2
dv	Dissolution parameter	0.05

3.4.2 Numerical results

The pore fluid pressure change is presented in Figure 3.3. As expected, fluid loses from the left boundary, and the pressure in the domain drops, as time goes by, pressure drops more and will finally reach equilibrium. The pressure distribution for swelling/non-swelling and dissolution/non-dissolution are the same, this is because the porosity change due to dissolution is not considered, and since the Biot coefficient is taken as 1, the porosity change due to swelling is 0, therefore, the transport equation for

swelling/non-swelling and dissolution/non-dissolution cases are the same, and the pressure distribution of them shows no difference.

Figures 3.4 and 3.5 show the horizontal displacement and strain of the domain. As water pressure drops, loading will be beard by the solid matrix, therefore, the domain consolidates. Since the left boundary is fixed but the right boundary is free, the right boundary moves toward the left direction (Figure 3.4). The negative displacement value in Figure 3.4 denotes the moving direction. The associated strain is presented in Figure 3.5. As the swelling or dissolution influence on displacement is associated with the pressure (as shown in equation (3.37)) and the pressure decrease with time (Figure 3.3), the displacement at a longer time (1 year) is larger than the displacement at a shorter time (0.5 years).

Biot theory describes the consolidation process, however, the swelling process would resist the consolidation and dissolution promote consolidation. In Figure 3.4, compared with the non-swelling and non-dissolution case (consolidation process, sw=0, dv=0), the swelling but non-dissolution case (sw=0.2, dv=0) shows a smaller displacement while the dissolution but non-swelling case (sw=0, dv=0.05) holds a greater displacement. Since dissolution and swelling have opposite influence on the consolidation process, the final displacement relies on the combined effect of swelling and dissolution. The corresponding strain is presented in figure 3.5.

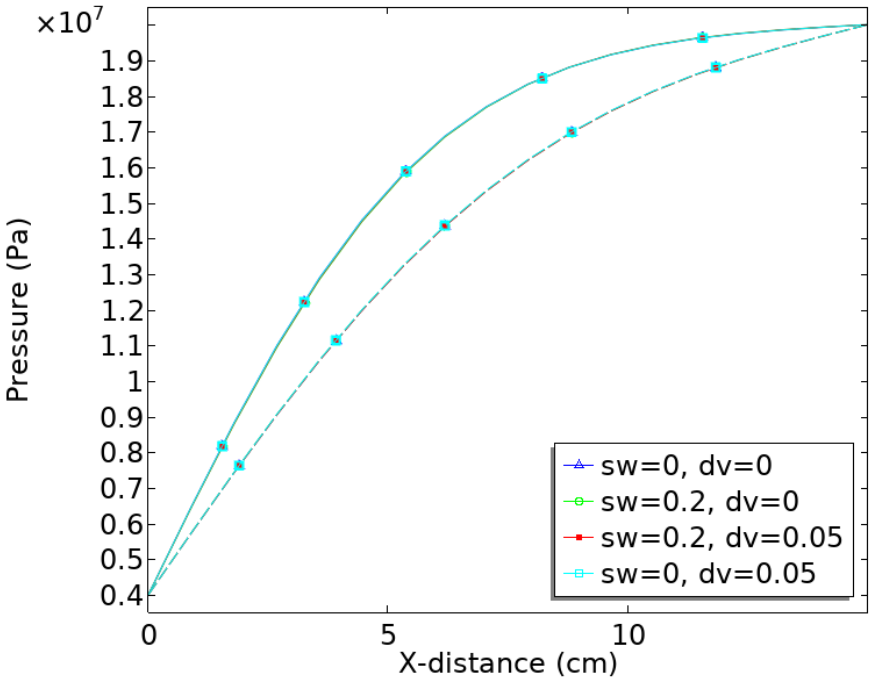

Figure 3. 3 Evolution of pore fluid pressure with time and space (solid line: 0.5 year; dashed line: 1 year)

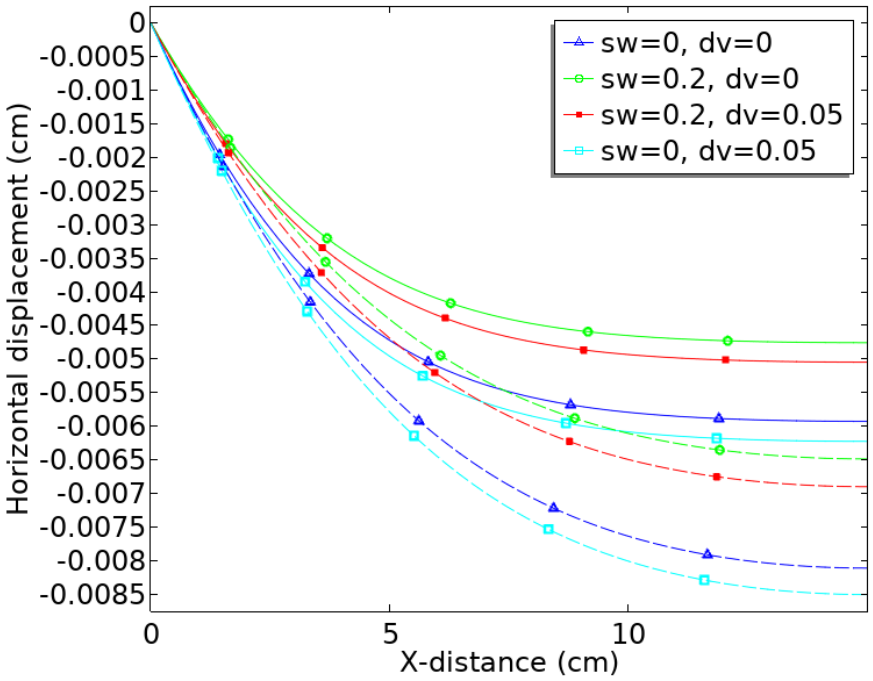

Figure 3. 4 Evolution of horizontal displacement with time and space (solid line: 0.5 year; dashed line: 1 year)

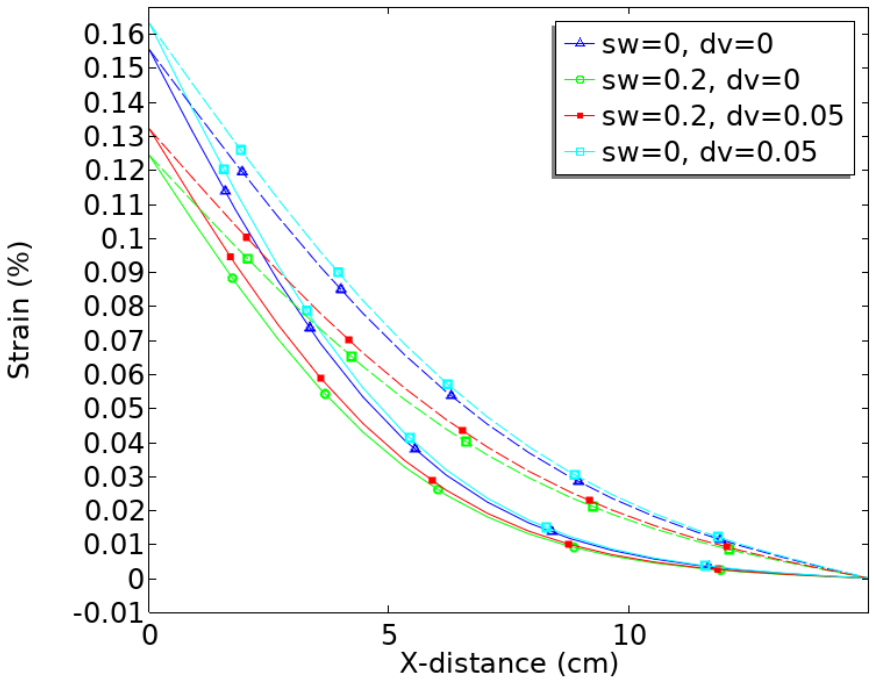

Figure 3. 5 Evolution of strain with time and space (solid line: 0.5 year; dashed line: 1 year)

3.4.3 Sensitivity analysis of swelling/dissolution coefficient

The swelling and dissolution coefficient are two important concepts introduced into the Biot poroelasticity theory, although they have not been determined theoretically or experimentally, their influence on mechanical behaviour can be explored by sensitivity analysis. In this section, the swelling and dissolution coefficients are given with different values, e.g., $sw = 0.1, 0.2, 0.3$ and $dv = 0.05, 0.1, 0.15$, to show their influence.

From the analysis in section 3.4.1, the influence of swelling and dissolution on the hydraulic process is neglected for simplification, hence, only the mechanical results are presented. The swelling influence on displacement and strain are given in Figures 3.6 and 3.7. From the numerical results, the larger the swelling coefficient is, the smaller the displacement/strain will be, showing a greater resistance effect of swelling on consolidation. The opposite trend of dissolution influence is shown in Figures 3.8 and 3.9: the larger the dissolution coefficient is, the greater the displacement/strain will be.

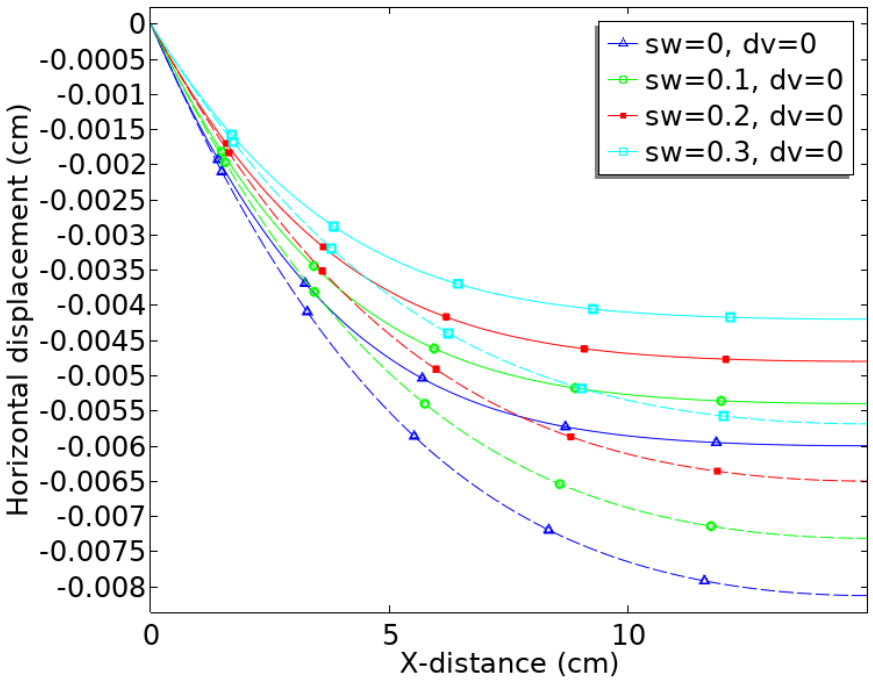

Figure 3. 6 Evolution of horizontal displacement with different swelling coefficients (solid line: 0.5 year; dashed line: 1 year)

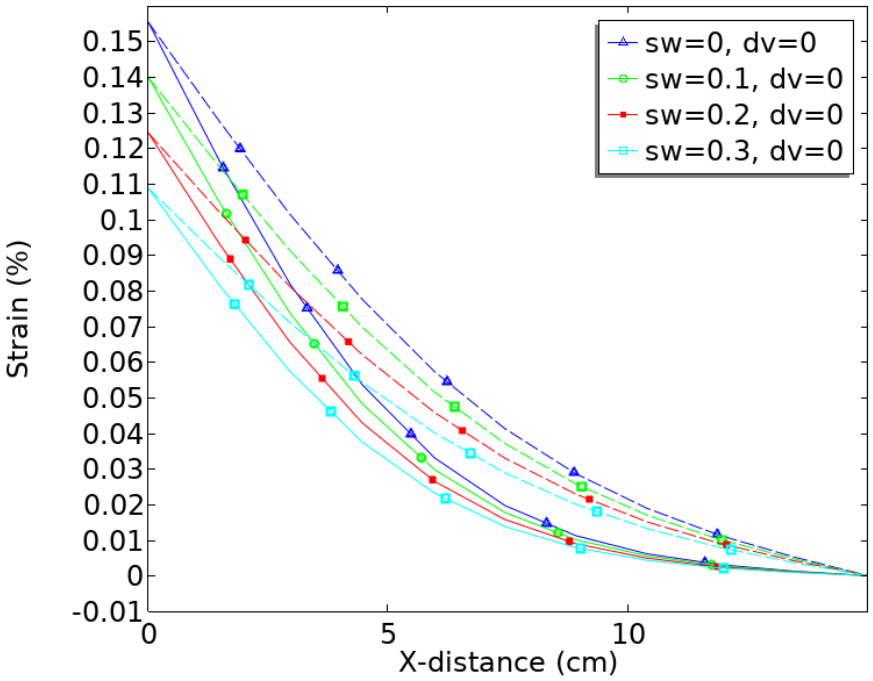

Figure 3. 7 Evolution of horizontal strain with different swelling coefficients (solid line: 0.5 year; dashed line: 1 year)

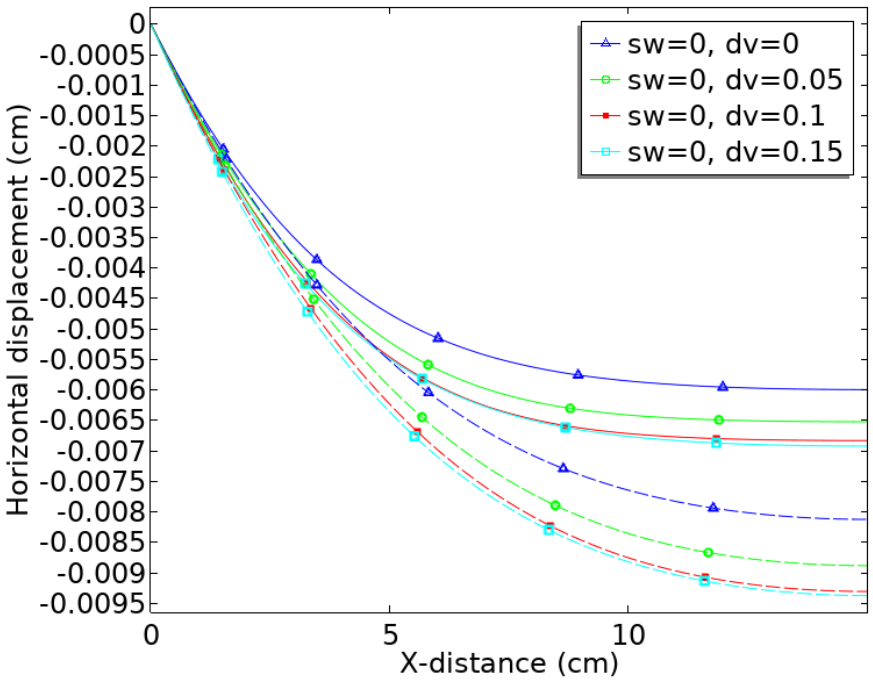

Figure 3. 8 Evolution of horizontal displacement with different dissolution coefficients (solid line: 0.5 year; dashed line: 1 year)

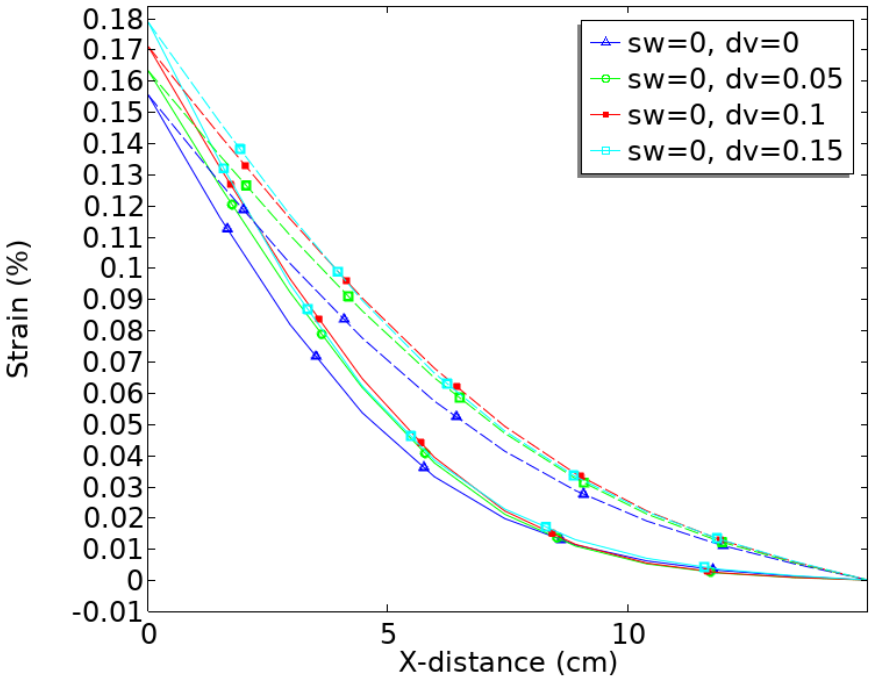

Figure 3. 9 Evolution of horizontal strain with different dissolution coefficients (solid line: 0.5 year; dashed line: 1 year)

3.5 Conclusions and limitations

This chapter developed a Hydro-Mechanical coupled model to consider the swelling and dissolution influence. Two parameters, namely the swelling parameter and the dissolution parameter, are incorporated into the mechanical equation of the Biot poroelasticity equation and are linked to the fluid pressure, and meanwhile, for simplification, the hydraulic equation ignored dissolution influence. The derivation extended the application of the Mixture-Coupling Theory and showed the capacity of Mixture-Coupling Theory to model complex problems in geotechnical engineering.

In the derivation process of equations (3.17) and (3.21), the dissolved chemical/solid flux $\mathbf{I}^d$ is ignored, following an assumption that the dissolved chemical/solid does not flow out the selected region, therefore, the $\mathbf{I}^d$ term in equation (3.4) should also vanishes. If assuming that the dissolved chemical/solid flux $\mathbf{I}^d$ can pass through the boundary, some equations presented before/and equation (3.22) may change, but the wetted matrix free energy equation (3.23) remains the same. This is because the free energy of the wetted matrix relies on the occurrence of dissolution, but not depends on migration of dissolved species. Since the stress-strain response is derived from equation (3.23), the final mechanical equation for the two assumptions is the same. When deriving the hydraulic equation, the influence of dissolution on porosity and the influence of dissolved chemicals on the fluid property are ignored, therefore, the transport equation for the two assumptions is also the same.

In the derivation of the hydraulic equation, the influence of dissolution on porosity and fluid mass is ignored for simplification, and the fluid mass density variation against space is also ignored. If the amount of dissolved species is very limited, such an assumption would be reasonable, but in extreme cases (for example, high acidity solution passing through carbonate rock), these assumptions are worth more notice. In chapter 6, the influence of dissolution on porosity and fluid mass will be considered, in

terms of fluid mass density variation against space, it can be easily considered in the mathematic equation, but its influence is not revealed numerically. Future research can be done to explore the density variation, which is especially useful in large scale engineering applications.

The thermodynamics approach adopts the chemical potential as the variable. Such a variable can represent either the chemical potential of the molecular, ion or cation brought by reactive dissolution, or the chemical potential of the constituent in the fluid which has the same chemical formula as the solid mineral brought by pressure solution, the developed model can be applied to both reactive dissolution and pressure solution.

The developed model can be viewed as an extension case of the classic Biot consolidation equation and the Biot theory is a specific or simplified case of the presented model, showing the correctness of the adopted theory and the power of the theory to deal with complex case.

The numerical simulation compared the mechanical deformation and strain of the swelling/dissolution case to those of the non-swelling/no-dissolution case and showed that the swelling process has a resistance effect on consolidation while dissolution has a promotion effect on consolidation. The simulation also showed that different values of the swelling parameter and dissolution parameter have different impacts on the mechanical behaviour, that is, the displacement/strain becomes smaller with a larger swelling coefficient and greater with a larger dissolution parameter.

The numerical simulation is conducted for up to one year, at this time scale, the pressure has not reached equilibrium yet. On a longer time scale, the pressure will reach equilibrium gradually, and meanwhile, the influence of swelling and dissolution will culminate.

The swelling coefficients and the dissolution coefficients are undetermined yet. It would be not easy to determine them through theoretical derivation, but experimental research can be possible. Potential experiments can be conducted to measure the stress change and pressure evolution subject to swelling/dissolution influence, so that the relevant coefficient can be matched through the stress-pressure relationship curve. Another possible way can also be considered: from equation (3.28) to (3.31), for isotropic material, since $H_{ij} = \omega_d \delta_{ij}$ (see equation (3.33)), the dissolution coefficient links the stress influence on the dissolved mass density, then, experiments can be done to explore the stress change and the dissolved mass density change. Similarly, the swelling coefficient can be explored through the stress influence on the bounded mass density, as presented in equation (3.30).

Chapter 4 Unsaturated coupled Hydraulic-mechanical constitutive model with swelling and dissolution

In this chapter, the Hydro-Mechanical model in chapter 3 is extended to the unsaturated condition. For unsaturated conditions, the free energy balance and mass balance equations are the same as those in chapter 3. The major difference is in the equations associated with hydraulic transport, as the unsaturated case must consider the fluid saturation ratio.

4.1 Balance equations and dissipative process

The same domain V with that in chapter 3 is selected. Since this chapter deals with the unsaturated case, the domain must be big enough to contain solid, water and gas. To simplify the discussion, the air phase is assumed to be continuous with atmospheric pressure $p_{atm} = 0$ (Neuman, 1975, Safai and Pinder, 1979)

4.1.1 Helmholtz Free Energy Density

Helmholtz free energy measures the useful work and is defined as the difference between internal energy and entropy (Haase, 1990). The balance equation for Helmholtz free energy can be derived based on the assumption of ignoring gas transport as (Chen, 2013):

$$\frac{D}{Dt}\int_V \psi dV = \int_S \boldsymbol{\sigma}\mathbf{n}\cdot\mathbf{v}^s dS - \int_S \mu^w \mathbf{I}^w \cdot \mathbf{n} dS - \int_S \mu^d \mathbf{I}^d \cdot \mathbf{n} dS - T\int_V \gamma dV \qquad (4.1)$$

where ψ is Helmholtz free energy density, $\boldsymbol{\sigma}$ is the Cauchy stress tensor, $\mathbf{v}^s$ is the velocity of the solid, μ^w is the chemical potential of water, μ^d is the chemical potential of dissolved chemical species, T is temperature, γ is the entropy production per unit volume, and the time derivative is

$$\frac{D}{Dt} = \partial_t + \mathbf{v}^s \cdot \nabla \tag{4.2}$$

in which ∂_t is the time derivative and ∇ is the gradient.

In equation (4.1), $\mathbf{I}^w$ and $\mathbf{I}^d$ are the mass flux of water and dissolved solid/chemical that can be defined as

$$\mathbf{I}^w = \rho^w \left(\mathbf{v}^w - \mathbf{v}^s \right) \text{ , and } \mathbf{I}^d = \rho^d \left(\mathbf{v}^d - \mathbf{v}^s \right) \tag{4.3}$$

where ρ^w and ρ^d are the mass density of water and dissolved chemical, $\mathbf{v}^w$, $\mathbf{v}^d$ are the velocity of water and dissolved chemical species.

The derivative version of the balance equation (4.1) for the free energy is expressed as

$$\dot{\psi} + \psi \nabla \cdot \mathbf{v}^s - \nabla \cdot \left(\boldsymbol{\sigma} \mathbf{v}^s \right) + \nabla \cdot \left(\mu^w \mathbf{I}^w \right) + \nabla \cdot \left(\mu^d \mathbf{I}^d \right) = -T\gamma \le 0 \tag{4.4}$$

(2) Balance equation for water mass is

$$\frac{D}{Dt} \left(\int_V \rho^w dV \right) = -\int_S \mathbf{I}^w \cdot \mathbf{n} da \tag{4.5}$$

The derivative version is

$$\dot{\rho}^w + \rho^w \nabla \cdot \mathbf{v}^s + \nabla \cdot \mathbf{I}^w = 0 \tag{4.6}$$

The mass density of water ρ^w is defined relative to the volume of the mixture. It is related to the phase density ρ_f^w, which is defined as the mass of water against the volume of fluid, through

$$\rho^w = \phi^f \rho_f^w \tag{4.7}$$

in which ϕ^f is the volume fraction of pore fluid. The relationship between ϕ^f and the porosity of the medium ϕ is

$$\phi^f = S^f \phi \tag{4.8}$$

where S^f is the saturation of the pore fluid.

Equation (4.6) or (4.7) also applies if change the subscribe ‘ w ’ into ‘ f ’ to denote the pore fluid as a whole if the fluid volume changes very limit by dissolution.

4.1.2 Dissipative progress and unsaturated Darcy’s law

The dissipation equation at the solid/fluid boundary can be obtained by using non-equilibrium thermodynamics, and the entropy production is described as (Katachalsky and Curran, 1965)

$$0 \le T\gamma = -\mathbf{I}^w \cdot \nabla \mu^w - \mathbf{I}^d \cdot \nabla \mu^d \tag{4.9}$$

where μ^w and μ^d are the chemical potential of the pore water and dissolved solids, respectively.

If assuming that the dissolved chemical species do not flow out through the boundary, the equation (4.9) becomes

$$0 \le T\gamma = -\mathbf{I}^w \cdot \nabla \mu^w \tag{4.10}$$

Through using Phenomenological Equations for equation (4.10), and the Gibbs-Duhem equation for the pore water giving the relationship between water pressure and water chemical potential, Darcy’s law can be obtained (Chen, 2013)

$$\mathbf{u} = -\frac{\mathrm{k}k_{rf}}{\nu} \nabla p^f \tag{4.11}$$

where $\mathbf{u}$ is the Darcy’s velocity, k is the permeability, k_{rf} is the relative permeability, ν is the viscosity of fluid, and p^f is the pore fluid pressure.

4.2 State equations for swelling and dissolving

4.2.1 Helmholtz free energy of pore space

Based on classical thermodynamics, the Helmholtz free energy density of pore space

ψ_{pore} can be written as

$$\psi_{pore} = -\bar{p} + S^f \rho_f^w \mu^w + S^f \rho_f^d \mu^d \tag{4.12}$$

where $\bar{p}$ is the average pressure in the pore space and the gas pressure has been ignored, ρ_f^w is the phase density of water, ρ_f^d is the phase density of dissolved solid/chemical.

The time derivative of equation (4.12) is

$$\dot{\psi}_{pore} = -\dot{\bar{p}} + \dot{\mu}^w S^f \rho_f^w + \mu^w \left(S^f \rho_f^w\right)^{\cdot} + \dot{\mu}^d S^f \rho_f^d + \mu^d \left(S^f \rho_f^d\right)^{\cdot} \tag{4.13}$$

Using the Gibbs-Duhem equation for the pore fluid, there is

$$\dot{\bar{p}} = S^f \rho_f^w \dot{\mu}^w + S^f \rho_f^d \dot{\mu}^d \tag{4.14}$$

Substituting equation (4.14) into (4.13), the time derivative of Helmholtz free energy can be simplified as

$$\dot{\psi}_{pore} = \mu^w \left(S^f \rho_f^w\right)^{\cdot} + \mu^d \left(S^f \rho_f^d\right)^{\cdot} \tag{4.15}$$

4.2.2 Basic equation for deformation

It is assumed that the rock maintains mechanical equilibrium so that $\nabla \cdot \boldsymbol{\sigma} = \mathbf{0}$. Substituting the entropy production equation (4.9) into the Helmholtz free energy balance equation (4.4) for the mixture and adopting the same assumption as that in section 3.2.2 (ignoring $\mathbf{I}^d$), it leads to

$$\dot{\psi} + \psi \nabla \cdot \mathbf{v}^s - \left(\boldsymbol{\sigma} : \nabla \mathbf{v}^s\right) + \mu^w \nabla \cdot \mathbf{I}^w = 0 \tag{4.16}$$

Equation (4.16) is the free energy at the current configuration. To measure the rock's deformation state, classic continuum mechanics has been considered here: an arbitrary reference configuration $\mathbf{X}$ is selected, then at the time t, the position is $\mathbf{x}$. The expression of Green strain $\mathbf{E}$, the deformation gradient $\mathbf{F}$,

$$\mathbf{F} = \frac{\partial \mathbf{x}}{\partial \mathbf{X}}(\mathbf{X}, t), \ \mathbf{E} = \frac{1}{2}\left(\mathbf{F}^{\mathrm{T}}\mathbf{F} - \mathbf{I}\right), \tag{4.17}$$

where $\mathbf{I}$ is a unit tensor. The relationship between second Piola-Kirchhoff stress $\mathbf{T}$ and Cauchy stress $\boldsymbol{\sigma}$ is

$$\mathbf{T} = J\mathbf{F}^{-1}\boldsymbol{\sigma}\mathbf{F}^{-T}$$

where J (the Jacobian of $\mathbf{F}$) is

$$J = \frac{dV}{dV_0},\ \dot{J} = Jdiv v_s$$

By further consideration partial masses equation (4.6) and (4.16), along with the equation (4.17), it leads to

$$\dot{\Psi} = tr\left(\mathbf{T}\dot{\mathbf{E}}\right) + \mu^w \dot{m}^w \tag{4.18}$$

$$\Psi = J\psi,\ m^w = J\rho = JS^f \phi \rho_f^w \tag{4.19}$$

4.2.3 Free energy density of the wetted mineral matrix

The free energy of the mineral matrix includes the fluid 'bounded' between clay platelet but excludes the solid minerals dissolved into the pore space. It can be obtained by subtracting the free energy of the pore space from the total free energy of the rock/ fluid mixture. Therefore, the free energy density of the wetted mineral matrix in the reference configuration is

$$\left(\Psi - J\phi\psi_{pore}\right)^{\cdot} = tr\left(\mathbf{T}\dot{\mathbf{E}}\right) + \mu^w \dot{m}_{bound} + \bar{p}\dot{\upsilon} - \mu^d \dot{m}_{dissolve} \tag{4.20}$$

where $\upsilon = J\phi$ is denoted as pore volume per unit referential volume and $m_{dissolve} = JS^f \phi \rho_f^d$ is the mass of dissolved species per unit referential volume

For the reason of convenience, the dual potential can be expressed as

$$W = \left(\Psi - J\phi\psi_{pore}\right) - \bar{p}\upsilon - \mu^w m_{bound} + \mu^d m_{dissolve} \tag{4.21}$$

where W is a function of $\mathbf{E}$, $\bar{p}$, μ^w, μ^d, so the expression of $\mathbf{T}, \upsilon$, m_{bound}, $m_{dissolve}$ can be given. Equation (4.21) implies the time derivative of $W\left(\mathbf{E}, \bar{p}, \mu^w, \mu^d\right)$ satisfies the relation

$$\dot{W}\left(\mathbf{E}, \bar{p}, \mu^w, \mu^d\right)^{\cdot} = tr\left(\mathbf{T}\dot{\mathbf{E}}\right) - \dot{\bar{p}}\upsilon - \dot{\mu}^w m_{bound} + \dot{\mu}^d m_{dissolve} \tag{4.22}$$

From which there must be

$$T_{ij}=\left(\frac{\partial W}{\partial E_{ij}}\right)_{\bar{p},\mu^w,\mu^d},\ \upsilon=-\left(\frac{\partial W}{\partial \bar{p}}\right)_{E_{ij},\mu^w,\mu^d},\ m_{bound}=-\left(\frac{\partial W}{\partial \mu}\right)_{E_{ij},\bar{p},\mu^d},m_{dissolve}=\left(\frac{\partial W}{\partial \mu^d}\right)_{E_{ij},\bar{p},\mu^w} \tag{4.23}$$

Then, equation (4.22) can be written as

$$\dot{W}(\mathbf{E},\bar{p},\mu^w,\mu^d)=\left(\frac{\partial W}{\partial E_{ij}}\right)_{\bar{p},\mu^w,\mu^d}\dot{E}_{ij}+\left(\frac{\partial W}{\partial \bar{p}}\right)_{E_{ij},\mu^w,\mu^d}\dot{\bar{p}}+\left(\frac{\partial W}{\partial \mu^w}\right)_{E_{ij},\bar{p},\mu^d}\dot{\mu}^w+\left(\frac{\partial W}{\partial \mu^d}\right)_{E_{ij},\bar{p},\mu^w}\dot{\mu}^d \tag{4.24}$$

If equation (4.23) is differentiated with respect to time, and by substituting equation (4.24) into the time derivative of equation (4.23), for the stress T_{ij}, there is

$$\dot{T}_{ij}=\frac{\partial T_{ij}}{\partial t}=\frac{\partial}{\partial t}\left(\frac{\partial W}{\partial E_{ij}}\right)_{\bar{p},\mu^w,\mu^d}=\left(\frac{\partial}{\partial E_{ij}}\left(\frac{\partial W}{\partial t}\right)\right)_{\bar{p},\mu^w,\mu^d}=\left(\frac{\partial \dot{W}}{\partial E_{ij}}\right)_{\bar{p},\mu^w,\mu^d} \tag{4.25}$$

Substituting Equation (4.24) into equation (4.25) leads to the constitutive equation for stress with associate variables E_{ij}, $\bar{p}$, μ^w, μ^d:

$$\begin{aligned}
\dot{T}_{ij}&=\left(\frac{\partial}{\partial E_{ij}}\left(\left(\frac{\partial W}{\partial E_{ij}}\right)_{\bar{p},\mu^w,\mu^d}\dot{E}_{ij}+\left(\frac{\partial W}{\partial \bar{p}}\right)_{E_{ij},\mu^w,\mu^d}\dot{\bar{p}}+\left(\frac{\partial W}{\partial \mu^w}\right)_{E_{ij},\bar{p},\mu^d}\dot{\mu}+\left(\frac{\partial W}{\partial \mu^d}\right)_{E_{ij},\bar{p},\mu^w}\dot{\mu}^d\right)\right)_{\bar{p},\mu,\mu^d}\\
&=\left(\frac{\partial}{\partial E_{ij}}\left(\frac{\partial W}{\partial E_{ij}}\right)_{\bar{p},\mu^w,\mu^d}\right)_{\bar{p},\mu^w,\mu^d}\dot{E}_{ij}+\left(\frac{\partial}{\partial E_{ij}}\left(\frac{\partial W}{\partial \bar{p}}\right)_{E_{ij},\mu^w,\mu^d}\right)_{\bar{p},\mu^w,\mu^d}\dot{\bar{p}}\\
&+\left(\frac{\partial}{\partial E_{ij}}\left(\frac{\partial W}{\partial \mu^w}\right)_{E_{ij},\bar{p},\mu^d}\right)_{\bar{p},\mu^w,\mu^d}\dot{\mu}+\left(\frac{\partial}{\partial E_{ij}}\left(\frac{\partial W}{\partial \mu^d}\right)_{E_{ij},\bar{p},\mu^w}\right)_{\bar{p},\mu^w,\mu^d}\dot{\mu}^d\\
&=\left(\frac{\partial^2 W}{\partial E_{ij}\partial E_{kl}}\right)_{\bar{p},\mu^w,\mu^d}\dot{E}_{ij}+\left(\frac{\partial^2 W}{\partial \bar{p}\partial E_{ij}}\right)_{\mu^w,\mu^d}\dot{\bar{p}}+\left(\frac{\partial^2 W}{\partial \mu^w\partial E_{ij}}\right)_{\bar{p},\mu^d}\dot{\mu}+\left(\frac{\partial^2 W}{\partial \mu^d\partial E_{ij}}\right)_{\bar{p},\mu^w}\dot{\mu}^d\\
&=\left(\frac{\partial T_{ij}}{\partial E_{kl}}\right)_{\bar{p},\mu^w,\mu^d}\dot{E}_{ij}-\left(\frac{\partial \upsilon}{\partial E_{ij}}\right)_{\bar{p},\mu^w,\mu^d}\dot{\bar{p}}-\left(\frac{\partial m_{bound}}{\partial E_{ij}}\right)_{\bar{p},\mu^w,\mu^d}\dot{\mu}+\left(\frac{\partial m_{dissolve}}{\partial E_{ij}}\right)_{\bar{p},\mu^w,\mu^d}\dot{\mu}^d
\end{aligned} \tag{4.26}$$

Similarly, the evolution of pore fraction, bounded water and dissolved chemicals can be obtained as:

$$\dot{\upsilon} = -\left(\frac{\partial}{\partial \overline{p}} \left(\left(\frac{\partial W}{\partial E_{ij}} \right)_{\overline{p},\mu^w,\mu^d} \dot{E}_{ij} + \left(\frac{\partial W}{\partial \overline{p}} \right)_{E_{ij},\mu^w,\mu^d} \dot{\overline{p}} + \left(\frac{\partial W}{\partial \mu}^w \right)_{E_{ij},\overline{p},\mu^d} \dot{\mu}^w + \left(\frac{\partial W}{\partial \mu^d} \right)_{E_{ij},\overline{p},\mu^w} \dot{\mu}^d \right) \right)_{E_{ij},\mu,\mu^d}$$

$$= -\left(\frac{\partial^2 W}{\partial E_{ij} \partial \overline{p}} \right)_{\mu^w,\mu^d} \dot{E}_{ij} - \left(\frac{\partial^2 W}{\partial \overline{p} \partial \overline{p}} \right)_{E_{ij},\mu^w,\mu^d} \dot{\overline{p}} - \left(\frac{\partial^2 W}{\partial \mu^w \partial \overline{p}} \right)_{E_{ij},\mu^d} \dot{\mu}^w - \left(\frac{\partial^2 W}{\partial \mu^d \partial \overline{p}} \right)_{E_{ij},\mu^w} \dot{\mu}^d$$

$$= -\left(\frac{\partial T_{ij}}{\partial \overline{p}} \right)_{E_{ij},\mu^w,\mu^d} \dot{E}_{ij} + \left(\frac{\partial \upsilon}{\partial \overline{p}} \right)_{E_{ij},\mu^w,\mu^d} \dot{\overline{p}} + \left(\frac{\partial m_{bound}}{\partial \overline{p}} \right)_{E_{ij},\mu^w,\mu^d} \dot{\mu} - \left(\frac{\partial m_{dissolve}}{\partial \overline{p}} \right)_{E_{ij},\mu^w,\mu^d} \dot{\mu}^d$$

(4.27)

$$\dot{m}_{bound} = -\left(\frac{\partial^2 W}{\partial E_{ij} \partial \mu^w} \right)_{\overline{p},\mu^d} \dot{E}_{ij} - \left(\frac{\partial^2 W}{\partial \overline{p} \partial \mu^w} \right)_{E_{ij},\mu^d} \dot{\overline{p}} - \left(\frac{\partial^2 W}{\partial \mu^w \partial \mu^w} \right)_{E_{ij},\overline{p},\mu^d} \dot{\mu}^w - \left(\frac{\partial^2 W}{\partial \mu^d \partial \mu^w} \right)_{E_{ij},\overline{p}} \dot{\mu}^d$$

$$= -\left(\frac{\partial T_{ij}}{\partial \mu^w} \right)_{E_{ij},\overline{p},\mu^d} \dot{E}_{ij} + \left(\frac{\partial \upsilon}{\partial \mu^w} \right)_{E_{ij},\overline{p},\mu^d} \dot{\overline{p}} + \left(\frac{\partial m_{bound}}{\partial \mu^w} \right)_{E_{ij},\overline{p},\mu^d} \dot{\mu}^w - \left(\frac{\partial m_{dissolve}}{\partial \mu^w} \right)_{E_{ij},\overline{p},\mu^d} \dot{\mu}^d$$

(4.28)

$$\dot{m}_{dissolve} = \left(\frac{\partial^2 W}{\partial E_{ij} \partial \mu^d} \right)_{\overline{p},\mu^w} \dot{E}_{ij} + \left(\frac{\partial^2 W}{\partial \overline{p} \partial \mu^d} \right)_{E_{ij},\mu^w} \dot{\overline{p}} + \left(\frac{\partial^2 W}{\partial \mu^w \partial \mu^d} \right)_{E_{ij},\overline{p}} \dot{\mu}^w + \left(\frac{\partial^2 W}{\partial \mu^d \partial \mu^d} \right)_{E_{ij},\overline{p},\mu^w} \dot{\mu}^d$$

$$= \left(\frac{\partial T_{ij}}{\partial \mu^d} \right)_{E_{ij},\overline{p},\mu^w} \dot{E}_{ij} - \left(\frac{\partial \upsilon}{\partial \mu^d} \right)_{E_{ij},\overline{p},\mu^w} \dot{\overline{p}} - \left(\frac{\partial m_{bound}}{\partial \mu^d} \right)_{E_{ij},\overline{p},\mu^w} \dot{\mu} + \left(\frac{\partial m_{dissolve}}{\partial \mu^d} \right)_{E_{ij},\overline{p},\mu^w} \dot{\mu}^d$$

(4.29)

Equation (4.26)-(4.29) can be written as

$$\dot{T}_{ij} = L_{ijkl} \dot{E}_{kl} - M_{ij} \dot{\overline{p}} + S_{ij} \dot{\mu}^w - H_{ij} \dot{\mu}^d \tag{4.30}$$

$$\dot{\upsilon} = M_{ij} \dot{E}_{ij} + Q \dot{\overline{p}} + B \dot{\mu}^w + B^d \dot{\mu}^d \tag{4.31}$$

$$\dot{m}_{bound} = -S_{ij} \dot{E}_{ij} + B \ \dot{\overline{p}} + Z \dot{\mu}^w + X \ \dot{\mu}^d \tag{4.32}$$

$$\dot{m}_{dissolve} = H_{ij} \dot{E}_{ij} - B^s \dot{\overline{p}} - X \dot{\mu}^w + Y \dot{\mu}^d \tag{4.33}$$

where the parameters L_{ijkl}, M_{ij}, S_{ij}, H_{ij}, B, X, Y, Z, B^d are as following group equations

$$L_{ijkl} = \left(\frac{\partial T_{ij}}{\partial E_{kl}} \right)_{\overline{p},\mu^w,\mu^d} = \left(\frac{\partial T_{kl}}{\partial E_{ij}} \right)_{\overline{p},\mu^w,\mu^d}$$

$$M_{ij} = -\left(\frac{\partial T_{ij}}{\partial \bar{p}}\right)_{E_{ij},\mu^w,\mu^d} = \left(\frac{\partial \upsilon}{\partial E_{ij}}\right)_{\bar{p},\mu^w,\mu^d}$$

$$S_{ij} = \left(\frac{\partial T_{ij}}{\partial \mu^w}\right)_{E_{ij},\bar{p},\mu^d} = -\left(\frac{\partial m_{bound}}{\partial E_{ij}}\right)_{\bar{p},\mu^w,\mu^d}$$

$$H_{ij} = \left(\frac{\partial T_{ij}}{\partial \mu^d}\right)_{E_{ij},\bar{p},\mu^w} = \left(\frac{\partial m_{dissolve}}{\partial E_{ij}}\right)_{\bar{p},\mu^w,\mu^d} \tag{4.34}$$

$$Z = \left(\frac{\partial m_{bound}}{\partial \mu^w}\right)_{E_{ij},\bar{p},\mu^d}$$

$$B = \left(\frac{\partial \upsilon}{\partial \mu^w}\right)_{E_{ij},\bar{p},\mu^d} = \left(\frac{\partial m_{bound}}{\partial \bar{p}}\right)_{E_{ij},\mu^w,\mu^d}$$

$$Q = \left(\frac{\partial \upsilon}{\partial \bar{p}}\right)_{E_{ij},\mu^w,\mu^d}$$

$$Y = \left(\frac{\partial m_{dissolve}}{\partial \mu^d}\right)_{E_{ij},\bar{p},\mu^w}$$

$$X = \left(\frac{\partial m_{bound}}{\partial \mu^d}\right)_{E_{ij},\bar{p},\mu^w} = -\left(\frac{\partial m_{dissolve}}{\partial \mu^w}\right)_{E_{ij},\bar{p},\mu^d}$$

$$B^d = -\left(\frac{\partial m_{dissolve}}{\partial \bar{p}}\right)_{E_{ij},\mu^w,\mu^d} = \left(\frac{\partial m_{bound}}{\partial \mu^d}\right)_{E_{ij},\bar{p},\mu^w}$$

Equations (4.30)-(4.33) give the general coupled equation for the mechanical behaviour, pore volume fraction, the mass density of bounded fluids and the mass density of the dissolved minerals. As the attention of this thesis is focused on the coupled dissolution and swelling influence for unsaturated swelling soil/rock, a few assumptions are made including

(i) Small strain assumption. This leads to the replacement of Green Strain tensor E_{ij} by strain tensor ε_{ij}, and Piola-Kirchhoff stress T_{ij} by Cauchy stress σ_{ij}.

(ii) Materials parameters assumption. The parameters L_{ijkl}, M_{ij}, S_{ij}, Z, B, Q, X, Y are material-dependent constants and the material is isotropic, therefore, the tensors M_{ij}, S_{ij}, H_{ij} are diagonal and can be written in the forms of scalars ζ, ω_s, ω_d as

$$M_{ij} = \zeta\delta_{ij},\ S_{ij} = \omega_s\delta_{ij},\ H_{ij} = \omega_d\delta_{ij} \tag{4.35}$$

(iii) Based on the assumption ii), the elastic stiffness L_{ijkl} can be a fourth-order isotropic tensor

$$L_{ijkl} = G\left(\delta_{ik}\delta_{jl} + \delta_{il}\delta_{jk}\right) + \left(K - \frac{2G}{3}\right)\delta_{ij}\delta_{kl} \tag{4.36}$$

where G is the rock's shear modulus and K is the bulk modulus.

4.3 Coupled Hydro-Mechanical constitutive equations

4.3.1 Mechanical behaviour

Based on the material parameters simplification from i-iii in the last section, the governing stress equation (4.30) can be simplified to

$$\dot{\sigma}_{ij} = \left(K - \frac{2G}{3}\right)\dot{\varepsilon}_{kk}\delta_{ij} + 2G\dot{\varepsilon}_{ij} - \zeta\dot{\bar{p}}\delta_{ij} + \omega_s\dot{\mu}^w\delta_{ij} - \omega_d\dot{\mu}^d\delta_{ij} \tag{4.37}$$

where ζ is the Biot coefficient, which is related to the bulk modulus of the matrix K and the bulk modulus of the grain K_s through $\zeta = 1 - \left(K / K_s\right)$.

By introducing equation (4.14) into (4.37), and assuming the linear relationship $\dot{\mu}^d = x\dot{\mu}^w$, then the stress equation (4.37) can be rewritten as

$$\dot{\sigma}_{ij} = \left(K - \frac{2G}{3}\right)\dot{\varepsilon}_{kk}\delta_{ij} + 2G\dot{\varepsilon}_{ij} - \left(\zeta - \frac{\omega_s}{S^f\left(\rho_f^w + x\rho_f^d\right)} + \frac{x\omega_d}{S^f\left(\rho_f^w + x\rho_f^d\right)}\right)\dot{\bar{p}}\delta_{ij} \tag{4.38}$$

Under mechanical equilibrium condition, $\partial\sigma_{ij}/\partial x_j = 0$, and using displacement variables $d_i\,(i=1,2,3)$ through $\varepsilon_{ij} = \frac{1}{2}\left(d_{i,j} + d_{j,i}\right)$, it leads to

$$G\nabla^2\mathbf{d} + \left(\frac{G}{1-2\theta}\right)\nabla(\nabla\cdot\mathbf{d}) - \left(\zeta - \frac{\omega_s}{S^f\left(\rho_f^w + x\rho_f^d\right)} + \frac{x\omega_d}{S^f\left(\rho_f^w + x\rho_f^d\right)}\right)\nabla\dot{\bar{p}} = 0 \quad (4.39)$$

where $\mathbf{d}$ is the displacement tensor, θ is Poisson's ratio.

Since the average pressure $\bar{p}$ can be interpreted as a function of pore fluid pressure and saturation, i.e., $\bar{p} = S^f p^f$ (Li and Zienkiewicz, 1992) and its time derivative is

$$\dot{\bar{p}} = S^f\frac{\partial p^f}{\partial t} + \frac{C_s}{\phi}p^f\frac{\partial p^f}{\partial t} = \left(S^f + \frac{C_s}{\phi}p^f\right)\frac{\partial p^f}{\partial t} \quad (4.40)$$

where $C_s = \phi\frac{\partial S^f}{\partial p^f}$ in the specific moisture content which is defined in terms of pressure.

By introducing equation (4.40), equation (4.39) can be rewritten as

$$\begin{aligned} &G\nabla^2\mathbf{d} + \left(\frac{G}{1-2\theta}\right)\nabla(\nabla\cdot\mathbf{d}) \\ &-\left(\zeta - \frac{\omega_s}{S^f\left(\rho_f^w + x\rho_f^d\right)} + \frac{x\omega_d}{S^f\left(\rho_f^w + x\rho_f^d\right)}\right)\nabla\left[\left(S^f + \frac{C_s}{\phi}p^f\right)\dot{p}^f\right] = 0 \end{aligned} \quad (4.41)$$

Equation (4.41) presents a formula including both the swelling and dissolution influence on the mechanical behaviour in the unsaturated case.

4.3.2 Fluid-phase

From the mass balance equation (4.6), density equation (4.7) and Euler identity, the conservation equation of pore fluid is (neglecting the pore fluid mass change due to swelling and dissolution)

$$\left(S^f\upsilon\rho_f^f\right)^{\cdot} + \nabla\cdot\left(\rho_f^f\mathbf{u}\right) = 0 \quad (4.42)$$

From equation (4.42), (4.11) and the porosity change equation (as given in chapter 3),

it leads to

$$\begin{aligned} & S^f \rho_f^f \zeta \nabla \cdot \dot{\mathbf{d}} + S^f \rho_f^f \left(Q + B / \rho_f^f \right) \dot{\bar{p}} \\ & + \phi \rho_f^f \frac{\partial S^f}{\partial t} + \phi S^f \frac{\partial \rho_f^f}{\partial t} + \rho_f^f \left[-\mathrm{k} \frac{k_{rf}}{\nu} \nabla^2 p^f \right] = 0 \end{aligned} \tag{4.43}$$

where Q is the void compressibility, relating to the scalar ζ through $Q = \left(1/K_s\right)/\left(\zeta - \phi\right)$, $B = 1/K\left(\zeta - 1\right)\omega_s$.

Considering the rate of change of saturation function and the rate of change of water density function

$$\phi \frac{\partial S^f}{\partial t} + \frac{\phi S^f}{\rho_f^f} \frac{\partial \rho_f^f}{\partial t} = C_S \frac{\partial p^f}{\partial t} + \phi \frac{S^f}{K_f} \frac{\partial p^f}{\partial t} = \left(C_S + \phi \frac{S^f}{K_f} \right) \frac{\partial p^f}{\partial t} \tag{4.44}$$

equation (4.43) can be rewritten as

$$\begin{aligned} & -\mathrm{k} \frac{k_{rf}}{\nu} \nabla^2 p^f + \left(C_S + \phi \frac{S^f}{K_f} \right) \frac{\partial p^f}{\partial t} \\ & + S^f \left(Q + B / \rho_f^f \right) \left(S^f + \frac{C_s}{\phi} p^f \right) \frac{\partial p^f}{\partial t} + S^f \zeta \nabla \cdot \dot{\mathbf{d}} = 0 \end{aligned} \tag{4.45}$$

4.3.3 Equation summary and validation

The coupled equations (4.41) and (4.45) can be validated by comparing with the unsaturated hydro-mechanical coupled equations derived from the mechanics approach which has been tested by a number of researchers. The stress-strain relationship and the hydraulic equations from the mechanics approach are (Lewis and Schrefler, 1987, Lewis and Schrefler, 1998)

Stress-strain: $\dot{\sigma}_{ij} = \left(K - \frac{2G}{3} \right) \dot{\varepsilon}_{kk} \delta_{ij} + 2G \dot{\varepsilon}_{ij} - \zeta \dot{\bar{p}} \delta_{ij}$

Hydro: $-\mathrm{k} \frac{k_{rf}}{\nu} \nabla^2 p^f + \left(C_S + \phi \frac{S^f}{K_f} \right) \frac{\partial p^f}{\partial t} + S^f Q \left(S^f + \frac{C_s}{\phi} p^f \right) \frac{\partial p^f}{\partial t} + S^f \zeta \nabla \cdot \dot{\mathbf{d}} = 0$

Without considering swelling and dissolution (ω_s, ω_d in stress-strain relationship and B/ρ_f^f in hydraulic equation), equations (4.41) and (4.45) can go back to classic equations derived from the mechanics approach by Lewis and Schrefler (1987), Lewis and Schrefler (1998). The difference is the coupled swelling and dissolution term $\frac{\omega_s}{S^f\left(\rho_f^w + x\rho_f^d\right)} + \frac{x\omega_d}{S^f\left(\rho_f^w + x\rho_f^d\right)}$, and these two terms require experimental determination.

4.4 Numerical simulation

In this section, numerical modelling is presented to show the coupled hydro-mechanical behaviour, with consideration of swelling and dissolution, for the host rock around a nuclear waste container. The host rock for nuclear waste works as a barrier to prevent radionuclides from leaching into the biosphere via underground water.

4.4.1 Conceptual model

4.4.1.1Model geometry and material parameters

Figure 4.1 shows a simplified one-dimensional model geometry (0.15m width and 0.3m height). Boundary A is fixed and permeable, and boundary B is free and permeable. The upper and lower boundaries are on rollers allowing only horizontal displacement and are set as impermeable.

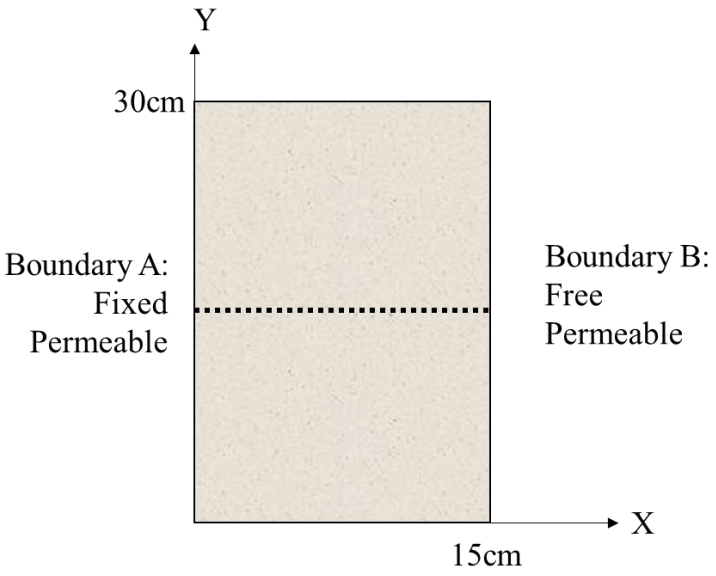

Figure 4. 1 Numerical modelling geometry and boundary condition

Table 4. 1 Material parameters (Rejeb and Cabrera, 2004, Maßmann et al., 2006)

Parameters	Physical meaning	Values and units
ρ_f^f	Density of pore fluid	1000kg/m^3
k/v	absolute permeability/dynamic viscosity	10^{-19}m/s
m	Van Genuchten parameter	0.43
M	Van Genuchten parameter	51Mpa
E	Young's modulus	9270MPa
θ	Poisson's ratio	0.2
ζ	Biot's coefficient	1
q	Void coefficient	0.0005MPa^{-1}
sw	Swelling parameter	0.2
dv	Dissolution parameter	0.05

4.4.1.2 Initial and boundary condition

The domain is assumed to contain water at a pressure of −4 MPa (unsaturated condition), with the corresponding degree of saturation as 0.995 obtained through using Van Genuchten relationship as

$$k_{rw} = \left(S^w\right)^{0.5}\left[1-\left(1-\left(S^w\right)^{1/m}\right)^m\right]^2$$

$$S^w = \left[\left(-P/M\right)^{1/(1-m)}+1\right]^{-m}$$

The whole domain is in equilibrium and the effective stress is zero.

4.4.1.3 Dissolution/swelling, and parameters

In equation (4.41), a dissolution term $\mathrm{dv} = \dfrac{x\omega_d}{S^f\left(\rho_f^w + x\rho_f^d\right)}$ and a swelling term $\mathrm{sw} = \dfrac{\omega_s}{S^f\left(\rho_f^w + x\rho_f^d\right)}$ have been included to account for the dissolution and swelling process. In realistic conditions, both dissolution and swelling are time-dependent processes. To simplify the analysis, the dissolution and swelling terms are assumed to be constant as dv=0.05 and sw=0.2, respectively. The material parameters are listed in table 4.1, more details about the adopted parameters can be found in section 3.4.1.

4.4.2 Numerical result

At the beginning of the numerical simulation, the pore fluid pressure at boundary A drops from -4MPa to -20MPa. Pore fluid pressure and degree of saturation are maintained to be the initial value at boundary B. The software COMSOL is used to solve the coupled constitutive equations.

4.4.2.1 pore fluid pressure and degree of saturation

Figure 4.2 and Figure 4.3 shows the distribution of pore fluid pressure and saturation throughout the domain at different time. Because there is a direct link between pore fluid pressure and saturation by Van Genuchten relationship, the two figures show a similar trend. As the absolute permeability is assumed to be constant, and swelling/dissolution is assumed to have little influence on the absolute and relative permeability, the pore pressure remains the same for both (sw=0.2) and non-swelling

(sw=0), dissolving (dv=0.05) and non-dissolving (dv=0).

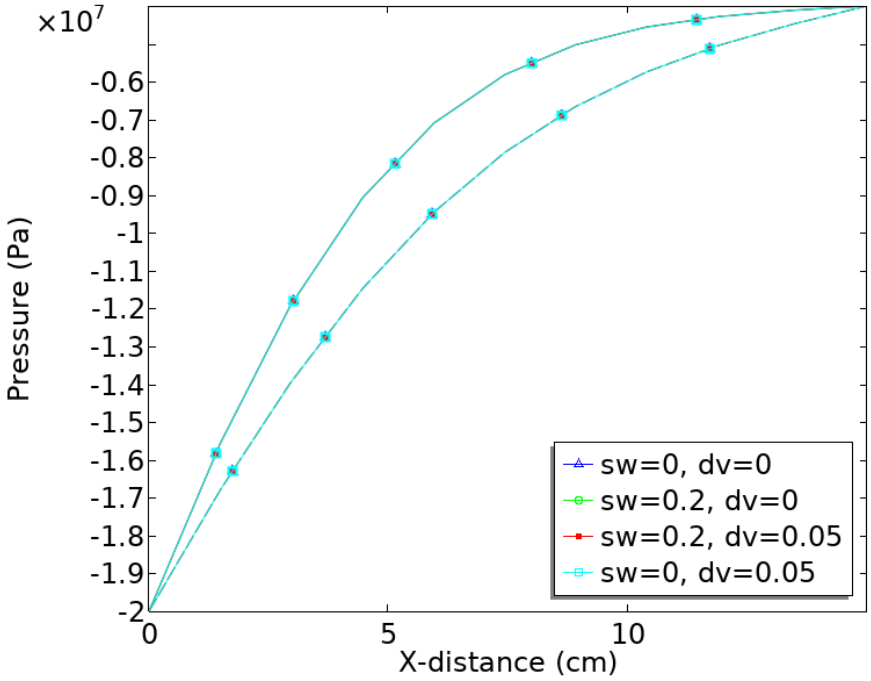

Figure 4. 2 Evolution of pore water pressure with time (solid line: t=0.5 year, dashed line: t=1 year)

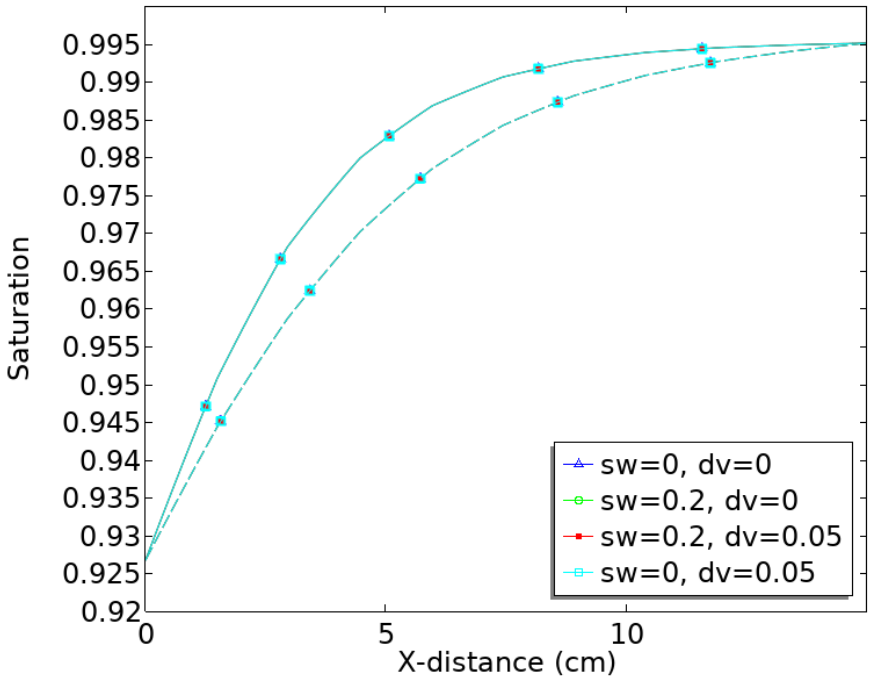

Figure 4. 3 Evolution of saturation distribution with time (solid line: t=0.5 year, dashed line: t=1 year)

4.4.2 Effective stress, strain and displacement

Figure 4.4 shows the change of horizontal effective stress. Effective stress at boundary B remains 0. At boundary A, 'swelling and non-dissolving case have the smallest effective stress, while 'non-swelling and dissolving case' has the largest effective stress. Compare the different lines in Figure 4.4, it can be concluded that the swelling process decreases the effective stress and the dissolution process increases the effective stress. This is because the swelling effect reduces the total stress influence on the solid skeleton whereas the dissolution effect enlarges such influence. A similar trend can be found in the horizontal strain and displacement (Figures 4.5 and 4.6). Since the swelling and dissolution process have contrary effects on the rock, the deformation of the rock depends on the combined impact of swelling and dissolution (Figure 4.6).

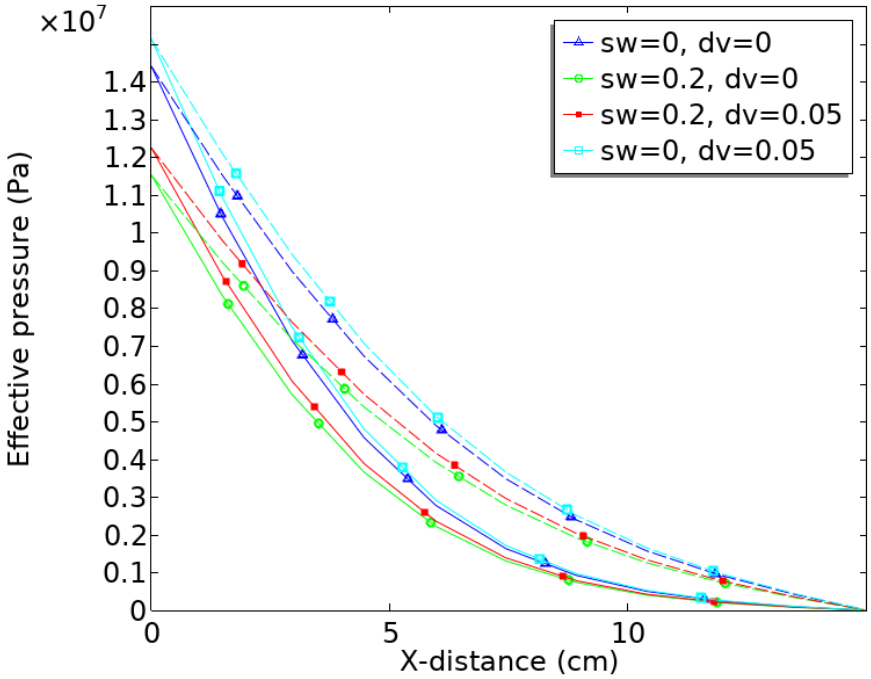

Figure 4. 4 Evolution of effective stress with time (solid line: t=0.5 year, dashed line: t=1 year)

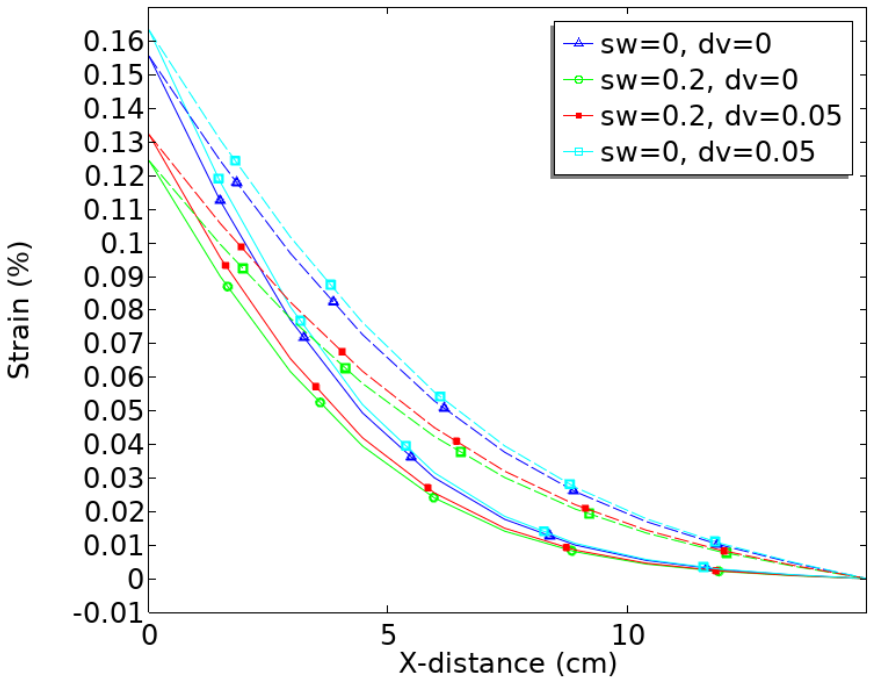

Figure 4. 5 Evolution of horizontal strain with time (solid line: t=0.5 year, dashed line: t=1 year)

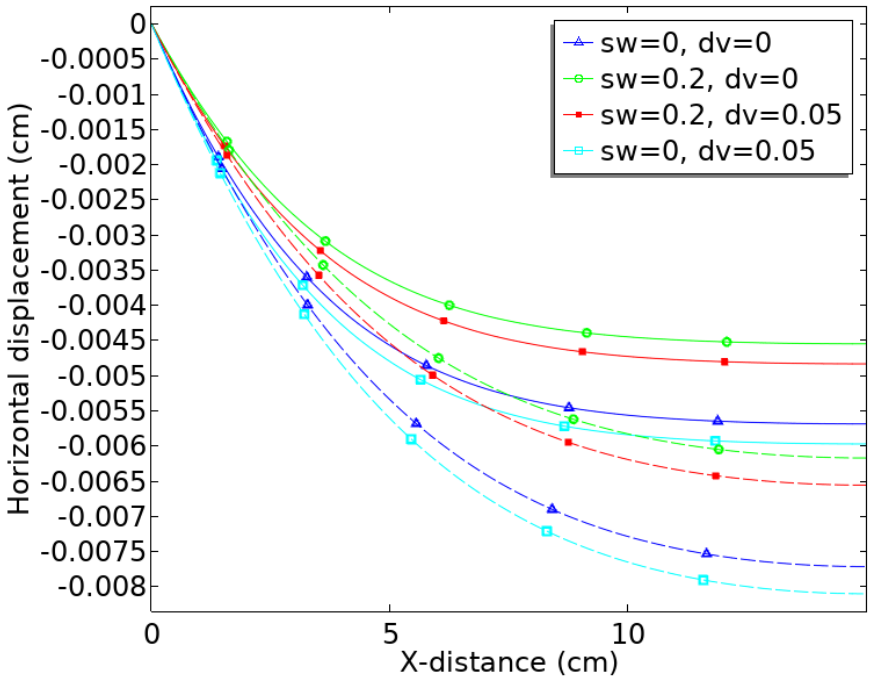

Figure 4. 6 Evolution of horizontal displacement with time (sw=0.2, dv=0.05) (solid line: t=0.5 year, dashed line: t=1 year)

4.4.3 Sensitivity analysis of permeability parameter

Permeability is very important in Hydro-Mechanical coupling. This section compares the influence of 'swelling + dissolving' on the deformation of rock, under different permeabilities: $k/\nu = 10^{-18}$ and $k/\nu = 10^{-19}$ at 0.5 years (Note k is used in the figure label to represent k/ν). The pore fluid pressure and saturation change much faster at larger permeability ($k/\nu = 10^{-18}$) (Figures 4.7 and 4.8). Effective stress, horizontal strain and displacement in high permeability ($k/\nu = 10^{-18}$) rock are all larger than in low permeability ($k/\nu = 10^{-19}$) at the same time (0.5 years) due to the faster increase of water pressure caused by higher permeability.

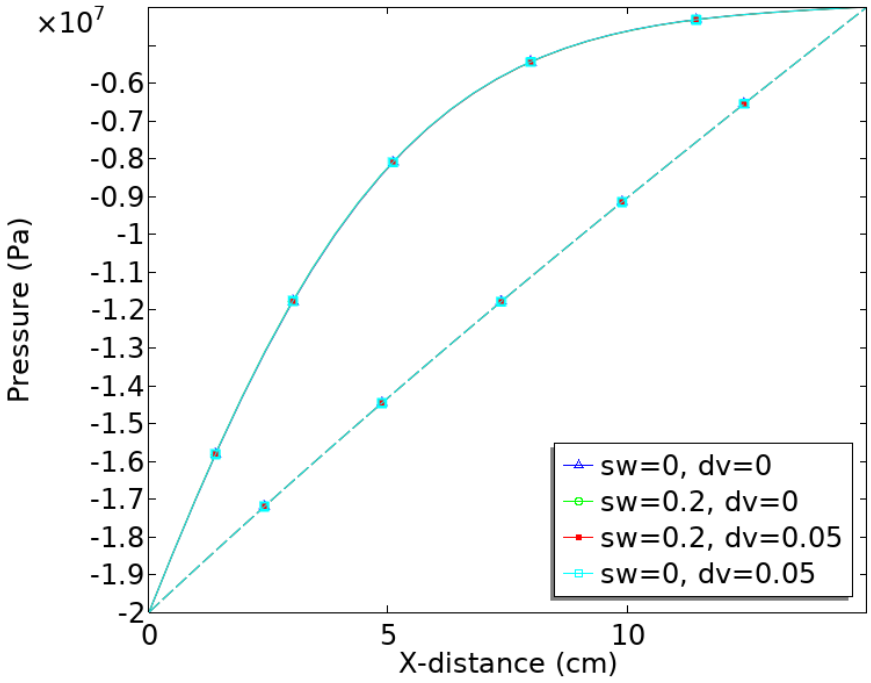

Figure 4. 7 Evolution of pore water pressure with time (solid line: $k/v=10^{-19}$, dashed line: $k/v=10^{-18}$)

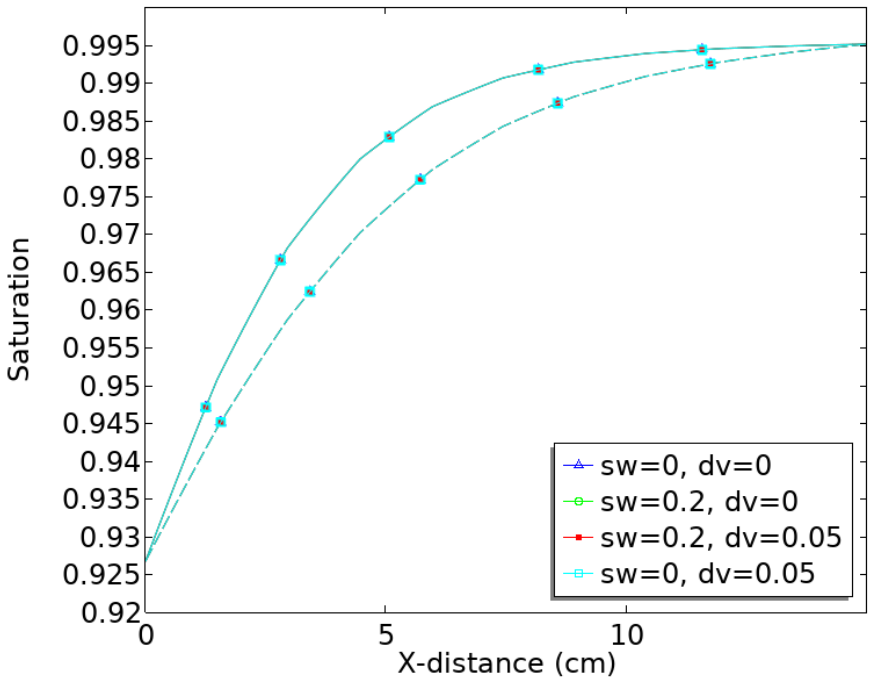

Figure 4. 8 Evolution of saturation with time (solid line: $k/v=10^{-19}$, dashed line: $k/v=10^{-18}$)

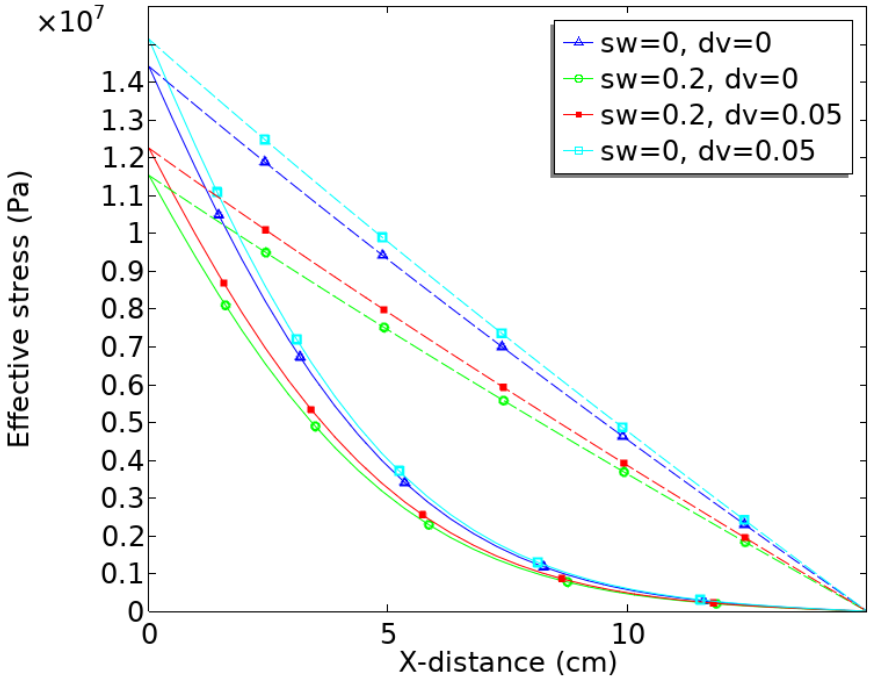

Figure 4. 9 Evolution of effective stress with time (solid line: $k/v=10^{-19}$, dashed line: $k/v=10^{-18}$)

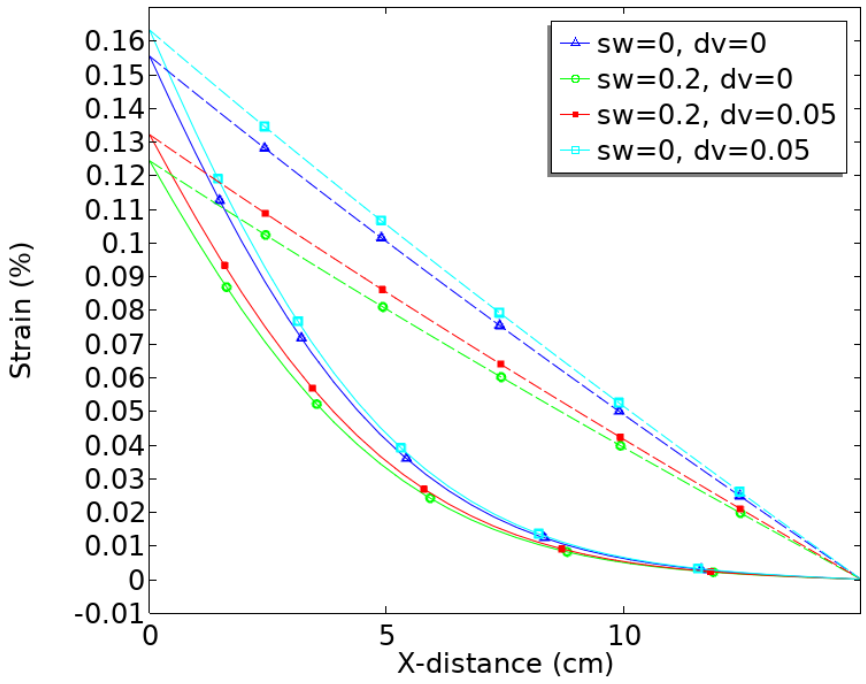

Figure 4. 10 Evolution of horizontal strain with time (solid line: $k/v=10^{-19}$, dashed line: $k/v=10^{-18}$)

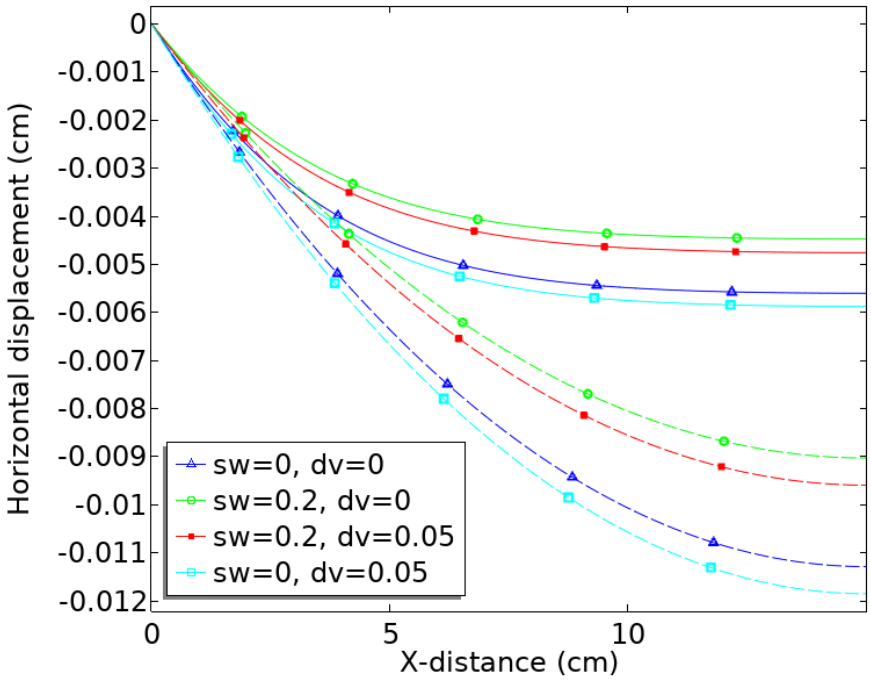

Figure 4. 11 Evolution of horizontal displacement with time (solid line: $k/v=10^{-19}$, dashed line: $k/v=10^{-18}$)

4.4.4 Limitation discussion and further work

The numerical simulation presented here is a simplified case for the demonstration purpose of the complex mathematical equations, with the assumptions made as 1) Swelling and dissolution do not impact permeability (or porosity) or concentrations, which presents only in very high saturation ratio and low kinetics reaction in a short period of time (e.g. < 1 year for quartz dissolution); 2) Variations of the chemical potential of water and of dissolved solids are linearly related. This only presents in the condition of low concentration of dissolved solids. The relationship between the chemical potential of water and of dissolved solid can be further modified according to a real situation; 3) The dissolution and swelling terms are assumed to be constant, however, they are functions of the state variables and need to be determined by experiments.

4.5 Conclusions

This chapter extends the Biot's elasticity theory by including the influence of swelling and dissolution based on Mixture-Coupling Theory. A general coupled structure for swelling and dissolvable materials has been formed. The rigorous derivation obtained by using Helmholtz free energy and non-equilibrium thermodynamics gives a deep insight into the inter-effects between molecular reaction, rock deformation, pore water and water molecules in the clay platelets.

The numerical simulation analyses the swelling and dissolution progress on the deformation of an unsaturated rock sample. The numerical results show that swelling and dissolution have a contrary influence on the rock deformation. The research has focussed on unsaturated water flow, without considering the chemical transport, which is important in nuclear waste disposal industry and will be conducted in future research.

Chapter 5 Unsaturated Hydro-Mechanical-Chemical coupling with consideration of swelling and dissolution

5.1 Introduction

Swelling clay-rich geomaterials have been widely used for waste management as engineered or host barriers (e.g., nuclear waste disposal, liquid mining waste, etc.). These barriers, however, will be exposed to coupled thermal (T), hydraulic (H), mechanical (M) and chemical (C) processes, and may be strongly influenced by acidic or alkaline leachate (e.g., the hyper-alkaline leachates from the cementitious barrier of intermediate/low-level waste). Research has been conducted to study the behaviour of engineered barriers under such coupled situations (Gens et al., 2004, Liu et al., 2011, Peter, 2011, Xiaodong et al., 2011), however, little research has been done on the coupled swelling and dissolution/precipitation processes.

In this chapter, Mixture-Coupling Theory has been further extended to consider the influence of coupled swelling and dissolution/precipitation. Entropy is used to link the dynamic dissipation and energy function. The evolution of stress and pore volume fraction are obtained by analyzing the free energy density of the wetted matrix. Numerical simulations demonstrate the advantages of the new theoretical and mathematical formulations.

5.2 Balance equations and dissipative process

An arbitrary domain V is selected within the material. It is assumed to be big enough to include solid, water and gas. S is the boundary attached to the solid phase and only fluid is allowed to pass through. The gas phase is assumed to be continuous with atmospheric pressure and p_{atm} is assumed to be zero to simplify the discussion (Neuman, 1975,

Safai and Pinder, 1979).

5.2.1 Flux and density

The flux is defined as

$$\mathbf{I}^{\beta} = \rho^{\beta}\left(\mathbf{v}^{\beta} - \mathbf{v}^{s}\right) \tag{5.1}$$

where $\mathbf{I}^{\beta}$, $\mathbf{v}^{\beta}$, and ρ^{β} are the flux, velocity and mixture density, respectively. β represents different fluid components: $\beta = w$ denotes water, $\beta = c$ denotes chemical (solute), $\beta = f$ denotes the fluid as a whole.

The fluid phase density (the concentration in mass per unit volume fluid) is defined as

$$\rho_f^{\beta} = mass^{\beta} / V_{fluid} \tag{5.2}$$

in which the mixture density ρ^{β} is related to phase density ρ_f^{β} through

$$\rho^{\beta} = S^{f}\phi\rho_f^{\beta} \tag{5.3}$$

where S^{f} is the saturation of pore fluid, ϕ is the porosity.

The total pore-fluid mixture density (e.g., water and a chemical) can be defined as:

$$\rho^{f} = \rho^{w} + \rho^{c} \tag{5.4}$$

and the barycentric velocity of the fluids can be defined as

$$\mathbf{v}^{f} = \left(\rho^{w} / \rho^{f}\right)\mathbf{v}^{w} + \left(\rho^{c} / \rho^{f}\right)\mathbf{v}^{c} \tag{5.5}$$

The diffusion flux of the water and chemical, which is relative to the barycentric motion, can be written as

$$\mathbf{J}^{\beta} = \rho^{\beta}\left(\mathbf{v}^{\beta} - \mathbf{v}^{f}\right) \tag{5.6}$$

by introducing the equation (5.1), the relationship between $\mathbf{J}^{\beta}$ and $\mathbf{I}^{\beta}$ can be obtained as

$$\mathbf{J}^{\beta} = \mathbf{I}^{\beta} - \rho^{\beta}\left(\mathbf{v}^{f} - \mathbf{v}^{s}\right) \tag{5.7}$$

where $\mathbf{v}^{s}$ is the velocity of the solid.

5.2.2 Balance equations

(1) *Energy balance*: The balance equation for Helmholtz free energy in iso-thermal condition can be derived based on the assumption of ignoring gas transport (Chen and Hicks, 2009, Chen, 2013)

$$\frac{D}{Dt}\int_V \psi dV = \int_S \boldsymbol{\sigma}\mathbf{n}\cdot\mathbf{v}^s dS \; - \int_S \mu^w \mathbf{I}^w \cdot \mathbf{n} dS - \int_S \mu^c \mathbf{I}^c \cdot \mathbf{n} dS - T\int_V \gamma dV \tag{5.8}$$

where the material time derivative is

$$\frac{D}{Dt} = \partial_t + \mathbf{v}^s \cdot \nabla \tag{5.9}$$

In equations (5.8), ψ is the Helmholtz free energy density, $\boldsymbol{\sigma}$ is the Cauchy stress tensor, $\mathbf{v}^s$ is the velocity of the solid, T is temperature, γ is the entropy produced per unit volume, ∂_t is the time derivative and ∇ is the gradient.

The derivative version of the equation (5.8) is expressed as

$$\dot{\psi} + \psi\nabla\cdot\mathbf{v}^s - \nabla\cdot\left(\boldsymbol{\sigma}\mathbf{v}^s\right) + \nabla\cdot\left(\mu^w\mathbf{I}^w\right) + \nabla\cdot\left(\mu^c\mathbf{I}^c\right) = -T\gamma \le 0 \tag{5.10}$$

(2) The general balance equation for mass can be written as

$$\frac{D}{Dt}\left(\int_V \rho^\beta dV\right) = -\int_S \mathbf{I}^\beta \cdot \mathbf{n} dS + \int_V \dot{m}_r^\beta dV \tag{5.11}$$

where $-\int_S \mathbf{I}^\beta \cdot \mathbf{n} dS$ represents the mass change due to transport through the boundary and $\int_V \dot{m}_r^\beta dV$ represents the mass change due to reaction inside the system.

According to equation (5.11), the balance equation for water mass and chemicals are:

Water balance: The balance equation for the water mass (assuming water change due to reaction is negligible):

$$\frac{D}{Dt}\left(\int_V \rho^w dV\right) = -\int_S \mathbf{I}^w \cdot \mathbf{n} dS \tag{5.12}$$

and the derivative version is

$$\dot{\rho}^w + \rho^w \nabla \cdot \mathbf{v}^s + \nabla \cdot \mathbf{I}^w = 0 \tag{5.13}$$

Chemical balance: considering a mineral reaction process (e.g., $\nu_b B \rightleftarrows \nu_c C$) the chemical component C in the solution will be either generated due to dissolution of mineral B or consumed due to precipitation (reverse process). The balance equation for the chemical component is

$$\frac{D}{Dt}\left(\int_V \rho^c dV\right) = -\int_S \mathbf{I}^c \cdot \mathbf{n} dS + \int_V \dot{m}_r dV \tag{5.14}$$

The derivative version of the equation (5.14) is

$$\dot{\rho}^c + \rho^c \nabla \cdot \mathbf{v}^s + \nabla \cdot \mathbf{I}^c - \dot{m}_r = 0 \tag{5.15}$$

where m_r is the source term, representing the generation or consumption of the chemical specie. m_r can be written as

$$m_r = \nu_c M_c \xi \tag{5.16}$$

where ξ (number of moles per unit mixture volume) is the extent of reaction, ν_c is the stoichiometric coefficient (positive for dissolution and negative for precipitation), and M_c is the molar mass of the *C*.

The time derivation of ξ can be linked to the dissolution/precipitation rate through

$$r = \nu_c \dot{\xi} \tag{5.17}$$

where r is the dissolution/precipitation rate.

5.2.3 Dissipative progress and dissolution entropy

The entropy change of the system could be categorized as (1) the friction generated at the solid/fluid boundary; (2) the transport of chemical species; (3) the dissolution or precipitation induced entropy. Therefore, the dissipation can be obtained by using non-equilibrium thermodynamics, and the entropy production function is described as (Katachalsky and Curran, 1965)

$$0 \le T\gamma = -\mathbf{I}^w \cdot \nabla \mu^w - \mathbf{I}^c \cdot \nabla \mu^c + \dot{\eta}^d \tag{5.18}$$

where $\dot{\eta}^d$ represents the entropy change due to dissolution/precipitation. To simply the discussion, the chemical entropy change influence on fluid transport is neglected (e.g. chemical osmosis and $\dot{\eta}^d = 0$), so the basic Darcy's law can be obtained by using phenomenological equations (Chen, 2013):

$$\mathbf{u} = -\frac{\mathrm{k}k_{rf}}{\nu}\nabla p^f \tag{5.19}$$

where $\mathbf{u}$ is Darcy's velocity, k is the permeability, k_{rf} is the relative permeability, and p^f is the pore fluid pressure.

The diffusion flux is (Chen and Hicks, 2013)

$$\mathbf{J}^c = -\rho_f^f D_{diff} \nabla w^c \tag{5.20}$$

where ρ_f^f is the fluid mass density, D_{diff} is the diffusion coefficient, and w^c is the mass fraction of the chemical component.

5.3 State equations for swelling and dissolution/precipitation

This chapter takes the same understanding as that in previous chapters: There are two types of water in a swelling/dissolving rock: 1) water in the pores which can be described using non-equilibrium thermodynamics, and 2) water in the clay platelets which is subjected to strong intermolecular and surface forces such that thermodynamics is not applicable (Israelachvili, 1991) (Figure 5.1). The solids can be classed into two types: 1) the solid structure, which follows the continuum thermodynamics (mechanics) and 2) the dissolved chemicals in the pore space, which do not support the structure strength (Figure 5.1).

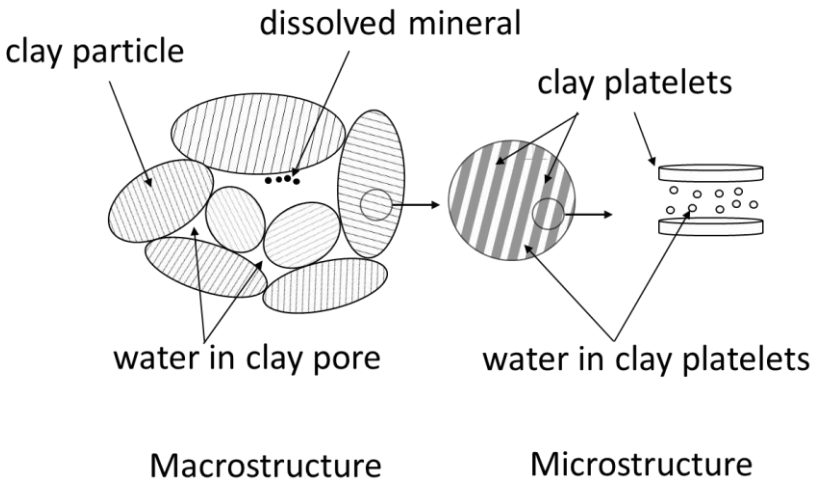

Figure 5. 1 Water types and solid types

5.3.1 Helmholtz free energy of pore space

Based on classical thermodynamics, the Helmholtz free energy density of the pore space ψ_{pore} can be written as

$$\psi_{pore} = -\overline{p} + S^f \rho_f^w \mu^w + S^f \rho_f^c \mu^c \tag{5.21}$$

where $\rho_f^\beta = mass^\beta / V_{fluid}$ denotes the mass of fluid component per unit volume fluid. $\overline{p}$ is the average fluid pressure in the pore space (the gas has been ignored). The time derivative of equation (5.21) leads to

$$\dot{\psi}_{pore} = -\dot{\overline{p}} + S^f \rho_f^w \dot{\mu}^w + \left(S^f \rho_f^w\right)^{\cdot} \mu^w + S^f \rho_f^c \dot{\mu}^c + \left(S^f \rho_f^c\right)^{\cdot} \mu^c \tag{5.22}$$

According to the Gibbs-Duhem equation in constant temperature as

$$\dot{\overline{p}} = S^f \rho_f^w \dot{\mu}^w + S^f \rho_f^c \dot{\mu}^c \tag{5.23}$$

and substituting equation (5.23) into equation (5.22) gives

$$\dot{\psi}_{pore} = \left(S^f \rho_f^w\right)^{\cdot} \mu^w + \left(S^f \rho_f^c\right)^{\cdot} \mu^c \tag{5.24}$$

5.3.2 Basic equation for deformation

It is assumed that the soil/rock maintains mechanical equilibrium so that $\nabla \cdot \boldsymbol{\sigma} = 0$. With the entropy production (5.18) and balance equation (5.10), the balance equation for ψ can be obtained as

$$\dot{\psi} + \psi \nabla \cdot \mathbf{v}^s - \left(\boldsymbol{\sigma} : \nabla \mathbf{v}^s \right) + \mu^w \nabla \cdot \mathbf{I}^w + \mu^c \nabla \cdot \mathbf{I}^c = 0 \tag{5.25}$$

To measure the rock's deformation state, classic continuum mechanics are considered here: An arbitrary reference configuration $\mathbf{X}$ is selected and at the time t, its position is $\mathbf{x}$. Some basic expressions are (Wriggers, 2008):

$$\mathbf{F} = \frac{\partial \mathbf{x}}{\partial \mathbf{X}}(\mathbf{X}, t), \mathbf{E} = \frac{1}{2}\left(\mathbf{F}^{\mathrm{T}} \mathbf{F} - \mathbf{I} \right), \mathbf{T} = J \mathbf{F}^{-1} \boldsymbol{\sigma} \mathbf{F}^{-T}, J = dV / dV_0 \ , \ \dot{J} = J \nabla \mathbf{v}_s \tag{5.26}$$

where $\mathbf{E}$ is the Green strain, $\mathbf{F}$ is the deformation gradient, $\mathbf{I}$ is a unit tensor. $\mathbf{T}$ is the second Piola-Kirchhoff stress and $\boldsymbol{\sigma}$ is the Cauchy stress.

From equation (5.25), using the mass balance equation (5.13), (5.15), and the mechanical relationship (5.26), it leads to:

$$\dot{\Psi} = tr\left(\mathbf{T}\dot{\mathbf{E}} \right) + \mu^w \dot{m}^w + \mu^c \dot{m}^c - \mu^c \dot{m}_r \tag{5.27}$$

$$\Psi = J\psi \ , \quad m^k = J\rho^k = JS^f \phi \rho_f^k \tag{5.28}$$

where Ψ is the free energy in the reference configuration, m^k $(k = w, c)$ is the mass density of the fluid component in the reference configuration, and S^f is the saturation of pore fluid.

5.3.3 Free energy density of the wetted mineral matrix

Because the free energy of the mineral matrix is inclusive of fluid 'bound' between platelets which do not follow non-equilibrium thermodynamics, the free energy of the mineral matrix can be obtained by subtracting the contribution of pore space from the total free energy of the combined solids/fluids system. Therefore, from equation (5.21), (5.24), (5.27) and (5.28), the free energy density of the wetted mineral matrix is written as:

$$\left(\Psi - J\phi\psi_{pore} \right)^{\cdot} = tr\left(\mathbf{T}\dot{\mathbf{E}} \right) + \bar{p}\dot{\upsilon} + \mu^w \dot{m}_{bound} - \mu^c \dot{m}_r \tag{5.29}$$

where $\bar{p} = S^f p^f$ is the average pressure in the pore space, $\upsilon = J\phi$ is denoted as the

pore volume per unit referential volume, $m_{bound} = m^w - JS^f \phi \rho_f^w$ is denoted as the referential mass density of bound water.

For the reason of convenience, the dual potential (deformation energy) can be expressed as

$$W = \left(\Psi - J\phi^w \psi_{pore}\right) - \bar{p}\upsilon - \mu^w m_{bound} + \mu^c m_r \tag{5.30}$$

where W is a function of $\mathbf{E}$, $\bar{p}$, μ^w, μ^c. The expressions for $\mathbf{T}$, υ, m_{bound} and m_r can be given. Equation (5.30) implies the time derivative of $W(\mathbf{E}, \bar{p}, \mu^w, \mu^c)$ satisfies the relation

$$\dot{W}\left(\mathbf{E}, \bar{p}, \mu^w, \mu^c\right) = tr\left(\mathbf{T}\dot{\mathbf{E}}\right) - \dot{\bar{p}}\upsilon - \dot{\mu}^w m_{bound} + \dot{\mu}^c m_r \tag{5.31}$$

Note: the variable for the reaction part in equation (5.31) is the chemical potential variation $\dot{\mu}^c$. This variable is not widely used as most dissolution/precipitation research focuses on dissolution/precipitation rate rather than the change of chemical potential. Using Legendre transforms leads to

$$\dot{\mu}^c m_r = \left(\mu^c m_r\right)^{\cdot} - \mu^c \dot{m}_r \tag{5.32}$$

Invoking equation (5.32) into equation (5.31) leads to

$$\dot{W}\left(\mathbf{E}, \bar{p}, \mu^w, \mu^c\right) - \left(\mu^c m_r\right)^{\cdot} = tr\left(\mathbf{T}\dot{\mathbf{E}}\right) - \dot{\bar{p}}\upsilon - \dot{\mu}^w m_{bound} - \dot{m}_r \mu^c \tag{5.33}$$

Substituting $W_0 = W - \mu^c m_r$, which can be expressed as total deformation energy considering reaction induced energy, into equation (5.33) leads to

$$\dot{W}_0\left(\mathbf{E}, \bar{p}, \mu^w, m_r\right) = tr\left(\mathbf{T}\dot{\mathbf{E}}\right) - \dot{\bar{p}}\upsilon - \dot{\mu}^w m_{bound} - \dot{m}_r \mu^c \tag{5.34}$$

or

$$\begin{aligned} \dot{W}_0\left(\mathbf{E}, \bar{p}, \mu^w, m_r\right) = & \left(\frac{\partial W_0}{\partial E_{ij}}\right)_{\bar{p}, \mu^w, m_r} \dot{E}_{ij} + \left(\frac{\partial W_0}{\partial \bar{p}}\right)_{E_{ij}, \mu^w, m_r} \dot{\bar{p}} \\ & + \left(\frac{\partial W_0}{\partial \mu^w}\right)_{E_{ij}, \bar{p}, m_r} \dot{\mu}^w + \left(\frac{\partial W_0}{\partial m_r}\right)_{E_{ij}, \bar{p}, \mu^w} \dot{m}_r \end{aligned} \tag{5.35}$$

Therefore,

$$T_{ij} = \left(\frac{\partial W_0}{\partial E_{ij}} \right)_{\bar{p},\mu^w,m_r} , \ \upsilon = -\left(\frac{\partial W_0}{\partial \bar{p}} \right)_{E_{ij},\mu^w,m_r} ,$$

$$m_{bound} = -\left(\frac{\partial W_0}{\partial \mu^w} \right)_{E_{ij},\bar{p},m_r} , \mu^c = -\left(\frac{\partial W_0}{\partial m_r} \right)_{E_{ij},\bar{p},\mu^w} \tag{5.36}$$

If equation (5.36) is differentiated with respect to time, the fundamental constitutive equations for the evolution of stress, pore volume fraction, the mass densities in the bound water and the chemical potential can be obtained

$$\dot{T}_{ij} = L_{ijkl}\dot{E}_{kl} - M_{ij}\dot{\bar{p}} + S_{ij}\dot{\mu}^w - H_{ij}\dot{m}_r \tag{5.37}$$

$$\dot{\upsilon} = M_{ij}\dot{E}_{ij} + Q\dot{\bar{p}} + B\dot{\mu}^w + D\dot{m}_r \tag{5.38}$$

$$\dot{m}_{bound} = -S_{ij}\dot{E}_{ij} + B\ \dot{\bar{p}} + Z\dot{\mu}^w + X\ \dot{m}_r \tag{5.39}$$

$$\dot{\mu}^c = H_{ij}\dot{E}_{ij} + D\dot{\bar{p}} + X\dot{\mu}^w + Y\dot{m}_r \tag{5.40}$$

where the parameters L_{ijkl}, M_{ij}, S_{ij}, H_{ij}, B, X, Y, Z are defined as the following group of equations:

$$L_{ijkl} = \left(\frac{\partial T_{ij}}{\partial E_{kl}} \right)_{\bar{p},\mu^w,m_r} = \left(\frac{\partial T_{kl}}{\partial E_{ij}} \right)_{\bar{p},\mu^w,m_r}$$

$$M_{ij} = -\left(\frac{\partial T_{ij}}{\partial \bar{p}} \right)_{E_{ij},\mu^w,m_r} = \left(\frac{\partial \upsilon}{\partial E_{ij}} \right)_{\bar{p},\mu^w,m_r}$$

$$S_{ij} = \left(\frac{\partial T_{ij}}{\partial \mu^w} \right)_{E_{ij},\bar{p},m_r} = -\left(\frac{\partial m_{bound}}{\partial E_{ij}} \right)_{\bar{p},\mu^w,m_r}$$

$$H_{ij} = -\left(\frac{\partial T_{ij}}{\partial m_r} \right)_{E_{ij},\bar{p},\mu^w} = \left(\frac{\partial \mu^c}{\partial E_{ij}} \right)_{\bar{p},\mu^w,m_r} \tag{5.41}$$

$$B = \left(\frac{\partial \upsilon}{\partial \mu^w} \right)_{E_{ij},\bar{p},\mu^c} = \left(\frac{\partial m_{bound}}{\partial \bar{p}} \right)_{E_{ij},\mu^w,m_r}$$

$$Z = -\left(\frac{\partial m_{bound}}{\partial \mu^w} \right)_{E_{ij},\bar{p},m_r} , \ Q = \left(\frac{\partial \upsilon}{\partial \bar{p}} \right)_{E_{ij},\mu^w,m_r}$$

$$Y = \left(\frac{\partial \mu^c}{\partial m_r} \right)_{E_{ij}, \bar{p}, \mu^w}, \; X = \left(\frac{\partial m_{bound}}{\partial m_r} \right)_{E_{ij}, \bar{p}, \mu^w} = \left(\frac{\partial \mu^c}{\partial m_r} \right)_{E_{ij}, \bar{p}, \mu^w}$$

5.4 Coupled Hydro-Mechanical-Chemical constitutive equations

5.4.1 Mechanical behaviour

Equations (5.37), (5.38), (5.39) and (5.40) give the general coupled equations for mechanical behaviour, porosity, mass density of the bounded water and chemical potential of the fluid component. These equations are for wide general cases like non-linear, large deformation, and anisotropic conditions. As the attention of this article is focused on the coupled dissolution and swelling influence, a few assumptions are made including (Chen & Hicks, 2013):

i. Small strains assumption that leads to the replacement of the Green Strain tensor E_{ij} by the strain tensor ε_{ij}, and the Piola-Kirchhoff stress T_{ij} by the Cauchy stress σ_{ij}.

ii. The parameters L_{ijkl}, M_{ij}, S_{ij}, Z, B and Q are material-dependent constants and the material is isotropic, therefore, the tensors M_{ij}, S_{ij} and H_{ij} are diagonal and can be written in the forms of scalars ζ, ω_s and ω_R, as

$$M_{ij} = \zeta \delta_{ij} \;,\; S_{ij} = \omega_s \delta_{ij}, H_{ij} = \omega_R \delta_{ij} \tag{5.42}$$

Based on assumption ii), the elastic stiffness L_{ijkl} can be a fourth-order isotropic tensor:

$$L_{ijkl} = G\left(\delta_{ik}\delta_{jl} + \delta_{il}\delta_{jk} \right) + \left(K - \frac{2G}{3} \right) \delta_{ij}\delta_{kl} \tag{5.43}$$

Here, G denotes the material's shear modulus and K denotes the bulk modulus.

With the assumptions i), ii), the stress equation (5.37) can be simplified to

$$\dot{\sigma}_{ij} = \left(K - \frac{2G}{3} \right) \dot{\varepsilon}_{kk}\delta_{ij} + 2G\dot{\varepsilon}_{ij} - \zeta \dot{\bar{p}}\delta_{ij} + \omega_s \dot{\mu}^w \delta_{ij} - \omega_R \dot{m}_r \delta_{ij} \tag{5.44}$$

where the quantity ζ is the Biot coefficient, which is related to the bulk modulus K and K_s in a manner from poroelasticity through the equation $\zeta = 1-\left(K / K_s\right)$. In this equation, the two terms, namely, ω_s and ω_R, have been introduced to represent the swelling and reactive dissolution/precipitation influence on the mechanical behaviour.

The term $\omega_R \dot{m}_r \delta_{ij}$ is interpreted as the stress change due to dissolution/precipitation. Since ω_R is related to the bulk modulus K, it can be expressed as $\omega_R = \omega_r K$. The dissolution/precipitation induced stress as

$$\dot{\sigma}_r = \omega_r K \dot{m}_r \tag{5.45}$$

Equation (5.45) can be compared with the thermal-induced stress as (Xia et al., 2014):

$$\dot{\sigma}_T = \alpha_s K \dot{T} \tag{5.46}$$

where α_s is the thermal expansion coefficient of the solid.

Substituting equation (5.45) into equation (5.44), the constitutive equation for stress response can be obtained as

$$\dot{\sigma}_{ij} = \left(K - \frac{2G}{3}\right)\dot{\varepsilon}_{kk}\delta_{ij} + 2G\dot{\varepsilon}_{ij} - \zeta \dot{\bar{p}}\delta_{ij} + \omega_s \dot{\mu}^w \delta_{ij} - \omega_r K \dot{m}_r \delta_{ij} \tag{5.47}$$

Assuming mechanical equilibrium ($\partial \sigma_{ij} / \partial x_j = 0$), and using displacement variables $d_i \left(i = 1,2,3\right)$ through $\varepsilon_{ij} = \frac{1}{2}\left(d_{i,j} + d_{j,i}\right)$, and introducing equation (5.23), equation (5.47) leads to

$$G\nabla^2 \dot{\mathbf{d}} + \left(\frac{G}{1-2\theta}\right)\nabla(\nabla \cdot \dot{\mathbf{d}}) - \left(\zeta - \frac{\omega_s}{S^f \rho_f^w}\right)\nabla \dot{\bar{p}} - \omega_r K \nabla \dot{m}_r = 0 \tag{5.48}$$

where θ is the Poisson's ratio, $\bar{p} = S^f p^f$ is the average pore pressure and its time derivative is (Lewis and Schrefler, 1987)

$$\dot{\bar{p}} = S^f \frac{\partial p^f}{\partial t} + \frac{C_s}{\phi} p^f \frac{\partial p^f}{\partial t} = \left(S^f + \frac{C_s}{\phi} p^f \right) \frac{\partial p^f}{\partial t}$$

in which $C_s = \phi \frac{\partial S^f}{\partial p^f}$ is the specific moisture content.

Equation (5.48) can then be rewritten as:

$$G\nabla^2 \dot{\mathbf{d}} + \left(\frac{G}{1-2\theta} \right) \nabla(\nabla \cdot \dot{\mathbf{d}}) - (\zeta - \frac{\omega_s}{S^f \rho_f^w}) \nabla \left[\left(S^f + \frac{C_s}{\phi} p^f \right) \dot{p}^f \right] - \omega_r K \nabla \dot{m}_r = 0 \quad (5.49)$$

Equation (5.49) presents a general formula including the influence of both the swelling and dissolution/precipitation on mechanical behaviour.

Considering the relationship in equation (5.16), the governing equation for both swelling and dissolution is

$$G\nabla^2 \dot{\mathbf{d}} + \left(\frac{G}{1-2\theta} \right) \nabla(\nabla \cdot \dot{\mathbf{d}}) - (\zeta - \frac{\omega_s}{S^f \rho_f^w}) \nabla \left[\left(S^f + \frac{C_s}{\phi} p^f \right)^f \right] - \omega_d \nu_c M_c K \nabla \dot{\xi} = 0 \quad (5.50)$$

And the governing equation for both swelling and precipitation is

$$G\nabla^2 \dot{\mathbf{d}} + \left(\frac{G}{1-2\theta} \right) \nabla(\nabla \cdot \dot{\mathbf{d}}) - (\zeta - \frac{\omega_s}{S^f \rho_f^w}) \nabla \left[\left(S^f + \frac{C_s}{\phi} p^f \right) \dot{p}^f \right] + \omega_p \nu_c M_c K \nabla \dot{\xi} = 0 \quad (5.51)$$

where ω_d and ω_p are the dissolution and precipitation coefficients, respectively.

5.4.2 Fluid-phase

From equation (5.3), the water density equation (5.13) and the Euler identity, the conservation equation of water is obtained as

$$\left(S^f \upsilon \rho_f^f \right)^{\cdot} + \nabla \cdot \left(\rho_f^f \mathbf{u} \right) = 0 \quad (5.52)$$

From equations (5.52), (5.13), (5.19) and (5.38), it leads to

$$\begin{aligned} & S^f \rho_f^f \zeta \nabla \cdot \dot{\mathbf{d}} + S^f \rho_f^f \left(Q + B / \rho_f^f \right) \dot{\bar{p}} \\ & + \phi \rho_f^f \frac{\partial S^f}{\partial t} + \phi S^f \frac{\partial \rho_f^f}{\partial t} + \rho_f^f \left[-\mathrm{k} \frac{k_{rf}}{\mu} \nabla^2 p^f \right] = 0 \end{aligned} \quad (5.53)$$

Considering the rate of change of saturation function and the rate of change of water

density function (Lewis and Schrefler, 1987)

$$\phi \frac{\partial S^f}{\partial t} + \frac{\phi S^f}{\rho_f^f} \frac{\partial \rho_f^f}{\partial t} = C_S \frac{\partial p^f}{\partial t} + \phi \frac{S^f}{K_f} \frac{\partial p^f}{\partial t} = \left(C_S + \phi \frac{S^f}{K_f} \right) \frac{\partial p^f}{\partial t} \tag{5.54}$$

Equation (5.53) can be rewritten as

$$-\mathrm{k} \frac{k_{rf}}{\nu} \nabla^2 p^f + \left(C_S + \phi \frac{S^f}{K_f} \right) \frac{\partial p^f}{\partial t} + S^f \left(Q + B / \rho_f^f \right) \left(S^f + \frac{C_s}{\phi} p^f \right) \frac{\partial p^f}{\partial t} + S^f \zeta \nabla \cdot \dot{\mathbf{d}} = 0 \tag{5.55}$$

5.4.3 Chemical-phase

From the partial mass equation(5.11), (5.13), (5.15) and the mass density equation (5.3), introducing equation (5.7) and using the Euler identity, leads to

$$\left(S^f \upsilon \rho_f^\beta \right)^{\cdot} + J \nabla \cdot \left(\rho^\beta \mathbf{u} \right) + J \nabla \cdot \mathbf{J}^\beta = \dot{m}_r^\beta \tag{5.56}$$

If the fluid is assumed to be incompressible, introducing the mass fraction $w^\beta = \rho_f^\beta / \rho_f^f$ and assuming $J = 1$, there is

$$\left(S^f \upsilon \rho_f^f w^\beta \right)^{\cdot} + \nabla \cdot \left(\rho_f^f w^\beta \mathbf{u} \right) + \nabla \cdot \mathbf{J}^\beta = \dot{m}_r^\beta \tag{5.57}$$

Because $\sum_\beta w^\beta = 1$ and $\sum_\beta \mathbf{J}^\beta = 0$, summing over all the fluid components leads to the relationship

$$\left(\upsilon S^f \rho_f^f \right)^{\cdot} + \nabla \cdot \left(\rho_f^f \mathbf{u} \right) = \sum \dot{m}_r^\beta \tag{5.58}$$

By invoking equation(5.58), equation (5.56) can be transformed to give

$$\left(S^f \upsilon \rho_f^f \right) \dot{w}^\beta + \rho_f^f \mathbf{u} \nabla \cdot w^\beta + \nabla \cdot \mathbf{J}^\beta = \dot{m}_r^\beta - w^\beta \sum \dot{m}_r^\beta \tag{5.59}$$

Because the dissolution/precipitation rate deals with mole concentration, with the relationship $w^\beta = \frac{c^\beta M_\beta}{\rho_f^f}$, equation (5.59) can be converted from mass fraction to mole concentration:

$$\upsilon S^f \dot{c}^\beta + \mathbf{u} \cdot \nabla \dot{c}^\beta + \frac{\nabla \cdot \mathbf{J}^\beta}{M_\beta} = r^\beta \tag{5.60}$$

where c^{β} is the mole concentration of the fluid component, and r^{β} is the dissolution/precipitation rate (moles per unit volume per unit time), the term $-w^{\beta}\sum \dot{m}_r^{\beta}$ has been neglected.

From equations (5.20) and (5.60), the chemical transport equation can be obtained as

$$S^f \phi \dot{c}^{\beta} - \left(\mathrm{k} \frac{k_{rf}}{\nu} \nabla p^f \right) \cdot \nabla c^{\beta} - D_{diff} \nabla^2 c^{\beta} = r^{\beta} \tag{5.61}$$

5.4.4 Equation validation

Equations (5.49), (5.55) and (5.61) represent the coupled mechanical, hydraulic, and chemical processes. The swelling and dissolution/precipitation influence, namely, $\frac{\omega_s}{S^f \rho_f^f}$ and ω_d / ω_p, have been incorporated into the coupled HMC framework. The new governing equations are a further extension of Chen's research (Chen, 2013), with considering the dissolution/precipitation influence. If the swelling and dissolution terms are ignored, the developed equations will be simplified to the governing equations proposed by Lewis (Lewis and Schrefler, 1987).

The dissolution part in equation (5.51) (or more general equation (5.47)) has the same equation stress-strain relationship as in the literature (Coussy, 2004, Zhang and Zhong, 2017b, Zhang and Zhong, 2018) with a rigorous mathematical derivation and further consideration of swelling/precipitation. Note: The name 'dissolution parameter' is to keep consistent with the name 'swelling parameter' in this paper, while it is called 'reaction dilation coefficient' or 'chemical dilation coefficient' in reference (Coussy, 2004, Zhang and Zhong, 2018)

5.5 Numerical simulation

5.5.1 Numerical model

Clay, which are used as part of the engineered barrier for nuclear waste disposal, will encounter the influences of swelling and dissolution/precipitation when in contact with hyper-alkaline leachates generated from the cement materials around the nuclear waste. (Note: In a geological disposal facility (GDF), cement and bentonite being in direct contact may be limited to plugs and/or seals, including borehole seals (a direct interaction), although leachate from cementitious backfill material used in association with one waste category could indeed migrate in groundwater to bentonite buffer material being used in another part of the GDF in association with a different waste category: an indirect interaction). In this section, a simple numerical simulation for demonstration purpose is presented to show the role of swelling and dissolution/precipitation in a coupled HMC process.

5.5.1.1 Geometry and boundary condition

Conceptual model: Figure 5.2 shows the prescribed geometry and boundary conditions, which represent a geomaterial sample around the nuclear waste container. The domain is a square with 1m width. The central line (the dashed line in figure 5.2) along the X direction is selected to track the change alone the horizontal direction and five observation points are selected to track the change at some points, as presented in Figure 5.2.

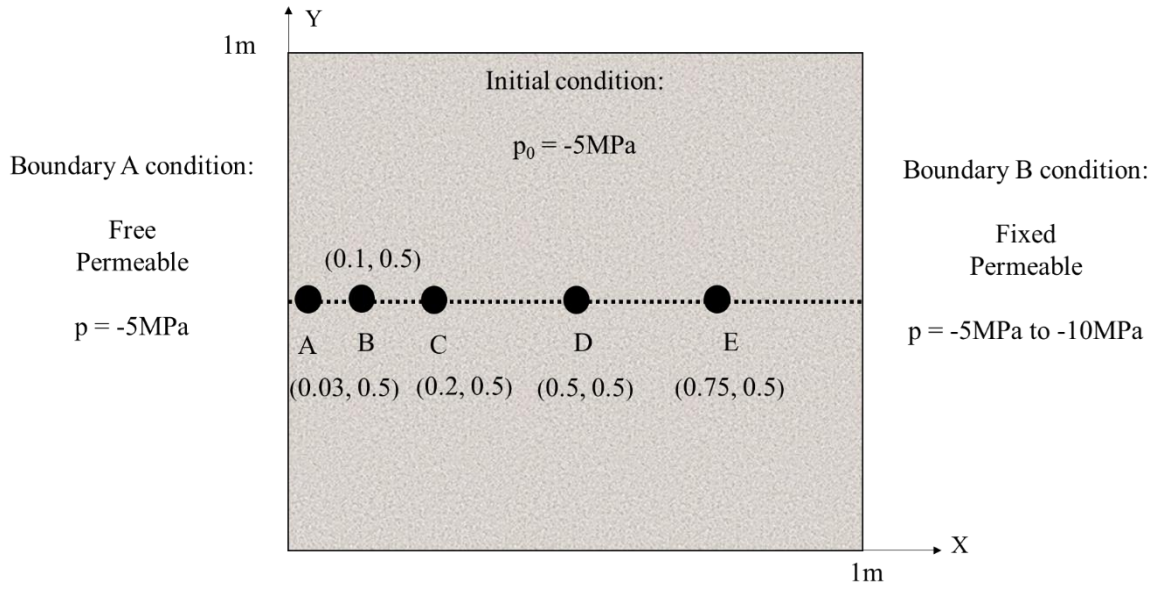

Figure 5. 2 Geometry and Boundary condition

Boundary condition: In this model, boundary A is free and permeable, while boundary B is fixed and permeable. The upper and lower boundaries are fixed and non-permeable so that no vertical displacement is allowed and no water passes through. At boundary B, water pressure decreases to -10 MPa at the start of the simulation.

Initial condition: The whole domain is assumed to be at mechanical equilibrium, with zero effective stress throughout. The domain initially contains water at a pressure of -5 MPa and a saturation degree of 0.995, according to van Genuchten's model, given by

$$k_{rw} = \left(S^w\right)^{0.5}\left[1-\left(1-\left(S^w\right)^{1/m}\right)^m\right]^2$$

$$S^w = \left[\left(-P/M\right)^{1/(1-m)}+1\right]^{-m}$$

Chemical condition: In the numerical simulation, it is assumed that quartz is the major mineral component of rock/clay, which will first form H_4SiO_4(solid) with water, and then react with hyper-alkaline leachate from the cement as (Haxaire and Djeran-Maigre, 2009)

$$\underset{solid}{H_4SiO_4} + 2\underset{liquid}{OH^-} = \underset{liquid}{H_2SiO_4^{2-}} + 2\underset{liquid}{H_2O}$$

The dissolution rate equation is (Savage et al., 2002)

$$r = k_{rate} A_{sf} \left(1 - \left(\frac{Q}{K_{eq}} \right)^{\vartheta} \right)^{\varpi} \tag{5.62}$$

in which r is the dissolution rate in moles per unit volume porous media, k_{rate} is the rate constant, A_{sf} is reactive surface area per unit volume of porous media, Q is the ion activity product, ϑ is a 'coefficient related to the stoichiometry of the reaction that forms an activated complex, but is often set to be 1' (Savage et al., 2002), ϖ is an empirical coefficient that is assumed to be 1 in this paper, and K_{eq} is the thermodynamic equilibrium constant described as

$$K_{eq} = \frac{\left[H_2SiO_4^{2-} \right]_{eq}}{\left[OH^- \right]_{eq}^2} \tag{5.63}$$

in which $\left[H_2SiO_4^{2-} \right]_{eq}$ is the concentration of $H_2SiO_4^{2-}$ and $\left[OH^- \right]_{eq}$ is the concentration of OH^- at equilibrium, respectively. Since K_{eq} is a constant value, $\left[H_2SiO_4^{2-} \right]_{eq}$ and $\left[OH^- \right]_{eq}$ will influence each other, i.e. the higher $\left[OH^- \right]_{eq}$ is, the higher $\left[H_2SiO_4^{2-} \right]_{eq}$ will be. So, in the numerical simulation, not only are the conditions for H_2SiO_4 required, but also the conditions for OH^-.

Chemical boundary and initial condition ($H_2SiO_4^{2-}$): The concentration of H_2SiO_4 on the left boundary is set to be $0.003 mol/L$ (t>0) to represent the H_2SiO_4 brought by the external groundwater. The domain contains no H_2SiO_4 initially, but the mineral will react with the hyper-alkaline leachates at t>0, and the concentration of OH^- from the hyper-alkaline leachates is $0.3 mol/L$ (pH=13.48) and applied to all the domain (t=0).

The hydraulic and mechanical parameters, including the Poisson's ration, shear

modulus, permeability, porosity and the Biot's coefficient are mainly for the Opalinus Clay, and are adopted from the experimental results by Wild et al. (2015) and the modelling case by Ziefle et al. (2018). The reactive rate constant is adopted for the case of base mechanism from Hu et al. (2012); the diffusion coefficient, surface area and equilibrium constant are collected from different research, they are the general values for quartz (Lichtner and Seth, 1996, Savage et al., 2002). Detailed parameters are listed in Table 5.1.

Table 5. 1 Material parameters

Parameters	Physical meaning	Values and units
ρ_t^w	Density of fluid	1000kg/m^3
ϕ	Porosity	0.16
k	permeability	6.8*10^{-20}m^{-2}
ν	Dynamics viscosity	1*10^{-3}Pa.s
m	van Genuchten parameter	0.54
M	van Genuchten parameter	44.4MPa
G	Shear modulus	1.2GPa
θ	Poisson's ratio	0.18
ζ	Biot's coefficient	1
D	Diffusion coefficient	10^{-9} m^2/s(Lichtner and Seth, 1996)
q	Void coefficient	5*10^{-10}
k_{rate}	Reactive rate constant	2.102*10^{-10} mol/m^2/s (Hu et al., 2012)
A	Reactive surface area	9.53*10^3 m^2/m (Savage et al., 2002)
K_{eq}	Equilibrium constant	1*10^{-4}

5.5.1.2 Simulation procedure

The swelling term $\frac{\omega_s}{S^f \rho_f^w}$ and the dissolution/precipitation term ω_d may be complicated expressions. To simplify the discussion, the swelling coefficient is

assumed to be $\frac{\omega_s}{S^f \rho_f^w} = 0.2$. The coefficient associated with the pressure variable in the hydraulic equation (5.55) is simplified as one simple and named as void coefficient $q = \left(C_S + \phi \frac{S^f}{K_f} \right) + S^f \left(Q + B / \rho_f^f \right) \left(S^f + \frac{C_s}{\phi} p^f \right)$. The strain resulting from dissolution can be expressed by considering the volumetric strain (Tao et al., 2019) as

$$\varepsilon_d = \frac{V_s^{rem}}{V_s^{ini}} - 1 = -\frac{M_b}{\rho_t^b} \frac{d(n)}{V_s} = -\frac{M_b}{\rho_t^b} \frac{1}{1-\phi} \frac{d(n)}{V} \tag{5.64}$$

where n is the change of the number of moles, V_s is the volume of the solid part, V is the total volume, M_b is the mole mass of mineral B, and ρ_t^b is the true mass density of mineral B.

If the dissolution rate is defined as the number of moles per unit time per unit volume of porous media as in equation (5.62), $\frac{d(n)}{V}$ in equation (5.64) becomes the reaction extent ξ. From the stress-strain relationship (5.47) with consideration of dissolution influence only, the corresponding stress-strain relationship (assuming the solid is homogeneous and linearly elastic) can be obtained as

$$\sigma_d = -K\varepsilon_d = -K \frac{M_b}{\rho_t^b} \frac{1}{1-\phi} \frac{d(n)}{V} = -\omega_d K m_r \tag{5.65}$$

With equation (5.65) and the relationship in equation (5.16), it leads to

$$\omega_d = \frac{1}{\nu_{ro} M_c} \frac{M_b}{\rho_t^b} \frac{1}{1-\phi} \tag{5.66}$$

Here, for $\nu_b B \rightleftarrows \nu_c C$, ν_{ro} is the proportion of the stoichiometric coefficient of the product against reactant, e.g., $\nu_{ro} = \nu_c / \nu_b$.

For example: Considering quartz (e.g. H_4SiO_4), as the density is 1800g/m^3 and molar

mass 96g/mol, using equation (5.65) leads to $\omega_d = \frac{5.3*10^{-4}}{(1-\phi)\nu_{ro}}$. The variable in equation (5.65) is m_d rather than ξ. In Equation (5.50), the variable has been switched to ξ, the coefficient before ξ changes to $\omega_d \nu_c M_c = \frac{5.3*10^{-3}\nu_b}{(1-\phi)}$, which is a similar value as the 'reaction dilation coefficient'($1*10^{-5}$) in recent literature (Zhang and Zhong, 2018).

To obtain a deep understanding of the influence caused by swelling and dissolving/precipitating, four scenarios are considered in the numerical simulation:

i). "No swelling and no dissolution". In this scenario, the influence of swelling or dissolution is not considered, this situation becomes the classic theory described by Lewis's research (Lewis and Schrefler, 1987).

ii). "Swelling only". In this scenario, only the influence of swelling is considered, this is the same as Chen's research (Chen, 2013).

iii). "Dissolution only".

iv). "Swelling and dissolution".

Note: By setting the dissolution parameter to be negative, the influence of precipitation can be analyzed.

5.5.2 1D numerical results

Figure 5.3 shows the distribution of pore water pressure along the middle line of the sample under the four scenarios at different times. The water pressure distributions in these scenarios are the same. This is because the porosity evolution, the water loss in the pore space due to swelling is ignored and the osmosis phenomena induced by chemical concentration variation are not considered to simplify the discussion. Figure 5.3 shows that the pressure in the domain decreases gradually with time and reaches equilibrium at t=1000h. From equation (5.55), the time required to reach equilibrium

not only depends on the pressure and strain variables, but also depends on the associated coefficients, i.e., permeability, void coefficient and Biot coefficient. Numerical investigations show that the permeability and void coefficient has a much more significant influence than the Biot coefficient. The greater void coefficient and smaller permeability would lead to longer time required to reach equilibrium. The permeability adopted in table 5.1 is much larger than the permeability in chapter 4, resulting in a much shorter time to reach equilibrium in spite of a larger domain size. Owing to the van Genuchten relationship between water pressure and saturation, the distribution of saturation (Figure 5.4) shows a similar trend as the pressure distribution in Figure 5.3.

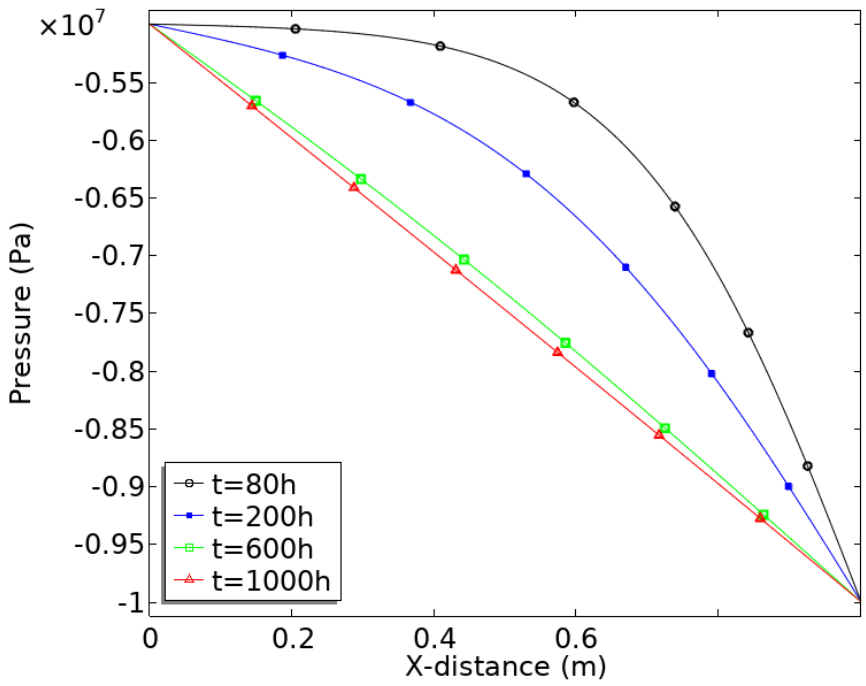

Figure 5. 3 Distribution of pore water pressure (scenario i, ii, iii, iv)

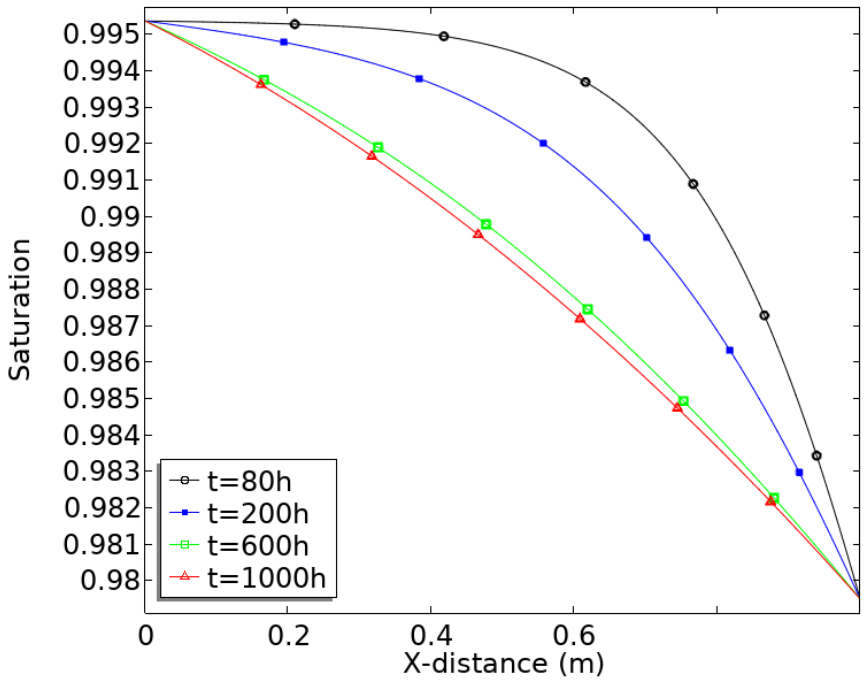

Figure 5. 4 Distribution of saturation (scenario i, ii, iii, iv)

Figure 5.5 shows the horizontal displacements according to the four scenarios at 240 hours and 600 hours. The displacement in scenarios i and iii looks like the "same", and means that dissolution has 'no' contribution to displacement. However, this is because the dissolution rate is so slow that the amount of quartz dissolved within 600 hours is very small. The contribution of dissolution on displacement is very limited, even not in the same magnitude with the contribution of water pressure, so there is no significant influence of dissolution displayed in Figure 5.5. This also explains why the displacement in scenarios ii and iv is the same. Comparing scenarios i and ii, when there is only the influence of swelling, the displacement is significantly decreased, which means that swelling has a negative influence on the consolidation process.

Because water pressure reaches equilibrium around 1000 hours, water pressure or swelling will no longer contribute to the displacement change after 1000 hours. The displacement change after 1000 hours is purely caused by dissolution. In Figure 5.6, at t=2000h, dissolution slightly enlarges the displacement, and at a longer time, the displacement is further enlarged. Considering the conclusion from Figure 5.5, it is clear

that swelling and dissolution have opposite influence on displacement.

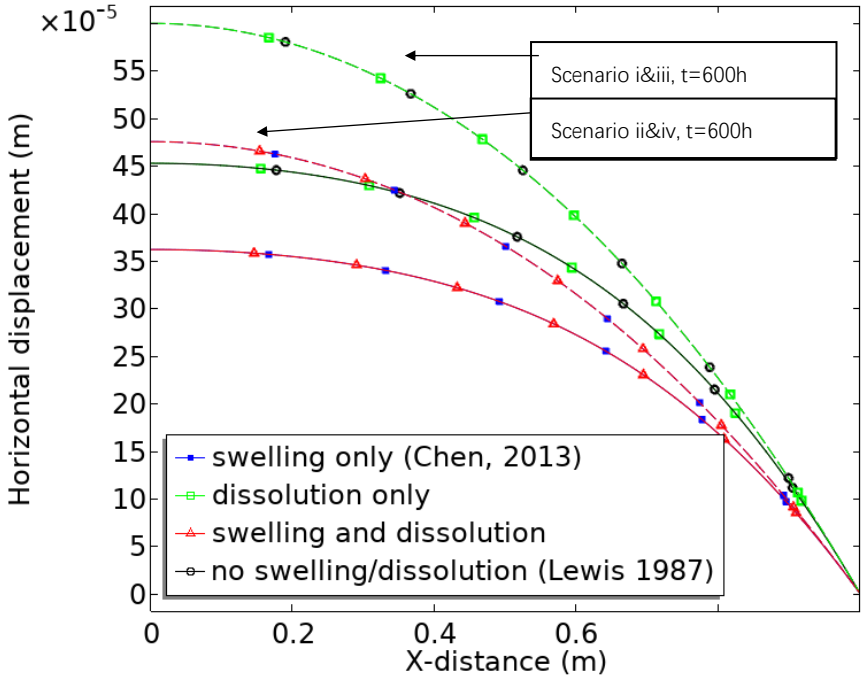

Figure 5. 5 Horizontal displacement (short time)

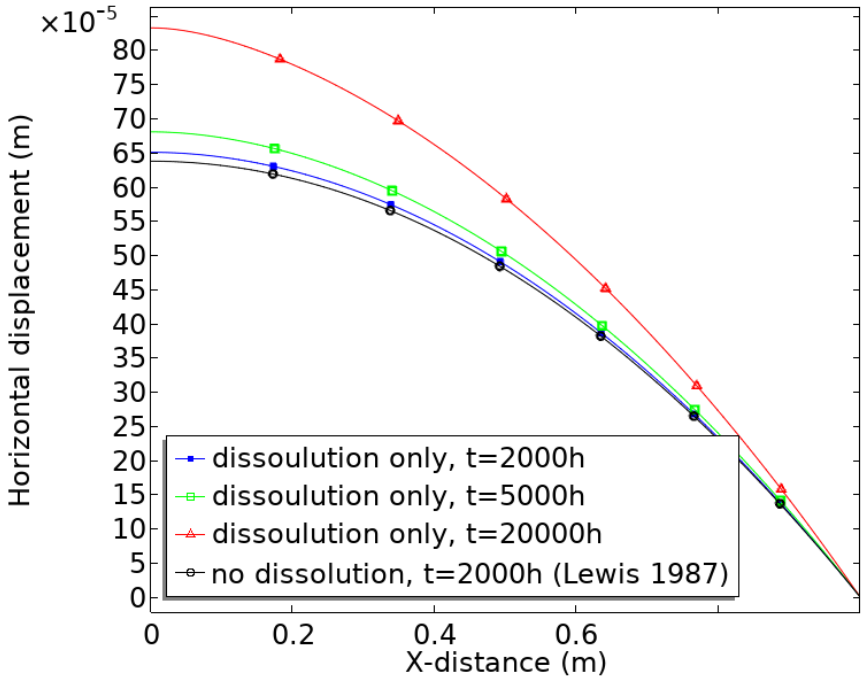

Figure 5. 6 Horizontal displacement (long time)

Figure 5.7 shows the H_2SiO_4 concentration distribution with time and space. In Figure 7 (a), at the early stage, the concentration near boundary A is dominated by diffusion,

whereas the concentration in the domain is dominated by the dissolution of quartz. As time increases, at t=120 hours, the concentration near boundary A exceeds the initial value (0.003 mol/L) due to the combined influence of dissolution and diffusion, however, the concentration in the domain is still dominated by dissolution, because the diffusion toward the right boundary B is slow. Later, the concentration in the domain exceeds the value on left boundary A and the diffusion direction reverse from B to A.

In Figure 5.7 (b), the concentration at point A is higher than the concentration at other points before t=200h. This is because, at the very early stage, the concentration is dominated by diffusion, since point A is closer to the high concentration boundary, the concentration is higher; then as time goes by, the influence of dissolution becomes significant, and the combined influence of dissolution and diffusion makes the concentration at points B increase but not exceed the concentration at point B. 200 hours later, the dissolution process takes the dominate role, resulting in a higher concentration at point B, C, D, E, F. The concentration at points D and E are the same, because these two points are far away from the diffusion source, i.e., the left boundary, therefore, the concentration at these two points is controlled mainly by the dissolution process but the diffusion process has very limited influence. The dissolution reaction here is the same so the concentration is the same. After a sufficiently long time, the concentration at all these points reaches equilibrium but the equilibrium concentration is different, this is because the concentration at A, B C points is controlled by the joint effects of dissolution and diffusion as they are close to the left boundary and the concentration at D, E points are dominated by dissolution only.

Figure 5.8 presents the influence of precipitation on horizontal displacement. Compared with Lewis' research (Lewis and Schrefler, 1987), precipitation and dissolution have opposite influences. This is because, theoretically, precipitation can be viewed as an opposite process of dissolution.

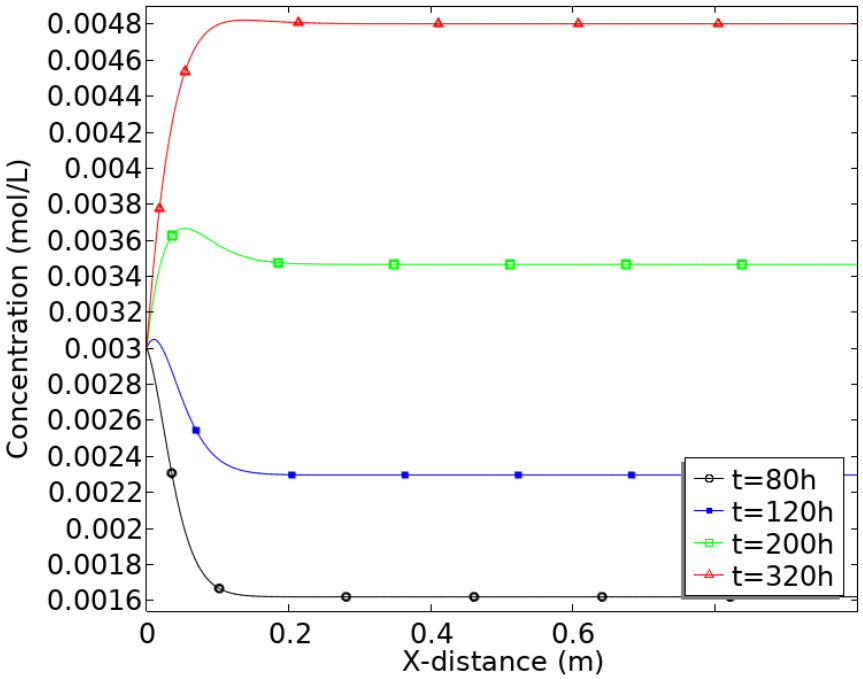

(a) concentration change along the observation line

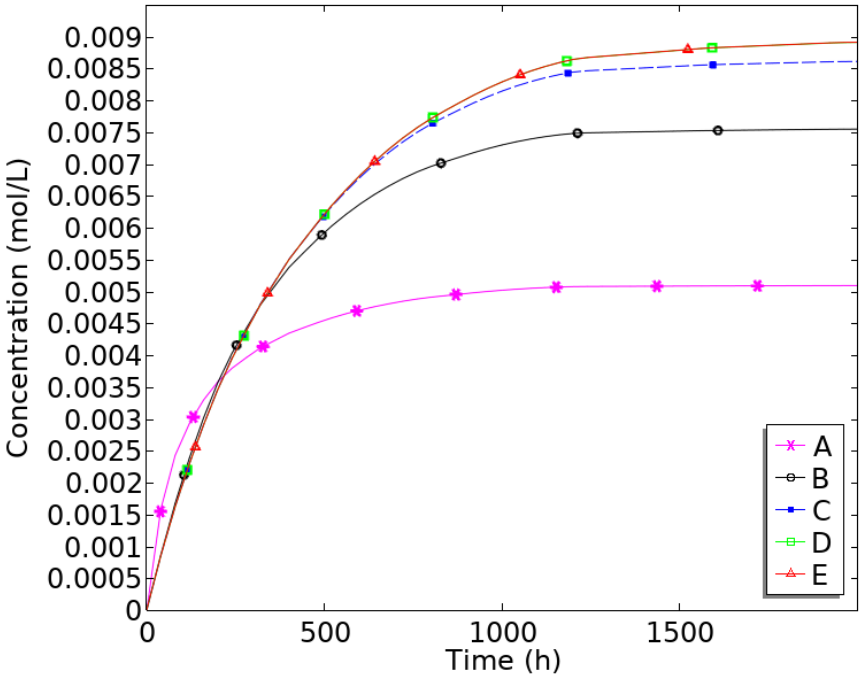

(b) concentration change at the observation points

Figure 5. 7 H_2SiO_4 concentration change with space (a) and time (b)

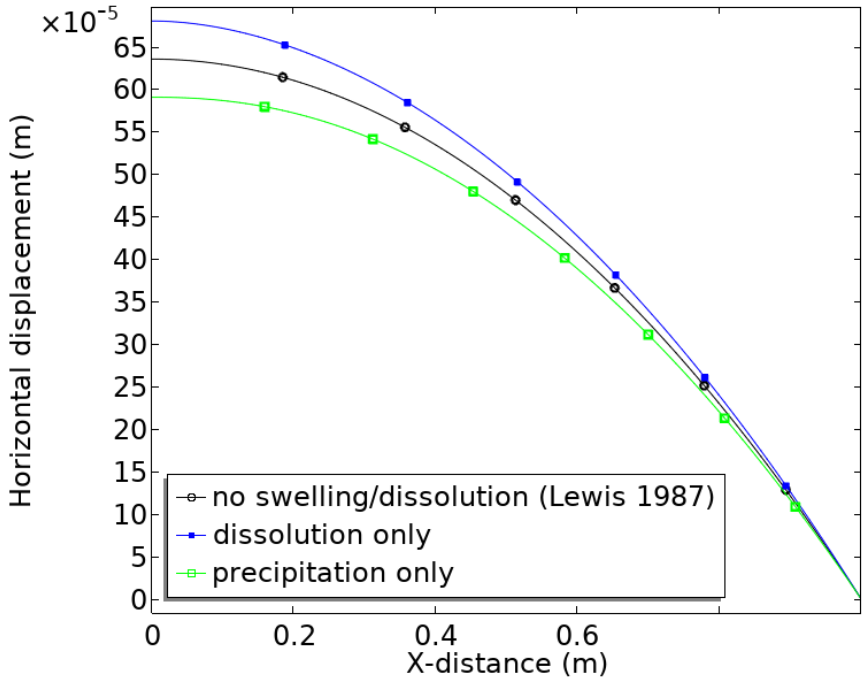

Figure 5. 8 Horizontal displacement at t=5000h (dissolution and precipitation)

5.5.3 2D numerical results

The above 1D numerical simulation presents the influence of swelling and dissolution/precipitation on the mechanical behaviour. In this section, a simple 2D model is presented for engineering applications. The basic parameters and boundaries are the same as the 1D model. The difference is that the pressure at the domain and the left boundary varies linearly from -5MPa to -10MPa, representing the pressure variation in natural situation (Figure 5.9). At the start of the simulation, pressure at the right-hand boundary drops by -5MPa to simulate pressure change caused by engineering disturbance (e.g., excavation).

The displacement distribution is presented in Figure 5.10. From (a) and (b), it can be found that at t=240h, the displacement in the “swelling only” situation is smaller than the displacement in “no swelling/dissolution” situation, which means the swelling process has a negative influence on displacement. From (a) and (c), dissolution has a very small influence on displacement as dissolution is kinetically controlled so that it doesn’t show influence in such a short time. Comparing (c) and (d) at a much longer

time (e.g., 20000 hours), the influence of dissolution becomes much more significant. This reveals the importance of including chemical reactions in the long term analysis for chemical disturbed soils/rocks.

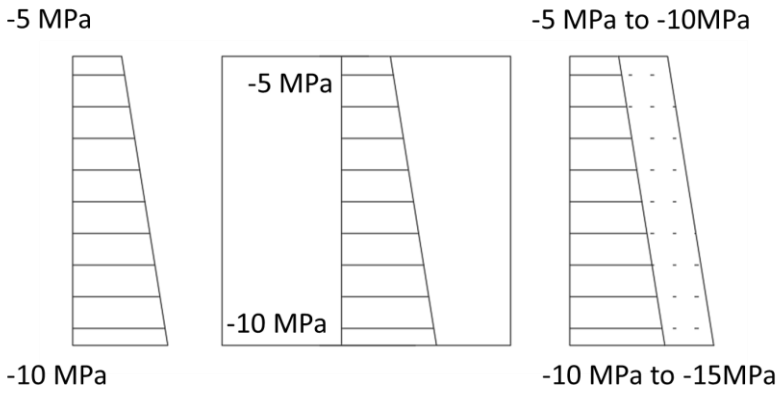

Figure 5. 8 Pressure condition in 2D model

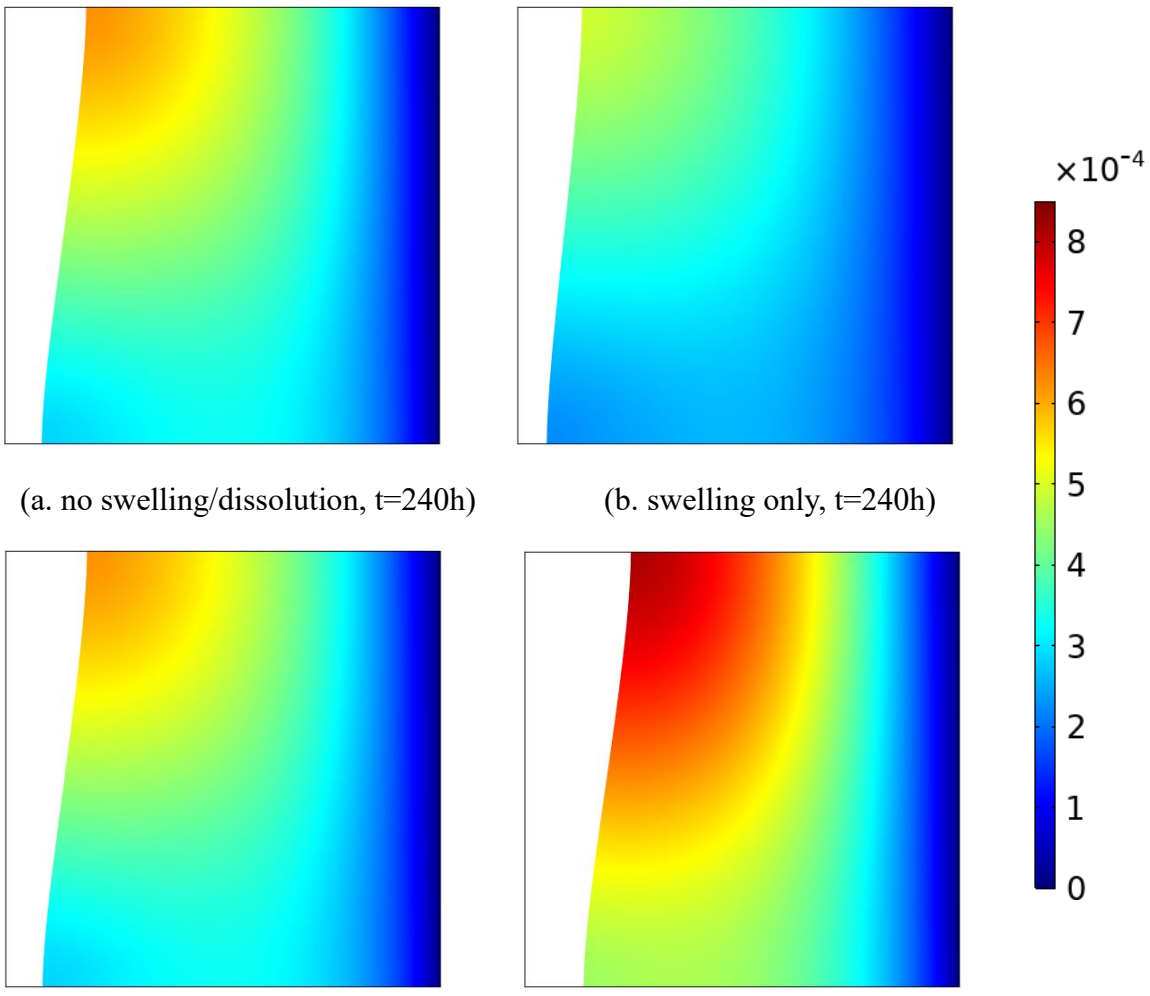

(a. no swelling/dissolution, t=240h)

(b. swelling only, t=240h)

(c. dissolution only, t=240h)

(d. dissolution only, t=20000h)

Figure 5. 9 Horizontal displacement distribution in different situations (unit: m)

5.5.4 Discussion and limitations

This research is a further extension of Biot's theory by incorporating the influence of swelling and dissolution/precipitation. Specific attention is paid to the chemical influence on mechanical behaviour. A group of general fully cross-coupling equations have been obtained as equations (5.37), (5.38), (5.39) and (5.40), and a further simplified equation for small strains is obtained in equation (5.44).

There are a few limitations of this chapter:

Theoretical derivation:

1: The key feature of dissolution is the solid mineral mass change and the corresponding free energy change. However, this feature could not be found in the derivation process, and the dissolution mechanism is hidden. Such a limitation further leads to an imprecise constitutive result, see limitation 2.

2: The dissolution term in the stress-strain equation (5.47) is derived from the reactive term in equation (5.27) and represents the stress caused by the dissolution of the solid mineral. Since equation (5.27) adopts the free energy change of the reaction product instead of that of the reactant, there will always be a $-\omega_r K\dot{m}_r \delta_{ij}$ term in the developed stress-strain relationship. Such a result is imprecise if the reaction occurs between the fluid components without changing the solid mineral, for example, $CO_2 + H_2O \rightarrow H_2CO_3$. In this reaction, no solid mineral is involved, and no stress-strain response generates from the reaction, but the constitutive relationship still contains a $-\omega_r K\dot{m}_r \delta_{ij}$ term.

3. Equation (5.27) indicates that the chemical potential of the free water in the pore space and the bounded water in the interlayer space is the same. This is a rather rough

assumption as the chemical potential of free water and bounded water differs.

4. The water in the interlayer space is strongly bounded by intermolecular force and does not flow. Since the bounded water mass is formerly part of the free pore water mass, it must be the 'sink source' of the free pore water mass. Although the equation for bounded mass has been derived in this chapter, it is not derived as the 'sink source' in the fluid transport equation, this is primarily because the mass density of pore fluid and bounded fluid is not distinguished and the entropy production due to free pore fluid becoming bounded fluid is not considered.

Numerical modelling:

1. As the attention of this paper has been focused on embedding the coupling of swelling and dissolution/precipitation terms into an HMC framework, the change of physical properties (e.g., permeability, bulk modulus) are ignored in the numerical simulation. But all of these physical properties can be incorporated into the final new constitutive equations.

2. The clay-rich sample considered in this research is idealized and is assumed to be homogeneous.

3. The water loss into the clay platelet is ignored. The osmosis phenomenon, induced by chemical components in the pore water, is not considered.

4. The swelling and dissolution/precipitation terms (e.g., $\frac{\omega_s}{S^f \rho_f^w}$, ω_d etc.) need to be determined by further experimental research. Although a theoretical expression for the dissolution coefficient has been derived, experimental validation is still required. The relationship between the stress change and the reaction extent obtained in experiments

can be used to validate the dissolution coefficient. Because reactions may be complex, it is suggested to use a sample and solution that involves only one reaction or one dominant reaction. The swelling coefficient may be obtained through the relationship between the stress change and water pressure change in a swelling test.

5.6 Conclusion

In this chapter, Mixture-Coupling Theory has been extended to derive a new coupled hydro-mechanical-chemical formulation accounting for the complex molecular-scale swelling and dissolution/precipitation interactions. The distributions of pore water pressure, degree of water saturation, and displacement have been analysed using numerical simulations under various scenarios for swelling/dissolution/precipitation. The results demonstrate that the molecular-scale interactions can have a significant influence on the macro-scale physical deformation. This indicates that molecular-scale influence should be sufficiently considered in a design of engineered barriers or a safety analysis of the natural barriers for waste management (e.g., nuclear waste disposal).

This chapter is focused on the theoretical and numerical study, and the swelling and dissolution/precipitation parameters need to be determined by further experimental research.

Chapter 6 Constitutive equations for coupled THMC model with consideration of swelling and dissolution based on Mixture-Coupling Theory

This chapter develops a new coupled Thermo-Hydro-Mechanical-Chemical (THMC) model with swelling and dissolution. It is not only an extension of the HMC model presented in chapter 5 by incorporating the thermal process but also a refinement and improvement of the derivation details discussed in section 5.5.4. The improvement of derivations includes:

1. The mass density in the mixture now has been divided into two parts: the free mass in the pore space and the bounded mass in the interlayer space. This enables rigorous consideration of (1). The mass movement into the interlayer space and the corresponding entropy production; (2). The pore fluid mass loss due to swelling.
2. The entropy production of free pore mass becoming bounded mass is considered, making the derivation more rigorous. This consideration, together with the above one, also brings a more precise description of the Helmholtz free energy of the mixture.
3. More detailed chemical reaction formula is considered.
4. The entropy production due to chemical reaction is quantified and employed in the derivation, and the reaction extent is adopted as a variable in the mechanical equation.
5. A new concept, solid affinity, is defined. This enables a deeper understanding of the free energy change in a reactive dissolution/precipitation process.
6. The dissolution/precipitation influence on porosity change is derived and quantified and incorporated into the fluid/chemical transport equation.
7. The bounded fluid mass is derived as a sink term in the fluid and chemical transport equation. It is also presented in the thermal transport equation to represent the influence of bounded mass on thermal transport.

6.1 Basic consideration

6.1.1 Swelling and density

As swelling is the result of fluid absorbed into the interlayers of clay, the fluid in the mixture system can be divided into two parts: the free fluid in the pore space and bounded fluid in the interlayer space, so, for the density of any fluid component, there is a relationship

$$\rho^{\beta} = \rho_{pore}^{\beta} + \rho_{bound}^{\beta} \tag{6.1}$$

in which ρ^{β}, ρ_{pore}^{β} and ρ_{bound}^{β} are the mixture density of overall fluid component β, pore fluid component β and bounded fluid component β. β represent the fluid component, when $\beta = f$, it represents the fluid as a whole.

From the density relationship, the mixture density of the pore fluid component ρ_{pore}^{β} is related to the phase density of the pore fluid component ρ_{f}^{β} through

$$\rho_{pore}^{\beta} = \phi S^{f} \rho_{f}^{\beta} \tag{6.2}$$

in which ϕ is the porosity, S^{f} is the saturation of pore fluid.

6.1.2 dissolution and reaction extent

For reactive dissolution/ precipitation, a general chemical reaction is considered as

$$\underset{solid}{\nu_A A} + \underset{fluid}{\nu_B B} \rightarrow \underset{fluid}{\nu_C C} + \underset{solid}{\nu_D D} \tag{6.3}$$

in which ν_A, ν_B, ν_C, ν_D are stoichiometric coefficients for reactants A, B and products C, D. Equation (6.3) describes a reactive process that involves the dissolution of mineral A, consumption of fluid component B, generation of fluid component C and precipitation of mineral D. It is easy to include more reactants or products in the reaction, but only limited items are listed for clarity and simplicity.

Let ξ be the extension of reaction. The change in the number of moles per unit mixture volume is

$$\frac{dn^A}{V} = -\nu_A d\xi \ , \ \frac{dn^B}{V} = -\nu_B d\xi \ , \frac{dn^C}{V} = \nu_C d\xi \ , \ \frac{dn^D}{V} = \nu_D d\xi \tag{6.4}$$

6.1.3 Flux

Since a part of fluid is bounded in the interlayer, only the pore fluid can flow out through the boundary, so the flux should be defined for the free pore fluid, instead of the overall fluid or bounded fluid.

$$\mathbf{I}^\beta = \rho_{pore}^\beta \left(\mathbf{v}^\beta - \mathbf{v}^s \right) \tag{6.5}$$

in which $\mathbf{v}^\beta$, $\mathbf{v}^s$ are the velocity of pore fluid component β and the solid.

The total pore-fluid mixture density is

$$\rho_{pore}^f = \sum \rho_{pore}^\beta \tag{6.6}$$

and the barycentric velocity of the fluids can be defined as

$$\mathbf{v}^f = \sum \left(\rho_{pore}^\beta / \rho_{pore}^f \right) \mathbf{v}^\beta \tag{6.7}$$

The diffusion flux of the chemical, which is relative to the barycentric motion, can be written as

$$\mathbf{J}^\beta = \rho_{pore}^\beta \left(\mathbf{v}^\beta - \mathbf{v}^f \right) \tag{6.8}$$

by introducing the equation (6.5), the relationship between $\mathbf{J}^\beta$ and $\mathbf{I}^\beta$ can be obtained as

$$\mathbf{J}^\beta = \mathbf{I}^\beta - \rho_{pore}^\beta \left(\mathbf{v}^f - \mathbf{v}^s \right) \tag{6.9}$$

If sum up all fluid components, with the help of equation (6.5), it is easy to find

$$\sum \mathbf{J}^\beta = 0 \tag{6.10}$$

The Darcy velocity for the unsaturated condition is described as

$$\mathbf{u}^{\beta} = S^{f}\phi\left(\mathbf{v}^{\beta} - \mathbf{v}^{s}\right) \tag{6.11}$$

6.2 Balance equations and entropy production

6.2.1 Mass balance equation

The mass balance equations in chapters 3, 4 and 5 are written for the overall fluid without distinguishing the pore fluid and bounded fluid. In this chapter, the balance equation is written for the pore fluid only, enabling one to set the bounded mass as the 'sink term' for the pore fluid and consider the entropy production due to pore mass becoming bounded mass.

For the free mass in the pore space, since some can be absorbed into the interlayers, some can be generated by the reaction, the mass balance for the fluid component β can be written as

$$\frac{D}{Dt}\left(\int_{V}\rho_{pore}^{\beta}dV\right) = -\int_{S}\mathbf{I}^{\beta}\cdot\mathbf{n}dS - \int_{V}\dot{\rho}_{ex}^{\beta}dV + \int_{V}\chi\nu_{\beta}M^{\beta}\dot{\xi}dV \tag{6.12}$$

where ρ_{ex}^{β} is the mass density of fluid component β that entered into the interlayer space; $\chi = -1$ for the reactant, $\chi = 1$ for the product and $\chi = 0$ if β does not join the reaction.

The balance for bounded mass is

$$\frac{D}{Dt}\left(\int_{V}\rho_{bound}^{\beta}dV\right) = \int_{V}\dot{\rho}_{ex}^{\beta}dV \tag{6.13}$$

Because the only source for bounded fluid is the fluid from the pore space, there must be

$$\dot{\rho}_{bound}^{\beta} = \dot{\rho}_{ex}^{\beta} \tag{6.14}$$

The time derivation form for equation (6.12) is

$$\dot{\rho}_{pore}^{\beta} + \rho_{pore}^{\beta}\nabla\cdot\mathbf{v}^{s} + \nabla\cdot\mathbf{I}^{\beta} + \dot{\rho}_{ex}^{\beta} = \chi\nu_{\beta}M^{\beta}\dot{\xi} \tag{6.15}$$

6.2.2 Heat balance equation

The heat change considered in the mixture system is only the influx and efflux of thermal flow across the boundary. Although the chemical reaction can release or absorb some heat, the amount is normally very limited and has very feebly influence, so it is not considered.

The total thermal flow $\mathbf{q}$ can be divided into two parts: the heat flow carried by the pore fluid $\mathbf{q}^f$, and the reduced heat flow $\mathbf{q}'$, which is the difference between the total heat flow and the heat flow caused by fluid (Katchalsky and Curran, 1965).

$$\mathbf{q} = \mathbf{q}' + \mathbf{q}^f \tag{6.16}$$

The heat flow carried by the fluid can be expressed as:

$$\mathbf{q}^f = \sum h^\beta \mathbf{I}^\beta = h^f \mathbf{I}^f \tag{6.17}$$

where h^β is the enthalpy of β th fluid component.

The balance equation for the heat of the mixture system can be written as

$$\frac{D}{Dt}\int_V \left(q^s + q^f_{pore} + q^f_{bound}\right)dV = -\int_S \mathbf{q}' \cdot \mathbf{n}dS - \int_S h^f \mathbf{I}^f \cdot \mathbf{n}dS \tag{6.18}$$

in which q^s, q^f_{pore}, q^f_{bound} are the heat mixture density of the solid, pore fluid and bounded fluid, they are defined as

$$q^s = \rho^s C^s T \ , \ q^f_{pore} = \rho^f_{pore} C^f T \tag{6.19}$$

where C^s, C^f are the specific heat capacities of solid and pore fluid. The fluid heat capacity C^f can be determined by experiments or estimated through

$$C^f = \sum w^\beta C^\beta \tag{6.20}$$

in which w^β, C^β are the mass fraction and specific heat capacity of pore fluid component β.

It should be noted that the fluid in the interlayer can feel the change of temperature so

that the heat density of the bounded mass changes with temperature, this is why equation (6.18) contains q^f_{bound} .

The time derivation of the heat balance equation (6.18) is

$$\left(q^s + q^f_{pore} + q^f_{bound}\right)^{\cdot} + \left(q^s + q^f_{pore} + q^f_{bound}\right)\nabla \cdot \mathbf{v}^s + \nabla \cdot \mathbf{q}' + \nabla \cdot h^f \mathbf{I}^f = 0 \qquad (6.21)$$

This equation shows that the heat change of the mixture system, including the solid, pore fluid ad bound fluid, equals to the heat leaves the system by conduction and fluid convection.

6.2.3 Internal energy balance equation

The internal energy balance equation for the mixture system can be written as

$$\frac{D}{Dt}\int_V \varepsilon dV = \int_V \left(\boldsymbol{\sigma}\mathbf{v}_s - \mathbf{q}'\right)\cdot \mathbf{n} dV - \sum \int_S h^\beta \mathbf{I}^\beta \cdot \mathbf{n} dS \qquad (6.22)$$

where ε is the internal energy density, $\boldsymbol{\sigma}$ is the Cauchy stress tensor.

The derivative version of the balance equation (6.22) is

$$\dot{\varepsilon} + \varepsilon \nabla \cdot \mathbf{v}^s - \nabla \cdot \left(\boldsymbol{\sigma}\mathbf{v}^s\right) + \nabla \cdot \mathbf{q}' + \nabla \cdot \sum h^\beta \mathbf{I}^\beta = 0 \qquad (6.23)$$

6.2.4 Entropy balance equation

In an irreversible process, the entropy change combines two parts: the entropy exchange with surroundings and the entropy produced irreversibly. The entropy balance equation can be written as (Katchalsky and Curran, 1965)

$$\frac{D}{Dt}\int_V \left(\eta^s + \eta^f_{pore} + \eta^f_{bound}\right) dV = -\int_S \mathbf{I}_\eta \cdot \mathbf{n} dS + \int_V \gamma dV \qquad (6.24)$$

where η^s, η^f_{pore}, η^f_{bound} are the entropy mixture density of the solid matrix, pore fluid and bounded fluid, respectively. $\mathbf{I}_\eta$ is the entropy flow exchange with the surroundings and γ is entropy produced irreversibly.

If only considering the influx and efflux of thermal flow, the expression of $\mathbf{I}_\eta$ can be written as

$$\mathbf{I}_\eta = \frac{\mathbf{q} - \sum \mu^\beta \mathbf{I}^\beta}{T} = \frac{\mathbf{q}'}{T} + \sum \eta^\beta \mathbf{I}^\beta \tag{6.25}$$

in which $\mu^\beta = h^\beta - T\eta^\beta$ is the chemical potential of the pore fluid component β.

The time derivation of equation (6.24) following the movement of the solid is

$$\left(\eta^s + \eta^f_{pore} + \eta^f_{bound}\right)^{\cdot} + \left(\eta^s + \eta^f_{pore} + \eta^f_{bound}\right)\nabla \cdot \mathbf{v}^s + \nabla \cdot \mathbf{I}_\eta - \gamma = 0 \tag{6.26}$$

For the sake of simplification, equation (6.26) could be written as

$$\dot{\eta}^{mix} + \eta^{mix}\nabla \cdot \mathbf{v}^s + \nabla \cdot \mathbf{I}_\eta - \gamma = 0 \tag{6.27}$$

where $\eta^{mix} = \eta^s + \eta^f_{pore} + \eta^f_{bound}$ is the entropy density of the solid-fluid mixture.

6.2.5 Helmholtz Free Energy balance equation

From the definition of Helmholtz free energy, for the solid-fluid mixture system, there must be

$$\frac{D}{Dt}\int_V \psi dV = \frac{D}{Dt}\int_V \varepsilon dV - \frac{D}{Dt}\int_V \left[T\left(\eta^s + \eta^f_{pore} + \eta^f_{bound}\right)\right] dV \tag{6.28}$$

where ψ is the Helmholtz free energy density of the solid-fluid mixture system.

So that with equation (6.24), (6.25) ,(6.26) and (6.27), the local version of equation (6.28) is

$$\dot{\psi} + \psi\nabla \cdot \mathbf{v}^s = \nabla \cdot (\boldsymbol{\sigma}\mathbf{v}^s) - \nabla \cdot \mathbf{q}' - \nabla \cdot \sum h^\beta \mathbf{I}^\beta - \left(\dot{T} + T\nabla \cdot \mathbf{v}^s\right)\eta^{mix} + T\nabla \cdot \mathbf{I}_\eta - T\gamma \tag{6.29}$$

6.3.6 Dissipative progress and entropy production

The entropy change of the system could be categorized as (1) the entropy production generated by fluid passing through the solid matrix; (2) the entropy production generated by free pore fluid becoming bounded fluid; (3) the dispassion of heat; (4) the entropy production caused by chemical reaction. The first, third and the fourth entropy

production can be obtained by using non-equilibrium thermodynamics (Katchalsky and Curran, 1965) and the second entropy production can refer to the result of Loret (Loret et al., 2002). The overall entropy production is

$$0 \le T\gamma = -\mathbf{I}_\eta \cdot \nabla T - \sum \mathbf{I}^\beta \cdot \nabla \mu^\beta + \left(\mu^\beta - \mu^\beta_{bound}\right)\dot{\rho}^\beta_{ex} + A\dot{\xi} \tag{6.30}$$

where μ^β, μ^β_{bound} are the chemical potential of pore fluid component and bounded fluid component.

In equation (6.30), the terms on the right hand of the equality are:

1: $-\mathbf{I}_\eta \cdot \nabla T = -\left(\frac{\mathbf{q} - \sum \mu^\beta \mathbf{I}^\beta}{T}\right)\cdot \nabla T = -\left(\frac{\mathbf{q}'}{T} + \sum \eta^\beta \mathbf{I}^\beta\right)\cdot \nabla T$, the entropy production caused by heat exchange, including heat by convection and heat by advection;

2: $-\sum \mathbf{I}^\beta \cdot \nabla \mu^\beta$, the entropy production caused by fluid flow, which includes the entropy by the fraction when pore fluid passes through the solid;

3: $\left(\mu^\beta - \mu^\beta_{bound}\right)\dot{\rho}^\beta_{ex}$, the entropy production generated when the free pore fluid entering into the interlayer space and becoming bounded fluid;

4: $A\dot{\xi}$, the entropy production caused by the chemical reaction.

The affinity A of the reaction is defined as $A = -\sum \nu_\beta \mu_t^\beta$ (Kondepudi and Prigogine, 2014)

$$A = \nu_A \mu_t^A + \nu_B \mu_t^B - \nu_C \mu_t^C - \nu_D \mu_t^D \tag{6.31}$$

where μ_t^β is the 'true' chemical potential, which is the potential that widely used in most chemical research, it is related to the chemical potential used in this thesis through:

$$\mu^\beta = \frac{\mu_t^\beta}{M_\beta} \tag{6.32}$$

With equation (6.32), the equation of affinity becomes

$$A = \nu_A M^A \mu^A + \nu_B M^B \mu^B - \nu_C M^C \mu^C - \nu_D M^D \mu^D \tag{6.33}$$

6.4 State equations for swelling/dissolution

This chapter deals with the state equations for swelling/dissolution. First, the free energy density of the pore space is analyzed by using classical thermodynamics. Then, the free energy density of the mixture system is obtained by non-equilibrium thermodynamics and continuum mechanics. Finally, the free energy of the wetted mineral matrix is obtained.

6.4.1 Helmholtz free energy density of pore space

From classical thermodynamics, the free energy density of the pore space ψ_{pore} is

$$\psi_{pore} = -\overline{p} + S^f \sum \rho_f^\beta \mu^\beta \tag{6.34}$$

where $\overline{p} = S^f p^f$ is the average pore pressure, p^f is the pore fluid pressure.

The time derivation of equation (6.34) is:

$$\dot{\psi}_{pore} = -\dot{\overline{p}} + \dot{S}^f \sum \rho_f^\beta \mu^\beta + S^f \sum \dot{\rho}_f^\beta \mu^\beta + S^f \sum \rho_f^\beta \dot{\mu}^\beta \tag{6.35}$$

According to the Gibbs-Duhem equation, for the pore fluid, there is

$$\dot{\overline{p}} = S^f \eta_f^f \dot{T} + S^f \sum \rho_f^\beta \dot{\mu}^\beta \tag{6.36}$$

where η_f^f is the phase density of pore fluid entropy, it is the summary of entropy of all fluid components, i.e. $\eta_f^f = \sum \eta_f^\beta$.

Substituting (6.36) into (6.35) leads to

$$\dot{\psi}_{pore} = -S^f \eta_f^f \dot{T} + S^f \sum \dot{\rho}_f^\beta \mu^\beta + \dot{S}^f \sum \rho_f^\beta \mu^\beta \tag{6.37}$$

6.4.2 Helmholtz free energy density of the mixture system

Assume that the rock maintains mechanical equilibrium so that $\nabla \cdot \boldsymbol{\sigma} = \mathbf{0}$. With the entropy production (6.30) and balance equation (6.29), the equation for the free energy ψ is

$$\dot{\psi}+\psi\nabla\cdot\mathbf{v}^{s}-\left(\boldsymbol{\sigma}:\nabla\mathbf{v}^{s}\right)+\sum\mu^{\beta}\nabla\cdot\mathbf{I}^{\beta}+\left(\dot{T}+T\nabla\cdot\mathbf{v}^{s}\right)\eta^{mix}+\sum\left(\mu^{\beta}-\mu_{bound}^{\beta}\right)\dot{\rho}_{ex}^{\beta}+A\dot{\xi}=0 \tag{6.38}$$

Recalling the continuum mechanics in chapter 3, from equation (6.38), it leads to the Helmholtz free energy density in the reference configuration as

$$\dot{\Psi}=tr\left(\mathbf{T}\dot{\mathbf{E}}\right)+\sum\mu^{\beta}\dot{m}_{pore}^{\beta}+\sum\mu_{bound}^{\beta}\dot{m}_{bound}^{\beta}+\mu^{B}\nu_{B}M^{B}\dot{\xi}-\mu^{C}\nu_{C}M^{C}\dot{\xi}-A\dot{\xi}-\mathrm{H}^{mix}\dot{T} \tag{6.39}$$

in which

$$\Psi=J\psi\,,\ m_{pore}^{\beta}=J\rho_{pore}^{\beta}\ ,m_{bound}^{\beta}=J\rho_{bound}^{\beta}\,,\ \mathrm{H}^{mix}=J\eta^{mix} \tag{6.40}$$

Ψ is the free energy in the reference configuration and m_{pore}^{β}, m_{bound}^{β} are the mass mixture density of the pore fluid component β and bounded fluid component β in the reference configuration; H^{mix} is the entropy density of the mixture in the reference configuration.

Invoking the affinity equation (6.33), equation (6.39) becomes

$$\dot{\Psi}=tr\left(\mathbf{T}\dot{\mathbf{E}}\right)+\sum\mu^{\beta}\dot{m}_{pore}^{\beta}+\sum\mu_{bound}^{\beta}\dot{m}_{bound}^{\beta}-\nu_{A}M^{A}\mu^{A}\dot{\xi}+\nu_{D}M^{D}\mu^{D}\dot{\xi}-\mathrm{H}^{mix}\dot{T} \tag{6.41}$$

Similar to the definition of affinity, a new concept A_s is defined as the 'solid affinity' to represent the affinity of the solid part in the reaction, written as

$$A_{s}=\nu_{A}M^{A}\mu^{A}-\nu_{D}M^{D}\mu^{D} \tag{6.42}$$

Then, equation (6.41) can be written as

$$\dot{\Psi}=tr\left(\mathbf{T}\dot{\mathbf{E}}\right)+\sum\mu^{\beta}\dot{m}_{pore}^{\beta}+\sum\mu_{bound}^{\beta}\dot{m}_{bound}^{\beta}-A_{s}\dot{\xi}-\mathrm{H}^{mix}\dot{T} \tag{6.43}$$

In equation (6.43), the term $-A_s\dot{\xi}$ represents the Helmholtz free energy change of the solid mineral due to reactive dissolution/precipitation. If the chemical reaction happens only within the fluids without changing the solid, A_s vanishes, and the free energy of the system will not be changed by the reaction. The terms $\mu^{\beta}\dot{m}_{pore}^{\beta}$, $\mu_{bound}^{\beta}\dot{m}_{bound}^{\beta}$ represent the free energy of the pore mass and bounded mass, respectively. They are associated with different chemical potentials, which is different from the equal chemical

potential assumption in equation (5.27). The different chemical potentials for free pore mass and bounded mass give a more precise description of the free energy change during a swelling process, which is more advanced than the equal chemical potential of pore mass and bounded mass in literature (Heidug and Wong, 1996, Roshan and Oeser, 2012, Gao et al., 2021).

6.4.3 Free energy density of the wetted matrix

As fluid has been absorbed into the solid matrix, the free energy of the wetted matrix includes the free energy of the matrix and the free energy of the bounded fluid. This can be obtained by subtracting the contribution of pore fluid free energy $\phi\psi_{pore}$ from the free energy of the mixture system Ψ.

With equation (6.39), (6.37) and (6.34), the free energy of the wetted matrix can be obtained as

$$(\Psi - J\phi\psi_{pore})^{\cdot} = tr\left(\mathbf{T}\dot{\mathbf{E}}\right) + \bar{p}\dot{\upsilon} + \sum \mu^{\beta}_{bound}\dot{m}^{\beta}_{bound} - A_s\dot{\xi} - \mathrm{H}^{wet}\dot{T} \tag{6.44}$$

where $\mathrm{H}^{wet} = \mathrm{H}^{mix} - \mathrm{H}^{f} = \mathrm{H}^{s} + \mathrm{H}^{f}_{bound} = J\eta^{wet}$ is the entropy density of the wetted matrix in the reference configuration, $\upsilon = J\phi$ is the pore volume fraction per unit referential volume.

For the reason of convenience, the dual potential (deformation energy) can be expressed as

$$W = \left(\Psi - J\phi^{w}\psi_{pore}\right) - \bar{p}\upsilon - \sum \mu^{\beta}_{bound}m^{\beta}_{bound} \tag{6.45}$$

where W is a function of $\mathbf{E}$, $\bar{p}$, μ^{β}_{bound}, ξ, T.

From Equation (6.44), there is

$$\dot{W}\left(\mathbf{E}, \bar{p}, \mu^{\beta}_{bound}, \xi, T\right) = tr\left(\mathbf{T}\dot{\mathbf{E}}\right) - \upsilon\dot{\bar{p}} - \sum m^{\beta}_{bound}\dot{\mu}^{\beta}_{bound} - A_s\dot{\xi} - \mathrm{H}^{wet}\dot{T} \tag{6.46}$$

Equation (6.46) must have

$$\dot{W}\left(\mathbf{E},\bar{p},\mu_{bound}^{\beta},\xi,T\right)=\left(\frac{\partial W}{\partial E_{ij}}\right)_{\bar{p},\mu_{bound}^{\beta},\xi}\dot{E}_{ij}+\left(\frac{\partial W}{\partial \bar{p}}\right)_{E_{ij},\mu_{bound}^{\beta},\xi}\dot{\bar{p}}$$
$$+\sum\left(\frac{\partial W}{\partial \mu_{bound}^{\beta}}\right)_{E_{ij},\bar{p},\xi}\dot{\mu}_{bound}^{\beta}+\left(\frac{\partial W}{\partial m_r}\right)_{E_{ij},\bar{p},\mu_{bound}^{\beta}}\dot{\xi}+\left(\frac{\partial W}{\partial T}\right)_{E_{ij},\bar{p},\mu_{bound}^{\beta}}\dot{T} \tag{6.47}$$

in which

$$T_{ij}=\left(\frac{\partial W}{\partial E_{ij}}\right)_{\bar{p},\mu^{w},\xi},\ \upsilon=-\left(\frac{\partial W}{\partial \bar{p}}\right)_{E_{ij},\mu^{w},\xi},\ m_{bound}^{\beta}=-\left(\frac{\partial W}{\partial \mu_{bound}^{\beta}}\right)_{E_{ij},\bar{p},\xi},$$
$$\mu^{c}=-\left(\frac{\partial W}{\partial \xi}\right)_{E_{ij},\bar{p},\mu^{w}},\ \mathrm{H}^{wet}=-\left(\frac{\partial W}{\partial T}\right)_{E_{ij},\bar{p},\mu_{bound}^{\beta}} \tag{6.48}$$

If equation (6.46) is differentiated with respect to time, the fundamental constitutive equations for the evolution of stress, pore volume fraction, the mass densities of the bound component, the solid affinity and the entropy of the wetted matrix can be obtained

$$\dot{T}_{ij}=L_{ijkl}\dot{E}_{kl}-M_{ij}\dot{\bar{p}}+\sum S_{ij}^{\beta}\dot{\mu}_{bound}^{\beta}-H_{ij}\dot{\xi}-F_{ij}\dot{T} \tag{6.49}$$

$$\dot{\upsilon}=M_{ij}\dot{E}_{ij}+Q\dot{\bar{p}}+\sum B^{\beta}\dot{\mu}_{bound}^{\beta}+D\dot{\xi}+N\dot{T} \tag{6.50}$$

$$\dot{m}_{bound}^{\beta}=-S_{ij}^{\beta}\dot{E}_{ij}+B^{\beta}\dot{\bar{p}}+Z^{\beta}\dot{\mu}_{bound}^{\beta}+X^{\beta}\dot{\xi}+R^{\beta}\dot{T} \tag{6.51}$$

$$\dot{A}_{\mathrm{s}}=F_{ij}\dot{E}_{ij}+N\dot{\bar{p}}+\sum R^{\beta}\dot{\mu}_{bound}^{\beta}+W\dot{\xi}+C\dot{T} \tag{6.52}$$

$$\dot{\mathrm{H}}^{wet}=H_{ij}\dot{E}_{ij}+D\dot{\bar{p}}+\sum R^{\beta}\dot{\mu}_{bound}^{\beta}+C\dot{\xi}+V\dot{T} \tag{6.53}$$

As the thesis introduces the solid affinity A_{s} to describe the Helmholtz free energy change by dissolution/precipitation, the cross-coupling group equations (6.49)-(6.53) are different from other research (e.g. Haxaire and Djeran-Maigre (2009), Karrech (2013), Zhang and Zhong (2017a)) in that equation (6.52) presents the solid affinity change instead of the overall affinity change.

6.5 Coupled field equation

6.5.1 Solid phase

Equation (6.49) represents the evolution of the Piola-Kirchhoff stress T_{ij}, volume fraction υ, mass density of bounded fluid component m^{β}_{bound}, solid affinity A_s and entropy of the wetted matrix H^{wet} with selected variables $\mathbf{E}, \bar{p}, \mu^{\beta}_{bound}, \xi, T$.

Since equation (6.49) is rather general, to obtain the governing equations, the mechanical behaviour of the clay/rock is restrained to be in small condition and isotropic, so that the Green Strain tensor E_{ij} and the Piola-Kirchhoff stress can be substituted by strain tensor ε_{ij} and Cauchy stress σ_{ij}, and the coefficients L_{ijkl}, M_{ij}, S^{β}_{ij}, F_{ij} are assumed to be diagonal and can be written with a scalar coefficient and Kronecker delta δ_{ij}.

The coefficients are then written as

$$M_{ij} = \zeta\delta_{ij},\ S^{\beta}_{ij} = \omega^{\beta}_{s}\delta_{ij},\ H_{ij} = \omega_{R}\delta_{ij},\ F_{ij} = \omega_{T}\delta_{ij} \tag{6.54}$$

If only consider the elastic deformation of rock, then, the stiffness L_{ijkl} can be written in a form of a fourth-order isotropic tensor

$$L_{ijkl} = G\left(\delta_{ik}\delta_{jl} + \delta_{il}\delta_{jk}\right) + \left(K - \frac{2G}{3}\right)\delta_{ij}\delta_{kl} \tag{6.55}$$

where G, K are the shear modulus and bulk modulus.

Based on the assumption and relationships in equation (6.54) and (6.55), equation (6.49) becomes

$$\dot{\sigma}_{ij} = \left(K - \frac{2G}{3} \right) \dot{\varepsilon}_{kk} \delta_{ij} + 2G\dot{\varepsilon}_{ij} - \zeta \dot{\bar{p}} \delta_{ij} + \sum \omega_s^{\beta} \dot{\mu}_{bound}^{\beta} \delta_{ij} - \omega_R \dot{\xi} \delta_{ij} - \omega_T \dot{T} \delta_{ij} \quad (6.56)$$

in which $\omega_T = K\alpha_s$ and α_s is the thermal expansion coefficient. The swelling coefficient ω_s^{β} is introduced to represent the influence of the bounded fluid component β on the mechanical behaviour. The value or expression of ω_s^{β} requires experimental determination or further theoretical investigation. The term $\dot{\xi}$ is introduced into the stress equation to represent the stress caused by chemical dissolution/precipitation.

From the discussion in chapter 5, equation (6.56) can be rewritten as (for dissolution only)

$$\dot{\sigma}_{ij} = \left(K - \frac{2G}{3} \right) \dot{\varepsilon}_{kk} \delta_{ij} + 2G\dot{\varepsilon}_{ij} - \zeta \dot{\bar{p}} \delta_{ij} + \sum \omega_s^{\beta} \dot{\mu}_{bound}^{\beta} \delta_{ij} - \omega_d K \dot{\xi} \delta_{ij} - \alpha_s K \dot{T} \delta_{ij} \quad (6.57)$$

where ω_d is the dissolution coefficient. Equation (6.57) is for dissolution case only, if considering precipitation, the coefficient ω_d can be substituted by other expressions.

6.5.2 Porosity

Equation (6.50) illustrates the dependence of porosity on Green Strain tensor E_{ij}, average pore pressure $\bar{p}$, chemical potential μ_{bound}^{β}, reaction extent ξ and temperature T. From the results in section 6.5.1 and chapter 5, equation (6.50) can be written as

$$\dot{\upsilon} = \zeta \dot{\varepsilon}_{ii} + Q\dot{\bar{p}} + \sum B^{\beta} \dot{\mu}_{bound}^{\beta} + D\dot{\xi} + N\dot{T} \quad (6.58)$$

The expressions for the coefficients are

$$Q = (1/K_s)(\zeta - \phi), \; B^{\beta} = (1/K)(\zeta - 1)\omega_s^{\beta}, \; N = (\phi - \zeta)\alpha_s \quad (6.59)$$

$$D = \begin{cases} \nu_A M_A / \rho_t^A & \textit{dissolution only} \\ -\nu_D M_D / \rho_t^D & \textit{precipitation only} \\ \nu_A M_A / \rho_t^A - \nu_D M_D / \rho_t^D & \textit{dissolution and precipitation} \end{cases} \quad (6.60)$$

where M_A/ρ_t^A, M_D/ρ_t^D are the molar volume of mineral A and D, respectively.

6.5.3 Bounded mass

Equation (6.51) gives the evolution of bounded mass with associated variables of stress, average pore pressure, chemical potential of bounded mass, reaction extent and temperature. From the assumptions and discussions in section 6.5.1 and 6.5.2, the bounded mass density can be simplified to:

$$\dot{m}_{bound}^{\beta} = -\omega_s^{\beta}\dot{\varepsilon}_{ij} + B^{\beta}\dot{\bar{p}} + Z^{\beta}\dot{\mu}_{bound}^{\beta} + X^{\beta}\dot{\xi} + R^{\beta}\dot{T} \tag{6.61}$$

With $B^{\beta} = (1/K)(\zeta - 1)\omega_s^{\beta}$.

The coefficients Z^{β}, X^{β}, R^{β} are undetermined in this thesis, which requires further exploration.

6.5.3 Fluid phase

The balance equation for the fluid as a whole is

$$\frac{D}{Dt}\left(\int_V \rho_{pore} dV\right) = -\sum\int_S \mathbf{I}^{\beta}\cdot\mathbf{n}dS - \sum\int_V \dot{\rho}_{bound}^{\beta} dV + \sum\int_{\Omega} \chi \nu_{\beta} M^{\beta}\dot{\xi} d\Omega \tag{6.62}$$

Because β represents fluid only, therefore the reaction term in equation (6.62) accounts for the reactant B and product C only.

The time derivation of equation (6.62) is

$$\dot{\rho}_{pore} + \rho_{pore}\nabla\cdot\mathbf{v}^s + \sum\nabla\cdot\mathbf{I}^{\beta} + \sum\dot{\rho}_{bound}^{\beta} - \sum\chi\nu_{\beta}M^{\beta}\dot{\xi} = 0 \tag{6.63}$$

From equation (6.63), fluid density equation (6.2), Darcy velocity (6.11), flux equation (6.5) and Euler identity, it leads to

$$\left(\upsilon S^f \rho_f^f\right)^{\cdot} + \nabla\cdot\left(\rho_f^f \mathbf{u}\right) + \sum\dot{m}_{bound}^{\beta} - \sum\chi\nu_{\beta}M^{\beta}\dot{\xi} = 0 \tag{6.64}$$

Expanding the first term in equation (6.64) gives

$$\upsilon\left(S^f\rho_f^f\right)^{\cdot} + S^f\rho_f^f\dot{\upsilon} + \nabla\cdot\left(\rho_f^f\mathbf{u}\right) + \sum\dot{m}_{bound}^{\beta} - \sum\chi\nu_{\beta}M^{\beta}\dot{\xi} = 0 \tag{6.65}$$

The fluid density is a function of pressure and temperature $\rho_f^f = \rho_f^f\left(p^f, T\right)$ (Hosking et al., 2020)

$$\dot{\rho}_f^f(T, p^f) = \rho_f^f\left(\frac{1}{K_f}\dot{p}^f - \alpha_f \dot{T}\right) \tag{66}$$

in which $\frac{1}{K_f} = \frac{1}{\rho_f^f}\left(\frac{\partial \rho_f^f}{\partial p^f}\right)_T$ is the compressibility of the fluid, $\alpha_f = -\frac{1}{\rho_f^f}\left(\frac{\partial \rho_f^f}{\partial T}\right)_{p^f}$ is the thermal expansion coefficient of the pore fluid.

Therefore, the first term in equation (6.65) becomes:

$$\upsilon\left(S^f \rho_f^f\right)^{\cdot} = \rho_f^f\left(C_s + \frac{\phi S^f}{K_f}\right)\dot{p}^f - \upsilon \rho_f^f \alpha_f \dot{T} \tag{6.67}$$

Invoking the porosity change equation (6.58), and with equation (6.67), (66), equation (6.65) becomes

$$\begin{aligned} &\nabla\cdot\left(\rho_f^f \mathbf{u}\right) + S^f \rho_f^f \zeta \dot{\varepsilon}_{ii} + \left[\rho_f^f\left(C_s + \frac{\phi S^f}{K_f}\right) + S^f \rho_f^f Q\left(S^f + \frac{C_s}{\phi} p^f\right)\right]\dot{p}^f \\ &+ S^f \rho_f^f B^\beta \sum \omega_s^\beta \dot{\mu}_{bound}^\beta + \left(S^f \rho_f^f N - \upsilon \rho_f^f \alpha_f\right)\dot{T} + S^f \rho_f^f D\,\dot{\xi} \\ &= -\left(\sum \dot{m}_{bound}^\beta - \sum \chi \nu_\beta M^\beta \dot{\xi}\right) \end{aligned} \tag{6.68}$$

In equation (6.68), if assuming $C_s = 0$, and neglecting the swelling ($\dot{\mu}_{bound}^\beta$ and $\dot{m}_{bound}^\beta$) and dissolution terms ($\dot{\xi}$), the equation will reduce to

$$\begin{aligned} &\nabla\cdot\left(\rho_f^f \mathbf{u}\right) + S^f \rho_f^f \zeta \dot{\varepsilon}_{ii} + \left[\rho_f^f\left(C_s + \frac{\phi S^f}{K_f}\right) + S^f \rho_f^f Q\left(S^f + \frac{C_s}{\phi} p^f\right)\right]\dot{p}^f \\ &+ \left(S^f \rho_f^f N - \upsilon \rho_f^f \alpha_f\right)\dot{T} = 0 \end{aligned} \tag{6.69}$$

This equation is very similar to the fluid transport equation under coupled THMC conditions in some literature, for example, the one in Yin et al. (2010).

If neglecting the space variation of ρ_f^f, e.g. $\nabla \rho_f^f = 0$, equation (6.68) can be further

simplified as

$$\begin{aligned}&\nabla\cdot\mathbf{u}+S^f\zeta\dot{\varepsilon}_{ii}+\left[\left(C_s+\frac{\phi S^f}{K_f}\right)+S^fQ\left(S^f+\frac{C_s}{\phi}p^f\right)\right]\dot{p}^f\\&+S^fB^\beta\sum\omega_s^\beta\dot{\mu}_{bound}^\beta+S^fD\,\dot{\xi}+\left(S^fN-\upsilon\alpha_f\right)\dot{T}\\&=-\frac{\sum\dot{m}_{bound}^\beta-\sum\chi\nu_\beta M^\beta\dot{\xi}}{\rho_f^f}\end{aligned}\tag{6.70}$$

6.5.4 Chemical phase

The balance equation for the chemical β is

$$\frac{D}{Dt}\left(\int_V\rho_{pore}^\beta dV\right)=-\int_S\mathbf{I}^\beta\cdot\mathbf{n}dS-\int_V\dot{\rho}_{ex}^\beta dV+\int_V\chi v^\beta M^\beta\dot{\xi}dV\tag{6.71}$$

And the time derivation form of equation (6.71) is

$$\dot{\rho}_{pore}^\beta+\rho_{pore}^\beta\nabla\cdot\mathbf{v}^s+\nabla\cdot\mathbf{I}^\beta=-\dot{\rho}_{bound}^\beta+\chi v^\beta M^\beta\dot{\xi}\tag{6.72}$$

With density relationship (6.2), flux relationship (6.9) and Euler identity, it leads to

$$\left(\upsilon S^f\rho_f^\beta\right)^{\cdot}+\nabla\cdot\mathbf{J}^\beta+\nabla\cdot\left(\rho_f^\beta\mathbf{u}^\beta\right)=-\dot{m}_{bound}^\beta+\chi v^\beta M^\beta\dot{\xi}\tag{6.73}$$

In the transport research, the pore fluid could be assumed to be incompressible. If the mass fraction of chemical β is defined as $w^\beta=\rho_f^\beta/\rho_f^f$, then equation (6.73) can be written as

$$\left(\phi S^f w^\beta\rho_f^f\right)^{\cdot}+\nabla\cdot\mathbf{J}^\beta+\nabla\cdot\left(w^\beta\rho_f^f\mathbf{u}^\beta\right)=-\dot{m}_{bound}^\beta+\chi v^\beta M^\beta\dot{\xi}\tag{6.74}$$

Because $\sum\mathbf{J}^\beta=0$, and $\sum w^\beta=1$, so that based on equation (6.74), summing over all fluid component leads to

$$w^\beta\left(\phi S^f\rho_f^f\right)^{\cdot}+w^\beta\nabla\cdot\left(\rho_f^f\mathbf{u}^\beta\right)=-w^\beta\left(\sum\dot{m}_{bound}^\beta-\chi v^\beta M^\beta\dot{\xi}\right)\tag{6.75}$$

Invoking equation (6.75) into equation (6.74), it leads to

$$\begin{aligned}&\phi S^f\rho_f^f\dot{w}^\beta+\nabla\cdot\mathbf{J}^\beta+\rho_f^f\mathbf{u}^\beta\cdot\nabla w^\beta\\&\quad=-\dot{m}_{bound}^\beta+v^\beta M^\beta\dot{\xi}+w^\beta\sum\left(\dot{m}_{bound}^\beta-\chi v^\beta M^\beta\dot{\xi}\right)\end{aligned}\tag{6.76}$$

The term $w^\beta\sum\left(\dot{m}_{bound}^\beta-\chi v^\beta M^\beta\dot{\xi}\right)$ in equation (6.76) is usually ignored since its

influence is insignificant for the dilute solution. Then, equation (6.76) becomes

$$\phi S^f \rho_f^f \dot{w}^\beta + \nabla \cdot \mathbf{J}^\beta + \rho_f^f \mathbf{u}^\beta \cdot \nabla w^\beta = -\dot{m}_{bound}^\beta + \chi v^\beta M^\beta \dot{\xi} \tag{6.77}$$

Compared to most advection-diffusion equations, $\dot{m}_{bound}^\beta$ is added to account for the loss of pore mass due to swelling. The expression $\dot{m}_{bound}^\beta$ is given in equation (6.61).

6.5.5 Thermal phase

Since q^s , q^f are related to the volume of the mixture, similar to the density relationship, they can be related to the volume of solid and fluid phases through

$$q^s = \phi_s q_s^s \,,\; q^f = q_f^f S^f \phi \tag{6.78}$$

where $\phi_s = 1 - \phi$ is the volume fraction of the solid; q_s^s , q_f^f are the heat phase density of the solid and the pore fluid.

Similar to equation (6.19), q_s^s and q_f^f are

$$q_s^s = \rho_s^s C^s T \;\;,\; q_f^f = \rho_f^f C^f T \tag{6.79}$$

where ρ_s^s is the phase density of the solid (relative to the solid volume), ρ_f^f is the phase density of the fluid (relative to the fluid volume).

With the help of the flux equation (6.5), density relationship (6.78) and Darcy velocity (6.11), the heat flow $\mathbf{q}_f$ in equation (6.17) can be written as

$$\mathbf{q}_f = h^f \mathbf{I}^f = \rho_f^f C^f T \mathbf{u}^f \tag{6.80}$$

where the expression $h^f = C^f T$ is adopted.

From balance equation (6.21), with the help of relationship (6.78), (6.79) and (6.80), the balance equation for heat can be written as

$$\left((1-\upsilon)\rho_s^s C^s T\right)^{\cdot} + \left(S^f \upsilon \rho_f^f C^f T\right)^{\cdot} + \left(q^{bound}\right)^{\cdot} + \nabla\cdot\mathbf{q}' + \nabla\cdot\mathbf{q}_f = 0 \qquad (6.81)$$

Assume that the bounded fluid has the same heat capacity as pore fluid, equation (6.81) can be written as

$$\left((1-\upsilon)\rho_s^s C^s T\right)^{\cdot} + \left(S^f \upsilon \rho_f^f C^f T\right)^{\cdot} + \left(m_{bound}^f C^f T\right)^{\cdot} + \nabla\cdot\mathbf{q}' + \nabla\cdot\left(\rho_f^f C^f T\mathbf{u}^f\right) = 0 \quad (6.82)$$

Equation (6.82) differs from most existing thermal transport equation in that the term $\left(m_{bound}^f C^f T\right)^{\cdot}$ is added to represent the influence of bounded mass on thermal transport.

6.6 Coupled Thermal-Hydro-Mechanical-Chemical constitutive equations for two fluid components case

The field equations in section 6.5 consider the general case that different chemical components in the pore space and the interlayer space, therefore, the variable denoting the chemical influence is the chemical potential. However, in geotechnical engineering, the chemical potential is not a well-accepted variable as it is difficult to obtain the change of chemical potential through experiments or apply it to engineering applications.

In this section, a two fluid components (water as the solvent and chemical as solute) case is considered to simplify the discussion and convert the variable of chemical potential to more friendly ones.

6.6.1 Assumption for Chemical potential

To simplify the discussion, it is assumed that only water (denoted by subscript w) and one solute (denoted by subscript c) are considered here, therefore the stress equation (6.56) reduces to

$$\dot{\sigma}_{ij} = \left(K - \frac{2G}{3}\right)\dot{\varepsilon}_{kk}\delta_{ij} + 2G\dot{\varepsilon}_{ij} - \zeta\dot{\bar{p}}\delta_{ij} + \left(\omega_s^w \dot{\mu}_{bound}^w + \omega_s^c \dot{\mu}_{bound}^c\right)\delta_{ij} - \omega_R\dot{\xi}\delta_{ij} - \omega_T\dot{T}\delta_{ij} \quad (6.83)$$

To deal with the variable $\dot{\mu}^{\beta}_{bound}$, this chapter follows the assumption made by Heidug and Wong (1996) that the bounded fluid holds the same chemical potential as pore fluid, so that $\dot{\mu}^{w}_{bound}$ satisfies the Gibbs-Duhem equation (6.36). In this assumption, the equilibrium between bounded and pore water may be disturbed but can be regained in a negligible time. Such an assumption is valid when loading is slow enough (Lei et al., 2016). According to the Gibbs-Duhem relationship, the evolution of bounded water chemical potential can then be described as

$$\dot{\mu}^{w}_{bound} = \dot{\mu}^{w} = \frac{\dot{\bar{p}}}{S^{f}\rho^{w}_{f}} - \frac{\eta^{f}_{f}}{\rho^{w}_{f}}\dot{T} - \frac{\rho^{c}_{f}}{\rho^{w}_{f}}\dot{u}^{c} \tag{6.84}$$

The above relationship could help to reduce the two chemical potential variables ($\dot{\mu}^{w}_{bound}$ and $\dot{\mu}^{c}_{bound}$) to one ($\dot{\mu}^{c}_{bound}$).

Next, to deal with $\dot{\mu}^{c}_{bound}$, the relationship of the chemical potential of ideal dilute solution is adopted. The chemical potential of ideal dilute solution is

$$\mu^{\beta} = g^{\beta}\left(p,T\right) + \frac{RT'}{M^{\beta}}\left(\ln x^{\beta}\right) \tag{6.85}$$

where R is the gas constant. x^{β} is the mole fraction of fluid component β. $g^{\beta}\left(p,T\right)$ is the dependence of chemical potential on pressure and temperature. T' means that this term holds for constant temperature.

Equation (6.85) describes the dependence of chemical potential on temperature, pressure (i.e. $g^{\beta}(p,T)$) and mole fraction. As derived by Katchalsky and Curran (1965), the dependence of chemical potential on pressure can be given by the dependence of volume on the number of moles. With the fact that many experimental evidences indicate the dependence of volume on the number of moles is weak, this chapter could neglect the pressure influence on chemical potential and consider the temperature influence only. As suggested by Job and Herrmann (2006), the dependence

of chemical potential on temperature can be approximated by a linear function as

$$\dot{\mu}^c = \alpha_\mu^c \dot{T} \tag{6.86}$$

Since the mass dependency part of equation (6.85) can be differential as

$$\dot{\mu}^c = \frac{RT'}{M^c}\frac{\partial \ln x^c}{\partial t} = \frac{RT'}{M^c}\frac{\partial \ln x^c}{\partial x^c}\frac{\partial x^c}{\partial t} = \frac{RT'}{M^c}\frac{1}{x^c}\dot{x}^c \tag{6.87}$$

The mole fraction x^c is related to a mass fraction w^c through

$$w^c = \frac{x^c M^c}{x^c M^c + \left(1 - x^c\right) M^w} \tag{6.88}$$

When the solution is sufficiently dilute, the relationship can be simplified as

$$w^c = x^c \frac{M^c}{M^w} \tag{6.89}$$

Therefore, combining equation (6.86), (6.87) and (6.89), the evolution of chemical potential with mass and temperature is

$$\dot{\mu}^c = \frac{RT'}{M^c}\frac{1}{x^c}\dot{x}^c + \alpha_\mu^c \dot{T} = \frac{RT'}{M^c}\frac{1}{w^c}\dot{w}^c + \alpha_\mu^c \dot{T} \tag{6.90}$$

6.6.2 stress, porosity, and bounded mass

1. Stress

Substituting equation (6.90), (6.84) and (6.89) into equation (6.83) leads to the stress evolution with strain, pressure, mass fraction, and temperature:

$$\dot{\sigma}_{ij} = \left(K - \frac{2G}{3}\right)\dot{\varepsilon}_{kk}\delta_{ij} + 2G\dot{\varepsilon}_{ij} - \left(\zeta - \frac{\omega_s^w}{S^f \rho_f^w}\right)\dot{\bar{p}}\delta_{ij} + \Upsilon_1 \dot{w}^c - \left(\omega_T + \Upsilon_2\right)\dot{T}\delta_{ij} - \omega_R \dot{\xi}\delta_{ij} \tag{6.91}$$

where Υ_1 and Υ_2 are

$$\Upsilon_1 = \left(\omega_s^c - \omega_s^w \frac{\rho_f^c}{\rho_f^w}\right)\frac{RT'}{M^c}\frac{1}{w^c}\ ,\ \Upsilon_2 = -\alpha_\mu^c\left(\omega_s^c - \omega_s^w \frac{\rho_f^c}{\rho_f^w}\right) + \omega_s^w \frac{\eta_f^f}{\rho_f^w} \tag{6.92}$$

In equation (6.91), the term $\Upsilon_1 \dot{w}^c$ is explained as the chemical 'chemically induced deformation' (Heidug and Wong, 1996). The term $\left(\omega_T + \Upsilon_2\right)\dot{T}\delta_{ij}$ represents the thermal

expansion of the wetted matrix, in which Υ_2 is the contribution of bounded mass. When swelling happens, the matrix no longer consists of dry grains but wetted matrix with fluid bounded inside. Since the bounded fluid does not migrate or evaporate, the greater thermal expansion capability of the fluid will make the wetted matrix hold a greater expansion volume than the dry matrix.

Once reaching the similar stress-strain relation as equation (6.92), some researchers (e.g. Ghassemi and Diek (2003), Roshan and Oeser (2012)) immediately adopts the assumption that the swelling coefficient for water and chemical is the same (i.e. $\omega_s^w = \omega_s^c = \omega_s^0$) to form their constitution equation. It should be mentioned that it is too early to make such as assumption as this assumption indicates the influence of different chemical components is the same, which is not very realistic. Such an assumption can make the equations simple but significantly limit the application of the equation and hide the swelling mechanism. Heidug and Wong (1996) made such an assumption only when doing the numerical simulation, following him, this chapter presents the constitutive equation with two different swelling coefficients and assumes their equality in the simulation part.

2. Porosity

With the two fluid components assumption, the porosity evolution equation (6.58) becomes

$$\dot{\upsilon} = \zeta \dot{\varepsilon}_{ii} + Q\dot{\bar{p}} + B^w \dot{\mu}^w_{bound} + B^c \dot{\mu}^c_{bound} + D\,\dot{\xi} + N\dot{T} \tag{6.93}$$

Then, introducing the chemical potential assumption and expression, the porosity evolution equation can be written as

$$\dot{\upsilon} = \zeta\dot{\varepsilon}_{ii} + \left(Q + \frac{B^w}{S^f \rho_f^w} \right) \dot{\bar{p}} + \left(B^c - B^w \frac{\rho_f^c}{\rho_f^w} \right) \frac{RT'}{M^c} \frac{1}{w^c} \dot{w}^c + \left(N - B^w \frac{\eta_f^f}{\rho_f^w} + \alpha_\mu^c \left(B^c - B^w \frac{\rho_f^c}{\rho_f^w} \right) \right) \dot{T} + D\,\dot{\xi} \tag{6.94}$$

With relationship (6.92) and (6.59), equation (6.94) can be written as

$$\dot{\upsilon} = \zeta\dot{\varepsilon}_{ii} + \left(Q + \frac{B^w}{S^f \rho_f^w} \right) \dot{\bar{p}} + \Upsilon_1 \frac{\zeta - 1}{K} \dot{w}^c + \left(N - \Upsilon_2 \frac{\zeta - 1}{K} \right) \dot{T} + D\,\dot{\xi} \tag{6.95}$$

3. Bounded Mass

The bounded mass equation (6.61) for the two fluid components case keeps the same as:

$$\dot{m}_{bound}^{\beta} = -\omega_s^{\beta} \dot{\varepsilon}_{ij} + B^{\beta} \dot{\bar{p}} + Z^{\beta} \dot{\mu}_{bound}^{\beta} + X^{\beta} \dot{\xi} + R^{\beta} \dot{T} \tag{6.96}$$

For the bounded chemical, involving the chemical potential equation (6.90) yields to

$$\dot{m}_{bound}^{c} = -\omega_s^{c} \dot{\varepsilon}_{ij} + B^{c} \dot{\bar{p}} + Z^{c} \frac{RT'}{M^c} \frac{1}{w^c} \dot{w}^c + X^{c} \dot{\xi} + \left(R^c + Z^c \alpha_\mu^c \right) \dot{T} \tag{6.97}$$

With then relationship (6.84), from equation (6.97), the bounded water mass density with associate variables of strain, pressure, mass fraction, reaction extent and temperature is

$$\dot{m}_{bound}^{w} = -\omega_s^{w} \dot{\varepsilon}_{ij} + \left(B^w + Z^w \frac{1}{S^f \rho_f^w} \right) \dot{\bar{p}} - Z^w \frac{\rho_f^c}{\rho_f^w} \dot{u}^c + X^w \dot{\xi} + \left(R^w - Z^w \frac{\eta_f^f}{\rho_f^w} \right) \dot{T} \tag{6.98}$$

Then, with the chemical potential equation (6.90), the bounded water equation can be obtained as

$$\dot{m}_{bound}^{w} = -\omega_s^{w} \dot{\varepsilon}_{ij} + \left(B^w + Z^w \frac{1}{S^f \rho_f^w} \right) \dot{\bar{p}} - Z^w \frac{\rho_f^c}{\rho_f^w} \frac{RT'}{M^c} \frac{1}{w^c} \dot{w}^c + X^w \dot{\xi} + \left(R^w - Z^w \frac{\eta_f^f}{\rho_f^w} - Z^w \frac{\rho_f^c}{\rho_f^w} \alpha_\mu^c \right) \dot{T} \tag{6.99}$$

6.6.1 Mechanical behaviour

Assuming mechanical equilibrium condition $\partial\sigma_{ij}/\partial x_j = 0$, and using displacement variables $d_i (i = 1,2,3)$ through $\varepsilon_{ij} = \frac{1}{2}(d_{i,j} + d_{j,i})$, from Equation (6.91), and incorporating the relationship $\dot{\bar{p}} = S^f \frac{\partial p^f}{\partial t} + \frac{C_s}{\phi} p^f \frac{\partial p^f}{\partial t} = \left(S^f + \frac{C_s}{\phi} p^f \right) \frac{\partial p^f}{\partial t}$ to convert average pressure to pore fluid pressure, the governing equation for solid phase (neglecting the spatial divergence of saturation/density) can be obtained as

$$G\nabla^2 \dot{\mathbf{d}} + \left(\frac{G}{1-2\theta} \right) \nabla \left(\nabla \cdot \dot{\mathbf{d}} \right) - \left(\zeta - \frac{\omega_s^w}{S^f \rho_f^w} \right) \nabla \left[\left(S^f + \frac{C_s}{\phi} p^f \right) \dot{p}^f \right] + \nabla \Upsilon_1 \dot{w}^c - \nabla \left(\omega_T + \Upsilon_2 \right) \dot{T} - \omega_R \nabla \dot{\xi} = 0 \tag{6.100}$$

with

$$\Upsilon_1 = \left(\omega_s^c - \frac{\rho_f^c}{\rho_f^w} \omega_s^w \right) \frac{RT'}{M^c} \frac{1}{x^c}, \quad \Upsilon_2 = -\alpha_\mu^c \left(\omega_s^c - \omega_s^w \frac{\rho_f^c}{\rho_f^w} \right) + \omega_s^w \frac{\eta_f^f}{\rho_f^w} \tag{101}$$

6.6.3 Hydraulic behaviour

The transport of fluid may be complicated if consider the thermal and chemical osmosis phenomenon. A lot of researchers have paid special attention to fluid transport (Ghassemi and Diek, 2003, Ghassemi et al., 2009, Zheng et al., 2011, Kanfar et al., 2017, Samper et al., 2020). The osmosis phenomenon can be derived in the framework of Mixture-Coupling Theory (Ma et al., 2022), however, the novelty of the thesis is the swelling and dissolution process, the complex coupling of thermal and chemical process is fluid transport is not the key issue, therefore, this chapter simply adopts Darcy's law for pore fluid:

$$\mathbf{u} = -\mathrm{k} \frac{k_{rf}}{\nu} \nabla p^f \tag{6.102}$$

where k_{rf} is the relative permeability, k is absolute permeability and ν is the viscosity of pore fluid.

Invoking the porosity change equation (6.95) and bounded mass equation (6.97), (6.99), and Darcy's law into the fluid conservation(6.65), we could have the final governing equation for pore fluid transport as(alternatively, substituting the chemical potential (6.84)and (6.90) relationship into equation (6.70))

$$
\begin{aligned}
&-\mathrm{k}\frac{k_{rf}}{\nu}\nabla^2 p^f + S^f\zeta\dot{\varepsilon}_{ii} + \left[S^f\left(Q+\frac{B^w}{S^f\rho_f^w}\right)(S^f+\frac{C_s}{\phi}p^f)+\left(C_s+\frac{\phi S^f}{K_f}\right)\right]\dot{p}^f \\
&+S^f\Upsilon_1\frac{\zeta-1}{K}\dot{x}^c+\left[S^f\left(N-\Upsilon_2\frac{\zeta-1}{K}\right)-\upsilon\alpha_f\right]\dot{T}+S^f D\,\dot{\xi} \qquad (6.103)\\
&=-\frac{1}{\rho_f^f}\left(\dot{m}^w_{bound}+\dot{m}^c_{bound}\right)+\frac{1}{\rho_f^f}\sum\chi\nu_\beta M^\beta\dot{\xi}
\end{aligned}
$$

On the right hand of equation (6.103), there is

$$
\begin{aligned}
&\dot{m}^w_{bound}+\dot{m}^c_{bound}= \\
&\quad\left(\omega_s^w+\omega_s^c\right)\dot{\varepsilon}_{ij}+\left(B^w+Z^w\frac{1}{S^f\rho_f^w}+B^c\right)\dot{\bar{p}}+\left(Z^c-Z^w\frac{\rho_f^c}{\rho_f^w}\right)\frac{RT'}{M^c}\frac{1}{x^c}\dot{x}^c \qquad (6.104)\\
&\quad+\left(R^w+R^c+\alpha_\mu^c\left(Z^c-Z^w\frac{\rho_f^c}{\rho_f^w}\right)-Z^w\frac{\eta_f^f}{\rho_f^w}\right)\dot{T}+\left(X^w+X^c\right)\dot{\xi}
\end{aligned}
$$

6.6.4 Chemical behaviour

The diffusion of chemicals is described by Fick's law

$$\mathbf{J}^\beta=\rho_f^f D^\beta_{diff}\nabla w^\beta \qquad (6.105)$$

where D^β_{diff} is the diffusion coefficient of $\beta\,th$ fluid component.

Invoking diffusion law and Darcy's law into equation (6.76), the governing equation for chemical transport can be obtained as

$$\phi S^f\rho_f^f\dot{w}^\beta+\rho_f^f D^\beta_{diff}\nabla^2 w^\beta-\rho_f^f k\frac{k_{rf}}{\nu}\nabla p^f\cdot\nabla w^\beta=-\dot{m}^\beta_{bound}+\chi\nu^\beta M^\beta\dot{\xi} \qquad (6.106)$$

6.6.5 Thermal behaviour

The heat transport can be described by the Fourier' Law

$$\mathbf{q}' = -\lambda \nabla T \tag{6.107}$$

where λ is the overall thermal conductivity coefficient.

With equation (6.82) and the thermal convection law, the governing equation for thermal transport can be obtained

$$\left((1-\upsilon)\rho_s^s C^s T\right)^{\cdot} + \left(S^f \upsilon \rho_f^f C^f T\right)^{\cdot} + \left(m_{bound}^f C^f T\right)^{\cdot} - \nabla^T \lambda \nabla T + \nabla \cdot \left(\rho_f^f C^f T \mathbf{u}\right) = 0 \tag{6.108}$$

in which C^f can be estimated through $C^f = w^w C^w + w^c C^c$, λ is the overall thermal conductivity coefficient of the porous media and for dry media, it can be written as $\lambda = (1-\upsilon)\lambda_s + \upsilon\lambda_f$, with λ_s, λ_f being the thermal conductivity coefficient of the solid and the fluid, however, for wetted media, no theoretical relationship is given in literature.

6.6.6 Equation discussion and validation

1. Discussion

The coupling equations (6.49), (6.50), (6.51), (6.52), (6.53) represent the very general cross-coupling between stress, pressure, chemical potential of bounded mass, reaction extent and temperature, they are appliable for general cases including large strain, anisotropy. Equation (6.57), (6.58), (6.70), (6.61), (6.77) are for small strain, isotropic and elastic deformation conditions, however, the variable for swelling is the chemical potential of bounded, although it is adopted by some researchers (Zhang and Zhong, 2017a), it is an unfamiliar concept in geotechnical engineering, and the physical meaning of the coefficient for this variable is unknown. Therefore, equation (6.100), (6.103), (6.106), (6.108) adopt the assumption that chemical potential of the bounded mass is the same as that of the pore mass, so as to switch the variable into mass fraction, making it more applicable.

The swelling coefficient, i.e., ω_s^β , has been added to describe the influence of swelling. The swelling coefficient ω_s^β requires experimental work to determine. Specifically, the thermal influence associated with swelling is derived, which, as far as the author's knowledge, although have been explored by experiments but is rarely described mathematically.

The influence of fluid loss due to sorption into the interlayers has been considered in the hydraulic, chemical, and thermal transport equation. This is a step forward, but also it opens the question that what is the density of the bounded fluid. Equation (6.99) provides the bounded mass density change equation under coupled THMC situation, but the coefficients are rather difficult to determine. The bounded mass density is relative to the volume of the mixture, rather than the volume of the bounded mas, this distracts us to determine the coefficient theoretically.

2. Validation

For swelling:

The mass equation (6.12) and free energy equations (6.38), (6.39), (6.43) in this thesis are different from those in existing papers such as Roshan and Oeser (2012), Gao et al. (2021), Roshan and Rahman (2011), Ghassemi et al. (2009), Heidug and Wong (1996), as the mass equation is written for the pore mass in the thesis while for overall mass in these papers, and the free energy equations in this thesis adopt different chemical potentials for pore mass and bounded mass while the same chemical potential for different mass in literature. Owing to the above difference, the final state equation (6.46) and the cross-coupling equations (6.49)-(6.53) are also different in that this adoptes the chemical potential $\dot{\mu}_{bound}^\beta$ while these papers adopt the chemical potential $\dot{\mu}^\beta$. If assuming the $\dot{\mu}_{bound}^\beta = \dot{\mu}^\beta$ at the very beginning of the derivations, the free energy

equations and cross coupling equations in the thesis will be the same as those in the literatures. This indicating that the equations in these papers are a specific case of the equations in this thesis, and this thesis has presented more general and more precise equations.

The stress-strain equation (6.91) adopts two different swelling coefficients, if using the same expression for the two swelling coefficients, the stress-strain equation will be the same as the one derived in Gao et al. (2021) and very similar to the one in Roshan and Oeser (2012). If neglecting the temperature influence on chemical potential, the stress-strain equation will be the same as that presented in Ghassemi et al. (2009). If reducing the stress-strain equation to iso-thermal condition, the equation will be the same as the those developed in Heidug and Wong (1996), Ghassemi and Diek (2003), Roshan and Rahman (2011), Kivi et al. (2015). Overall, the present stress-strain relationship is the extension of the aforementioned research by including the temperature influence and the temperature dependency of chemical potential, and the aforementioned models can be viewed as simplified cases of the presented model.

The transport equations for the swelling case in this thesis are different from those in the aforementioned papers: 1. The transport equations are written for pore fluid instead of overall fluid; 2. The bounded mass is incorporated as the sink term while the papers do not consider it. If considering the bounded mass to be negligible and the pore fluid density to be the same as overall fluid density, the transport equations will be the same as those in these papers. This also indicates that the transport equations in these papers are a specific case of the transport equations developed in this thesis when the bounded mass density is sufficiently small.

For dissolution:

The dissolution part can be compared to those presented in Coussy (2004), Haxaire and

Djeran-Maigre (2009), Karrech (2013), Zhang and Zhong (2017b), Zhang and Zhong (2017a), Zhang and Zhong (2018). The equations and methods for the derivations are different from those in these papers as this thesis provides a more advanced approach and gives a more precise free energy equation by defining the solid affinity A_s concept. The final state equation (6.46) and the cross-coupling equations (6.49)-(6.53) are also different in that this thesis adopts the solid affinity A_s as the coefficient for variable reaction extent $\dot{\xi}$ while these papers adopt the overall affinity A as the coefficient. However, the final stress-strain equation (6.56) is the same, because, following the thermodynamics way, the variables adopted to represent the dissolution process are all reaction extent $\dot{\xi}$. This thesis also managed to derive the coefficient but these existing papers made no attempt.

6.7 Numerical simulation

This section presents the role of dissolution/swelling in the THMC framework by numerical simulation. Although the dissolved chemicals may influence the swelling state and the swelling absorbed chemicals may affect the dissolution process, the mechanism and equations for each process are so complicated. To have a better understanding of the influence of swelling and dissolution, the numerical simulation part ignores their interaction and focuses on each process only. Therefore, the numerical simulation presented in this section does not include both swelling and dissolution in one THMC framework but separates them into two independent THMC frameworks.

6.7.1 Numerical simulation for THMC-swelling

This section presents the swelling influence in the THMC framework, it is a further extension of the HMC-swelling simulation in chapter 5 with specific attention to the thermal process and its influence on other processes. To do this, an iso-thermal

condition is set as a comparison to show the influence of temperature on the pressure and mass fraction change. Later, the swelling influence in non-isothermal condition is present, which is very similar to that in chapter 5; the swelling influence under non-isothermal condition shows a very strong influence with the adopted parameters, the expansion capacity of the wetted matrix is ten times greater than that of the dry matrix.

6.7.1.1 Numerical model

6.7.1.1.1 equation assumption

In this section, the classic finite element method is adopted to solve the governing equations (6.100), (6.103), (6.106), (6.108). Since the equations are so complicated and comprehensive, some assumptions and simplifications are made to simplify the discussion:

1. Although the bounded masses have been derived as the sink source for the fluid/chemical transport equation, they are not considered in the numerical simulation as the coefficients of bounded mass are rather difficult to obtain.

2. Although the spatial variation of density may exist due to temperature or chemical distribution, but this variation is ignored.

3. The swelling coefficient, i.e., ω_s^w and ω_s^c , maybe complicated expression, for simplification, they are roughly assumed to be $\frac{\omega_s^w}{S^f \rho_f^w} = 0.2$. Since the saturation S^f adopted is very close to 1, the value of ω_s^w is assumed to be 180, regardless of the change in saturation and density. Till now, the equal swelling coefficient made by Heidug and Wong (1996) is adopted as $\omega_s^w = \omega_s^c = 180$.

4. The term $\Upsilon_1 \dot{w}^c$ in the mechanical equation, which is explained as the 'chemically induced deformation' (Heidug and Wong, 1996), has been explored extensively by some researchers (Heidug and Wong, 1996, Ghassemi and Diek, 2003, Roshan and Rahman, 2011, Kivi et al., 2015), it is not considered in this numerical simulation.

5. C_s is assumed to be 0, and the term $S^f\left(Q+\frac{B^w}{S^f\rho_f^w}\right)(S^f+\frac{C_s}{\phi}p^f)+\left(C_s+\frac{\phi S^f}{K_f}\right)$ is regarded to be a constant value $q=5*10^{-10}$.

Based on the above assumptions, the numerical modelling focuses more on the swelling phenomenon and the thermal impact on other processes, especially the swelling process. The governing equations are now reduced to:

$$G\nabla^2\dot{\mathbf{d}}+\left(\frac{G}{1-2\theta}\right)\nabla(\nabla\cdot\dot{\mathbf{d}})-\left(\zeta-\frac{\omega_s^w}{S^f\rho_f^w}\right)\nabla\left(S^f\dot{p}^f\right)-\nabla\left(\omega_T+\Upsilon_2\right)\dot{T}=0 \qquad (6.109)$$

$$-\mathrm{k}\frac{k_{rf}}{\nu}\nabla^2 p^f+S^f\zeta\dot{\varepsilon}_{ii}+q\dot{p}^f+S^f\Upsilon_1\frac{\zeta-1}{K}\dot{x}^c+\left[S^f\left(N-\Upsilon_2\frac{\zeta-1}{K}\right)-\upsilon\alpha_f\right]\dot{T}=0 \qquad (6.110)$$

$$\phi S^f\dot{w}^\beta+D_{diff}^\beta\nabla^2 w^\beta-\mathrm{k}\frac{k_{rf}}{\nu}\nabla p^f\cdot\nabla w^\beta=0 \qquad (6.111)$$

$$\left((1-\upsilon)\rho_s^s C^s T\right)^{\cdot}+\left(S^f\upsilon\rho_f^f C^f T\right)^{\cdot}-\nabla^T\lambda\nabla T+\nabla\cdot\left(\rho_f^f C^f T\mathbf{u}^f\right)=0 \qquad (6.112)$$

6.7.1.1.2 Geometry and boundary condition

Geometry: the model adopted is a 1m*1m plane rectangle, as shown in Figure 6.1.

Mechanical condition: The left boundary A is set to be free whereas the right boundary B is fixed. The upper and lower boundaries are constrained with no displacement allowed. The whole domain is at mechanical equilibrium and has no initial effective stress.

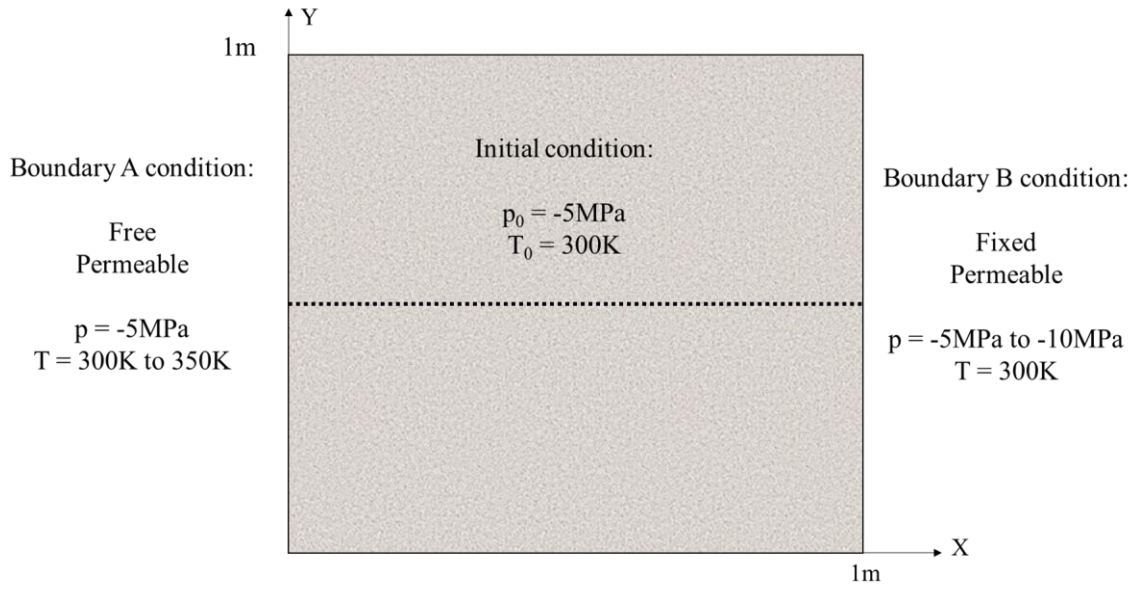

Figure 6. 1 Geometry and Boundary condition

Hydraulic condition: The domain is unsaturated and filled with water of -5 MPa pressure. According to van Genuchten's model in pre-chapters, the initial saturation is 0.995. The pressure at boundary A is set to be -5MPa and maintains constant. At the beginning of the simulation, pressure at boundary B drops to -10MPa.

To involve the temperature influence, the fluid viscosity is set to be a function of temperature (Zheng et al., 2011), as:

$$\nu(T) = 0.661(T - 229)^{-1.562} \tag{6.113}$$

Chemical condition: The chemical mass fraction on the right boundary is set to be 0.1 and keeps constant during the whole simulation. On the left boundary, a mass fraction at 0.2 is applied to represent external chemicals brought by groundwater. In the domain, the initial value is 0.1 and could change due to diffusion from the left to the right.

The diffusion coefficient relates to temperature and viscosity through (Zheng and Samper, 2008)

$$D_{diff}(T) = D_{diff}(T_0)\frac{T}{T_0}\frac{\nu(T_0)}{\nu(T)} \tag{6.114}$$

with $D_{diff}(T_0) = 5.95E-9m^2/s$ (Lichtner and Seth, 1996), $T_0 = 300K$

The conductivity coefficient λ is estimated through

$$\lambda = (1-\phi)\lambda_s + \phi\lambda_f \tag{6.115}$$

where . λ_s ., λ_f are the conductivity coefficient of the solid and pore fluid.

Thermal condition: the thermal condition is very similar to that of chemical condition with a fixed 300K on the right boundary, 350K applied on the left boundary and an initial 300K in the domain.

The basic material considered is the same as that in Chapter 5: the hydraulic and mechanical parameters are taken from the experimental and numerical case for the Opalinus Clay by Wild et al. (2015) and Ziefle et al. (2018), which are the same are the parameters adopted in chapter 5. The thermal properties are taken from the experimental results (Zheng et al., 2011); the fluid entropy and the coefficient for chemical potential are taken from the modeling work of Roshan and Oeser (2012). Detailed parameters are listed in Table 6.1.

Table 6. 1 Material parameter (Zheng et al., 2011, Roshan and Oeser, 2012, Ziefle et al., 2018)

Parameter	Physical meaning	Values and units
ρ_f^f	Density of fluid	1000kg/m^3, with ρ_f^w =900kg/m^3, ρ_f^c =100kg/m^3
ϕ	Porosity	0.16
k	Permeability	6.8*10^{-20}m^{-2}
m	Van Genuchten parameter	0.54
M	Van Genuchten parameter	44.4Mpa

G	Shear modulus	1.2GPa
E	Young's modulus	3.6E9GPa
K	Bulk modulus	1.875GPa
θ	Poisson's ratio	0.18
ζ	Biot's coefficient	1
q	Void coefficient	$5*10^{-10}$
λ_s	Solid thermal conductivity	1.23W/m/K
λ_f	Fluid thermal conductivity	1.5W/m/K
α_s	Thermal expansion coefficient of solid	$2*10^{-5}$/K
α_f	Thermal expansion coefficient of fluid	$2.1*10^{-4}$/K
C^s	Specific heat capacity of solid	835.5J/kg/K
C^w	Specific heat capacity of water	4202J/kg/K
η_f^f	Entropy of fluid	3683J/kg/K
α_μ^c	Coefficient for chemical potential	-1060J/kg/K

6.7.1.2 Numerical results

6.7.1.2.1 thermal impact in non-swelling condition

By setting an iso-thermal condition as contrast and neglecting the swelling term, the temperature influence is presented below:

The temperature distribution within the domain at different times is presented in Figure 6.2. Since viscosity and diffusion are functions of temperature, they also change (Figure 6.3): the higher temperature is, the greater the diffusion coefficient is, the lower the viscosity is. Figure 6.4 shows the temperature influence of chemical distribution. Compared to the isothermal condition (T=300K), the mass fraction in the non-isothermal condition changes quicker, this is because, as illustrated in figure 6.3, the diffusion coefficient increase with temperature.

Intuitively, a high temperature leads to a lower viscosity and thus quicker fluid transport. At the early time (t=50h, 200h), the pressure change under higher temperature (iso-

thermal) is quicker than that under low temperature (Figure 6.5). At a long time scale (t=500h), the pressure reaches equilibrium. The pressure distribution curves for non-isothermal condition at 500h hours looks fall behind that in iso-thermal condition, but it does not mean the pressure change is slower. Actually, the curved line is the final status, and can never reach a straight line like that in the isothermal condition, which mainly results from the ununiform distribution of viscosity.

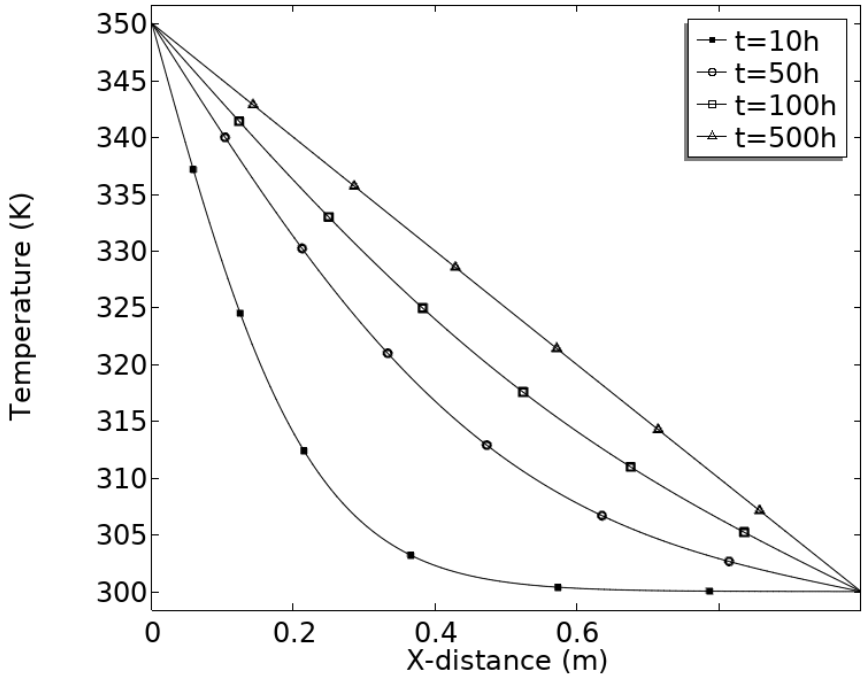

Figure 6. 2 Temperature distribution with time and space

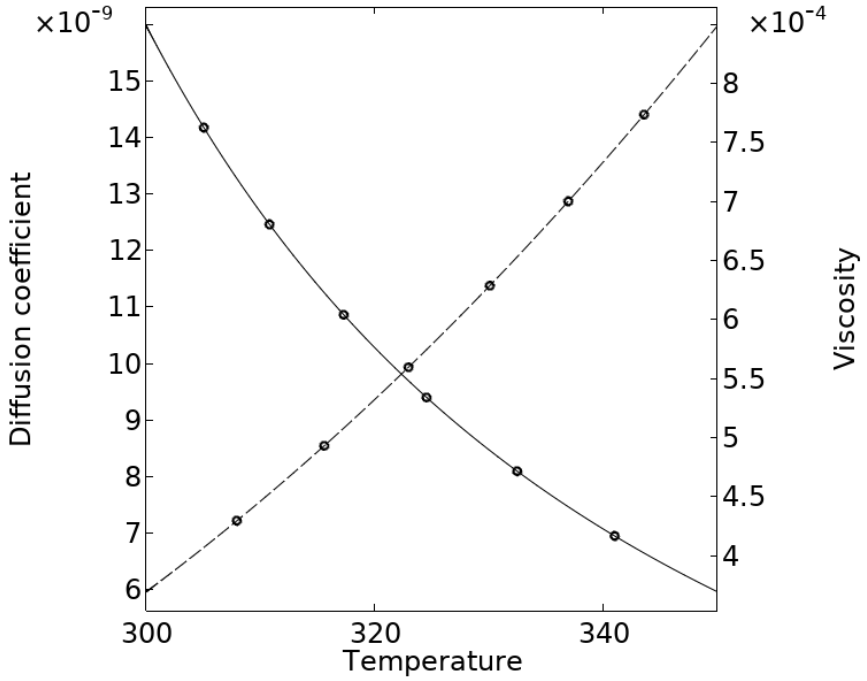

(a)

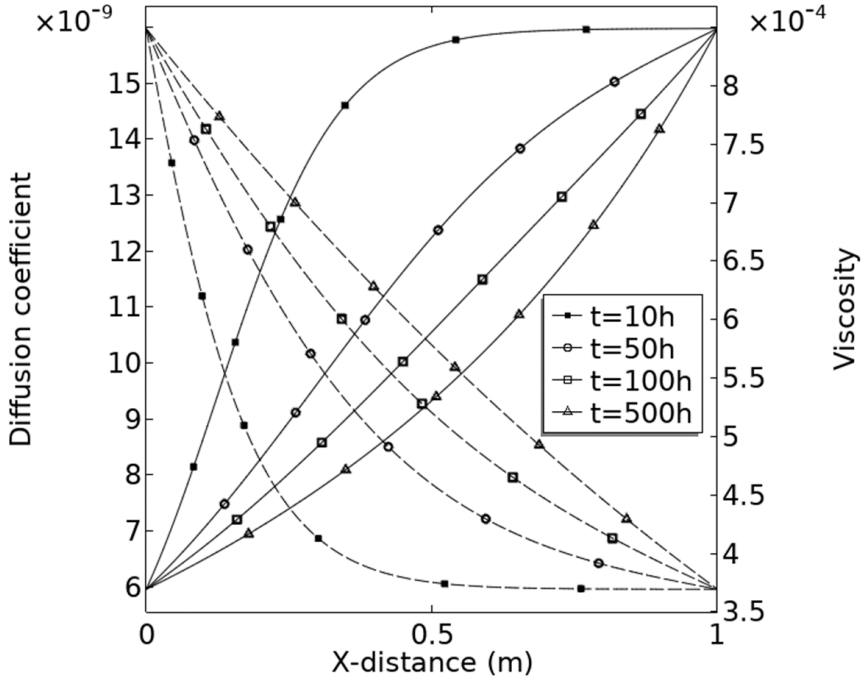

(b)

Figure 6. 3 Viscosity (solid line)/diffusion coefficient (dashed line) change with temperature (a) and space (b)

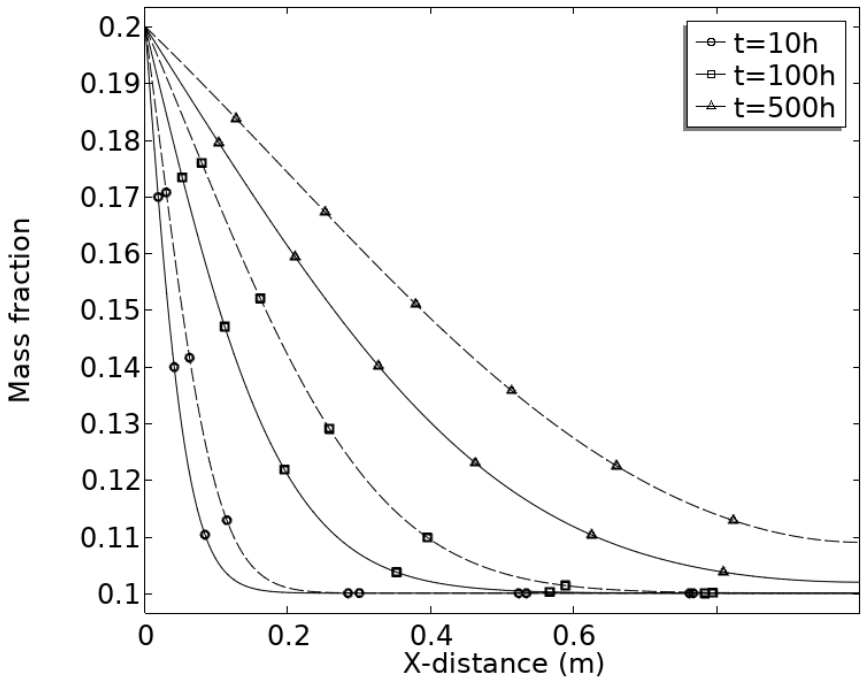

Figure 6. 4 Mass fraction distribution with time and space (Isothermal: solid line, non-isothermal: dashed line)

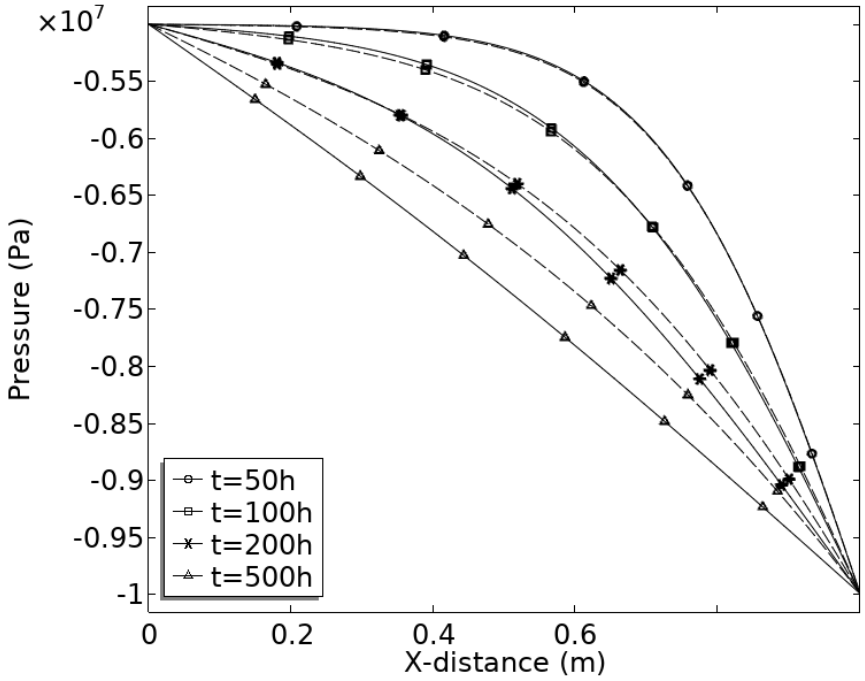

Figure 6.5 Pressure distribution with time and space (Isothermal: solid line, non-isothermal: dashed line)

Figures 6.6 and 6.7 show the displacement and strain of the domain under iso-thermal and non-isothermal conditions. Since pressure drops on the right boundary, fluid within

the domain flows out and fluid pressure changes. The change of fluid pressure leads to the stress working on the solid matrix, and thereby, the domain consolidates and a displacement field generate (Figure 6.6, solid line). As fluid pressure loss more and more, the displacement becomes larger. When there is a high temperature applied on the left boundary, the domain will expand. The expansion of the left part of the domain occurs earlier than that in the right part, leading to a movement toward the left side. The coaction effects of consolidation induced by pressure and expansion caused by temperature result in a complicated trend of displacement and strain, as shown in Figures 6.6 and 6.7. A noticeable point is that under isothermal condition, there is only the consolidation process, and the strain shows to be positive. However, under non-isothermal condition, the domain may expand due to thermal expansion phenomenon, when the thermal expansion exceeds the consolidation process, the strain presents to be positive.

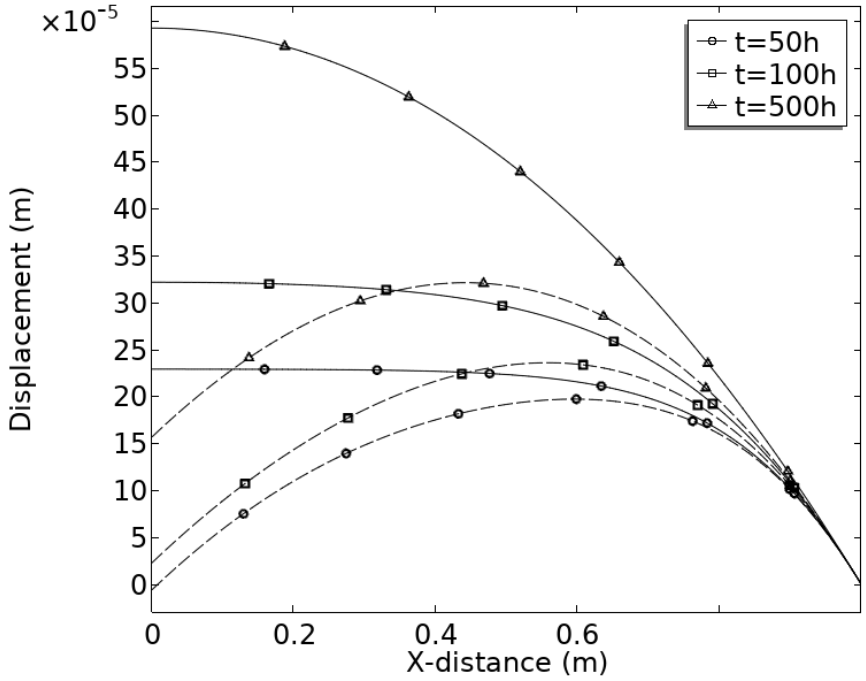

Figure 6. 6 Displacement distribution with time and space (Isothermal: solid line, non-isothermal: dashed line)

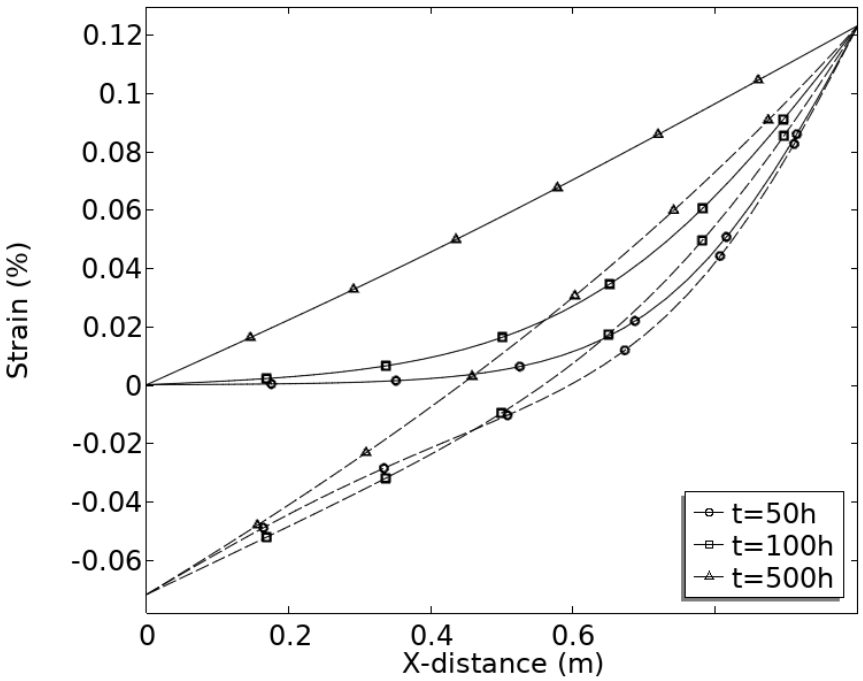

Figure 6. 7 Strain distribution with time and space (Isothermal: solid line, non-isothermal: dashed line)

6.7.1.2.2 thermal impact in non-swelling condition

Enabling the swelling term and considering the non-isothermal condition, the following part shows the influence of swelling and the temperature influence on swelling behaviour.

Figures 6.8 and 6.9 give the displacement and strain of swelling and non-swelling domain under isothermal condition. Clearly, the swelling process has a negative contribution to the displacement (Figure 6.8) which means that the pressure loss leads the sample to be consolidated but the swelling process resists such consolidation. This conclusion has been concluded in previous chapters.

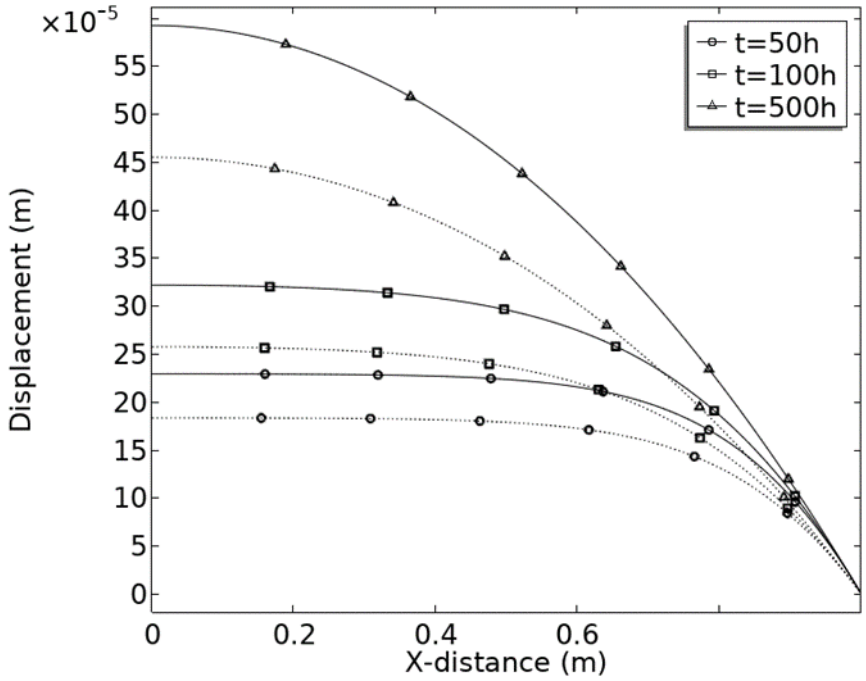

Figure 6. 8 Displacement distribution with time and space (non-swelling: solid line, swelling: dashed line)

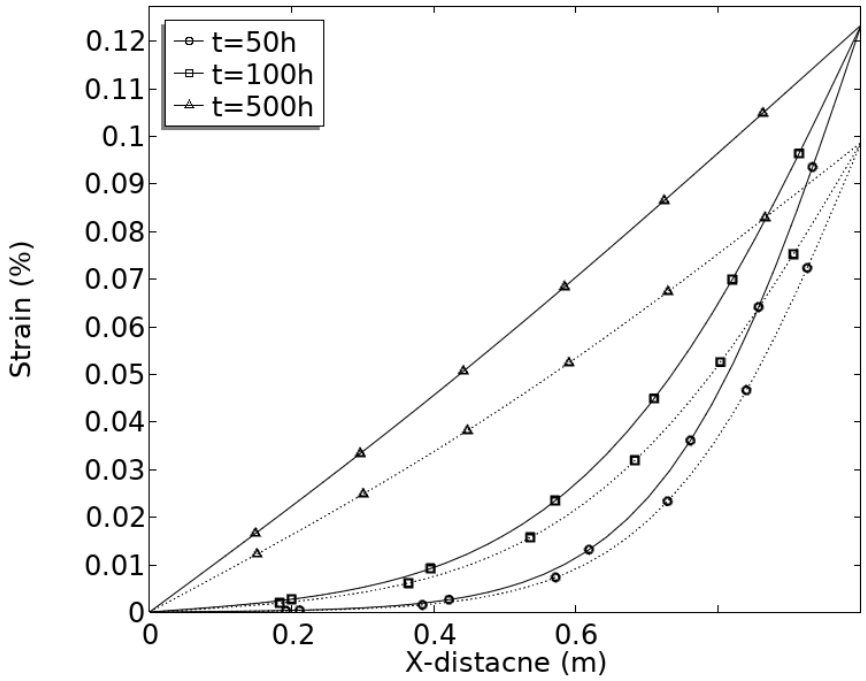

Figure 6. 9 Strain distribution with time and space (non-swelling: solid line, swelling: dashed line)

Figures 6.10 and 6.11 show the displacement and strain distribution of swelling rock under non-isothermal condition. Compared to the non-swelling case in figure 6.6, the

left boundary undergoes a much larger displacement toward the left direction, meaning that the thermal expansion exceeds the contribution of consolidation, and caused the left boundary to move toward the left.

This is because, due to swelling, water has been bounded into the matrix, the wetted matrix now has a greater thermal expansion capacity, based on the adopted parameters, the coefficient Υ_2 can be determined as $\Upsilon_2 = 1.70*10^5$, it can be found that the contribution of thermal stress of dry matrix is

$$\dot{\sigma}_T = -\omega_T \dot{T} = 0.1875*10^5 \dot{T} \tag{6.116}$$

when swelling is caused by both water and chemical, it becomes

$$\dot{\sigma}_T = -(\omega_T + \Upsilon_2)\dot{T} = 1.9375*10^5 \dot{T} \tag{6.117}$$

It can be found that the thermal stress of the wetted matrix is more than 10 times greater than that of the dry matrix. when swelling happens, the matrix is no longer consisting of dry grains but a wetted matrix with fluid bounded inside. Since the bounded fluid does not migrate or evaporate, the greater thermal expansion capability of the fluid will make the wetted matrix hold a greater expansion capacity than the dry matrix. Because the wetted matrix includes both solid and fluid, the thermal expansion capability could not exceed the thermal expansion capability of bounded fluid.

The thermal expansion capacity of the wetted matrix highly depends on the swelling coefficient and the temperature dependency of chemical potential α_μ^c. Unfortunately, the α_μ^c value is difficult to determine or find in literature. If considering a less swelling influence, that is taking $\omega_s^w = \omega_s^c = 90$ and $\Upsilon_2 = 0.852*10^5$, the corresponding displacement and strain distribution are presented in Figures 6.12 and 6.13, from which we could find that the influence from thermal expansion of the wetted matrix becomes smaller but still very significant compared to iso-thermal condition. If neglecting the

temperature dependency of chemical potential, then $\Upsilon_2 = 768\,(\omega_s^w = \omega_s^c = 180)$, this is a much smaller value compared to $\omega_T = 0.1875 * 10^5$, it can be predicted that in this case, the swelling has little influence on the thermal expansion capacity of the matrix.

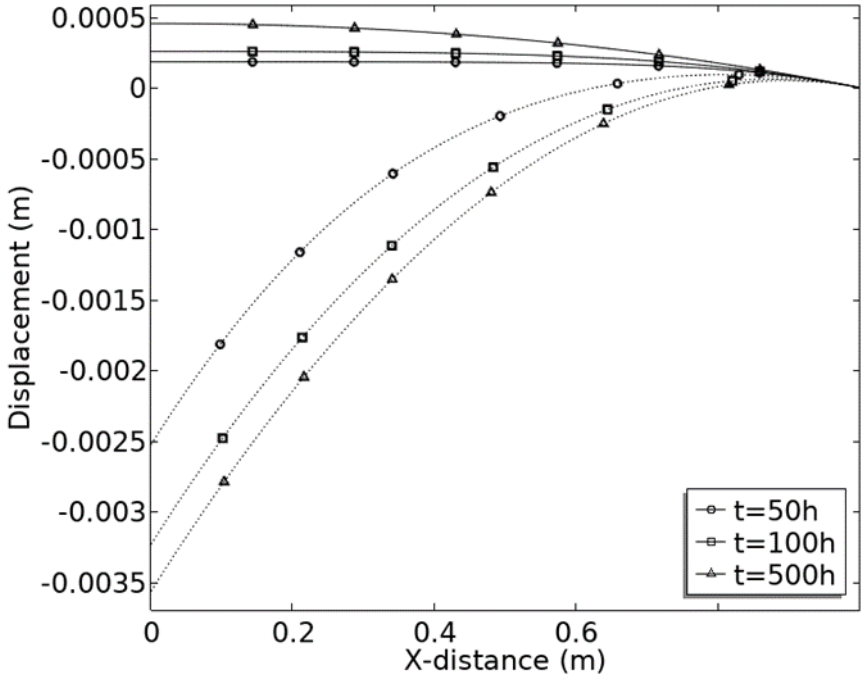

Figure 6. 10 Displacement distribution with time and space (Isothermal: solid line, non-isothermal: dashed line)

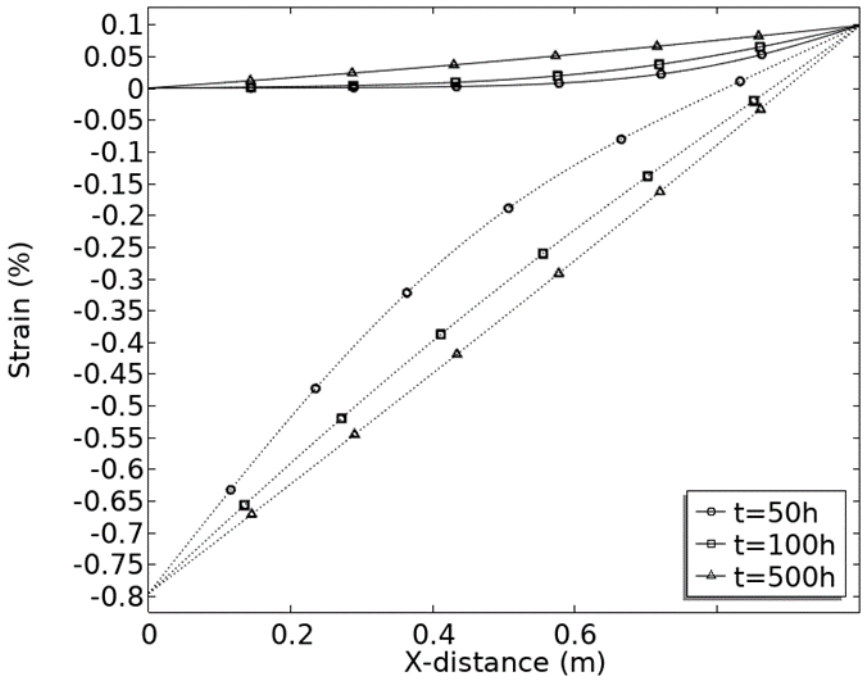

Figure 6. 11 Strain distribution with time and space (Isothermal: solid line, non-

isothermal: dashed line)

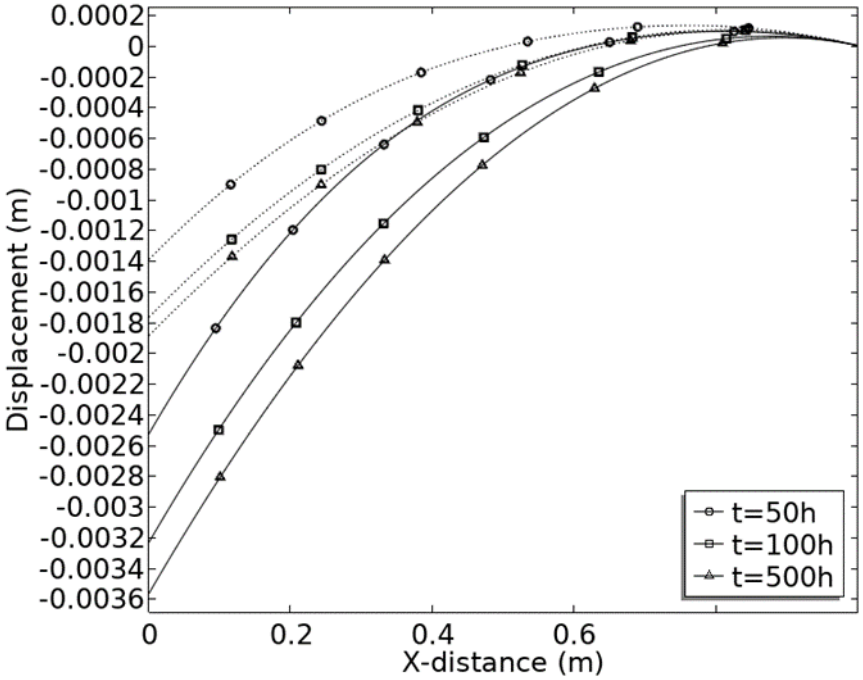

Figure 6. 12 Displacement distribution with time and space ($\omega_s^w = 180$: solid line, $\omega_s^w = 90$: dashed line)

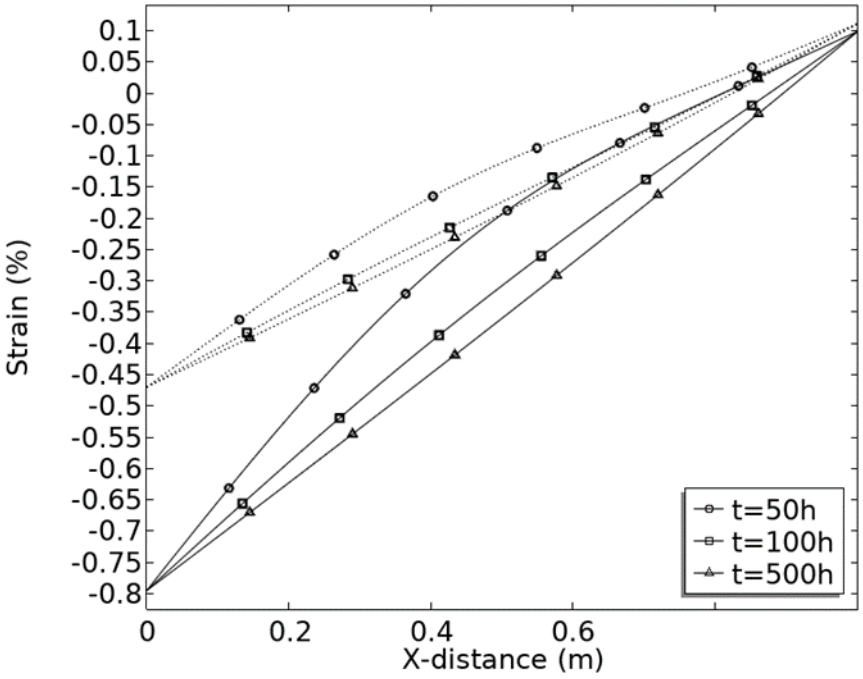

Figure 6.13 Strain distribution with time and space ($\omega_s^w = 180$: solid line, $\omega_s^w = 90$: dashed line)

6.7.1.3 Conclusion

The numerical simulation shows in a higher temperature condition, the change of mass fraction and fluid pressure can be faster. When there is a temperature gradient in the system, the pressure distribution shows a different status from that in uniform temperature condition, which mainly results from the ununiform distribution of viscosity. The swelling process has a negative influence on the consolidation process; however, it is highly influenced by temperature and the swelling coefficient. The temperature dependency of chemical potential adopted in the simulation shows a great influence on the expansion of the wetted matrix, however, this coefficient needs further theoretical or experimental determination.

6.7.2 Numerical simulation for THMC-dissolution

This section presents the dissolution process in a coupled THMC framework through numerical simulation. It takes quartz dissolution in pure water solution as an example. The temperature influence on dissolution is first presented for a closed system scenario, which may be considered as dissolution taking place between an engineering facility and an aquitard. Later, the dissolution is modelled in an open system, the concentration change, as well as the dissolution rate and reaction extent, subject to dissolution-advection, are presented. The porosity and strain change in a long time scale are predicted.

6.7.2.1 Numerical model

The numerical model considers the dissolution of quartz in a 2-dimensional rectangle with 0.5m width and 0.2m height. Quartz is the major mineral composition of clay /rock, and its dissolution and corresponding influence are of significant interest to many research fields. The dissolution of quartz in water can be written as

$$SiO_2 + 2H_2O \rightarrow H_4SiO_4 \tag{6.118}$$

The dissolution rate equation is (Savage et al., 2002)

$$r = k_{rate} A_{sf} \left(1 - \left(\frac{Q}{K_{eq}} \right)^{\vartheta} \right)^{\varpi} \tag{6.119}$$

in which r, k_{rate}, A_{sf}, Q, K_{eq} are the dissolution rate in moles per unit volume of porous media, rate constant, reactive surface area per unit volume of porous media, the ion activity product and the thermodynamic equilibrium constant. ϑ and ϖ are two coefficients and set to be 1.

The dissolution rate constant k_{rate} is temperature-dependent, its simplified relationship with temperature is (Nguyen et al., 2016)

$$k_{rate} = k_{rate}^{25} \exp\left[-\frac{E_a}{R} \left(\frac{1}{T} - \frac{1}{298.15} \right) \right] \tag{6.120}$$

where k_{rate}^{25} is the rate constant at $25°C$, E_a is the activation energy, R is the gas constant. The temperature of 25 degree is called the Standard Reference Ambient Temperature, which is determined internationally as the reference temperature and any measurement at a different ambient temperature can be compared to the value measured at this stand temperature.

The equilibrium constant K_{eq} is also temperature-dependent. A lot of experiments have been done to investigate the solubility of quartz under different temperatures, pressure or pH (Morey et al., 1962, Fournier and Potter II, 1982, Manning, 1994, Rimstidt, 1997), here, the empirical relationship proposed by Fournier and Potter II (1982) is adopted in the simulation:

$$\log K_{eq} = -4.66206 + 0.0034063T + \frac{2179.7}{T} - \frac{1.1292*10^6}{T^2} + \frac{1.3543*10^8}{T^3} \tag{6.121}$$

The properties for quartz are: molar mass: 60.086g/mol, molar volume: 22.68cm^3/mol

surface area: $9.53*10^3 m^2/m^3$ (Guthrie and Carey, 2015), $\log k_{rate}^{25} = 1*10^{-16.3}$ (Savage et al., 2002). Other data adopted are listed in table 6.2

Table 6. 2 Parameters adopted for the simulation

Parameters	Physical meaning	Values and units
ϕ	porosity	0.2
K	Bulk modulus	1.875GPa
C^s	Specific heat capacity of solid	835.5J/kg/K
C^w	Specific heat capacity of water	4202J/kg/K
λ_f	Thermal conductivity of fluid	1.5W/m/K
λ_s	Thermal conductivity of solid	1.23W/m/K

6.7.2.2 Numerical result

6.7.2.2.1 THMC-dissolution in Closed system

1. Isothermal condition

Assume a closed system where there is no chemical exchange with the surroundings, but a chemical reaction takes place inside the system. The quartz will dissolve until equilibrium. Since the rate constant and equilibrium constant are temperature-dependent (Figure 6.13), the time it takes to reach equilibrium and the corresponding concentration must be different, as shown in Figure 6.14. At 298.15K, from the adopted parameters, the dissolution will reach equilibrium at around 4 years with a H_4SiO_4 concentration of $1.18*10^{-4}$mol/L. When the temperature rises to 350K, 380K and 400K, it takes 1000 hours, 200 hours, and 80 hours to reach equilibrium with H_4SiO_4 concentration of $5.00*10^{-4}$ mol/L, $10.37*10^{-4}$ mol/L and $16.14*10^{-4}$ mol/L.

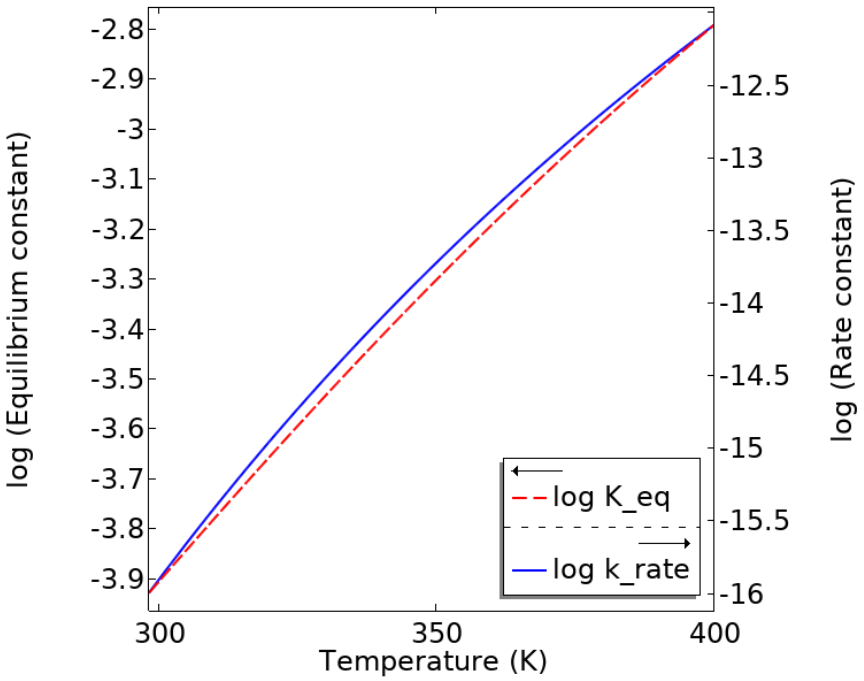

Figure 6. 13 Equilibrium constant and rate constant change with temperature

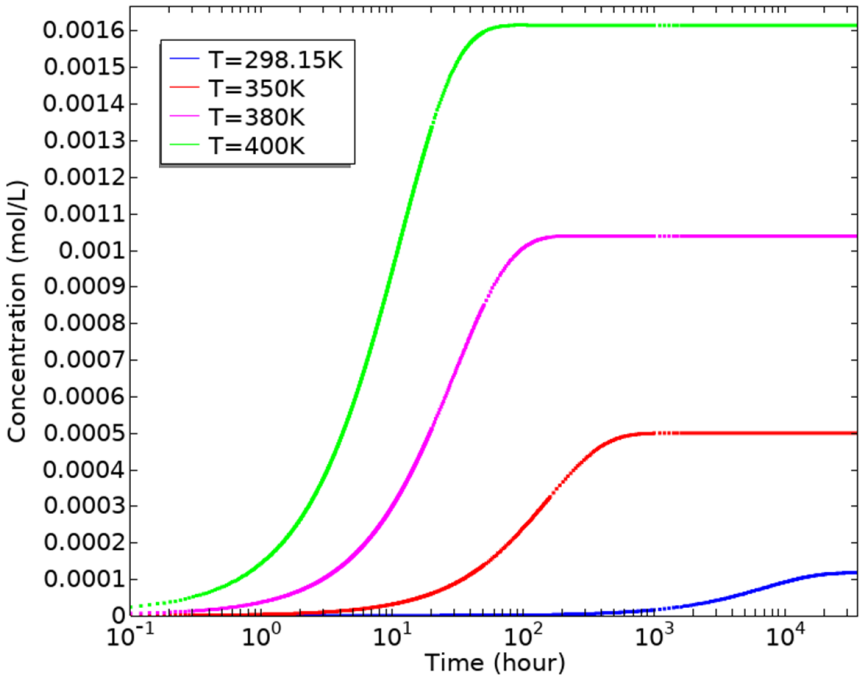

Figure 6. 14 Concentration change with time under different temperature

2. Non-isothermal condition

The above section explored the temperature influence on the dissolution by assuming a unform temperature situation. This section shall explore the chemical distribution in non-unform temperature condition. To achieve this, a high temperature (T_left=350K

or 400K) is applied on the left boundary and the domain is given a low temperature (298.15K). Due to the temperature gradient, heat will transfer from the left side to the right side gradually and resulting in time-dependent non-uniform temperature distribution, as shown in Figures 6.15 and 6.17, the trend in the two situations are very similar.

Since the left side holds a higher temperature, the dissolution rate on the left side will be quicker than that on the right side, resulting in a high chemical concentration in the left domain. The concentration difference in the domain will further lead to a diffusion of chemicals from the left side toward the right side. Assuming a diffusion coefficient of $1.17*10^{-9}$ (Rebreanu et al., 2008), the concentration distribution of H_4SiO_4 subject to dissolution and diffusion are presented in Figures 6.16 and 6.18, from which it could be found that the concentration change in higher temperature is quicker.

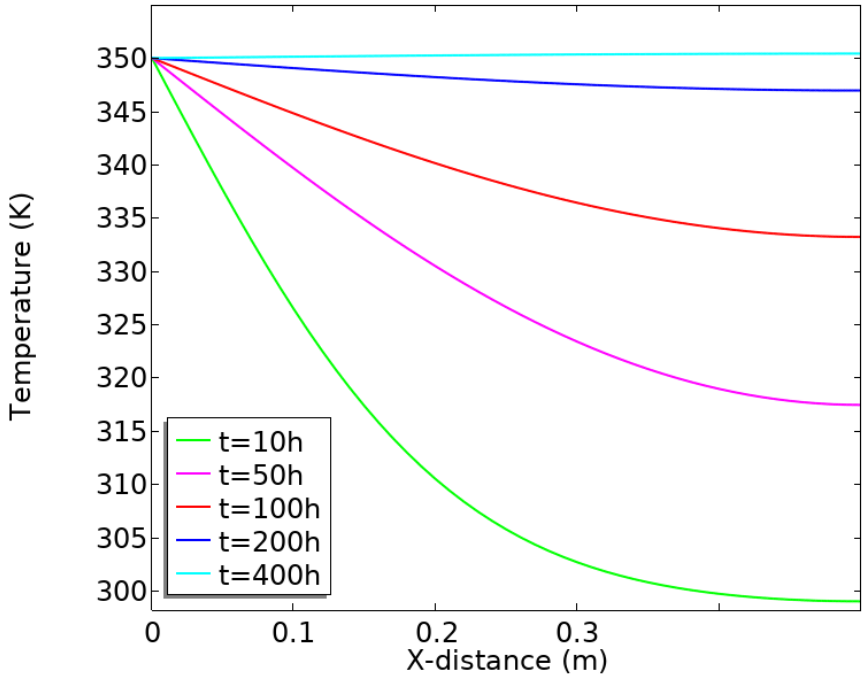

Figure 6. 15 Temperature distribution with time and space (T_left=350K)

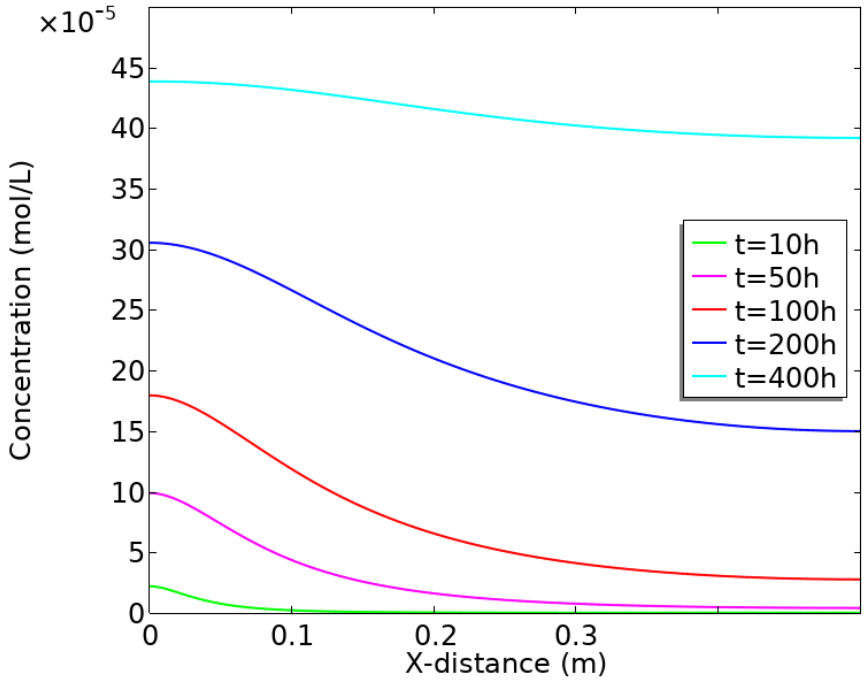

Figure 6. 16 Concentration distribution with time and space (T_left=350K)

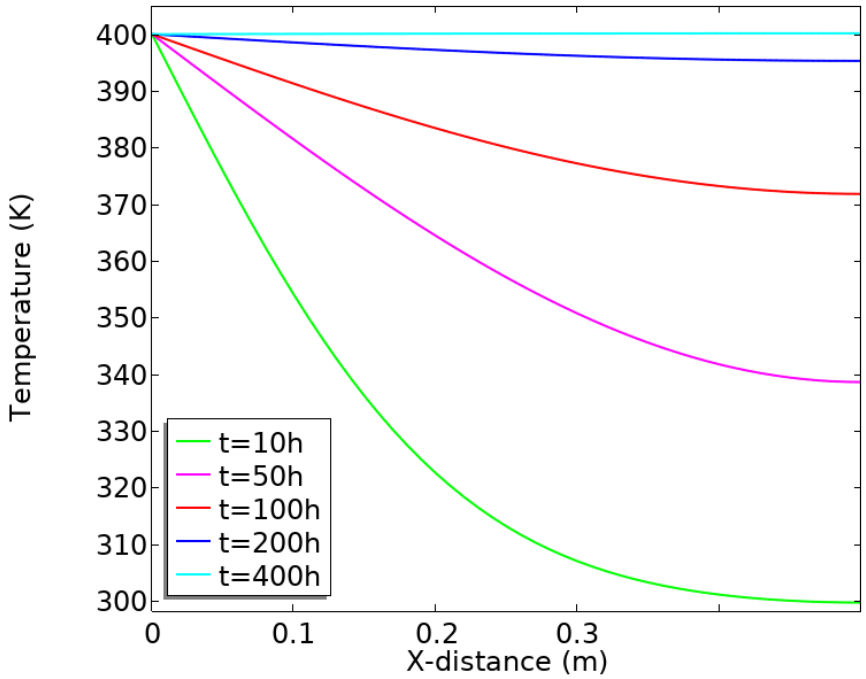

Figure 6. 17 Temperature distribution with time and space (T_left=400K)

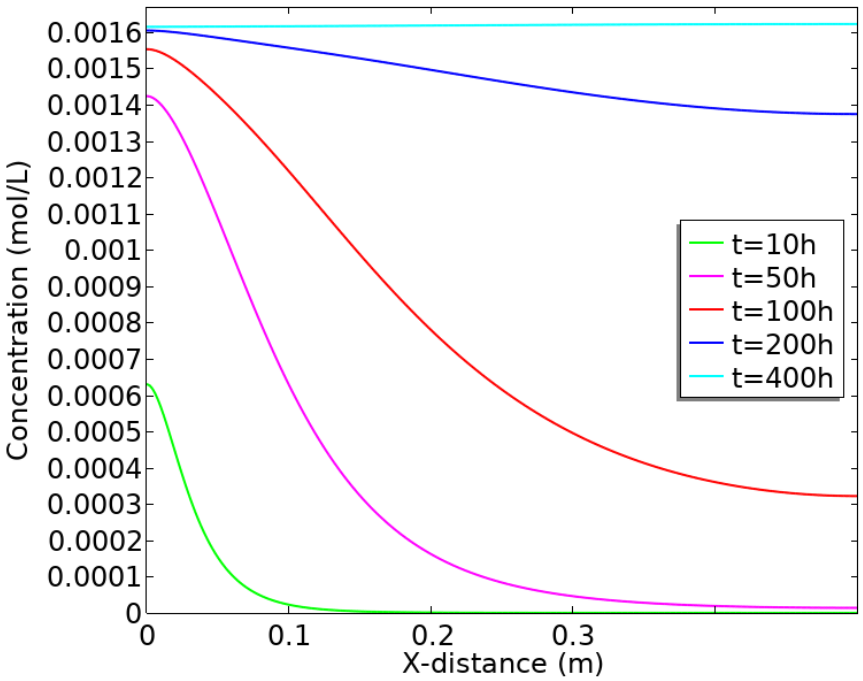

Figure 6. 18 Concentration distribution with time and space (T_left=400K)

6.7.2.2.1 THMC-dissolution in Open system

The above research investigated the temperature dependence of dissolution in a closed system, However, the dissolution process in a closed system, once reaches equilibrium, will no longer go further, which means that no more quartz can be further dissolved. Due to the very low solubility of quartz, the amount of quartz that can be dissolved is so limited that no significant influence on strain/porosity can be observed.

This section investigates the dissolution process in an open system. When reaching equilibrium, the concentration of dissolved species will no longer change, but the dissolution process keeps going, the chemicals generated from dissolution is the same as that been brought away by advection, reaching a dynamic equilibrium status.

This time, it is assumed that the porous media is under a constant and uniform temperature of 350K. A fluid flow is injected into the media at a constant Darcy velocity of $1*10^{-7}$m/s from the left toward the right. The concentration distribution will be controlled by advection, diffusion, and reaction, as shown in Figure 6.19. It can be

found that the concentration in the domain increase with time, after 400 hours, the concentration reaches a maximum value of $4.20*10^{-4}$mol/L, which is less than the value in Figure 6.14. After 400 hours, the concentration does not change anymore, however, the dissolution rate is nonzero (Figure 6.20), meaning that the dissolution process keeps going on, this is the same as the estimation before. As given in equation (6.119), the dissolution is only associated with the concentration if assuming the reactive surface area to be constant, therefore, the trend in Figures 6.19 and 6.20 are very similar.

The incessant dissolution process will result in an increasing amount of reaction extent (Figure 6.21): at 10 years, the reaction extent is less than 0.1 moles per unit volume porous media, but at 400 years, it reaches over 1.1 moles per unit volume porous media. Since the dissolution varies with space, the reaction extent also varies with space: the amount of quartz dissolved in the left domain is much more than that in the right domain, as shown in Figure 6.21.

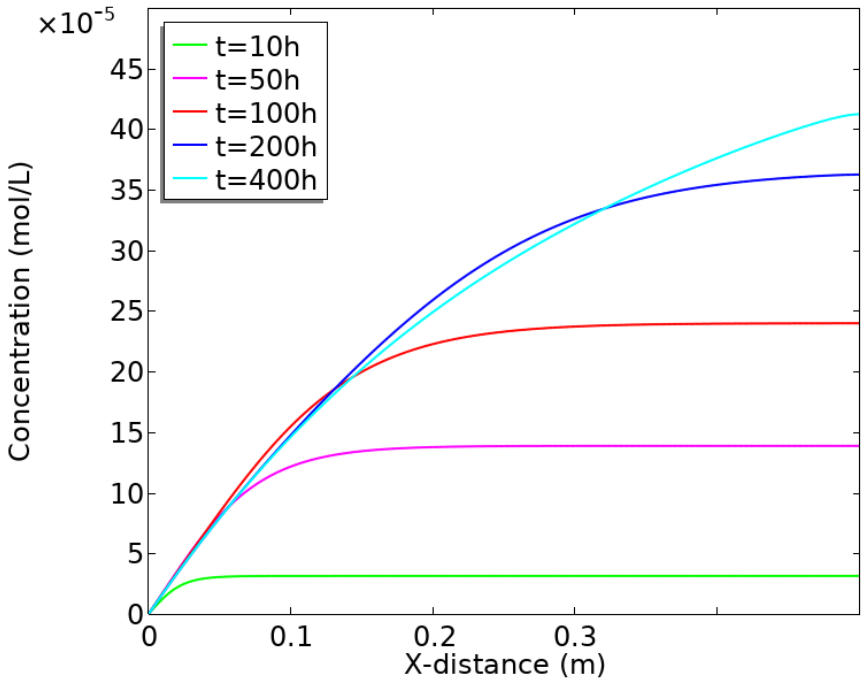

Figure 6. 19 Concentration distribution with time and space (350K)

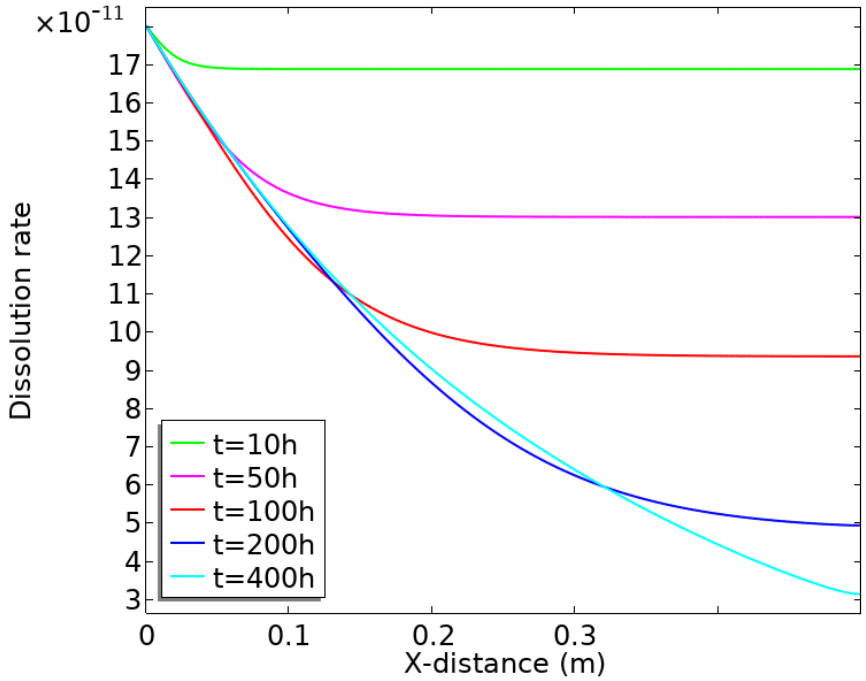

Figure 6. 20 Dissolution rate distribution with time and space (350K)

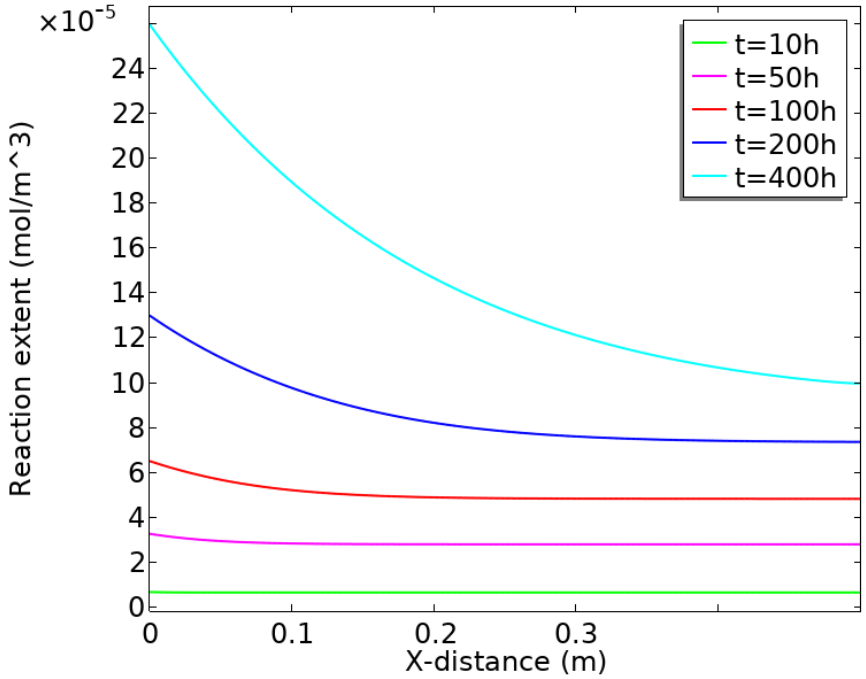

Figure 6. 21 Reaction extent distribution with time and space (350K)

The porosity change is linked to the reaction extent through:

$$\triangle\phi = \frac{M^{qz}}{\rho_t^{qz}}\xi \tag{6.122}$$

where $\frac{M^{qz}}{\rho_t^{qz}} = 22.68cm^3 / mol$ is the molar volume of quartz, $M^{qz} = 60.084g / mol$ is the molar mass of quartz and ρ_t^{qz} is the true density of quartz.

According to Tao et al. (2019), the strain resulting from dissolution is

$$\varepsilon_d = \frac{V_s^{rem}}{V_s^{ini}} - 1 = -\frac{M^{qz}}{\rho_t^{qz}} \frac{d(n)}{V_s} = -\frac{M^{qz}}{\rho_t^{qz}} \frac{1}{1-\phi} \xi \tag{6.123}$$

It can be found that the strain change and porosity change are both related to reaction extent and molar volume. Because the molar volume is very small and the reaction extent within 400 hours is very tiny (Figure 6.21), there couldn't be observable porosity/strain change within 400 hours. If the dissolution process takes place for a sufficiently long time, the amount of quartz that has been dissolved increases to a certain level, and there could be a significant influence. As shown in Figure 6.22, when it comes to 10000 years, the porosity will increase by nearly 0.0013.

If the dissolution reaction is quicker, that is temperature at 400K and Darcy velocity at $1*10^{-6}$m/s, the porosity change can be more significant, as shown in Figure 6.23. The corresponding strain and porosity resulting from dissolution can be easily estimated through relationship (6.123) and (6.122), and are presented in Figure 6.22 and 6.23 (strain switched to positive to fit the strain definition in geotechnical engineering)

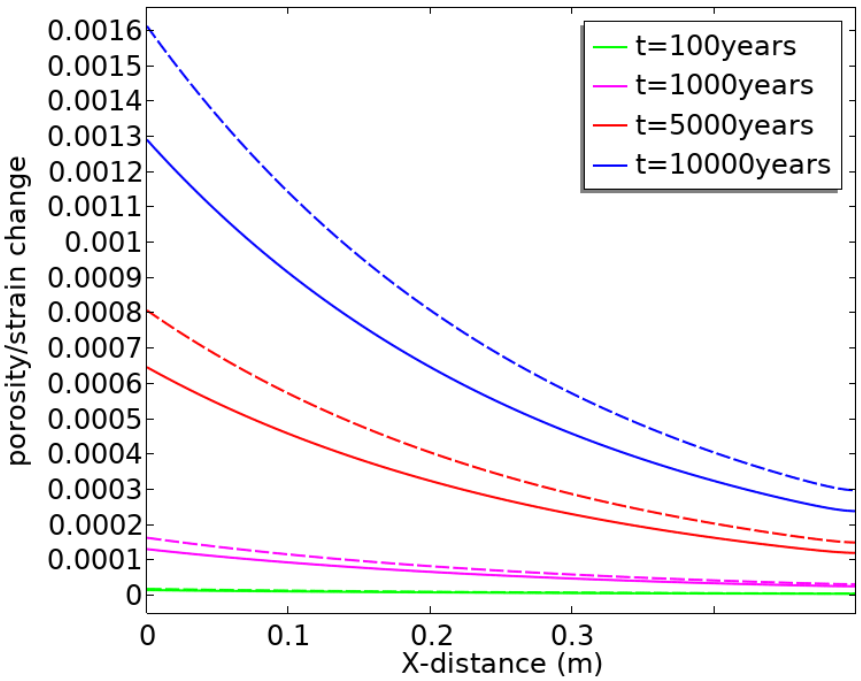

Figure 6. 22 Porosity and strain change with time and space (350K) (Porosity: solid line, strain: dashed line)

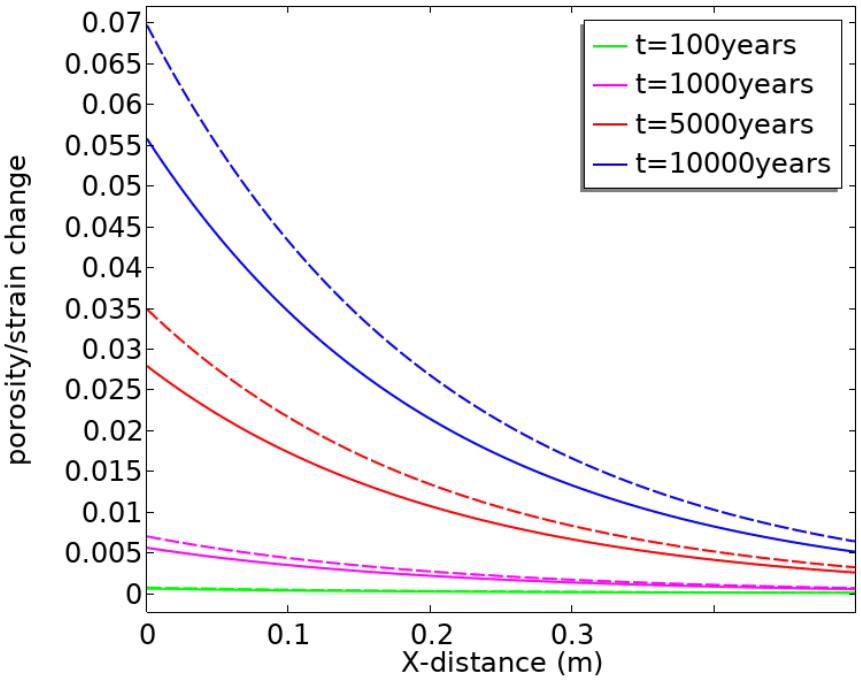

Figure 6. 23 Porosity and strain change with time and space (400K) (Porosity: solid line, strain: dashed line)

6.7.2.3 Conclusion

The numerical simulation shows that the dissolution in a closed system in a high-temperature situation is much quicker than that in low-temperature condition and the equilibrium concentration is also higher under a high temperature. In an open system, dissolution may reach a dynamics equilibrium status, in which case the dissolution keeps going on while the concentration remains constant. However, due to the sluggish dissolution rate, the amount of quartz that can be dissolved in a short time is very limited. If the dissolution keeps going on for over 100 years, the porosity change of strain can be significant.

Although quartz is the major mineral of soil/rock, the dissolution rate is quite slow and solubility quite is low, therefore, in the presented simulation, a long time scale is required to show the influence. If for some minerals of quick dissolution rate, e.g., calcite in acid solution, less time scale may be required.

Chapter 7 Conclusion and recommendations

7.1 Conclusion

A series of new governing equations have been developed using Mixture-Coupling Theory and are summarized as:

1. In chapter 3, the classic Biot's consolidation theory has been extended to include the swelling and dissolution influence by using the Mixture-Coupling Theory. A general coupled structure for swelling and dissolvable materials has been formed. Two parameters, namely, the swelling coefficient and the dissolution coefficient, have been incorporated into the stress-strain equation to represent the influence of swelling and dissolution. The rigorous derivation obtained by using the Mixture-Coupling Theory gives a deep insight of the effects between reaction, deformation, and water pressure, and also extends the application of the Mixture-Coupling Theory. The numerical simulation shows that when there is swelling process, the displacement and strain will be smaller than the no-swelling case, which means that swelling has a resistance effect on consolidation and modelling also shows that the larger the swelling coefficient is, the greater the resistance effect will be. Meanwhile, the dissolution process could promote the consolidation, and the greater dissolution coefficient will lead to a larger displacement and strain. The overall mechanical behaviour depends on the joint influence of swelling and dissolution

2. In chapter 4, the model developed in chapter 3 has been extended to the unsaturated condition. The saturation of pore fluid has been added to the mechanical and hydraulic equation to represent the unsaturated case. The governing equation is the same as those derived from the classic mechanics approach, if neglecting the swelling and dissolution parameter, proving the validity of the approach and the model for the unsaturated case.

The numerical results show that swelling and dissolution have a contrary influence on the rock deformation. The sensitivity analysis shows that the pressure changes faster with a larger permeability, and the mechanical behaviour also changes faster.

3. In chapter 5, the Mixture-Coupling Theory has been further extended to incorporate the swelling and dissolution in the coupled HMC framework. The model considers a detailed reaction type, giving a deep insight into the stress response with dissolution process. The model is very appliable to geotechnical engineering since the concept of reaction extent is friendly to engineers and reachable in either lab experiments or field experiments. The numerical simulation shows the swelling and dissolution process have opposite influence on the displacement, but the swelling influence starts with the pressure change and is effective in a short time period (depending on pressure change) while the dissolution process shows its influence in a long time scale. The simulation also shows that the concentration near the left boundary is dominated by diffusion at the early stage and dominated by diffusion and dissolution at a long time scale; in the middle and right part, the concentration is dominated by dissolution only.

4. In chapter 6, the model in chapter 5 has been further extended to THMC conditions. The entropy change due to fluid transforming from pore space to inter platelet place is considered, and the reaction inducted entropy is also considered. A new term, solid affinity, is introduced to describe the energy change due to the dissolution of solid minerals, providing a more accurate energy change equation during the swelling and dissolution process and making the derivations more rigorous. The fluid loss due to sorption into the interlayer space has been incorporated into the pore fluid transport equation and the chemical mass transport equation as sink terms. The thermal expansion capacity change of the wetted matrix is derived. The influence of bounded mass on heat transport is also derived in the heat transport equation. The new model provides a comprehensive framework to study the swelling and dissolution influence in the

coupled THMC condition. The numerical result shows that the thermal process has a significant influence on the hydraulic and chemical processes, and the swelling process significantly changed the expansion capacity of the wetted matrix. The dissolution of quartz by pure water can be much quicker in a high-temperature situation, however, due to the very low dissolution rate and solubility, the dissolution can only bring significant influence on porosity and strain on a sufficient long-time scale,

7.2 Recommendation for future work

The thesis significantly extends the Mixture-Coupling Theory and the research on THMC coupling. More work could be done in the future:

1. The gas pressure is assumed to be zero in this work, however, on most occasions, gas pressure is non-zero, and it may have a significant influence on the Thermo, Hydro, Mechanical, Chemical process. Meanwhile, the gas transport can be of significant importance in some geotechnical applications like landfill where the gas is poisonous or flammable.

2. The mechanical behaviour of clay/rock has been assumed to be isotropic, homogeneous, and elastic conditions. In real engineering applications, clay often exabit anisotropic, heterogeneous and elastic-plastic features, such characteristics can be taken into account to obtain more realistic mechanical behaviour.

3.The swelling coefficient and dissolution coefficient adopted in this thesis are assumed values. However, it is suggested to determine the swelling coefficient and dissolution through experiments. In the model presented in chapter 3 and 4, the dissolution and swelling influence are linked to the mechanical behaviour through pressure, the relevant coefficient can be obtained through the stress-pressure relationship in the experiments subject to swelling/dissolution influence. In the model presented in chapter 5 and 6,

the reaction extent is adopted as the variable to denote the dissolution influence. The dissolution coefficient can be validated through the relationship between the stress change and the reaction extent obtained in experiments. The swelling coefficient may be obtained through the relationship between the stress change and water pressure change in a swelling test.

4. The entropy production due to mass exchange and reactive dissolution are ignored in chapter 5 but are considered in chapter 6, the derived constitutive relations are very similar. Why do different considerations lead to similar results? In what condition can the entropy production be ignored?

5. From the numerical result, the temperature dependency coefficient of chemical potential has a great influence on the thermal expansion capacity of the wetted matrix. More experiments and theoretical work are required to determine this coefficient and verify its sensitivity to the expansion capacity change.

6. The dissolution process in geotechnical engineering also takes place in a long time scale, therefore, it would be of significance to study the influence of dissolution together with the creep phenomenon.

7. The numerical simulation considers only the dissolution of quartz for demonstration purposes. However, in engineering applications, such as carbon capture and storage, the mineral composition may include quartz, silica, mica, feldspar, etc. The dissolution of these minerals, as well as the precipitation of secondary minerals, can all be taken in account to model more complex reactions and corresponding couplings with other processes.

8. The numerical simulation presented in the thesis are simple 1D or 2D for isotropic

condition. More complex 2D or 3D models with real geometry and boundary condition, as well as anisotropic and heterogeneous properties would be more helpful to predict the mechanical, hydraulic, chemical and thermal behaviour of engineering applications like nuclear waste disposal, carbon capture and storage.

9. The presented models are highly theoretical, more work is required to apply the model to practice. In the first step, proper numerical algorithm should be adopted to solve the equations. In the second step, reasonable simplification can be made based on engineering problems. The presented mathematical equations include almost every aspect of the THMC coupling, however, some of them can be neglected to meet the engineering requirement, for example, the temperature influence in isothermal condition. Then, material parameters from field or lab experiments are required. It should be noticed that when doing the fully coupled modelling of dissolution, the mechanical property degradation much be considered. It is suggested to develop an engineer-friendly Graphical User Interface (GUI) which allows the users to select modulus by simple click instead of editing equations or programming work.

References

Aghighi, MA, Lv, A,Roshan, H 2021. Non-equilibrium thermodynamics approach to mass transport in sorptive dual continuum porous media: A theoretical foundation and numerical simulation. *Journal of Natural Gas Science and Engineering,* 87**,** 103757.

Akaki, T,Kimoto, S 2020. Numerical modelling of internal erosion during hydrate dissociation based on multiphase mixture theory. *International Journal for Numerical and Analytical Methods in Geomechanics,* 44**,** 327-350.

Al-Fattah, SM, Barghouty, MF,Dabbousi, BO 2011. *Carbon capture and storage: technologies, policies, economics, and implementation strategies,* CRC Press.

Alexander, WR,Mckinley, L 2011. Deep geological disposal of radioactive waste.

Amanullah, M, Marsden, J,Shaw, H. Effects of rock-fluid interactions on the petrofabric and stress-strain behaviour of mudrocks. Rock Mechanics in Petroleum Engineering, 1994. OnePetro.

Amorim, C, Lopes, R, Barroso, R, Queiroz, J, Alves, D, Perez, C,Schelin, H 2007. Effect of clay–water interactions on clay swelling by X-ray diffraction. *Nuclear Instruments and Methods in Physics Research Section A: Accelerators, Spectrometers, Detectors and Associated Equipment,* 580**,** 768-770.

Anderson, R, Ratcliffe, I, Greenwell, H, Williams, P, Cliffe, S,Coveney, P 2010. Clay swelling—a challenge in the oilfield. *Earth-Science Reviews,* 98**,** 201-216.

Atkin, RJ,Craine, RE 1976. Continuum Theories of Mixtures: Basic Theory and Historical Development. *The Quarterly Journal of Mechanics and Applied Mathematics,* 29.

Bandyopadhyay, A 2014. *Carbon Capture and Storage: CO2 Management Technologies,* CRC Press.

Bea, SA, Mayer, U,Macquarrie, K 2016. Reactive transport and thermo‐hydro‐mechanical coupling in deep sedimentary basins affected by glaciation cycles:

model development, verification, and illustrative example. *Geofluids,* 16**,** 279-300.

Beis 2018. IMPLEMENTING GEOLOGICAL DISPOSAL – WORKING WITH COMMUNITIES. Department for Business, Energy & Industrial Strategy, UK.

Bennethum, LS,Cushman, JH 1996. Multiscale, hybrid mixture theory for swelling systems—II: Constitutive theory. *International Journal of Engineering Science,* 34**,** 147-169.

Berryman, JG 2002. Extension of poroelastic analysis to double-porosity materials: New technique in microgeomechanics. *Journal of engineering mechanics,* 128**,** 840-847.

Berryman, JG,Wang, HF 1995. The elastic coefficients of double‐porosity models for fluid transport in jointed rock. *Journal of Geophysical Research: Solid Earth,* 100**,** 24611-24627.

Biot, MA 1941. General theory of three-dimensional consolidation. *Journal of applied physics,* 12**,** 155-164.

Biot, MA 1955. Theory of deformation of a porous viscoelastic anisotropic solid. *Journal of applied physics,* 27**,** 459-467.

Biot, MA 1962. Mechanics of deformation and acoustic propagation in porous media. *Journal of applied physics,* 33**,** 1482-1498.

Biot, MA 1973. Nonlinear and semilinear rheology of porous solids. *Journal of Geophysical Research,* 78**,** 4924-4937.

Biot, MA,Temple, G 1972. Theory of finite deformations of porous solids. *Indiana University Mathematics Journal,* 21**,** 597-620.

Borja, RI,Koliji, A 2009. On the effective stress in unsaturated porous continua with double porosity. *Journal of the Mechanics and Physics of Solids,* 57**,** 1182-1193.

Boutin, C,Royer, P 2015. On models of double porosity poroelastic media. *Geophysical Supplements to the Monthly Notices of the Royal Astronomical Society,* 203**,** 1694-1725.

Bowen, RM 1976. Theory of mixtures. *In:* ERINGEN, A. C. (ed.) *Continuum Physics* New York Academic Press.

Bowen, RM 1980. Incompressible Porous-Media Models by Use of the Theory of Mixtures. *International Journal of Engineering Science,* 18**,** 1129-1148.

Bowen, RM 1982. Compressible porous media models by use of the theory of mixtures. *International Journal of Engineering Science,* 20**,** 697-735.

Bowen, RM 1984. Diffusion models implied by the theory of mixtures. *In:* TRUESDELL, C. (ed.) *Rational Thermodynamics* New York: Springer-Verlag.

Bricker, OP 1988. The Global Water Cycle Geochemistry, and Environment. *Eos, Transactions American Geophysical Union,* 69**,** 51-51.

Brown, G 1982. *Crystal structures of clay minerals and their X-ray identification,* The Mineralogical Society of Great Britain and Ireland.

Callari, C,Federico, F 2000. FEM validation of a double porosity elastic model for consolidation of structurally complex clayey soils. *International journal for numerical and analytical methods in geomechanics,* 24**,** 367-402.

Castellanos, E, Villar, M, Romero, E, Lloret, A,Gens, A 2008. Chemical impact on the hydro-mechanical behaviour of high-density FEBEX bentonite. *Physics and Chemistry of the Earth, Parts A/B/C,* 33**,** S516-S526.

Chan, T, Khair, K,Vuillod, E 1996. Generic study of coupled THM processes of nuclear waste repositories as near-field initial boundary value problems (BMT2). *Developments in geotechnical engineering,* 79**,** 281-309.

Chavali, RVP, Vindula, SK, Babu, A,Pillai, RJ 2017. Swelling behavior of kaolinitic clays contaminated with alkali solutions: a micro-level study. *Applied Clay Science,* 135**,** 575-582.

Chen, C, Zhang, L,Shen, P 2020. Influence of mineral dissolution on the mechanical behaviour of a granular assembly under complex stress states. *International Journal of Rock Mechanics and Mining Sciences,* 136**,** 104546.

Chen, D, Yurtdas, I, Burlion, N,Shao, J-F 2007. Elastoplastic damage behavior of a mortar subjected to compression and desiccation. *Journal of engineering mechanics,* 133**,** 464-472.

Chen, X 2013. Constitutive unsaturated hydro-mechanical model based on modified mixture theory with consideration of hydration swelling. *International Journal of Solids and Structures,* 50**,** 3266-3273.

Chen, X,Hicks, MA 2009. Influence of water chemical potential on the swelling of water sensitive materials. *Computers & structures,* 88**,** 1498-1505.

Chen, X,Hicks, MA 2011. A constitutive model based on modified mixture theory for unsaturated rocks. *Computers and Geotechnics,* 38**,** 925-933.

Chen, X,Hicks, MA 2013. Unsaturated hydro-mechanical-chemo coupled constitutive model with consideration of osmotic flow. *Computers and Geotechnics,* 54**,** 94-103.

Chen, X, Pao, W,Li, X 2013. Coupled thermo-hydro-mechanical model with consideration of thermal-osmosis based on modified mixture theory. *International Journal of Engineering Science,* 64**,** 1-13.

Chen, X, Pao, W, Thornton, S,Small, J 2016. Unsaturated hydro-mechanical–chemical constitutive coupled model based on mixture coupling theory: Hydration swelling and chemical osmosis. *International Journal of Engineering Science,* 104**,** 97-109.

Chen, X, Thornton, SF,Pao, WJIJOES 2018. Mathematical model of coupled dual chemical osmosis based on mixture-coupling theory. *International Journal of Engineering Science,* 129**,** 145-155.

Chen, X, Thornton, SF,Small, J 2015. Influence of hyper-alkaline pH leachate on mineral and porosity evolution in the chemically disturbed zone developed in the near-field host rock for a nuclear waste repository. *Transport in Porous Media,* 107**,** 489-505.

Chen, Z-G, Tang, C-S, Zhu, C, Shi, B,Liu, Y-M 2017. Compression, swelling and rebound behavior of GMZ bentonite/additive mixture under coupled hydro-mechanical condition. *Engineering Geology,* 221**,** 50-60.

Choo, J, White, JA,Borja, RI 2016. Hydromechanical modeling of unsaturated flow in double porosity media. *International Journal of Geomechanics,* 16**,** D4016002.

Ciantia, MO, Castellanza, R, Crosta, GB,Hueckel, T 2015. Effects of mineral suspension and dissolution on strength and compressibility of soft carbonate rocks. *Engineering Geology,* 184**,** 1-18.

Cosenza, P, Ghoreychi, M, De Marsily, G, Vasseur, G,Violette, S 2002. Theoretical prediction of poroelastic properties of argillaceous rocks from in situ specific storage coefficient. *Water Resources Research,* 38**,** 25-1-25-12.

Coussy, O 1995. *Mechanics of porous continua*, Wiley.

Coussy, O 2004. *Poromechanics*, John Wiley & Sons.

Cui, L,Fall, M 2015. A coupled thermo–hydro-mechanical–chemical model for underground cemented tailings backfill. *Tunnelling and Underground Space Technology*, 50**,** 396-414.

Cuisinier, O,Masrouri, F 2004. Testing the hydromechanical behavior of a compacted swelling soil. *Geotechnical Testing Journal,* 27**,** 598-606.

Cuisinier, O,Masrouri, F 2005. Hydromechanical behaviour of a compacted swelling soil over a wide suction range. *Engineering Geology,* 81**,** 204-212.

Detournay, E,Cheng, A 1993. *Fundamentals of poroelasticity*.

Diaz-Perez, A, Cortes-Monroy, I,Roegiers, J 2007. The role of water/clay interaction in the shale characterization. *Journal of petroleum Science and Engineering,* 58**,** 83-98.

Drits, V, Środoń, J,Eberl, D 1997. XRD measurement of mean crystallite thickness of illite and illite/smectite: Reappraisal of the Kubler index and the Scherrer equation. *Clays and clay minerals,* 45**,** 461-475.

Einstein, H 1996. Tunnelling in difficult ground—swelling behaviour and identification of swelling rocks. *Rock mechanics and rock engineering,* 29**,** 113-124.

Emmanuel, S,Berkowitz, B 2007. Effects of pore‐size controlled solubility on reactive transport in heterogeneous rock. *Geophysical Research Letters,* 34.

Ericsson, LO 1999. Geoscientific R&D for high level radioactive waste disposal in Sweden — current status and future plans. *Engineering Geology,* 52**,** 305-317.

Esrl. 2017. Available: https://www.esrl.noaa.gov/gmd/ccgg/trends/global.html#global_data [Accessed 29,Nov 2017].

Fan, C, Luo, M, Li, S, Zhang, H, Yang, Z,Liu, Z 2019. A thermo-hydro-mechanical-chemical coupling model and its application in acid fracturing enhanced coalbed methane recovery simulation. *Energies,* 12**,** 626.

Fournier, RO,Potter Ii, RW 1982. An equation correlating the solubility of quartz in water from 25 to 900 C at pressures up to 10,000 bars. *Geochimica et Cosmochimica Acta,* 46**,** 1969-1973.

Fredd, CN,Fogler, HS 1998. Influence of transport and reaction on wormhole formation in porous media. *AIChE journal,* 44**,** 1933-1949.

Freiesleben, H 2013. Final disposal of radioactive waste. *The European Physical Journal. Web of Conferences : Proceedings,* 54**,** 01006-01006.

Fukushima, Y, Okada, A, Kawasumi, M, Kurauchi, T,Kamigaito, O 1988. Swelling behaviour of montmorillonite by poly-6-amide. *Clay Minerals,* 23**,** 27-34.

Gao, J, Lin, H, Wu, B, Deng, J,Liu, H 2021. Porochemothermoelastic solutions considering fully coupled thermo-hydro-mechanical-chemical processes to analyze the stability of inclined boreholes in chemically active porous media. *Computers and Geotechnics,* 134**,** 104019.

Gawin, D, Pesavento, F,Schrefler, B 2003. Modelling of hygro-thermal behaviour of concrete at high temperature with thermo-chemical and mechanical material

degradation. *Computer methods in applied mechanics and engineering,* 192**,** 1731-1771.

Gawin, D, Pesavento, F,Schrefler, BA 2008. Modeling of cementitious materials exposed to isothermal calcium leaching, considering process kinetics and advective water flow. Part 1: Theoretical model. *International journal of solids and structures,* 45**,** 6221-6240.

Gens, A,Alonso, E 1992. A framework for the behaviour of unsaturated expansive clays. *Canadian Geotechnical Journal,* 29**,** 1013-1032.

Gens, A, Guimarães, LDN,Olivella, S 2002. Coupled chemomechanical analysis for saturated and unsaturated soils. *Environmental geomechanics***,** 109-123.

Gens, A, Guimarães, LDN,Olivella, S 2005. THMC coupling in partially saturated geomaterials. *Revue européenne de génie civil,* 9**,** 747-765.

Gens, A, Guimarães, LDN, Olivella, S,Sánchez, M 2004. Analysis of the THMC behaviour of compacted swelling clay for radioactive waste isolation. *Elsevier Geo-Engineering Book Series,* 2**,** 317-322.

Gens, A, Guimaräes, LDN, Olivella, S, Sánchez, MJJORM,Engineering, G 2010. Modelling thermo-hydro-mechano-chemical interactions for nuclear waste disposal. *Journal of Rock Mechanics and Geotechnical Engineering,* 2**,** 97-102.

Gerard, B, Pijaudier-Cabot, G,Laborderie, C 1998. Coupled diffusion-damage modelling and the implications on failure due to strain localisation. *International Journal of Solids and Structures,* 35**,** 4107-4120.

Ghassemi, A,Diek, A 2003. Linear chemo-poroelasticity for swelling shales: theory and application. *Journal of Petroleum Science and Engineering,* 38**,** 199-212.

Ghassemi, A, Tao, Q,Diek, A 2009. Influence of coupled chemo-poro-thermoelastic processes on pore pressure and stress distributions around a wellbore in swelling shale. *Journal of petroleum science and Engineering,* 67**,** 57-64.

Ghirian, A. 2016. *Coupled Thermo-Hydro-Mechanical-Chemical (THMC) Processes in Cemented Tailings Backfill Structures and Implications for their Engineering Design.* Université d'Ottawa/University of Ottawa.

Ghirian, A,Fall, M. Experimental investigations of the thermo-hydro-mechanical-chemical behavior of cemented paste backfill. 23rd World Mining Congress. Montreal, Canada, 2013. 21.

Gluyas, J,Mathias, S 2013. *Geological storage of carbon dioxide (CO2): Geoscience, technologies, environmental aspects and legal frameworks*, Elsevier.

Grasley, Z,Rajagopal, K 2012. Revisiting total, matric, and osmotic suction in partially saturated geomaterials. *Zeitschrift für angewandte Mathematik und Physik,* 63**,** 373-394.

Gray, WG,Miller, CT 2014. *Introduction to the thermodynamically constrained averaging theory for porous medium systems*, Springer.

Guimaraes, LDN, Gens, A, Sanchez, M,Olivella, S 2006. THM and reactive transport analysis of expansive clay barrier in radioactive waste isolation. *Communications in numerical methods in engineering,* 22**,** 849-859.

Guimarães, LDN, Gens, A, Sánchez, M,Olivella, S. A chemo-mechanical constitutive model accounting for cation exchange in expansive clays. Bio-and Chemo-Mechanical Processes in Geotechnical Engineering: Géotechnique Symposium in Print 2013, 2014. ICE Publishing, 18-31.

Guthrie, GD,Carey, JW 2015. A thermodynamic and kinetic model for paste–aggregate interactions and the alkali–silica reaction. *Cement and Concrete Research,* 76**,** 107-120.

Haase, R 1990. *Thermodynamics of irreversible processes,* New York, Dover.

Han, WS, Mcpherson, BJ, Lichtner, PC,Wang, FP 2010. Evaluation of trapping mechanisms in geologic CO2 sequestration: Case study of SACROC northern platform, a 35-year CO2 injection site. *American Journal of Science,* 310**,** 282-324.

Haxaire, A,Djeran-Maigre, I 2009. Influence of dissolution on the mechanical behaviour of saturated deep argillaceous rocks. *Engineering geology,* 109**,** 255-261.

Heidug, W,Wong, SW 1996. Hydration swelling of water ‐ absorbing rocks: a constitutive model. *International Journal for Numerical and Analytical Methods in Geomechanics,* 20**,** 403-430.

Hosking, LJ, Chen, M,Thomas, HR 2020. Numerical analysis of dual porosity coupled thermo-hydro-mechanical behaviour during CO2 sequestration in coal. *International Journal of Rock Mechanics and Mining Sciences,* 135**,** 104473.

Hu, D, Zhou, H, Hu, Q, Shao, J, Feng, X,Xiao, H 2012. A hydro-mechanical-chemical coupling model for geomaterial with both mechanical and chemical damages considered. *Acta Mechanica Solida Sinica,* 25**,** 361-376.

Hueckel, TA 1992. Water–mineral interaction in hygromechanics of clays exposed to environmental loads: a mixture-theory approach. *Canadian Geotechnical Journal,* 29**,** 1071-1086.

Humphrey, J,Rajagopal, K 2002. A constrained mixture model for growth and remodeling of soft tissues. *Mathematical models and methods in applied sciences,* 12**,** 407-430.

Humphrey, J,Rajagopal, K 2003. A constrained mixture model for arterial adaptations to a sustained step change in blood flow. *Biomechanics and modeling in mechanobiology,* 2**,** 109-126.

Huyghe, J,Janssen, J 1999. Thermo-chemo-electro-mechanical formulation of saturated charged porous solids. *Transport in Porous Media,* 34**,** 129-141.

Israelachvili, JN 1991. *Intermolecular and surface forces,* London, Academic Press.

Isrm. Commission on swelling rock and working group on swelling-rock of the commission on testing methods (suggested methods for laboratory testing of argillaceous swelling rocks). International Journal of Rock Mechanics, Mining Sciences & Geomechanics Abstracts, 1989. 415-426.

Jia, Y, Bian, H, Xie, S, Burlion, N,Shao, J 2017. A numerical study of mechanical behavior of a cement paste under mechanical loading and chemical leaching. *International Journal for Numerical and Analytical Methods in Geomechanics,* 41**,** 1848-1869.

Jing, L,Feng, X 2003. NUMERICAL MODELING FOR COUPLED THERMO-HYDRO-MECHANICAL AND CHEMICAL PROCESSES (THMC) OF GEOLOGICAL MEDIA——INTERNATIONAL AND CHINESE EXPERIENCES. *Chinese Journal of Rock Mechanics and Engineering,* 22**,** 1715.

Job, G,Herrmann, F 2006. Chemical potential—a quantity in search of recognition. *European Journal of Physics,* 27**,** 353.

Kanfar, MF, Chen, Z,Rahman, SS 2017. Analyzing wellbore stability in chemically-active anisotropic formations under thermal, hydraulic, mechanical and chemical loadings. *Journal of Natural Gas Science and Engineering,* 41**,** 93-111.

Karaborni, S, Smit, B, Heidug, W, Urai, J,Van Oort, E 1996. The swelling of clays: molecular simulations of the hydration of montmorillonite. *Science,* 271**,** 1102-1104.

Karalis, TK 1992. Thermodynamics of soils swelling non-hydrostatically. *Mechanics of Swelling.* Springer.

Karrech, A 2013. Non-equilibrium thermodynamics for fully coupled thermal hydraulic mechanical chemical processes. *Journal of the Mechanics and Physics of Solids,* 61**,** 819-837.

Katachalsky, A,Curran, PF 1965. *Nonequilibrium thermodynamics in biophysics,* Cambridge, MA, Harvard University Press.

Katchalsky, A,Curran, PF 1965. *Nonequilibrium thermodynamics in biophysics,* Cambridge, MA, Harvard University Press.

Katsube, N,Carroll, MM 1987. The Modified Mixture Theory for Fluid-Filled Porous Materials: Theory. *Journal of Applied Mechanics,* 54**,** 35-40.

Keeling, CD, Bacastow, RB, Bainbridge, AE, Ekdahl Jr, CA, Guenther, PR, Waterman, LS,Chin, JF 1976. Atmospheric carbon dioxide variations at Mauna Loa observatory, Hawaii. *Tellus,* 28**,** 538-551.

Khalili, N 2003. Coupling effects in double porosity media with deformable matrix. *Geophysical Research Letters,* 30.

Kivi, IR, Ameri, MJ,Ghassemi, A 2015. Chemoporoelastic characterization of Ghom shale. *Journal of Petroleum Science and Engineering,* 127**,** 115-123.

Kleinfelter, N, Park, M,Cushman, JH 2007. Mixture theory and unsaturated flow in swelling soils. *Transport in porous media,* 68**,** 69-89.

Kondepudi, D,Prigogine, I 2014. *Modern thermodynamics: from heat engines to dissipative structures,* John Wiley & Sons.

Kowalsky, U, Bente, S,Dinkler, D 2014. Modeling of coupled THMC processes in porous media. *Coupled systems mechanics,* 3**,** 27-52.

Kuhl, D, Bangert, F,Meschke, G 2004. Coupled chemo-mechanical deterioration of cementitious materials. Part I: Modeling. *International Journal of Solids and Structures,* 41**,** 15-40.

Lai, Y, Wu, Z, Zhu, Y,Zhu, L 1999. Nonlinear analysis for the coupled problem of temperature and seepage fields in cold regions tunnels. *Cold Regions Science and Technology,* 29**,** 89-96.

Laloui, L, Klubertanz, G,Vulliet, L 2003. Solid-liquid-air coupling in multiphase porous media. *International Journal for Numerical and Analytical Methods in Geomechanics,* 27**,** 183-206.

Lei, X, Wong, H, Fabbri, A, Limam, A,Cheng, Y 2014. A thermo-chemo-electro-mechanical framework of unsaturated expansive clays. *Computers and Geotechnics,* 62**,** 175-192.

Lei, X, Wong, H, Fabbri, A, Limam, A,Cheng, Y 2016. A chemo-elastic–plastic model for unsaturated expansive clays. *International Journal of Solids and Structures,* 88**,** 354-378.

Lewis, RW,Schrefler, BA 1987. *The finite-element method in deformation and consolidation of porous media,* New York, Wiley.

Lewis, RW,Schrefler, BA 1998. *The Finite Element Method in the Static and Dynamic Deformation and Consolidation of Porous Media,* New York, John willey & sons.

Li, X,Zienkiewicz, OC 1992. Multiphase flow in deforming porous media and finite element solutions. *Computers & structures,* 45**,** 2l 1-227.

Lichtner, P,Seth, M 1996. User's manual for MULTIFLO: Part II MULTIFLO 1.0 and GEM 1.0 Multicomponent-multiphase reactive transport model. *Southwest Research Institute*.

Lin, Y, Zhou, K, Li, J, Ke, B,Gao, R 2020. Weakening laws of mechanical properties of sandstone under the effect of chemical corrosion. *Rock Mechanics and Rock Engineering,* 53**,** 1857-1877.

Liu, Y, Wang, J, Zhao, X, Ke, D, Xie, J, Cao, S, Ma, L, Jiang, W,Chen, L. Design and development of a large-scale THMC experiment of compacted bentonite for geological disposal of high level radioactive waste in China. 12th ISRM Congress, 2011. International Society for Rock Mechanics.

Loret, B, Hueckel, T,Gajo, A 2002. Chemo-mechanical coupling in saturated porous media: elastic–plastic behaviour of homoionic expansive clays. *International Journal of Solids and Structures,* 39**,** 2773-2806.

Lu, G, Fall, M,Cui, L 2017. A multiphysics-viscoplastic cap model for simulating blast response of cemented tailings backfill. *Journal of Rock Mechanics and Geotechnical Engineering,* 9**,** 551-564.

Lyu, Q, Long, X, Ranjith, P, Tan, J, Kang, Y,Luo, W 2018. A damage constitutive model for the effects of CO2-brine-rock interactions on the brittleness of a low-clay shale. *Geofluids,* 2018.

Ma, T, Chen, Y,Duan, M 2018. Chemo-poroelastic coupling method for wellbore stability analysis in shale gas formation with weakness planes. *Geotechnical and Geological Engineering,* 36**,** 1817-1831.

Ma, Y, Chen, X-H,Yu, H-S 2020. An extension of Biot's theory with molecular influence based on mixture coupling theory: Mathematical model. *International Journal of Solids and Structures,* 191**,** 76-86.

Ma, Y, Chen, X, Hosking, LJ, Yu, H-S,Thomas, HR 2022. THMC constitutive model for membrane geomaterials based on Mixture Coupling Theory. *International Journal of Engineering Science,* 171**,** 103605.

Manning, CE 1994. The solubility of quartz in H2O in the lower crust and upper mantle. *Geochimica et Cosmochimica Acta,* 58**,** 4831-4839.

Maßmann, J, Ziefle, G, Kohlmeier, M, Zielke, W,Shao, H. Coupled hydro-mechanical modeling of seasonally affected unsaturated claystone. GeoProc 2006 – Proc. of 2nd Int. Conf. on Coupled T-H-M-C Processes in Geo-systems: Fundamentals, Modeling, Experiments and Applications, 05/2006 2006 Nanjing, China. 555-560.

Massoudi, M 2003. Constitutive relations for the interaction force in multicomponent particulate flows. *International Journal of Non-Linear Mechanics,* 38**,** 313-336.

Massoudi, M 2010. A Mixture Theory formulation for hydraulic or pneumatic transport of solid particles. *International Journal of Engineering Science,* 48**,** 1440-1461.

Massoudi, M,Antaki, JF 2008. An anisotropic constitutive equation for the stress tensor of blood based on mixture theory. *Mathematical Problems in Engineering,* 2008.

Meroi, E, Schrefler, B,Zienkiewicz, O 1995. Large strain static and dynamic semisaturated soil behaviour. *International Journal for Numerical and Analytical Methods in Geomechanics,* 19**,** 81-106.

Merxhani, A 2016. An introduction to linear poroelasticity. *arXiv preprint arXiv:1607.04274*.

Miao, T, Niu, Y, Guo, L,Zhang, C 1999. Modeling on coupled heat and moisture transfer in freezing soil using mixture theory. *Science in China Series D: Earth Sciences,* 42**,** 9-16.

Mohammed, HQ 2017. *Geomechanical analysis of the wellbore instability problems in Nahr Umr Formation southern Iraq,* Missouri University of Science and Technology.

Momeni, A, Hashemi, S, Khanlari, G,Heidari, M 2017. The effect of weathering on durability and deformability properties of granitoid rocks. *Bulletin of Engineering Geology and the Environment,* 76**,** 1037-1049.

Mooney, R, Keenan, A,Wood, L 1952. Adsorption of water vapor by montmorillonite. II. Effect of exchangeable ions and lattice swelling as measured by X-ray diffraction. *Journal of the American Chemical Society,* 74**,** 1371-1374.

Morey, G, Fournier, R,Rowe, J 1962. The solubility of quartz in water in the temperature interval from 25 to 300 C. *Geochimica et Cosmochimica Acta,* 26**,** 1029-1043.

Morland, L 1972. A simple constitutive theory for a fluid‐saturated porous solid. *Journal of geophysical research,* 77**,** 890-900.

Moyce, EB, Rochelle, C, Morris, K, Milodowski, AE, Chen, X, Thornton, S, Small, JS,Shaw, S 2014. Rock alteration in alkaline cement waters over 15 years and its relevance to the geological disposal of nuclear waste. *Applied Geochemistry,* 50**,** 91-105.

Moyne, C,Murad, MA 2002. Electro-chemo-mechanical couplings in swelling clays derived from a micro/macro-homogenization procedure. *International Journal of Solids and Structures,* 39**,** 6159-6190.

Murad, MA, Bennethum, LS,Cushman, JH 1995. A multi-scale theory of swelling porous media: I. Application to one-dimensional consolidation. *Transport in Porous Media,* 19**,** 93-122.

Murad, MA,Cushman, JH 2000. Thermomechanical theories for swelling porous media with microstructure. *International Journal of Engineering Science,* 38**,** 517-564.

Nandanwar, MS,Anderson, BJ. Coupled Reservoir, Wellbore and Surface Plant Simulations for Enhanced Geothermal Systems. Proceedings, 2014.

Nasir, O, Fall, M,Evgin, E 2014. A simulator for modeling of porosity and permeability changes in near field sedimentary host rocks for nuclear waste under climate change influences. *Tunnelling and underground space technology,* 42**,** 122-135.

Nasir, O, Fall, M, Nguyen, ST,Evgin, E 2013. Modeling of the thermo-hydro-mechanical–chemical response of sedimentary rocks to past glaciations. *International Journal of Rock Mechanics and Mining Sciences,* 64**,** 160-174.

Nda 2015. Geological disposal—How the world is dealing with its radioactive wastes.

Nda 2019. 2019 UK RADIOACTIVE WASTE INVENTORY. Nuclear Decommissioning Authority.

Nea, O 2008. Moving Forward with Geological Disposal of Radioactive Waste, A Collective Statement by the NEA Radioactive Waste Management Committee (RWMC). Nuclear Energy Agency(NEA), Organisation for Economic Co-operation and Development,.

Nea, O 2013. The nature and purpose of the post-closure safety cases for geological repositories. Nuclear Energy Agency(NEA), Organisation for Economic Co-operation and Development,.

Neuman, SP 1975. Galerkin approach to saturated–unsaturated flow in porous media. *In:* GALLAGHER, R. H., ODEN, J. T., TAYLOR, C. & ZIENKIEWICZ, O. C. (eds.) *Finite Elements in Fluids.* New York: John Wiley & Sons.

Nguyen, BN, Hou, Z, Bacon, DH, Murray, CJ,White, MD 2016. Three-dimensional modeling of the reactive transport of CO2 and its impact on geomechanical

properties of reservoir rocks and seals. *International Journal of Greenhouse Gas Control,* 46**,** 100-115.

Nnl 2016. Summary of the BIGRAD project and its implications for a geological disposal facility. *A report prepared for and on behalf of Radioactive Waste Management Ltd.*

Norrish, K 1954. The swelling of montmorillonite. *Discussions of the Faraday society,* 18**,** 120-134.

Nowamooz, H, Mrad, M, Abdallah, A,Masrouri, F 2009. Experimental and numerical studies of the hydromechanical behaviour of a natural unsaturated swelling soil. *Canadian Geotechnical Journal,* 46**,** 393-410.

Ogata, S, Yasuhara, H, Aoyagi, K,Kishida, K. Coupled THMC analysis for predicting hydro-mechanical evolution in siliceous mudstone. 53rd US Rock Mechanics/Geomechanics Symposium, 2019. OnePetro.

Peng, S,Zhang, J 2007. *Engineering geology for underground rocks*, Springer Science & Business Media.

Peter, GJ. Application of Coupled Thermo-Hydro-Mechanical-Chemical (THMC) Processes in Hydrothermal Systems to Processes Near a High-Level Nuclear Waste Repository. ASME 2011 14th International Conference on Environmental Remediation and Radioactive Waste Management, 2011. American Society of Mechanical Engineers, 737-745.

Prevost, JH 1982. Nonlinear transient phenomena in saturated porous media. *Computer Methods in Applied Mechanics and Engineering,* 30**,** 3-18.

Prévost, JH 1980. Mechanics of continuous porous media. *International Journal of Engineering Science,* 18**,** 787-800.

Qi, S, Yue, ZQ, Liu, C,Zhou, Y 2009. Significance of outward dipping strata in argillaceous limestones in the area of the Three Gorges reservoir, China. *Bulletin of engineering geology and the environment,* 68**,** 195-200.

Quirk, J,Marcelja, S 1997. Application of double-layer theories to the extensive crystalline swelling of Li-montmorillonite. *Langmuir,* 13**,** 6241-6248.

Rajagopal, K 2007. On a hierarchy of approximate models for flows of incompressible fluids through porous solids. *Mathematical Models and Methods in Applied Sciences,* 17**,** 215-252.

Rajagopal, K,Tao, L 2005. On the propagation of waves through porous solids. *International Journal of Non-Linear Mechanics,* 40**,** 373-380.

Rajagopal, KR,Tao, L 1995. *Mechanics of mixtures,* Singapore, World scientific publishing.

Rebreanu, L, Vanderborght, J-P,Chou, L 2008. The diffusion coefficient of dissolved silica revisited. *Marine chemistry,* 112**,** 230-233.

Rejeb, A,Cabrera, J 2004. DECOVALEX-THMC, Description for Task C, Excavation Disturbed Zone (EDZ) in the argillaceous Tournemire site (France). *Technical report.* France Institute of Radioprotection and Nuclear Safety (IRSN).

Rice, JR,Cleary, MP 1976. Some basic stress diffusion solutions for fluid - saturated elastic porous media with compressible constituents. *Reviews of Geophysics,* 14**,** 227-241.

Rimstidt, JD 1997. Quartz solubility at low temperatures. *Geochimica et Cosmochimica Acta,* 61**,** 2553-2558.

Roshan, H,Aghighi, MA 2012. Chemo-poroelastic analysis of pore pressure and stress distribution around a wellbore in swelling shale: effect of undrained response and horizontal permeability anisotropy. *Geomechanics and Geoengineering,* 7**,** 209-218.

Roshan, H,Oeser, M 2012. A non-isothermal constitutive model for chemically active elastoplastic rocks. *Rock mechanics and rock engineering,* 45**,** 361-374.

Roshan, H,Rahman, S 2011. A fully coupled chemo-poroelastic analysis of pore pressure and stress distribution around a wellbore in water active rocks. *Rock mechanics and rock engineering,* 44**,** 199-210.

Rutqvist, J,Stephansson, O 2003. The role of hydromechanical coupling in fractured rock engineering. *Hydrogeology Journal,* 11**,** 7-40.

Saadatpoor, E, Bryant, SL,Sepehrnoori, K 2010. New trapping mechanism in carbon sequestration. *Transport in porous media,* 82**,** 3-17.

Safai, NM,Pinder, GF 1979. Vertical and horizontal land deformation in a desaturating porous medium. *Advances in Water Resources,* 2**,** 19-25.

Samper, J, Mon, A, Montenegro, L,Naves, A 2020. THCM numerical simulations of the engineered barrier system for radioactive waste disposal. *Environmental Geotechnics,* 8**,** 92-112.

Sánchez, M, Gens, A, Do Nascimento Guimarães, L,Olivella, S 2005. A double structure generalized plasticity model for expansive materials. *International Journal for numerical and analytical methods in geomechanics,* 29**,** 751-787.

Savage, D, Noy, D,Mihara, M 2002. Modelling the interaction of bentonite with hyperalkaline fluids. *Applied Geochemistry,* 17**,** 207-223.

Schrefler, BA,Scotta, R 2001. A fully coupled dynamic model for two-phase fluid flow in deformable porous media. *Computer methods in applied mechanics and engineering,* 190**,** 3223-3246.

Seetharam, S, Thomas, H,Cleall, PJ 2007. Coupled thermo/hydro/chemical/mechanical model for unsaturated soils—Numerical algorithm. *International Journal for Numerical Methods in Engineering,* 70**,** 1480-1511.

Shanmugharaj, A, Rhee, KY,Ryu, SH 2006. Influence of dispersing medium on grafting of aminopropyltriethoxysilane in swelling clay materials. *Journal of colloid and interface science,* 298**,** 854-859.

Shroll, RM,Smith, DE 1999. Molecular dynamics simulations in the grand canonical ensemble: Application to clay mineral swelling. *The Journal of chemical physics,* 111**,** 9025-9033.

Siddique, JI, Ahmed, A, Aziz, A,Khalique, CM 2017. A Review of Mixture Theory for Deformable Porous Media and Applications. *Applied Sciences,* 7**,** 917.

Sijing, W,Enzhi, W 2004. Recent study of coupled processes in geotechnical and geoenvironmental fields in china. *Elsevier Geo-Engineering Book Series,* 2**,** 81-91.

Skipper, NT, Chang, F-RC,Sposito, G 1995. Monte Carlo simulation of interlayer molecular structure in swelling clay minerals. 1. Methodology. *Clays and Clay minerals,* 43**,** 285-293.

Song, Z, Liang, F, Lin, C,Xiang, Y 2019. Interaction of pore pressures in double-porosity medium: Fluid injection in borehole. *Computers and Geotechnics,* 107**,** 142-149.

Sun, L, Zhang, Y, Qin, Z, Wang, T,Zhang, S 2020. A Damage Constitutive Model of Rock under Hydrochemical Cyclic Invasion. *Advances in Civil Engineering,* 2020.

Sun, P 2005. *Advances in Coupled Modeling in Geomechanics*, China Environmental Science Press.

Sun, W,Sun, DA 2012. Coupled modelling of hydro‐mechanical behaviour of unsaturated compacted expansive soils. *International Journal for Numerical and Analytical Methods in Geomechanics,* 36**,** 1002-1022.

Tambach, TJ, Hensen, EJ,Smit, B 2004. Molecular simulations of swelling clay minerals. *The Journal of Physical Chemistry B,* 108**,** 7586-7596.

Tao, J, Wu, Y, Elsworth, D, Li, P,Hao, Y 2019. Coupled thermo-hydro-mechanical-chemical modeling of permeability evolution in a CO2-circulated geothermal reservoir. *Geofluids,* 2019.

Taron, J,Elsworth, D 2010. Coupled mechanical and chemical processes in engineered geothermal reservoirs with dynamic permeability. *International Journal of Rock Mechanics and Mining Sciences,* 47**,** 1339-1348.

Terzaghi, K 1943. Theory of consolidation. *Theoretical Soil Mechanics***,** 265-296.

Thomas, H 1985. Modelling two - dimensional heat and moisture transfer in unsaturated soils, including gravity effects. *International journal for numerical and analytical methods in geomechanics,* 9**,** 573-588.

Thomas, H 1988. A nonlinear analysis of two - dimensional heat and moisture transfer in partly saturated soil. *International journal for numerical and analytical methods in geomechanics,* 12**,** 31-44.

Thomas, H, Cleall, P,Hashm, A 2001. Thermal/hydraulic/chemical/mechanical (THCM) behaviour of partly saturated soil. *Computer Methods and Advances on Geomechanics,* 1**,** 743-748.

Thomas, H, Cleall, P,Seetharam, S 2002. Numerical modelling of the thermalhydraulic-chemical-mechanical behaviour of unsaturated clay. *Environmental Geomechanics. Monte Verità***,** 125-136.

Thomas, H, Rees, S,Sloper, N 1998. Three - dimensional heat, moisture and air transfer in unsaturated soils. *International journal for numerical and analytical methods in geomechanics,* 22**,** 75-95.

Tong, F, Jing, L,Zimmerman, RW 2010. A fully coupled thermo-hydro-mechanical model for simulating multiphase flow, deformation and heat transfer in buffer material and rock masses. *International Journal of Rock Mechanics and Mining Sciences,* 47**,** 205-217.

Truesdell, C 1957. Sulle basi della termomeccanica. *Rend. Lincei,* 22**,** 33-38.

Tsang, C-F, Stephansson, O, Jing, L,Kautsky, F 2009. DECOVALEX Project: from 1992 to 2007. *Environmental Geology,* 57**,** 1221-1237.

Vaunat, J, Romero, E,Jommi, C 2000. An elastoplastic hydro-mechanical model for unsaturated soils. *Experimental evidence and theoretical approaches in unsaturated soils,* 20**,** 0.

Verruijt, A 1969. Elastic storage of aquifers. *Flow through porous media,* 1**,** 331-376.

Viani, BE, Low, PF,Roth, CB 1983. Direct measurement of the relation between interlayer force and interlayer distance in the swelling of montmorillonite. *Journal of colloid and interface science,* 96**,** 229-244.

Von Terzaghi, K 1923. Die Berechnung der Durchassigkeitsziffer des Tones aus dem Verlauf der hydrodynamischen Spannungs. erscheinungen. *Sitzungsber. Akad. Wiss. Math. Naturwiss. Kl. Abt. 2A,* 132**,** 105-124.

Weimin, MY, Zhang, F, Chen, B, Chen, Y-G, Wang, Q,Cui, Y-JJEES 2014. Effects of salt solutions on the hydro-mechanical behavior of compacted GMZ01 Bentonite. *Environmental earth sciences,* 72**,** 2621-2630.

Wielopolski, L 2011. Geological carbon sequestration: a new approach for near-surface assurance monitoring. *International journal of environmental research and public health,* 8**,** 818-829.

Wild, KM, Wymann, LP, Zimmer, S, Thoeny, R,Amann, F 2015. Water retention characteristics and state-dependent mechanical and petro-physical properties of a clay shale. *Rock Mechanics and Rock Engineering,* 48**,** 427-439.

Wna. 2022. *Nuclear Power in the World Today* [Online]. Available: https://world-nuclear.org/information-library/current-and-future-generation/nuclear-power-in-the-world-today.aspx [Accessed 26/01 2022].

Wriggers, P 2008. *Nonlinear finite element methods*, Springer Science & Business Media.

Xia, T, Zhou, F, Liu, J, Kang, J,Gao, F 2014. A fully coupled hydro-thermo-mechanical model for the spontaneous combustion of underground coal seams. *Fuel,* 125**,** 106-115.

Xiaodong, L, Prikryl, R,Pusch, R 2011. THMC-testing of three expandable clays of potential use in HLW repositories. *Applied Clay Science,* 52**,** 419-427.

Xikui, L,Zienkiewicz, O 1992. Multiphase flow in deforming porous media and finite element solutions. *Computers & structures,* 45**,** 211-227.

Xiong, Y, Hu, L,Wu, Y-S. Coupled geomechanical and reactive geochemical simulations for fluid and heat flow in enhanced geothermal reservoirs. PROCEEDINGS, Thirty-Eighth Workshop on Geothermal Reservoir Engineering Stanford University, 2013.

Yadav, SK,Chakrapani, G 2006. Dissolution kinetics of rock–water interactions and its implications. *Current Science***,** 932-937.

Yan, C, Deng, J,Yu, B 2013. Wellbore stability in oil and gas drilling with chemical-mechanical coupling. *The Scientific World Journal,* 2013.

Yasuhara, H, Kinoshita, N, Ogata, S, Cheon, D-S,Kishida, K 2016. Coupled thermo-hydro-mechanical-chemical modeling by incorporating pressure solution for estimating the evolution of rock permeability. *International Journal of Rock Mechanics and Mining Sciences,* 86**,** 104-114.

Yin, S, Dusseault, MB,Rothenburg, L 2011. Coupled THMC modeling of CO2 injection by finite element methods. *Journal of Petroleum Science and Engineering,* 80**,** 53-60.

Yin, S, Towler, BF, Dusseault, MB,Rothenburg, L 2010. Fully coupled THMC modeling of wellbore stability with thermal and solute convection considered. *Transport in porous media,* 84**,** 773-798.

Zhang, C-L, Rothfuchs, T, Su, K,Hoteit, N 2007. Experimental study of the thermo-hydro-mechanical behaviour of indurated clays. *Physics and Chemistry of the Earth, Parts A/B/C,* 32**,** 957-965.

Zhang, J, Hu, W, Zhang, L, Li, T, Cai, D,Chen, G 2019. Investigation of ammonium–lauric salt as shale swelling inhibitor and a mechanism study. *Adsorption Science & Technology,* 37**,** 49-60.

Zhang, R, Winterfeld, PH, Yin, X, Xiong, Y,Wu, Y-S 2015. Sequentially coupled THMC model for CO 2 geological sequestration into a 2D heterogeneous saline aquifer. *Journal of Natural Gas Science and Engineering,* 27**,** 579-615.

Zhang, R, Xiong, Y, Winterfeld, PH, Yin, X,Wu, YS 2016a. A novel computational framework for thermal - hydrological - mechanical - chemical processes of CO2 geological sequestration into a layered saline aquifer and a naturally fractured enhanced geothermal system. *Greenhouse Gases: Science and Technology,* 6**,** 370-400.

Zhang, R, Yin, X, Winterfeld, PH,Wu, Y-S 2016b. A fully coupled thermal-hydrological-mechanical-chemical model for CO 2 geological sequestration. *Journal of Natural Gas Science and Engineering,* 28**,** 280-304.

Zhang, R, Yin, X, Wu, Y-S,Winterfeld, P. A fully coupled model of nonisothermal multiphase flow, solute transport and reactive chemistry in porous media. SPE Annual Technical Conference and Exhibition, 2012. Society of Petroleum Engineers.

Zhang, X,Zhong, Z 2017a. A coupled theory for chemically active and deformable solids with mass diffusion and heat conduction. *Journal of the Mechanics and Physics of Solids,* 107**,** 49-75.

Zhang, X,Zhong, Z 2017b. A thermodynamic framework for thermo-chemo-elastic interactions in chemically active materials. *SCIENCE CHINA Physics, Mechanics & Astronomy,* 60**,** 084611.

Zhang, X,Zhong, Z 2018. Thermo-chemo-elasticity considering solid state reaction and the displacement potential approach to quasi-static chemo-mechanical problems. *International Journal of Applied Mechanics,* 10**,** 1850112.

Zhao, C 2014. Physical and chemical dissolution front instability in porous media. *Cham, Switzerland: Springer*.

Zheng, L, Samper, J, Montenegro, L,Fernández, AM 2010. A coupled THMC model of a heating and hydration laboratory experiment in unsaturated compacted FEBEX bentonite. *Journal of Hydrology,* 386**,** 80-94.

Zheng, L, Samper, J,Montenegro, LJ 2011. A coupled THC model of the FEBEX in situ test with bentonite swelling and chemical and thermal osmosis. *Journal of contaminant hydrology,* 126**,** 45-60.

Zheng, L,Samper, JJP 2008. A coupled THMC model of FEBEX mock-up test. *Physics and Chemistry of the Earth, Parts A/B/C,* 33**,** S486-S498.

Zhou, A,Sheng, D 2015. An advanced hydro-mechanical constitutive model for unsaturated soils with different initial densities. *Computers and Geotechnics,* 63**,** 46-66.

Zhou, X,Ghassemi, A 2009. Finite element analysis of coupled chemo-poro-thermo-mechanical effects around a wellbore in swelling shale. *International Journal of Rock Mechanics and Mining Sciences,* 46**,** 769-778.

Zhou, Z 1995. Construction and application of clay-swelling diagrams by use of XRD methods. *Journal of Petroleum Technology,* 47**,** 306-306.

Ziefle, G, Matray, J-M, Maßmann, J,Möri, A 2018. Coupled hydraulic-mechanical simulation of seasonally induced processes in the Mont Terri rock laboratory (Switzerland). *Mont Terri Rock Laboratory, 20 Years.* Springer.